Development of biosensors for early detection of anastomotic leak and sepsis

by

Natalie Anne Hirst

Submitted in accordance with the requirements for the degree of Doctor of Philosophy

The University of Leeds

School of Biomedical Sciences,

Faculty of Biological Sciences

August 2014

Declaration

The candidate confirms that the work submitted is her own, except where work which has formed part of jointly-authored publications has been included. The contribution of the candidate and the other authors to this work has been explicitly indicated below. The candidate confirms that appropriate credit has been given within the thesis where reference has been made to the work of others.

Some of Chapter 1 (Introduction) was based on work from the publication entitled *'Systematic review of methods to predict and detect anastomotic leakage in colorectal surgery',* Colorectal Disease, Volume 16, Issue 2, February 2014, Pages 81-154. This review was written by the candidate and the manuscript edited by the candidate's supervisors Professor D. G. Jayne and Professor P. A. Millner before publication. Sections of Chapter 1 were also based on work from the publication entitled *'Impedimetric biosensors for medical applications: Current progress and challenges'*, Biomedical & Nanomedical Technologies – Concise Monograph, Momentum Press, October 2013. The monograph was jointly-authored with laboratory members Dr J. V. Rushworth, J. A. Goode, D. J. Pike, A. Ahmed and supervisor Professor P. A. Millner. Chapter 2 of the monograph was written by the candidate before editing by Dr J. V. Rushworth and Professor P. A. Millner.

Some of the results from Chapter 4 have been published as *'An amperometric lactate biosensor using H_2O_2 reduction via a Prussian Blue impregnated poly(ethyleneimine) surface on screen printed carbon electrodes to detect anastomotic leak and sepsis'*, Sensors and Actuators B: Chemical, Volume 186, September 2013, Pages 674-680. This original research article was jointly-authored with the candidates supervisors Professor P. A. Millner and Professor D. G. Jayne and statistician Dr L. D. Hazelwood. The candidate carried out the work published and wrote the paper, which was edited by her supervisors before submission for publication. Assistance with statistical analysis was kindly given by Dr L. D. Hazelwood.

Acknowledgements

I gratefully acknowledge the financial support of the Leeds Teaching Hospitals NHS Trust Charitable Foundation and the Bowel Disease Research Foundation for this research.

I would like to express my gratitude to both my supervisors Professor David Jayne and Professor Paul Millner for their continuous support, expertise, and enthusiasm. Their confidence in me has enabled me to not only complete the research but to give me the self-belief to present the work on an international stage, to high commendation, amongst other achievements during these years.

Past and present lab members from the Millner group including Jo Rushworth and Tim Gibson who taught me electrochemistry and other techniques such as Midland blotting were invaluable to this work. I thank the surgical research group for always giving an honest opinion and helping me to keep the project moving forward, particularly Sarah Perry and Tom Hughes. Members of affiliated labs such as that of Vas Ponnambalam provided the secondary antibodies used in the work as well as humour in the lab, and special thanks to Anne Neville from the Engineering department for technical expertise and support. Lee Hazelwood, Helene Thygesen and Andrew Blance helped enormously with statistical assistance. Gareth Howell provided technical assistance with flow cytometry, as did John Harrington and Martin Fuller with SEM. I gratefully acknowledge John Wright for providing the *E. coli* strains used in the *E. coli* biosensor development. Thanks go to all the staff in the animal facility for assistance and advice, particularly Khawar Abbas.

Last but not least my family and Andy, the husband I gained whilst undertaking this work, who have kept me sane and made this all worthwhile, my biggest thanks are to you.

Abstract

Anastomotic leak is a catastrophic surgical complication leading to high morbidity, mortality and cancer recurrence. Currently detection is difficult, with a paucity of available diagnostic tests that have variable sensitivity and specificity. The work described in this thesis evaluated the use of local biomarkers within the anastomotic environment coupled with a biosensor application to assess proof-of-concept feasibility as a point-of-care diagnostic tool for anastomotic leak. Using a small animal model of caecal ligation and puncture to replicate abdominal sepsis, local abdominal biomarkers lactate, TNFα, and *E. coli* were all found to significantly increase compared to sham control models at 24 and 36 hours. Chronoamperometry and electrochemical impedance spectroscopy (EIS) interrogation of biosensors were then used to detect and quantitate levels of these respective biomarkers in real patient samples, and data compared to that obtained by existing commercial assays to evaluate accuracy. Characterisation of each biosensor utilised cyclic voltammetry, SEM, Midland blotting, SDS-PAGE and dot blotting techniques to optimise the fabrication methodology. The lactate biosensor consisted of a pre-impregnated Prussian Blue carbon electrode with lactate oxidase enzyme immobilised onto the surface *via* polyethyleneimine. Using chronoamperometry, the lactate biosensor gave significantly similar results to a commercial enzyme-based lactate colorimetric assay in ten abdominal fluid patient samples. *E. coli* immunosensors were constructed using a polytyramine matrix onto which half polyclonal antibody fragments raised against multiple strains of *E. coli* were immobilised. EIS was used to measure the charge transfer resistance of the biosensors when incubated with a varying concentration of *E. coli*, with a limit of detection found to be 10^4 cells ml^{-1}. EIS of *E. coli* biosensors in the ten patient samples showed statistically significant equivalent results to those from flow cytometry. Immunosensors to TNFα were constructed using a similar methodology to *E. coli*, with whole antibody to TNFα immobilised onto a polytyramine electrode surface. Initial EIS results in buffered solution showed good biosensor response to varying concentrations of TNFα, but further studies are required for complete biosensor development.

Abbreviations

2-ABA	2-aminobenzylamine
2-MEA	2-mercaptoethylamine•HCl
4-AAP	4-aminoantipyrine
AFM	Atomic force microscopy
AL	Anastomotic leak
APE	Abdominoperineal excision
ATP	Adenosine triphosphate
AUC	Area under curve
AXR	Abdominal X-ray
Biotin-IgG	Biotin tagged immunoglobulin G
Biotin-NHS	Biotin-N-hydroxysuccimide
BSA	Bovine serum albumin
CARS	Compensatory anti-inflammatory response syndrome
C_{dl}	Double layer capacitance
CL	Caecal ligation
CLP	Caecal ligation and puncture
CoPc	Cobalt phthalocyanine
CPE	Constant phase element
CRP	C-reactive protein
CT	Computerised tomography
CV	Cyclic voltammetry
DMSO	Dimethyl sulfoxide
DNA	Deoxyribonucleic acid
DRE	Digital rectal examination
ECL	Enhanced chemiluminescence
E. coli	Escherichia coli
EDTA	Ethylenediamine tetraacetic acid
E. faecalis	Enterococcus faecalis
EIS	Electrochemical impedance spectroscopy
ELISA	Enzyme-linked immunosorbent assay
FAD	Flavin adenine dinucleotide

FDG-PET	F-18-fluorodeoxyglucose positron emission tomography
FITC	Fluorescein isothiocyanate
FRA	Frequency response analyser
GI	Gastrointestinal
HRP	Horseradish peroxidase
ICG	Indocyanine green
Ig	Immunoglobulin
Il	Interleukin
K_d	Dissociation constant
KDa	Kilodalton
LAL	*Limulus* amebocyte lysate
LED	Light emitting diode
LOD	Limit of detection
LOx	Lactate oxidase
LPS	Lipopolysaccharide
MMP	Matrix metalloproteinase
mSAM	Mixed self assembled monolayer
NAD	Nicotinamide adenine dinucleotide
NCS	Newborn calf serum
NHS	National health service
NIR	Near infrared
NRES	National research ethics service
P(ANI/2-ABA)	Copolymer of aniline and 2-ABA
PANI	Polyaniline
PB	Prussian Blue
PBS	Phosphate buffered saline
PCR	Polymerase chain reaction
PEI	Polyethyleneimine
Phloretic acid	(3-(4-Hydroxyphenyl)propanoic acid)
PI	Propidium iodide
POC	Point of care
POD	Post-operative day
PSA	Phenol-4-sulphonic acid or prostate specific antigen
QCM	Quartz crystal microbalance

R&D	Research and development
R_{ct}	Charge transfer resistance
RI	Refractive index
RNA	Ribonucleic acid
ROC	Receiver operating characteristics
R_s	Solution resistance
SAM	Self assembled monolayer
SDS-PAGE	Sodium dodecyl sulphate polyacrylamide gel electrophoresis
SELEX	Systematic evolution of ligands by exponential enrichment
SEM	Scanning electron microscopy
SIRS	Systemic inflammatory response syndrome
SPCE	Screen printed carbon electrodes
SPR	Surface plasmon resonance
Sulfo-SMCC	Sulfosuccinimidyl 4-[N-maleimidomethyl] cyclohexane-1-carboxylate
TACE	TNFα-converting enzyme
TIMP	Tissue inhibitors of metalloproteinase
TMB	Tetramethylbenzidine
TNFα	Tumour necrosis factor alpha
Tris	Tris(hydroxymethyl) aminomethane
W	Warburg impedance
WSCE	Water-soluble contrast enema

Table of contents

List of Tables

List of Figures

Chapter 1:

Introduction

Chapter 1. Introduction

1.1 Overview

Septic complications from gastrointestinal (GI) surgery, such as anastomotic leak (AL), are catastrophic, conferring high morbidity and mortality and severely impacting on patient quality of life (Kube et al., 2010, Marra et al., 2009, Nesbakken et al., 2001). The incidence of anastomotic leak is 1-30%, with the wide range attributable to the lack of standardised definition, and a number of risk factors identified (Kingham and Pachter, 2009, Boccola et al., 2011). The early detection of anastomotic leak is crucial to allow remedial intervention. Evidence shows that each hour in delay of antibiotic administration and any delay to reoperation are associated with a measurable increase in mortality from sepsis and organ failure (Dellinger et al., 2008, den Dulk et al., 2009). Unfortunately the diagnosis of anastomotic leak is often difficult. The signs and symptoms that patients exhibit are largely subjective, non-specific, or may not be present. Anastomotic leaks present on a spectrum, ranging from an insidious onset, to the sudden development of fulminant sepsis. Interpretation and the correct management are therefore difficult.

Current diagnostic tests for anastomotic leak are largely limited to radiological tests (Hyman, 2009). Intraoperative "preventative" modalities also exist, but with a paucity of robust outcomes data. Literature on the available imaging modalities, including computerised tomography (CT) and water-soluble contrast enema (WSCE), demonstrate a wide range of sensitivity and specificity, and problems with expense and the need for experienced radiologists. Recently, strategies involving the measurement of pathophysiological biomarkers locally in the abdominal environment have been put forward as potentially more sensitive and specific for

anastomotic leak, although there is little data from human studies or animal experiments to prove their validity (Komen et al., 2008). These available studies provide early pilot data and have established proof of principle. The most common methodology for measurement of biomarkers is enzyme-linked immunosorbent assay (ELISA), with others including flow cytometry, electrophoresis and laser emitting diode (LED) devices. All of these methodologies involve complex protocols, additional reagents, specialist equipment, and user proficiency. Crucially, they also take time, with electrophoresis described as taking a number of days including an overnight soaking step, rendering them of limited usefulness for routine clinical application.

Electrochemical biosensors, as in a glucose monitor, have the advantage of being inexpensive, robust and negating the requirement for sophisticated high-tech equipment and trained users (Rushworth et al., 2013). Most importantly they provide rapid point-of-care results that can be frequently repeated to monitor clinical change and allow early intervention as necessary; properties that are ideal for time-sensitive anastomotic leak. Amperometric biosensors lend themselves to measurement of ischaemic markers because enzymes to generate products from glucose and lactate are readily available. Immunosensors using an antibody to capture inflammatory and bacterial analytes are a relatively new field in biosensing, but with rapidly expanding interest and huge potential. A sensitive and specific biomarker coupled with an appropriate electrochemical biosensor device has the potential to revolutionise postoperative detection of adverse events, such as anastomotic leak and sepsis, greatly reducing morbidity and mortality.

1.2 Abdominal sepsis

Sepsis is defined as a systemic inflammatory response to infection, progressing to severe sepsis if there is concurrent organ dysfunction, and septic shock classified as the presence of hypotension refractory to fluid resuscitation (Bone et al., 1992,

Dellinger et al., 2008). Extrapolated data suggest there may be up to 19 million cases of sepsis worldwide per year, although these figures are thought to be an underestimation (Adhikari et al., 2010). The pathophysiological features of sepsis are discussed in detail in **Section 1.6.3** but briefly there is a complex, as yet incompletely understood, excessive host inflammatory response invoking both pro- and anti-inflammatory cells and mediators**.** Intra-abdominal infection is the second most common cause of sepsis after pneumonia (Angus and van der Poll, 2013). It is a source of high morbidity and mortality, with intra-abdominal infections present in up to 25% patients with multi-organ failure (Merrell and Latifi, 2001). Common causes include infective pathologies such as appendicitis and diverticulitis, inflammatory conditions with secondary infection including pancreatitis and cholecystitis, ischaemic change, and iatrogenic complications such as anastomotic leak. This thesis will focus on sepsis due to anastomotic leak, but has relevance to the detection from any intra-abdominal septic complication.

1.3 Gastrointestinal surgery

1.3.1 Bowel anastomosis

"Anastomosis" is a term that broadly describes any connection of two luminal structures. An intestinal anastomosis may be defined as "a surgical procedure to establish communication between two formerly distant portions of the intestine" (Kate, 2014). The formation of a bowel (intestinal) anastomosis serves to restore intestinal continuity after removal of pathology affecting the bowel; commonly cancer, but also including benign disease. Descriptions of different anastomotic techniques date back to the 19th century (Senn, 1893). Subsequent improvements in understanding of the importance of serosal (outer wall) apposition, aseptic technique, and more recently in the 1980's the introduction of the modern stapling device, have rendered the anastomosis a routinely performed surgical procedure (Chen, 2012). An anastomosis may be formed by a stapling device, or be hand-sewn using sutures. Prospective, multicentre randomised studies have not shown

any difference in outcomes between the two techniques, and it remains the surgeon's preference at operation (Docherty et al., 1995, Chandramohan et al., 2013). **Figure 1.1** shows the steps in forming an anastomosis. In A, the caecum and ileum portions of the bowel are resected. B shows the free ends anastomosed together to restore continuity.

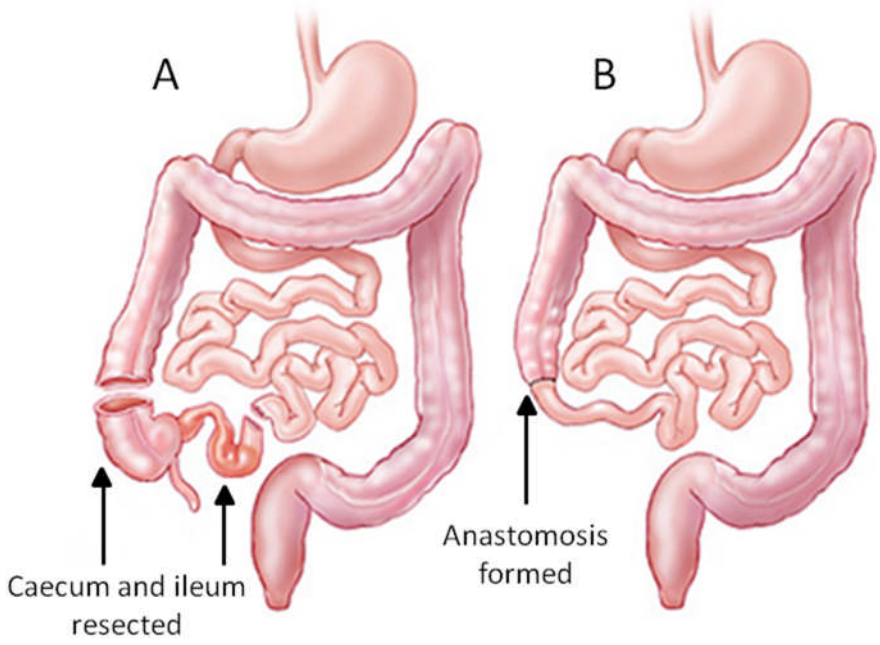

Figure 1.1: Schematic of the formation of an intestinal anastomosis. (A) Bowel resected, (B) The subsequent anastomosis formed from attachment of the free ends. Adapted from (Johns Hopkins Medicine, 2014).

Resection of part of the gastrointestinal tract is frequently performed for cancer treatment, either with curative intent or for disease management (Rahbari et al., 2010). Bowel cancer is the 4th most common cancer in the UK, with 40,695 new cases diagnosed in 2010 and a lifetime risk of 1 in 14 for men and 1 in 19 for women (Office for National Statistics, 2012). Incidence rates have increased in the UK since the mid-1970's, with the introduction of the National Bowel Cancer Screening Programme in 2006 and a shift to detection of earlier stage disease. These trends are echoed globally, as worldwide bowel cancer is the 3rd most common cancer with an estimated 1.2 million new cases diagnosed in 2008 (Ferlay et al., 2010).

Approximately 80% of bowel cancers diagnosed will undergo an operative surgical procedure with or without adjuvant treatment such as chemo or radiotherapy (Cancer Research UK, 2009). Almost all bowel resection operations for bowel cancer involve the formation of an anastomosis, notable exceptions being for rectal cancers in which an abdominoperineal excision (APE) or Hartmann's procedure may be performed if the tumour is too low to restore gastrointestinal continuity, or in emergency cases respectively. However, the most common operation for rectal cancer is an anterior resection in which a colo-rectal/anal anastomosis is formed (Morris et al., 2011). All resections elsewhere in the GI tract necessitate an anastomosis. The rate of anastomoses performed annually is therefore vast. **Table 1.1** shows the potential number of gastrointestinal anastomoses created per year in the UK based on the number of new diagnoses, and the proportion of patients whom undergo surgery. This includes inflammatory bowel disease (Crohn's disease and Ulcerative Colitis) and the corresponding percentage lifetime risk of surgical resection. It can be seen that for colorectal cancer alone, up to 32,556 patients will undergo bowel resection with an anastomosis annually (Cancer Research UK, 2009). Anastomoses are also performed for a number of other pathologies not mentioned e.g. diverticular disease, polyposis.

Disease	Location/Type	No. of new diagnoses per year UK (2010)	% of diagnoses resected surgically	Maximum anastomoses formed annually
Cancer	Colorectal (bowel)	40,695	80%	32,556
	Oesophageal	8,477	25%	2,119
	Gastric (stomach)	7,300	48%	3,504
Benign	Crohn's disease	3,000-6,000	70-80% (lifetime risk)	2,100-4,800
	Ulcerative Colitis	6,000-12,000	20-30% (lifetime risk)	1,200-3,600

Table 1.1: Summary of number of anastomoses formed annually. Table showing the numbers of new diagnoses and GI resections by each disease type in the UK annually, with maximum number of anastomoses formed (Cancer Research UK, 2009) and British Society of Gastroenterology guidelines (Mowat et al., 2010).

1.4 Anastomotic leak

Anastomotic leak is the breakdown of an anastomosis, and is one of the most feared complications of gastrointestinal surgery. It causes considerable morbidity and mortality, and contributes to local cancer recurrence (Kube et al., 2010, Marra et al., 2009, Branagan and Finnis, 2005, Boccola et al., 2011). Quality of life is often affected due to poor functional outcomes with high rates of permanent stoma formation (Nesbakken et al., 2001).

The incidence of anastomotic leak varies widely, with reported rates of between 1% and 30% (Kingham and Pachter, 2009). Risk factors include: i) patient-specific factors, such as male gender, older age, poor nutritional status, and advanced tumour stage, and ii) technical factors, including local ischaemia, anastomotic

tension, local sepsis, and the presence of distal obstruction (Boccola et al., 2011, Lipska et al., 2006, Matthiessen et al., 2004, Rullier et al., 1998). The risk also varies with the site of the anastomosis with low rectal anastomoses, less than 5 cm from the anal verge, being particularly vulnerable (Lipska et al., 2006, Rullier et al., 1998).

The definition of anastomotic leak has always been divisive and the primary reason for the wide range in reported incidence. In 1991, the United Kingdom Surgical Infection Study Group offered the definition: "a leak of luminal contents from a surgical join between two hollow viscera" (Peel and Taylor, 1991), but this definition has rarely been referenced since. A review of 97 studies from 1993 to 1999 demonstrated 56 different definitions of anastomotic leak after gastrointestinal surgery (Bruce et al., 2001), illustrating the lack of uniformity and difficulties interpreting outcomes from different studies. A more recent attempt to standardise terminology after rectal resection offered the definition: "a communication between the intra- and extraluminal compartments owing to a defect of the integrity of the intestinal wall at the anastomosis between the colon and rectum or the colon and anus" (Rahbari et al., 2010). The authors proceeded to offer a clinical grading system based on severity of leakage, in order to further standardise terms for valid comparison of studies. Difficulty in an agreed definition leads to problems with interpreting reported rates, and in diagnosis and consensus on correct clinical management.

Treatment options for anastomotic leak include conservative management with intravenous antibiotics and local percutaneous drainage, or reoperation with diversion (stoma) or takedown of the anastomosis (Murrell and Stamos, 2006). **Figure 1.2** shows the typical presentation at reoperation for anastomotic leak. The bowel appears "stuck down" with inflammatory exudate secondary to the peritoneal contamination. Treatment choice is largely dependent on localisation of the leak and the clinical picture (Phitayakorn et al., 2008).

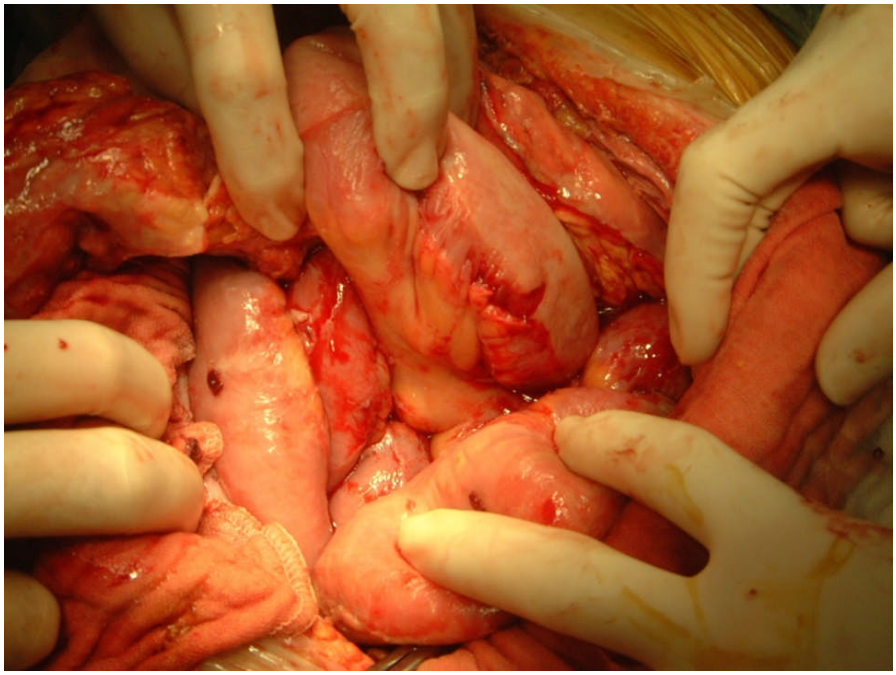

Figure 1.2: Photograph of typical appearance inside the abdomen at reoperation for anastomotic leak (intraoperative photograph courtesy of DG Jayne).

Early diagnosis and management of anastomotic leak are critical to a good outcome, with any time delay correlating directly with increased morbidity and mortality as a result of sepsis and multiorgan failure (Hyman, 2009, Murrell and Stamos, 2006). In 2004, the "Surviving Sepsis" campaign, spearheaded by critical care experts, published the first international guidance for the management of sepsis and noted that each hour of delay in administration of antibiotics from the onset of septic shock was associated with a decrease in survival of 7.6% (Dellinger et al., 2008). Similarly, in one study a delay of 2.5 days to reoperation or definitive intervention for anastomotic leak was associated with an increase in mortality from 24% to 39% (den Dulk et al., 2009).

Timely diagnosis of anastomotic leak is therefore of utmost importance, yet there is still ongoing difficulty in early detection of AL, without a consensus on the current best diagnostic test. Practice varies between hospitals and, because of the acute nature of the condition, there is a paucity of data comparing the sensitivity and

specificity of the various tests. Anastomotic leak may also present in varying guises, ranging from the sudden onset of fulminant sepsis with multiorgan failure, to a more insidious presentation with ileus (paralysis of gut motility) and general failure to progress in the postoperative period, or may even be subclinical and only detectable on radiological imaging (Hyman, 2009). Assessment and standardisation of diagnostic approaches is therefore challenging, which impacts upon research into the development of superior diagnostic tests (Hirst et al., 2014).

1.5 Current methods of diagnosis

1.5.1 Intraoperative prevention

Intraoperative assessment is used by some to confirm anastomotic integrity and pre-empt postoperative problems. Strategies include direct endoscopic visualisation, air leak testing, and assessment of completeness of anastomotic doughnuts. Air leak testing is a well-established technique. Beard *et al* demonstrated a reduction from 14% to 4% in postoperative clinical anastomotic leak, and 29% to 11% in radiological leak, with the use of intraoperative air leak testing and repair (Beard et al., 1990). Other studies show similar results (Ivanov et al., 2011). Air leak testing is easy, quick and cheap and confers little or no risk, therefore it is considered standard in some centres. Intraoperative endoscopy has the benefits of real-time assessment of anastomotic integrity, bleeding complications, vascular compromise, iatrogenic bowel wall injury, tumour margins and missed distal pathology. It also provides a robust air leak test (Li et al., 2009). Li *et al* compared outcomes in laparoscopic colorectal patients undergoing either routine intraoperative endoscopy (RIOE) or selective intraoperative endoscopy (SIOE) where there was doubt about anastomotic integrity (Li et al., 2009). Abnormalities including staple line bleeding, distal polyps and positive air leaks were observed in 10.3% of RIOE patients. 21.9% of patients underwent SIOE and 10% of these were found to have anastomotic abnormalities. The SIOE group had a higher incidence of anastomotic leak, but this failed to reach significance due to the

small sample size. Two further studies have corroborated the potential benefits of intraoperative endoscopy, but again the sample sizes were too small to draw any meaningful conclusions (Shamiyeh et al., 2012, Brugiotti et al., 2011). A sufficiently powered, randomised control trial would be needed before any conclusive recommendations could be made, although the proponents of intraoperative endoscopy highlight the advantages of low cost and minimal time associated with the additional procedure.

Other methods of intraoperative assessment include measurement of local tissue oxygenation as a predictor of anastomotic complications. Disruption of microcirculatory blood flow at the anastomosis leads to diminished tissue perfusion with impaired healing (Thompson et al., 2006, Enestvedt et al., 2006). Karliczek *et al* used visible light spectroscopy to measure saturated oxygen levels in 80 patients before and after colorectal resection and found that decreased oxygen values immediately after resection were predictive for later anastomotic leakage (Karliczek et al., 2010). Specifically, a significant rise in tissue oxygen saturation (from 72.1 ± 9.0 % to 76.7 ± 8.0 %) was seen in the proximal part of the anastomosis in those patients that did not leak, with no such rise observed in those who sustained an anastomotic leak (73.9 ± 7.9 % to 73.1 ± 7.4 %). The levels of oxygenation were found to be stable and reproducible, suggesting this technique may have merit as a predictive test. Two animal studies support these findings, comparing tissue oxygenation over a range of staple sizes, and using a novel wireless pulse oximeter to assess colonic tissue perfusion (Myers et al., 2009, Servais et al., 2011). To date, the level of tissue oxygenation that unavoidably leads to ischaemia has not been clearly defined and further work to stratify the risk of anastomotic leak is required.

Near infrared (NIR) fluorescent imaging is an emerging method for tissue assessment during surgery. Near infrared, rather than ultraviolet or narrow band imaging, holds great potential for abdominal imaging, as it is capable of penetrating relatively deeply into the bowel and mesenteric tissues without causing thermal

damage (Cahill and Mortensen, 2010). Coupled with the contrast agent indocyanine green (ICG), arteries, capillaries and veins can be mapped out, and vascular flow used as a surrogate for tissue perfusion. The first uses of NIR-ICG have been for assessment of skin flaps after plastic surgery (Krishnan et al., 2005), and in breast cancer sentinel lymph node mapping (Troyan et al., 2009). To apply the concept in gastrointestinal surgery, Matsui *et al* assessed the use of NIR-ICG in predicting long-term viability of ischaemic bowel during surgery (Matsui et al., 2011). The group showed increased prediction of survival (90%) and visible necrosis at postoperative day 3 (92%), using the imaging modality compared to clinical evaluation in ischaemic bowel animal models. Using NIR angiography to assess intraoperative human bowel integrity, Kudszus *et al* performed a retrospective matched-pairs analysis on 402 patients who underwent elective colorectal surgery (Kudszus et al., 2010). Twenty two patients subsequently developed anastomotic leak requiring revision, 7 (3.5%) in the imaging group and 15 (7.5%) in the control group. The use of imaging therefore effectively halved the absolute revision rate, as well as reducing revision rates on subgroup analyses, and significantly reducing the length of hospital stay. A current phase 1 multicentre clinical trial (PILLAR II) is in progress evaluating NIR-ICG administration in conjunction with a trans-anal endoscopic application (PINPOINT© system) to evaluate the planned area of colonic division and subsequent colorectal anastomosis during laparoscopic left sided bowel resection (Stamos, 2013). Initial results in nine patients have demonstrated proof of principle of the technique. NIR-ICG is a promising non-invasive intraoperative technique, but requires further study with assessment of predictive capability. A summary of intraoperative strategies is shown in **Table 1.2**.

Reference	Number of patients	Procedures	Modality	Results
(Beard et al., 1990)	145 (143 in final analysis)	Colo-rectal anastomosis	Air leak testing	Air leak test group vs. non air leak test group: Clinical AL: 4% vs. 14% Radiological AL: 11% vs. 29%
(Ivanov et al., 2011)	60	Stapled colo-rectal anastomosis	Air leak testing	AL: Air leak test group 10% vs. non air leak test group 20%
(Li et al., 2009)	144	Colo-rectal resection with distal anastomosis	Routine intraoperative endoscopy (RIOE) vs. selective intraoperative endoscopy (SIOE)	Abnormalities e.g. staple line bleeding in 10.3% RIOE. 21.9% underwent SIOE, with 10% anastomotic abnormalities Overt AL: 0% RIOE, 1.5% SIOE
(Shamiyeh et al., 2012)	338	Colonic resection	Routine endoscopy vs. non routine	Routine vs. non-routine: Anastomotic bleeding, 5.6% vs. 4.3% AL: 1.2% vs. 1.6%
(Brugiotti et al., 2011)	67	Anterior resection	Air leak testing and endoscopy	4 patients diagnosed AL by both modalities, 2 patients only by endoscopy
(Karliczek et al., 2010)	77	Colo-rectal resection with anastomosis	Oxygen saturation using visible light spectroscopy	Non AL: Increase in proximal anastomosis tissue oxygen saturation (72.1±9.0% to 76.7±8.0%) AL: No increase (73.9±7.9% to 73.1±7.4%)
(Myers et al., 2009)	Animal model	Stapling of small bowel and colon	Oxygen saturation using tissue haemoglobin oxygen saturation probe	Reduced oxygen saturation small bowel and colonic mucosa adjacent to staple lines (30±14.2%, 25±13% respectively) compared to baseline (50±6.6%, 46±14.2%) and 2 cm away (46±7.7%, 45±13.7%), with all stapler sizes (figures given for green)
(Servais et al., 2011)	Animal model	Clamping of stomach (and kidney)	Oxygen saturation using wireless pulse oximeter	Reduced oxygen saturation in devascularised stomach vs. control: serosa 74 vs. 96%, mucosa 52 vs. 88%
(Matsui et al., 2011)	Animal model	Strangulated small bowel vs. control	NIR- ICG	Increased prediction of survival (90%), visible necrosis at postoperative day 3 (92%), compared to clinical evaluation
(Kudszus et al., 2010)	402	Colo-rectal cancer resection	Laser fluorescence angiography	22 relaparotomy for AL: 3.5% angiography group vs. 7.5% control group
(Stamos, 2013)	9	Laparoscopic left colectomy with anastomosis	NIR-ICG with trans-anal endoscopic imaging system	9 patients to establish proof of principle of technique

Table 1.2: Overview of intraoperative modalities used in prediction of colorectal anastomotic leak. AL, Anastomotic leak; NIR-ICG, Near infrared–indocyanine green; RIOE, Routine intraoperative endoscopy; SIOE, Selective intraoperative endoscopy.

1.5.2 Radiological techniques

The most commonly used imaging techniques for postoperative diagnosis of anastomotic leak are CT scanning and water-soluble contrast studies/enemas (WSCE) (Hyman, 2009). In upper gastrointestinal surgery, radiological imaging is in routine use and its value is supported by large clinical datasets (Nicksa et al., 2007, Leslie et al., 2012, Madan et al., 2007, Raman et al., 2007, Toppino et al., 2001, Carucci et al., 2006), particularly in situations where there is diagnostic uncertainty (Igor et al., 2010, Katasani et al., 2005, Schiesser et al., 2011, Doraiswamy et al., 2007). One large series assessing 2,099 patients undergoing laparoscopic Roux-en-Y gastric bypass surgery reported a diagnostic sensitivity of 88% and a specificity of 99% for routine contrast study performed on all patients on postoperative day 1 (Leslie et al., 2012). Suspicion of an anastomotic leak on contrast imaging prompted an early return to theatre with a zero mortality rate. In comparison, clinical predictors, including tachycardia, were not as reliable. There is a paucity of studies assessing CT and WSCE for the detection of anastomotic leak after lower gastrointestinal surgery. Available data suggest that the accuracy of CT and WSCE varies widely, as a result of anastomosis location, study timing, and radiological expertise (Essani and Bergamaschi, 2009).

1.5.2.1 Water-soluble contrast enema

Water-soluble contrast enema has been used in the evaluation of colorectal anastomoses for over 30 years and has been shown to be safe, despite fears about disruption of the anastomosis (Shorthouse et al., 1982). However, over 90% of patients undergoing WSCE do not develop an anastomotic leak, making its routine use controversial and as a result it is largely discouraged (Essani and Bergamaschi, 2009). A landmark study by Goligher in 1970 investigated a series of 73 anterior resection patients in whom anastomotic leak was diagnosed by contrast enema on postoperative day 14 (Goligher et al., 1970). The authors found the contrast study superfluous to digital rectal examination (DRE) and/or sigmoidoscopy in making a diagnosis of dehiscence, particularly for low resections, although commented on its

value in providing a permanent record of the severity of the leak. Williams *et al* in 1991 assessed WSCE as a diagnostic test for anastomotic leak after rectal and colorectal anastomoses and compared it to plain abdominal X-ray (AXR) (Williams et al., 1991). Ten out of the 31 patients suffered an anastomotic leak, in whom 9 were found to have a visibly disrupted staple line on AXR. The authors concluded that AXR is a useful supporting test for anastomotic leak, with WSCE only indicated when an intact staple line was present on AXR yet clinical signs persisted. Further studies assessing WSCE also found it to be a poor diagnostic test for anastomotic leak. Akyol *et al* found a diagnostic sensitivity of 52.2% and a specificity of 86.7% for WSCE after colorectal or left-sided colonic anastomoses, concluding the test provides little useful impact on early postoperative morbidity (Akyol et al., 1992). In a comparison to digital rectal examination to assess staple line integrity prior to reversal of a defunctioning stoma, WSCE was found to be the inferior test with a false positive rate of 6.4% as compared to 3.5% for DRE (Tang and Seow-Choen, 2005). The sensitivity of DRE was 98%, leading the authors to conclude that this was the better test in the hands of an experienced surgeon, as well as being more economical and easier to perform. However, there is conflicting evidence. Nicksa *et al* compared WSCE with CT in a retrospective study of 36 colorectal patients with an anastomotic leak (Nicksa et al., 2007). Of the patients who suffered an anastomotic leak, 15/18 (83.3%) had a positive WSCE, compared to 4/27 (14.8%) who had a positive CT scan. This difference was most pronounced in the patients with a distal anastomotic leak, leading to the conclusion that WSCE may be most useful in assessing distal anastomoses, presumably due to dilution of contrast and/or inability to maintain pressure through a more proximal anastomosis. Further review showed that 9/27 (33.3%) of the CT scans were “descriptive positive”, with air or fluid in the peritoneal cavity but no extravasation of contrast, highlighting the importance of an experienced radiologist together with corroboration of the clinical data.

1.5.2.2 Computerised tomography

CT assessment of anastomotic leak is the preferred imaging method in some centres (Power et al., 2007, Khan et al., 2008), although there is inconsistent data regarding its accuracy and the diagnostic criteria. Power *et al* evaluated CT predictors for anastomotic leak and found that a peri-anastomotic collection containing fluid and air was the only feature significantly more common in patients with a clinically important leak (Power et al., 2007). The authors also found an overlap in CT signs between patients with and without anastomotic leak, and stressed the importance of clinical information in radiological interpretation. A study by Nesbakken *et al* showed that the sensitivity and specificity of CT scanning was 57% and 100% respectively for anastomotic leak after total mesorectal excision for rectal cancer (Nesbakken et al., 2005). This compared to conventional rectal contrast radiography, which gave a sensitivity of 60% and specificity of 100%. Clinical assessment yielded 50% sensitivity and 89% specificity, demonstrating that CT and contrast studies, whilst giving some false negative results, are equally good diagnostic tests. One of the main reasons given for the false negatives was imaging performed before an anastomotic dehiscence was radiologically apparent. This highlights one of the major drawbacks of imaging; the timing of investigation and a reluctance to perform repeated testing due to logistics, radiation exposure, and costs. Other drawbacks include the inherent delay when imaging is performed prior to definitive treatment (Komen et al., 2008). In a retrospective study, Khoury *et al* showed that only 47% of CT scans performed within 72 hours of re-laparotomy for anastomotic leak were positive (Khoury et al., 2009). CT in isolation cannot, therefore, be relied on. Combining pelvic CT scanning with rectal contrast, however, may be superior for low rectal anastomoses, requiring less radiological expertise and being better tolerated in comparison to CT or WSCE alone. Using this combination, Bertoni *et al* showed a 100% sensitivity and 96% specificity for anastomotic leak prior to closure of stoma (Bertoni et al., 2009). However, this was a small isolated study and use of CT in combination with rectal contrast has not yet been prospectively evaluated in the acute post operative setting. Large scale studies are required to evaluate its clinical use.

1.5.2.3 Other radiological techniques

Other radiological techniques have been assessed for the superior detection of anastomotic leak. A case report by Eininkel showed that transvaginal ultrasound scan helped to diagnose anastomotic leak in a colorectal anastomosis following debulking surgery for ovarian cancer (Eininkel et al., 2011). Teeuwen *et al* undertook a pilot study evaluating F-18-fluorodeoxyglucose positron emission tomography (FDG-PET), and was able to show low uptake of FDG in patients with normal, uncomplicated recovery after colorectal surgery, thus giving potential use as a diagnostic test with high sensitivity for anastomotic leak (Teeuwen et al., 2010). The sensitivity and specificity of the different radiological methods discussed is shown in **Table 1.3.**

Ultimately, there remains no consensus on which imaging modality is best for the early diagnosis of anastomotic leak. CT and WSCE are both shown to vary widely in sensitivity and specificity, attributed to a variety of reasons including the wide spectrum of radiological leak presentation and subsequent dependence on radiologist experience, timing of the study, quality of radiological technique, and fundamental differences in study design and definition of anastomotic leak. CT and WSCE both have their relative advantages and limitations and a combination of the two may have some additional benefit, dependent on the evolving clinical situation, although as yet this is largely unproven.

Reference	Number of patients	Procedures	Imaging	Sensitivity (%)	Specificity (%)	Recommendations
(Goligher et al., 1970)	73	Anterior resection	Barium enema study vs. DRE/sigmoidoscopy	Barium study: 97	-	Contrast study superfluous to DRE and sigmoidoscopy
(Williams et al., 1991)	31	Colo-rectal anastomosis	Plain AXR vs. WSCE	AXR: 90	AXR: 100	AXR superior to WSCE
(Akyol et al., 1992)	233	Colorectal/left sided anastomosis	WSCE	52.2	86.7	Poor technique for diagnosis of AL
(Tang and Seow-Choen, 2005)	195	Colo-rectal, colo-anal or ileo-anal pouch anastomosis with diversion stoma	DRE vs. WSCE	DRE: 98.4	DRE: 100	DRE superior test for AL
(Nicksa et al., 2007)	36 (all AL)	Lower GI anastomosis	CT vs. WSCE	CT: 14.8 WSCE: 83.3	-	WSCE superior to CT
(Power et al., 2007)	99	GI anastomosis	CT	Peri-anastomotic fluid and air collection seen in 30.4% of AL vs. 10% non-AL	-	Overlap of CT signs in AL
(Nesbakken et al., 2005)	56	Anterior resection	CT vs. Contrast radiography vs. clinical assessment	CT: 57 Contrast radiography: 60 Clinical assessment: 50	CT: 100 Contrast radiography: 100 Clinical assessment: 89	CT and contrast radiography are equally good tests
(Khoury et al., 2009)	70 (all AL)	Lower GI anastomosis	CT	47%	-	CT alone is not reliable
(Bertoni et al., 2009)	28	Anterior resection with diversion stoma	Pelvic CT with rectal contrast	100	96	Recommended as first line study for suspected AL
(Eininkel et al., 2011)	1 (case report)	Debulking ovarian ca surgery with colorectal anastomosis	Transvaginal USS	-	-	Promising modality for low anastomoses
(Teeuwen et al., 2010)	15 (all non-AL)	Colo-rectal anastomosis	FDG-PET	-	-	Promising novel detection method

Table 1.3: Overview of imaging modalities used to evaluate colorectal anastomotic leak. AL, Anastomotic leak; AXR, Abdominal X-ray; DRE, Digital rectal examination; CT, Computerised tomography; FDG-PET, F-18-fluorodeoxyglucose positron emission tomography; GI, Gastrointestinal; USS, Ultrasound scan; WSCE, Water-soluble contrast enema.

1.6 Emerging methods of diagnosis

To attempt to overcome the problem of non-specific and insensitive diagnostic modalities, various novel methodologies are under investigation. A new shift in focus has been to observe local molecular changes at the anastomosis during anastomotic failure and leak. The term biomarker has been used to describe such molecules which may be measured locally at the anastomotic site and utilised as a diagnostic tool by monitoring real time levels (Komen et al., 2008). **Figure 1.3** shows several of these potential biomarkers (discussed in more detail later) that increase over characteristic time points and may be diagnostic of anastomotic leak. Biomarkers are readily measurable in patient abdominal drain fluid, although the routine use of drains in surgery is declining due to enhanced recovery programmes and a lack of support for their perceived benefit (Kehlet, 1997). A superior diagnostic test based on biomarkers in the abdominal environment would potentially initiate the resurgence of drain use, or spawn another improved sampling method. Serum markers are also viable, although biomarkers from the locality of the anastomosis would intuitively be more sensitive than those that have then reached the systemic circulation.

Komen *et al* suggest the following criteria for an objective biomarker for anastomotic leak in peritoneal drain fluid (Komen et al., 2008):

i) Significant change in biomarker concentration in anastomotic leak
ii) Stability of the biomarker in the peritoneal environment and drain fluid
iii) Biomarker level not influenced by the primary disease
iv) Biomarker with sufficient sensitivity and specificity for anastomotic leak
v) Biomarker allows for easy, fast, and cheap real-time testing

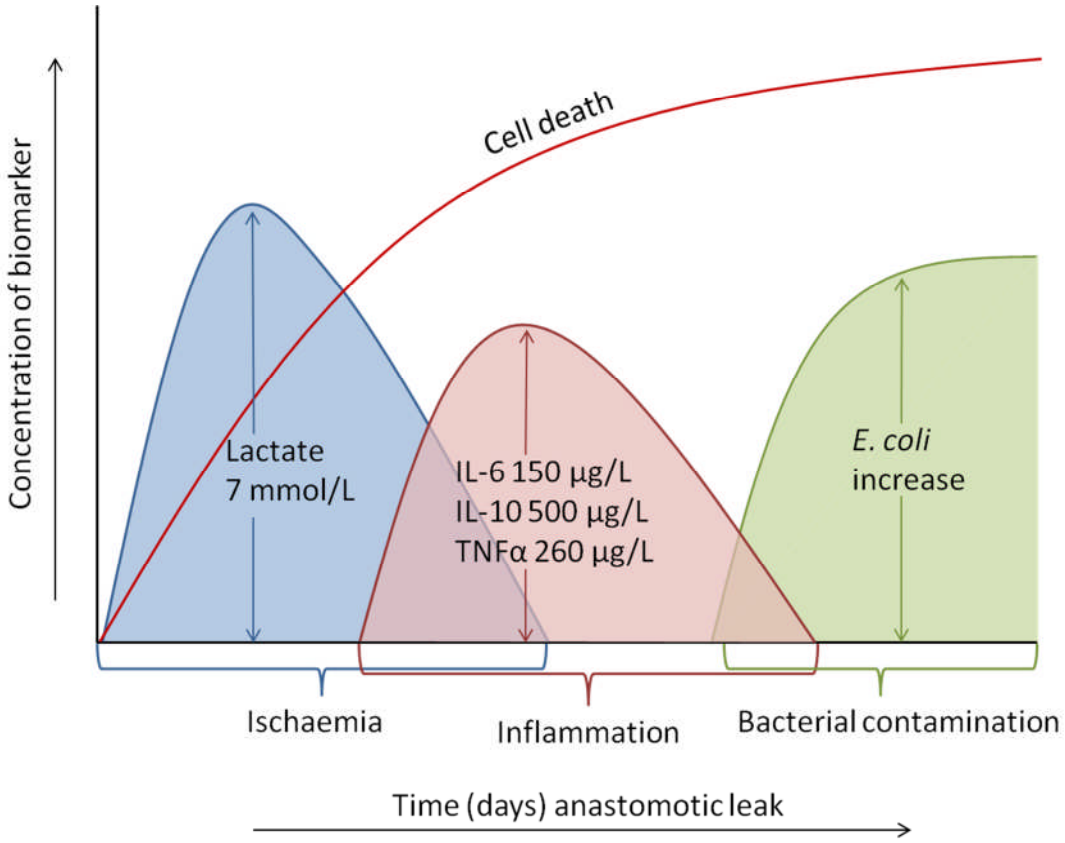

Figure 1.3: Schematic of average time-sensitive peak concentrations of various pathophysiological biomarkers in the abdominal environment implicated for use in early detection of anastomotic leak.

1.6.1 Pathophysiology of GI healing

The cellular pathophysiology of both normal gastrointestinal healing and of failure of an anastomosis must be understood in order to predict profiles of molecules which may then act as biomarkers for an anastomotic leak. Wound healing in general is a complex process, with a number of overlapping phases each involving a variety of coordinated cellular, humoral and molecular responses (Li et al., 2007, Robson et al., 2001). Four phases (in some papers considered as three stages) have been studied extensively in skin and comprise: i) haemostasis, ii) inflammation, iii) proliferation, and iv) remodelling and scar maturation (Enoch and Leaper, 2005, Dubay and Franz, 2003).

Haemostasis: Immediately after insult or injury, blood vessels are disrupted causing bleeding. Haemostasis (the state at which bleeding is ceased) is achieved by two main processes after initial blood vessel constriction: fibrin clot formation and coagulation (Li et al., 2007). Platelets are recruited to the area and activated by the vascular wall extracellular matrix causing adhesion and degranulation with release of a host of mediators, adhesive proteins and growth factors. These include serotonin and adenosine diphosphate, fibrinogen and fibronectin, and platelet derived growth factor and epidermal growth factor respectively. These mediators attract and activate fibroblasts, endothelial cells and macrophages, as well as activate the compliment and kinin cascades with plasmin generation (Enoch and Leaper, 2005). Fibrinogen is converted to fibrin by locally released thrombin which, with the platelet aggregate, forms the fibrin clot. Both the intrinsic and extrinsic coagulation cascades are activated by the action of platelet aggregation and tissue factor release from damaged tissue respectively.

Inflammation: The inflammatory phase is chiefly characterised by the mass influx of leukocytes, initially neutrophils and monocytes, up to 48 hours after the insult. These cells are recruited by the release of chemotactic factors including kallikrein, fibrinopeptides, growth factors, and mast cell products, such as tumour necrosis factor alpha (TNFα), histamine, interleukins and leukotrienes (Li et al., 2007). They act to kill and phagocytose bacteria and other foreign bodies to minimise bacterial contamination, as well as any native damaged proteins. TNFα is particularly chemotactic for other inflammatory cells (Robson et al., 2001). Macrophages (tissue-derived monocytes) dominate later in the inflammatory stage at days 2-3. They are recruited by complement and clotting components as well as some of the same chemoattractants that draw neutrophils, and have a key role in regulating tissue repair (Enoch and Leaper, 2005). Macrophages phagocytose pathogens, dispose of residual neutrophils, and produce growth factors to initiate healing *via* proliferation of fibroblasts, smooth muscle cells and endothelial cells for angiogenesis (Dubay and Franz, 2003). They also release proteolytic enzymes, such as collagenase, for wound debridement.

Proliferation: The duration of the proliferation phase is approximately 2-4 weeks. The principle functions are reinforcement of the damaged tissues and reestablishment of a blood supply. Fibroblasts migrate to the area under the influence of platelet-derived growth factor and transforming growth factor-β and proliferate, producing fibronectin and collagen to form new extracellular matrix for structural support as well as acting as a reservoir for cytokines and growth factors (Li et al., 2007, Robson et al., 2001). The initial extracellular matrix consists of collagens (largely type III) and elastin with an interstitial component of glycoproteins in proteoglycan and glycosaminoglycan gel, all produced by fibroblasts. This matrix evolves to become highly organised around epithelial, endothelial and smooth muscle cells, with a specialised basement membrane (Enoch and Leaper, 2005). Angiogenesis occurs as this granulation tissue begins to replace the extracellular matrix. A number of factors including vascular endothelial growth factor, platelet-derived growth factor, basic fibroblast growth factor and transforming growth factor-β induce angiogenesis (Enoch and Leaper, 2005). Capillary sprouts begin to infiltrate the matrix before organisation into a rich microvascular network throughout the granulation tissue. The proliferation phase is completed with the epithelialisation of the damaged tissue.

Remodelling and scar maturation: The final remodelling phase is characterised by the replacement of granulation tissue with a predominantly type I collagenous scar, and is present for several weeks (Li et al., 2007). The extracellular matrix undergoes continuous remodelling with coordinaed lysis and synthesis of collagen (Enoch and Leaper, 2005). Fibroblasts, neutrophils and macrophages produce metalloproteinases (MMP's), which cause collagen breakdown *via* a number of degradation and cleavage actions. Collagen synthesis is controlled by growth factors, such as transforming growth factor-β and fibroblast growth factor. Collagen degradation and synthesis is under tight control and as healing progresses MMP's decrease, leaving predominately type I collagen bundles. Cellular and vascular activities diminish and collagen bundles increase in diameter as the scar

matures, corresponding with the wound increasing in tensile strength. A summary of the overlapping four phases of wound healing is shown in **Figure 1.4**.

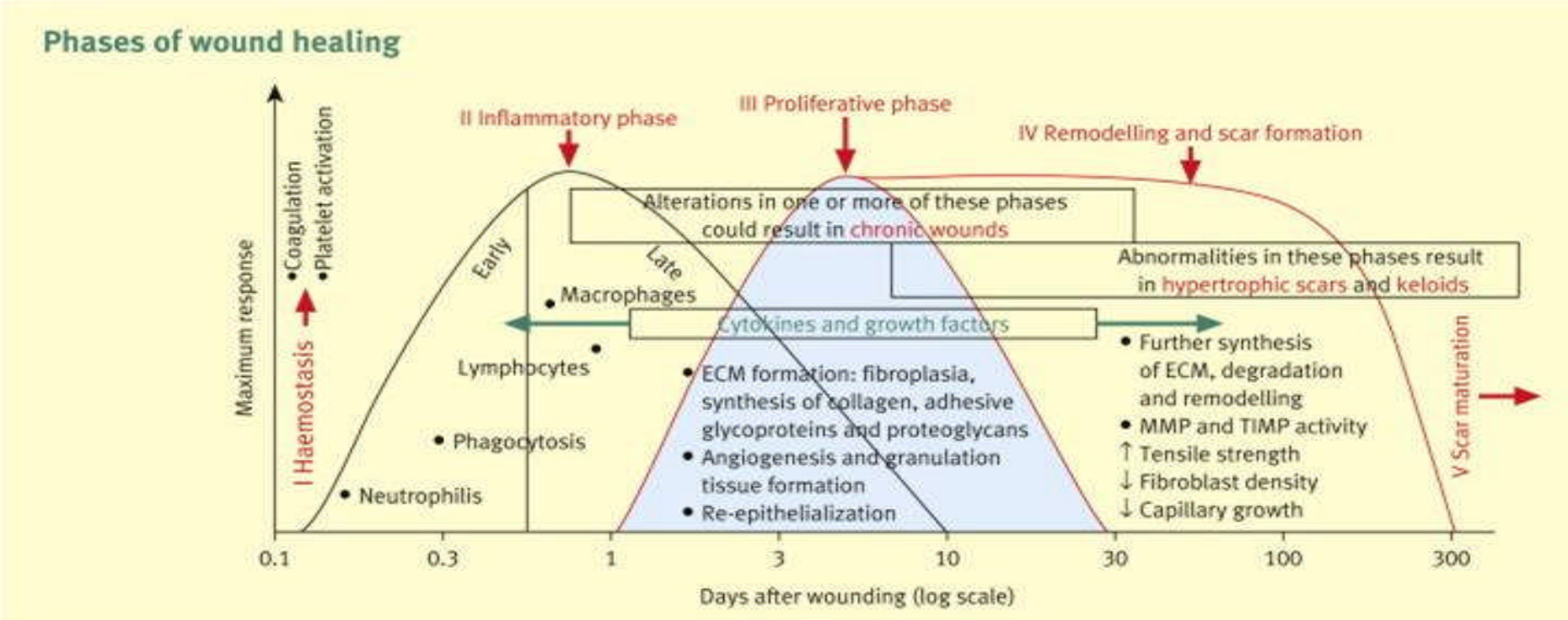

Figure 1.4: The four phases of wound healing and characteristic cell types present (Enoch and Leaper, 2005). Reproduced with permission.

There are discrete differences between this classically described healing of the skin and healing of the bowel, based on the differing structure and mechanics of function. The anatomy of the intraperitoneal gastrointestinal tract comprises four layers: the mucosa, submucosa, muscularis propria and serosa (Thompson et al., 2006). These four layers are shown in the schematic in **Figure 1.5**. The mucosa is the luminal (innermost) layer and has three components: an epithelial cell layer, loose connective tissue with collagen named lamina propria, and smooth muscle cells of the muscularis mucosa. If breached, the mucosa apposes by migration and hyperplasia of epithelial cells to act as a barrier to prevent leakage of luminal contents (Thompson et al., 2006). The submucosal layer contains the blood vessels, lymphatics and nerve plexus of the bowel. It contains an abundance of collagen (68% type I, 20% type III, 12% type V) and provides the gastrointestinal tract with the majority of its tensile strength (Halsted, 1887). The muscularis propria is the muscular portion of the bowel, containing smooth muscle cells in two distinct orientations: longitudinal and circular. The outermost layer, the serosa, is comprised of a thin layer of connective tissue covered mesothelium. During the surgical formation of an anastomosis, apposition of the serosa has been shown to be of great importance in minimising anastomotic leak (Thornton and Barbul, 1997).

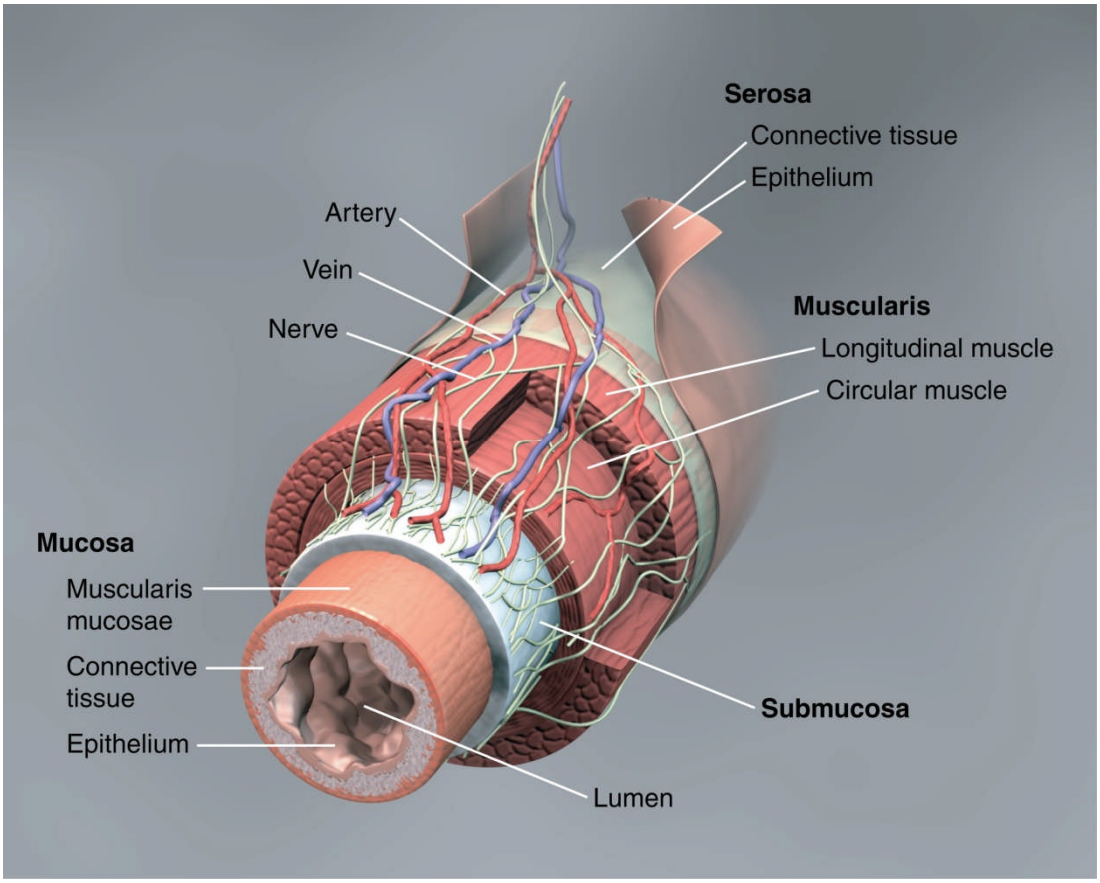

Figure 1.5: Cross section of the large intestine detailing the four principle layers and blood and nerve supply (Lamb, 2013). Reproduced with permission**.**

In similarity to skin, bowel healing begins with a haemostatic response before inflammatory cell migration and phagocytic activity. During the proliferation and remodelling phases, however, collagen is produced by both fibroblasts and smooth muscle cells in the muscularis mucosa and muscularis propria (Thornton and Barbul, 1997). This allows a more rapid increase in tensile strength than in skin to accommodate the shear stresses associated with peristalsis. The regulation of collagen lysis and synthesis also differs; in the bowel this is largely under the control of collagenase. There are three types of collagen produced in the bowel in contrast to cutaneous tissue; types I and III common to both with type V being specific to bowel. In clinical terms this translates as low anastomotic strength in the first few postoperative days as collagen degradation *via* collagenase dominates, with anastomotic strength completely dependent on the suture or staple holding capacity of the existing collagen (Thompson et al., 2006). The anastomosis is

therefore weakest and most vulnerable to leakage at this time. The final phase of bowel healing is again comparable to cutaneous tissue, with decrease in cellular activity and reorganisation of collagen bundles into contractile units.

A number of factors are implicated in the failure of gastrointestinal healing. Local factors include inadequate blood supply, anastomotic tension, local infection, and distal bowel obstruction. Systemic factors include hypovolaemia/shock, poor nutrition, and various metabolic disorders (uraemia, diabetes etc.) (Thornton and Barbul, 1997). During anastomotic failure the molecular environment of the anastomosis changes from that of normal healing. The presence of infection, for example, impairs wound healing by prolonging the inflammatory phase, leading to increased levels of inflammatory cells (Thompson et al., 2006). **Figure 1.6** shows a schematic of how some of these pathological processes may then become targets for measurement of adverse events. Sequential time points in the failure of anastomotic healing are considered below, with assessment of the current literature on the correspondingly increased (or decreased) molecules which may be exploited as diagnostic biomarkers for anastomotic leak.

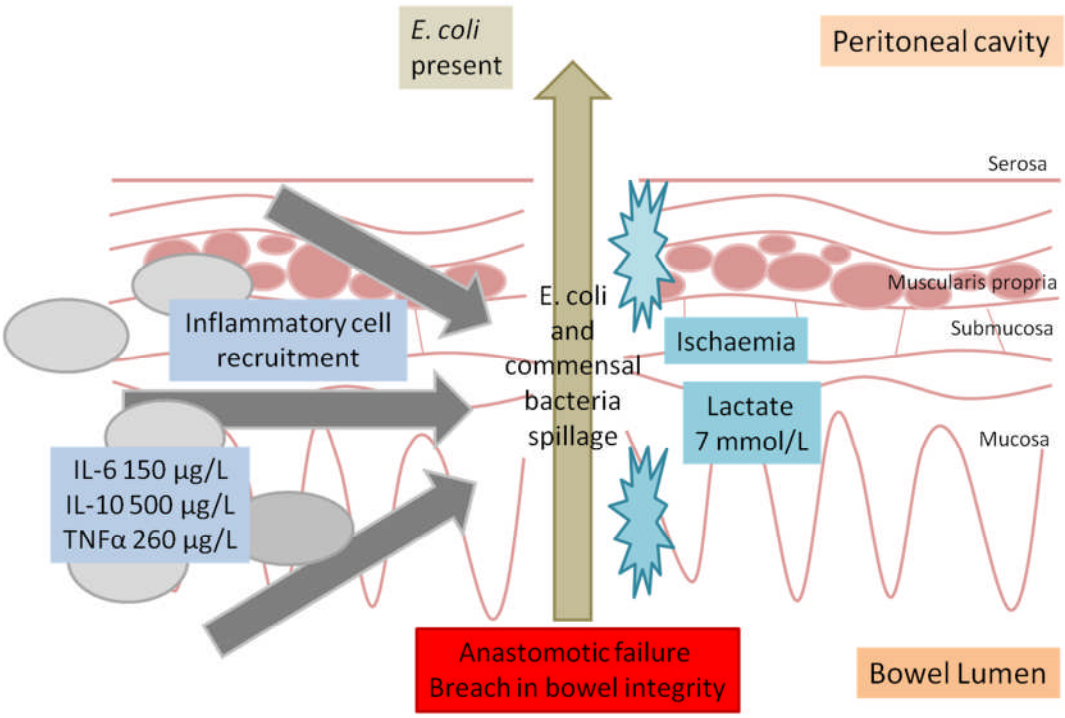

Figure 1.6: Schematic overview of some of the pathological processes seen during failure of gastrointestinal wound healing which may be exploited in diagnostic testing.

1.6.2 Biomarkers of ischaemia

Ischaemia is one of the earliest events in anastomotic leak, and its negative effect on the anastomosis is well documented. Disruption of microcirculatory blood flow at the anastomosis leads to diminished tissue perfusion and an inability to synthesise collagen (Thompson et al., 2006, Enestvedt et al., 2006). Decreased tissue perfusion may begin as early as intraoperatively, and over a period of hours leads to tissue breakdown with infarction of the epithelium and villi destruction progressing to full thickness necrosis, perforation, and inevitable failure of the anastomosis with peritonitis (Corke, 2001). Biomarkers for ischaemia therefore have the potential to detect anastomotic complications early in their evolution. General biomarkers of ischaemia that are detectable in the blood have been in clinical use for some time, and include phosphate, liver function tests and creatinine kinase. However, they have generally been shown to be non-specific for

intestinal ischaemia (Corke, 2001). Faecal examination for biomarkers has likewise found little success.

A number of studies have focused on local changes in metabolites that correlate with ischaemia and can be repeatedly measured in the postoperative period. These include glucose, lactic acid/lactate, and pyruvate, which are related through cellular glucose metabolism. Under aerobic conditions, cells covert glucose into pyruvate, a process known as glycolysis (Phypers and Pierce, 2006). Pyruvate is then oxidised in Krebs cycle to ultimately generate ATP for cellular energy. Under anaerobic conditions, pyruvate cannot be oxidised and undergoes fermentation catalysed by lactate dehydrogenase to form lactic acid (Robergs et al., 2004). This is a less efficient energy cycle although it still produces ATP. Under anaerobic conditions, whether physiological, as in exercise, or pathological, anaerobic metabolism dominates leading to increased lactic acid. Lactate is the ion of lactic acid, formed in solution after loss of a proton and thus the terms are used interchangeably.

Using tonometry *via* an intraluminal catheter at the anastomosis, Millan *et al* demonstrated a significant local decrease in pH at 24 hours in patients who went on to develop a colorectal anastomotic leak, indicative of increasingly acidic ischaemic conditions (Millan et al., 2006). Pedersen *et al* used a locally implanted microdialysis catheter in 45 patients following low anterior resection to obtain 4 hourly fluid samples, and found significant increases in lactate and lactate/pyruvate ratio in 4 patients who developed anastomotic leak (Pedersen et al., 2009b). Crucially, in 3 patients who had a delayed leak (after 10 days), the lactate and lactate/pyruvate ratio increases were observed several days prior to the leak being clinically apparent. Similar findings were recorded following oesophageal cancer resection (Pedersen et al., 2009a). The microdialysis method allowed for rapid analysis at multiple time-points, although it was invasive. Deeba *et al* also used a microdialysis catheter technique to obtain local fluid samples immediately before and after colonic resection and showed a significant decrease in glucose and

increase in lactate after resection (Deeba et al., 2008). There therefore appears to be merit in further exploring the role of ischaemic biomarkers as predictors of early anastomotic leak.

1.6.3 Biomarkers of inflammation

Abdominal surgery induces a complex inflammatory cascade with the release of cytokines and other inflammatory markers into the peritoneal cavity and bloodstream (Badia et al., 1996). After 24 hours these cytokine levels usually begin to decline (Guillou, 1993). However, if the normal postoperative course is not followed or in the presence of any insult, there is an inflammatory host response, considered to be a self-defence mechanism. This response is termed the systemic inflammatory response syndrome (SIRS), specifically defined as sepsis in the presence of documented or presumed infection (Bone et al., 1992). The pathophysiology of SIRS has been described in three stages (Bone, 1996). In stage I and II following an insult, normal wound repair is commenced as described in **Section 1.6.1**, with cytokines produced and recruitment of phagocytic cells to restore homeostasis. If homeostasis is not achieved, stage III (SIRS) develops. Stage III comprises a significant inflammatory reaction with mass cytokine release, becoming destructive instead of protective. There is a flood of inflammatory mediators triggering the sustained, inappropriate action of monocytes and leading to end organ dysfunction. TNFα, interleukin-1 (Il-1) and Il-6 are considered the primary pro-inflammatory mediators in SIRS/sepsis (Davies and Hagen, 1997). These pro-inflammatory cytokines act to initiate production of other pro-inflammatory cytokines (Il-8, γ-interferon), activate the coagulation and complement cascades, and lead to the release of nitric oxide, platelet activating factor, leukotrienes and prostaglandins, and culminating in a sustained, uncontrolled response causing widespread tissue injury and organ dysfunction (MacFie, 2013, Davies and Hagen, 1997). The counteraction of the host to this imbalance is an anti-inflammatory response, termed the compensatory anti-inflammatory response syndrome (CARS) (Ward et al., 2008). Anti-inflammatory

cytokines, such as Il-4 and Il-13, act to decrease production of pro-inflammatory cytokines *via* direct inhibition and indirect mechanisms (Collighan et al., 2004). The balance of SIRS and CARS largely determines the clinical outcome, with domination of SIRS conferring uncontrolled inflammation, or CARS becoming harmful in allowing secondary infections to overwhelm the patient if unchecked (Ward et al., 2008). Although as yet incompletely understood, SIRS and CARS have been the focus of therapeutic strategies for sepsis (Dinarello et al., 1993, Ward et al., 2008). The characteristic increase in specific cytokines also gives potential to exploit these molecules as biomarkers for diagnosis of progressing septic complications.

Serum C-reactive protein (CRP) has long been considered a primary clinical inflammatory indicator of postoperative complications despite poor specificity (Matthiessen, 2007). CRP is a plasma protein synthesised in the liver. When activated by macrophages, CRP binds to dying cells to activate the compliment system, amongst other complex functions (Black et al., 2004). Studies have shown that serum CRP is significantly elevated in the preceding days before anastomotic leak after colorectal surgery, as compared to a normal postoperative course (Matthiessen, 2007, Woeste et al., 2010, Almeida et al., 2012). However, in all these studies only an overt clinical presentation was defined as anastomotic leak, with radiological leaks expressly excluded in one study (Matthiessen, 2007). Garcia-Granero *et al* recently demonstrated that CRP was not reliable in the early detection of minor anastomotic leak, only reaching significance preceding a major presentation of leak (Garcia-Granero et al., 2013). Thus, CRP may not be as sensitive as previously considered, potentially as a result of measuring a local complication using a systemic marker.

Crucially, inflammatory cytokines and growth factors released at the site of tissue injury are present in much greater concentration in peritoneal fluid than the systemic circulation (Chuang et al., 2006). Increased local levels of interleukin-1β (Il-1β), Il-6, epidermal growth factor, and platelet derived growth factor have been

measured in drain fluid from patients who developed anastomotic leak and sepsis following colorectal surgery, as compared to those with an uneventful postoperative course (Baker et al., 2003). The levels of inflammatory and growth mediators also show a positive correlation with increasing severity of the complication. Fouda *et al* studied cytokine levels sampled *via* peritoneal drain fluid in 56 patients undergoing elective low anterior resection (Fouda et al., 2011). Cytokines Il-6, Il-10 and TNFα were measured by ELISA and were all significantly higher, particularly on postoperative day 3, in the 8 patients who developed anastomotic leak, as compared to those with no leak (Il-6 76% higher, Il-10 33% higher, TNFα 72% higher). A number of other studies support these findings, demonstrating an early increase in one or all of Il-6, Il-10 and TNFα in patients who develop anastomotic leak (Ugras et al., 2008, Matthiessen et al., 2007, Herwig et al., 2002). All of the studies used ELISA assays, which provide a relatively rapid result but require specialist laboratory facilities, user expertise, and are labour intensive (Shinde et al., 2012).

Lysozyme is a component of the host inflammatory response to trauma and sepsis. It is formed in macrophages and acts to destroy the cell wall of Gram-negative bacteria. Using an electrophoretic technique, Miller *et al* demonstrated that lysozyme levels in drain fluid after low anterior resection were significantly raised in patients with clinical and radiological evidence of anastomotic leak (Miller et al., 1996). Importantly, lysozyme levels were significantly increased as early as postoperative day 1. However, the methodology had major practical limitations, as the electrophorectic gel required overnight soaking, negating its usefulness as a rapid diagnostic test.

Matrix metalloproteinases are involved in remodelling of the extracellular matrix by collagen degradation during healing (Stumpf et al., 2005). Tissue inhibitors of metalloproteinase (TIMP's) are the natural inhibitors of MMP's, and wound repair is dependent on the balance between these mediators. In animal models,

anastomotic healing may be enhanced by administration of an MMP inhibitor, as evidenced by higher anastomotic burst pressures (Kiyama et al., 2001). The levels of MMP's and TIMP's might therefore prove a time sensitive test for anastomotic healing. Using human peritoneal fluid taken 4 hours after low anterior resection, Pasternak *et al* analysed levels of MMP-1, 2, 3, 7, 8, 9, and 13 by multiplex flow-cytometry. MMP-8 and 9 were significantly increased in the 10 patients who developed anastomotic leak, as compared to the 19 patients who had an uneventful postoperative course (Pasternak et al., 2010). Flow cytometry is a highly sensitive methodology but, similar to ELISA, requires specialist operators and costly equipment (Maher and Fletcher, 2005).

1.6.4 Bacterial biomarkers

Anastomotic integrity is initially dependent on apposition of the serosa and mucosal hyperplasia to create a barrier to luminal bacteria (Thompson et al., 2006). Failure of anastomotic healing, from whatever cause, leads to spillage of bowel contents into the peritoneal cavity. The human gastrointestinal tract contains a vast indigenous flora of microorganisms of which the majority, thought to be approximately 10^{13} in number, reside in the colon (Rakoff-Nahoum et al., 2004). The function of this flora is incompletely understood and is recently thought to be more mutualistic than inertly commensal, but includes metabolism of carbohydrates and fatty acids, regulation of epithelial and vasculature integrity, and provision of colonisation resistance to pathogenic strains (Hooper and Gordon, 2001).

In a 5-year prospective study, de Ruiter *et al* demonstrated that a number of micro-organisms could be cultured from abdominal fluid taken from patients with a perforated digestive tract (De Ruiter et al., 2009). Over half of the cultures, taken intraoperatively after colorectal perforation, contained aerobic Gram-negative bacteria, the majority of which were *E. coli*. Gram-positive bacteria, predominantly

Enterococci, were found in 42.5% of abdominal fluid cultures. Over the following 4 weeks as antibiotic treatment was administered, aerobic Gram-negative bacterial counts dropped, as interestingly, Gram-positive bacterial counts increased. Other studies have found a similar distribution of bacteria cultured in peritoneal fluid after intestinal perforation (Brook and Frazier, 2000). Although bacterial culture is not rapid enough to be of diagnostic use, the measurement of specific bacteria or bacterial components/products may have a role as biomarkers of anastomotic leak.

Komen *et al* utilised real-time polymerase chain reaction (PCR) as a rapid and sensitive method for detecting *E. coli* and *E. faecalis* in drain fluid (Komen et al., 2009). Testing on 10 known culture positive and 7 culture negative fluid samples, the PCR results were concordant with culture results except for 4 false positives, indicating that the method is too sensitive and susceptible to over-diagnosis. On-line infrared absorption and near-infrared LED devices are two other techniques that have been studied as potential diagnostic tools for bacteria (Pakula et al., 2005, Chaeron et al., 2007). Both these methods use optical sensor systems to spectroscopically detect bacteria in drain fluid. Using solutions with known concentrations of *E. coli*, the LED system was shown to rapidly distinguish between the different samples, although not quantitatively. The on-line infrared absorption technique also generally distinguished between differently contaminated drain fluid samples. The authors conceded that more detail would be required to use optical systems as a diagnostic tool for anastomotic leak, although the methodology was promising.

Endotoxin, or lipopolysaccharide (LPS), forms the outer wall of Gram-negative bacteria, including commmensals of the GI tract, and may serve as a biomarker for anastomotic leak. Junger *et al* measured LPS in peritoneal drain fluid from 22 patients after colonic resection and showed significantly increased LPS levels at day 1 and day 3 in the 3 patients who developed anastomotic leak (Junger et al., 1996). The day 3 levels, in particular, gave threshold results with high sensitivity.

Currently, LPS is not routinely measured in clinical laboratories, and improvements in the assay are required before there can be any clinical application.

1.6.5 Other biomarker approaches

A recent novel method for detection of anastomotic leak using electrical resistance changes has been studied in animal models. DeArmond *et al* compared negative controls to rats that were given gastrotomies to simulate anastomotic leak (DeArmond et al., 2010). Electrolyte contrast solution was introduced into the stomach and resistance measurements were taken *via* electrodes sutured around the gastrotomy. The authors were able to demonstrate a significant drop in electrical resistance following the extravasation of electrolyte contrast in animals with gastrotomies compared to negative controls. The application has the advantage of providing rapid results, which may be obtained at the bedside, and was shown to be sensitive and specific in these preliminary animal model tests. **Table 1.4** outlines the range of biomarkers and their respective research methodologies as early detection strategies for anastomotic leak.

Reference	Number of patients	Procedures	Biomarker(s) measured	Time interval	Methodology	Significant results (means unless stated)
Ischaemia						
(Millan et al., 2006)	90	Anterior resection	pH	24 and 48 hours	Intraluminal tonometry	pH < 7.28 in AL
(Pedersen et al., 2009b)	50	Low anterior resection	Glucose, lactate, pyruvate, glycerol, lactate/pyruvate ratio (L/P ratio)	4 hourly for maximum of 10 days	Microdialysis catheter	Lactate: 7.0 mmol/L AL, 3.0 mmol/L non AL. L/P ratio: 44.7 AL, 18.3 non AL
(Deeba et al., 2008)	7	Left colectomy	Glucose, lactate, lactate/glucose ratio (L/G ratio)	Operatively – over 60 mins	Microdialysis catheter	Glucose decrease to 1.89 mM. Lactate increase to 1.47 mM. L/G ratio increase to 8.1
Inflammation						
(Baker et al., 2003)	52	Colorectal resection	IL-6, IL-1β, TNFα epidermal growth factor, platelet-derived growth factor, vascular endothelial derived growth factor, basic fibroblast growth factor, transforming growth factor-β1	Daily, post operative day 1 until drain removal	ELISA on peritoneal drain fluid	IL-1β (days 1,3,6), EGF (day 5), PDGF (day 3), IL-6 (day 6) increased in complication with severity
(Fouda et al., 2011)	56	Low anterior resection	Bacterial cultures, IL-6, IL-10, TNFα	Daily, post operative day 1,3,5	Bacterial culture, ELISA	Day 3 (all pg/ml) IL-6: 115,450 AL, 28,159 non AL, IL-10: 33,355 AL, 22,209 non AL, TNFα: 511 AL, 141 non AL
(Ugras et al., 2008)	34	Colorectal anastomosis	IL-6, IL-10, TNFα	Daily, post operative day 1,2,3,4,5	ELISA on peritoneal drain fluid	Day 1 (all pg/ml) IL-6: ~140,000 AL, ~30,000 non AL, IL-10: ~125,000 AL, ~20,000 non AL, TNFα: ~120,000 AL, ~40,000 non AL
(Matthiessen et al., 2007)	23	Anterior resection	Lactate, pyruvate, glucose IL-6, IL-10, TNFα	Until post operative day 2	Lactate, pyruvate, glucose microdialysis IL-6, IL-10, TNFα ELISA on peritoneal drain fluid	Day 5 L/P ratio: ~18 AL, ~12 non AL Day 1 (all µg/L) IL-6: ~150 AL, ~80 non AL, IL-10: ~500 AL, ~100 non AL, TNFα: ~260 AL, ~100 non AL
(Herwig et al., 2002)	24	Colorectal resection	IL-6, IL-1β, TNFα	Daily, until post operative day 4	ELISA on peritoneal drain fluid	Day 1 (all pg/ml) IL-6: 162,500 AL, 27,940 non AL, TNFα: ~500 AL, ~200 non AL. Day 3 IL-1β: ~1500 AL, ~100 non AL

(Miller et al., 1996)	42	Low anterior resection	Lysozyme	Daily, until post operative day 4	Laurel's electroimmunodiffusion on peritoneal drain fluid	Day 1 (mg/dl) ~16 AL, ~6 non AL
(Pasternak et al., 2010)	29	Low anterior resection	MMP-1,2,3,7,8,9,13 TIMP-1,2	4 hours postoperatively	MMP by multiplex flow-cytometry, TIMP by ELISA, on peritoneal drain fluid	(All ng/ml) MMP-8: 704 AL, 445 non AL, MMP-9: 5300 AL, 4120 non AL
Reference	**Number of patients**	**Procedures**	**Biomarker(s) measured**	**Time interval**	**Methodology**	**Significant results (means unless stated)**
Bacterial contamination						
(Komen et al., 2009)	9 (17 samples, all non AL)	Colorectal resection	*E. coli, E. faecalis*	Daily, post operative day 1 until drain removal	PCR on peritoneal drain fluid	Entirely concordant results with PCR except 4 false positive PCR
(Pakula et al., 2005)	2	Lower GI surgery	Bacterial contamination	Post operatively	On-line infrared absorption on drain fluid	Differences in transmission of differently mixed "% contaminated" samples
(Chaeron et al., 2007)	N/A	N/A	Bacterial contamination	N/A	Near infrared LED on samples taken from a hospital laboratory	Differences in transmission of "0%" and "10%" contaminated samples
(Junger et al., 1996)	22	Colorectal resection	LPS, leukocyte count, thrombocyte count, urea, creatinine, temperature	Daily, until postoperative day 8	Chromogenic limulus amoebocyte lysate test on peritoneal drain fluid	LPS (all pg/ml) Day 1: 3165 AL, 904 non AL. Day 3: 6257 AL, 419 non AL
Other approaches						
(DeArmond et al., 2010)	Animal model	N/A	Electrical resistance	N/A	Electrical resistance across gastrotomy	Mean max rate of change in resistance gastrotomy: -310 ohms, control: -15 ohms

Table 1.4: Summary of the biomarkers evaluated for detection of anastomotic leak. AL, Anastomotic leak; EGF, Epidermal growth factor; LPS, Lipopolysaccharide; MMP, Matrix metalloproteinase; PDGF, Platelet-derived growth factor; TIMP, Tissue inhibitors of metalloproteinase; TNFα, Tumour necrosis factor alpha.

There is therefore a wealth of potential targets for a sensitive pathophysiological biomarker measured in the abdominal environment for early diagnosis of anastomotic leak. Although a number of these biomarkers appear to hold potential, few have been formally assessed under controlled conditions, with none clinically validated in randomised controlled trials. The ideal biomarker for anastomotic leak should express concentration changes early in the anastomotic leak process, remain stable, and confer high sensitivity and specificity. The biomarker measurement methodology should be user-friendly, inexpensive and give rapid, at the bedside, results. Currently, no detection method in the literature fulfils these criteria, with the majority requiring costly laboratory equipment and a lengthy time period.

1.7 Animal model of biomarkers

1.7.1 Caecal ligation and puncture

Despite extensive research, the pathophysiology of sepsis in humans from anastomotic leak and other causes is still not fully understood. Caecal ligation and puncture (CLP) is considered the gold-standard animal model in sepsis research, deemed by many investigators to be the crucial pre-clinical test for any new treatment of human sepsis (Rittirsch et al., 2009, Dejager et al., 2011). It is the most widely used model for experimental sepsis since being developed more than 30 years ago (Dejager et al., 2011). There is still no viable alternative for modelling sepsis other than to use *in vivo* models. Sepsis is a dynamic process, with biological markers changing in concentration at different time points as sepsis evolves in a living host. Therefore a live model is irreplaceable for this purpose, as cells or organs in isolation *in vitro* would not produce the same whole system complex immune response, allowing meaningful comparison to that of humans.

The CLP procedure consists of a midline laparotomy to gain access to the abdominal cavity, after which the caecum is ligated to provide an inflammatory source of necrotic tissue. Caecal perforation then allows faecal material to leak into the usually sterile peritoneal cavity resulting in bacterial peritonitis, triggering the systemic inflammatory response, inevitably leading to septic shock, organ dysfunction, and death (Rittirsch et al., 2009). As the pathogens (such as *E. coli*) originate from the host enteric system, there is a high degree of similarity to human sepsis. The haemodynamic and metabolic phases of sepsis as well as the pro- and anti-inflammatory stages have been shown to be comparable to those of humans (Dejager et al., 2011). Another advantage of the CLP model is its relative simplicity.

To date, CLP has been used to measure a wealth of mediators implicated in sepsis, to further our understanding of its pathophysiology, and to increase our knowledge of potential diagnostic markers and novel therapeutic targets (Dejager et al., 2011). However, very few studies have measured levels of these potential markers in fluid from the abdominal cavity, with most focusing on serum markers (Ebong et al., 1999, Brooks et al., 2007, Dragica et al., 2004). This is despite the logical premise that peritoneal fluid markers will be the earliest and most sensitive for detection as they are in the direct locality of the abdominal corruption. The therapeutic strategies for sepsis in humans arising from knowledge gained from the CLP animal model have so far largely been ineffective, which may in part be due to the overreliance on systemic features.

The few studies with a focus on measurement of peritoneal markers in caecal ligation and puncture and other animal models have revealed interesting results. Haji-Michael *et al* measured the glycolytic metabolism of rat leukocytes from the peritoneum in CLP versus sham laparotomy (Haji-Michael et al., 1999). At 24 hours, basal and glucose stimulated lactate output was significantly increased in CLP animals. To examine prediction of survival, cytokine levels Il-6, Il-10 and TNFα were measured in the peritoneal fluid of 48 rats following intraperitoneal injection of a

faecal/bacterial mixture (Hendriks et al., 2010). Measurements were taken at 24 and 72 hours. The authors found that cytokine levels at 24 hours discriminated between animals who subsequently survived and those who died within the next 24 hours. The levels of each marker that strongly correlated with mortality were determined. Levels of all three cytokines were also significantly higher at 72 hours in animals that were ultimately non-survivors compared to survivors. Using a mouse CLP model, Ebong *et al* measured Il-1β, TNFα, Il-6 and Il-10 in both plasma and peritoneal fluid between 2 and 24 hours versus sham controls (Ebong et al., 1999). Crucially, whilst raised levels of cytokines correlated with increased sepsis in most cases, the levels were consistently higher in the peritoneal fluid than systemically in the plasma. TNFα in particular was below limit of detection in plasma at all time points in the study. Thus, biomarkers for sepsis were more reliable in peritoneal fluid than in plasma. Two other studies corroborate these findings (Walley et al., 1996, Figueiredo et al., 2012). Figueiredo *et al* also showed an increase in the number of bacteria locally at the infective focus of the caecal ligation in a CLP rat model.

CLP and peritoneal sampling therefore confers many benefits in understanding the pathophysiology of intra-abdominal sepsis with relative simplicity and allowing sufficient numbers of animals to attain significant results. There is the additional benefit of strictly controlled experimental conditions. CLP serves as a proxy method for analysing potential biomarkers in postoperative patient drain fluid, providing information about the local biochemical and cellular profile directly at the site of abdominal sepsis. This has specific implications for abdominal sepsis pathophysiology and the elucidation of optimum biomarkers of sepsis, but also more generic implications for research into inflammation and healing.

1.8 Biosensors: Basic concepts

In recent times there have been great developments in biosensing technology research, for a wide variety of applications including environmental monitoring, food and water quality control and medical diagnostics and treatment. The advantages of adaptability, immediate point-of-care testing, speed, portable sampling, low cost and ease of use have rendered biosensing an important alternative to conventional bioanalytical systems such as ELISA (Cosnier, 2005, Rushworth et al., 2013). Applications are numerous, and areas of growth are particularly seen in the clinical setting, one example being DNA biosensors for detection of genetic diseases (Minunni et al., 2003). The detection of antigenic proteins including those identifying bacteria, viruses and parasites may be achieved at low concentration by antibody-based biosensors with high specificity. Currently, the blood glucose sensor is still the most widespread example of a biosensor, used by the estimated 347 million diabetics worldwide and now accounting for approximately 85% of the biosensor market globally at an estimated US$8.8 billion (Newman and Turner, 2005, Hughes, 2009). Biosensor development for a range of biomarkers, including those implicated in sepsis, is readily achievable with current knowledge and technologies.

1.8.1 Brief history of biosensor development

A biosensor in its most simple form may be described as a device comprising three parts: a biological recognition system, a transducer, and a signal processing display (Conroy et al., 2009). Interaction of the analyte of interest with the biorecognition element is converted to a measurable signal by the transducer, before conversion to the readout or display (Vo-Dinh and Cullum, 2000). The basic structure of a biosensor is illustrated in **Figure 1.7**.

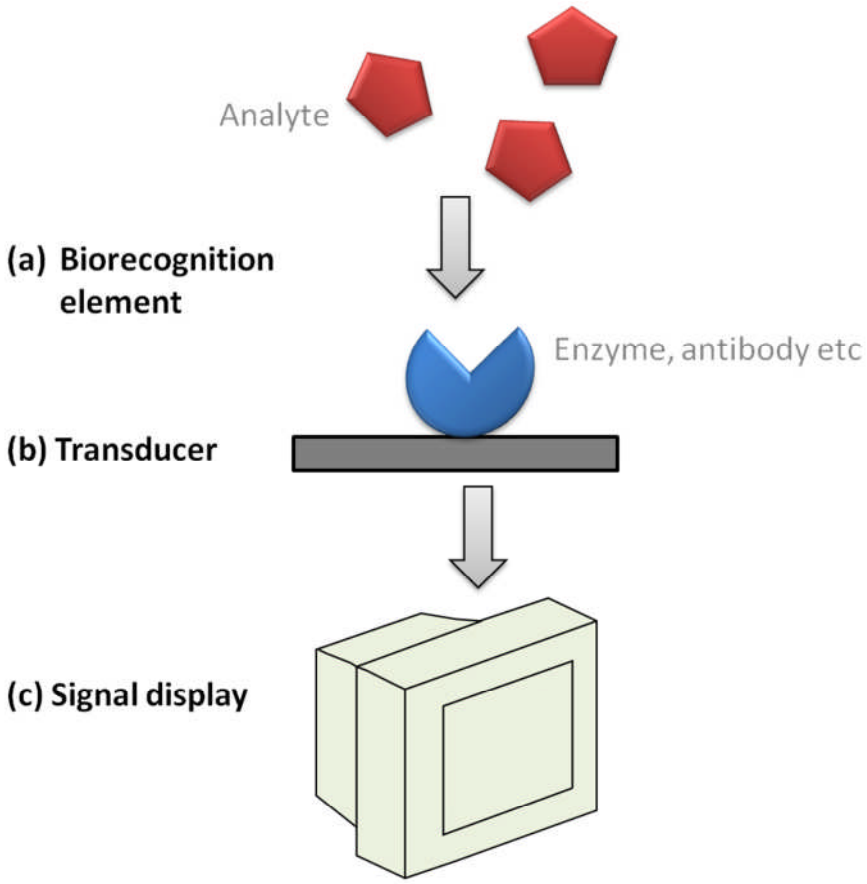

Figure 1.7: Schematic of a biosensor depicting the three main components.

Biosensors were first developed in the 1960's, with the first biosensor described by Clark and Lyons in 1962 at the Cincinnati Children's Hospital for monitoring during cardiovascular surgery. Their original method utilised an oxygen electrode with glucose oxidase entrapped between semi-permeable dialysis membranes. The electrode measured the oxygen consumption during the enzyme reaction, to consequently give a glucose concentration (Clark and Lyons, 1962). Errors caused by variation in O_2 levels in the solution however, led to the reaction product hydrogen peroxide becoming the product of interest to be measured. These so called "first generation" of amperometric sensors directly measured the electroactive species enzymically produced or consumed. Second generation biosensors were developed in the 1980's to overcome the requirement for a high potential in order to measure the electroactive species, which decreased specificity (Wang, 2001). The use of electron mediators such as ferrocene, to shuttle electrons

to the electrode from the enzyme, allowed a lower working potential to be used and thus decreased interference from other redox species present. Mediators may be free in the electrolyte, or immobilised on to the working electrode with the enzyme. The development of third generation biosensors in the 1990's progressed biosensing technology further by allowing direct, unmediated electron transfer between the enzyme's redox centre and the working electrode surface, using an enzyme capable of direct electron transfer such as horseradish peroxidise or cytochrome c. Clearly this may only be achieved with very small enzymes that have redox centres close to their surface, or those whose structure is appropriate.

In recent times biosensors have progressed from being predominantly enzymatic to encompass a wide variety of bioreceptors such as DNA, antibodies and aptamers, and using a range of transduction methodologies including electrochemical, optical and piezoelectric (Song et al., 2006). Within electrochemical approaches, an increased emphasis on impedimetric sensor interrogation is evident, with antibodies the predominant bioreceptors seen (immunosensors). However, other binding proteins have been used and recently evolved affinity proteins have emerged as useful alternative bioreceptors (Conroy et al., 2010, Rodgers et al., 2010). Each approach can be tailored to solving a specific challenge, for example the use of impedance sensors to measure non-electroactive species, to which amperometric biosensors are confined. Generic areas of ongoing biosensing research include design of integrated systems to allow multiplexed sensing, miniaturisation, and methods for continually improving sensitivity, selectivity and stability (Turner, 1996). Work to date has also focussed on the development of electrode surfaces that not only facilitate electron transfer but also provide a structural matrix to immobilise biorecognition molecules (Millner et al., 2009).

1.8.2 Biosensor architecture

Biosensors may be classified either by their biological recognition element e.g. antibody, enzyme, DNA, or by their type of transducer (Vo-Dinh and Cullum, 2000). Electrochemical transducers are the most commonly used type in biosensing (Conroy et al., 2009). They utilise a biological event from analyte interaction with a bioreceptor to generate or to modulate an electrical signal which is related to the analyte concentration (Ronkainen et al., 2010). Typically a three electrode system is used, in which current flows between the working and counter electrodes, with respect to the reference electrode. Working electrodes are commonly noble metals such as gold, or other conducting substances such as carbon. The complete electrochemical cell must contain an electrolytic medium, capable of carrying the ionic charges (Korotcenkov, 2010). In a clinical setting, this is usually the fluid in which the analytes are found e.g. blood, urine, peritoneal fluid etc.

There are many different transducer surfaces used in biosensing to which the bioreceptors can be tethered. Generally, these may be divided into two categories: insulating films, and polymer matrices (Millner et al., 2009). Insulating film based surfaces are mainly self-assembled monolayers (SAMs). SAMs consist of an ordered layer of molecules with a functional head group with affinity for the surface substrate, and a tail group facing into the solution. SAMs may then be modified as mSAMs – mixed self assembled monolayers - by addition of functionalised lipids or cross-linkers, in order to construct a platform for immobilisation. The biotin-avidin system is one way by which this can be achieved, where tetravalent avidin is able to link the biotinylated bioreceptor to the biotin-tagged surface. This method has been previously been used in biosensors for detection of haemoglobin (Hays et al., 2006).

Conducting polymer matrix surfaces are typically formed on the working electrode surface by electro-polymerisation using cyclic voltammetry (Millner et al., 2009),

which allows for fine control of the surface thickness. The formed polymer layer can then be used to immobilise electrochemical mediators and/or enzymes and other biological recognition elements by electrostatic absorption, covalent bonding, biotin-avidin coupling, or other methods (Gerard et al., 2002). Alternatively, proteins may be entrapped within the polymer matrix itself, although this can reduce activity due to decreased diffusion of analyte through the polymer layer to the redox site. Common polymers used are formed from monomers such as pyrrole, aniline and their derivatives, as they are easily electro-polymerised at relatively low redox potentials and have a high stability.

1.9 Biological recognition elements

The biorecognition element of a biosensor consists of a bioreceptor that is attached to a matrix support on a transducer surface. The bioreceptor is chosen to specifically interact with an analyte or material of interest, which leads to transduction and signal generation (Katz and Willner, 2003). Bioreceptors are commonly proteins such as enzymes, antibodies, cellular receptor proteins, non-antibody binding proteins and antigens, or nucleic acids such as oligonucleotides and DNA or RNA aptamers. The properties of the bioreceptor are of great importance, as they essentially confer the sensitivity and specificity of the overall biosensor (Hock et al., 2002, Conroy et al., 2009). Other important considerations are the method of immobilisation of the bioreceptors onto the supportive matrix, and their correct orientation, homogeneity and stability (Cosnier, 2005, Rushworth et al., 2013).

1.9.1 Enzymes

Enzymes as bioreceptors are arguably the most common type, doubtless due to their use in the vast market of glucose monitoring (Luong et al., 2008), although measurement of other analytes such as cholesterol and lactate are emergent systems, using the relevant oxidase enzymes. They are relatively easy to use and to

attach onto transducer surfaces, confer efficient biocatalytic activity, and are very selective, rendering them a popular option (Miscoria et al., 2006, Higson, 2012). A native enzyme may be used in which the concentration of analyte is equal to the enzyme substrate, or the analyte may function as an enzyme inhibitor (Pohanka and Skladai, 2008). Affinity based sensors may also be constructed using enzymes as labels bound to antibodies, antigens and oligonucleotides with a specific sequence. The oxidoreductases are the most widely used family of enzymes for electrochemical application (Ricci and Palleschi, 2005, Pohanka and Skladai, 2008) with glucose oxidase the most common, for glucose monitoring (Wilson and Turner, 1992). Other examples of oxidase enzymes in use are glucose dehydrogenase, lactate oxidase and dehydrogenase for lactate detection and alcohol oxidase for ethanol. Lactate oxidase (LOx) (EC 1.13.12.4) is an FAD-dependant enzyme, readily available from *Pediococcus* species (Perez and Fabregas, 2012). The FAD redox cofactor required for the enzyme to function as a catalyst is inherent within its structure, rendering the enzyme suitable for biosensor application as enzymes which require external additions of cofactors typically show rate limitation. LOx is negatively charged at neutral pH. LOx catalyses the conversion of lactate and oxygen to pyruvate and hydrogen peroxide (H_2O_2), of which the hydrogen peroxide may be detected amperometrically *via* an oxidative or reductive current signal (Romero et al., 2008). The cofactor FAD is correspondingly reduced or oxidised before regeneration (re-oxidation/reduction) for further reactions. The more common oxidative reaction steps are shown:

$$\text{Lactate} + LOx_{ox} \longrightarrow \text{pyruvate} + LOx_{red} \quad (1)$$

$$LOx_{red} + O_2 \longrightarrow LOx_{ox} + H_2O_2 \quad (2)$$

$$H_2O_2 \longrightarrow O_2 + 2e^- \quad (3)$$

Fundamental problems with this direct method include interference from electroactive substances, such as ascorbic acid (vitamin C), which undergo redox reactions at relatively low working potentials and thus reduce the selectivity of the biosensor. The use of mediators such as ferrocene and Prussian Blue to allow low potential, selective detection of hydrogen peroxide and other reaction products has since found wide use to overcome this difficulty (Wilson and Turner, 1992, Karyakin et al., 1995). Another key limitation of enzymes as bioreceptors is the necessity for the analyte of interest to be a substrate for an enzymatic reaction, of which the products can then be measured at the transducer. This restricts the range of enzyme biosensors that can be constructed.

1.9.2 Antibodies

Antibodies, or immunoglobulins, (IgG, IgM, IgA, IgE) are produced as part of the host immune response to pathogenic organisms and toxins (Holliger and Hudson, 2005). IgG is known as the main serum antibody in mammals and is the immunoglobulin that is almost exclusively used in clinical therapeutics. The IgG molecule is a 150 kDa hetero-tetramer which comprises four polypeptide chains - two light (25 kDa) and two heavy (50 kDa). These chains are linked by disulphide bonds and non-covalent interactions. The four chains are grouped into different domains, with two F_{ab} and one F_c segment forming the characteristic Y shaped configuration (Giacomelli et al., 1999). The antigen binding sites are located at the distal arms of the Y at the variable regions, the constant region forming the rest of the molecule. A schematic of this structure is seen in **Figure 1.8**. It is thus clear that the antibody must be orientated with the F_c portion to the biosensor surface and the F_{ab} segments facing into the analyte in solution, to function optimally as a biosensor.

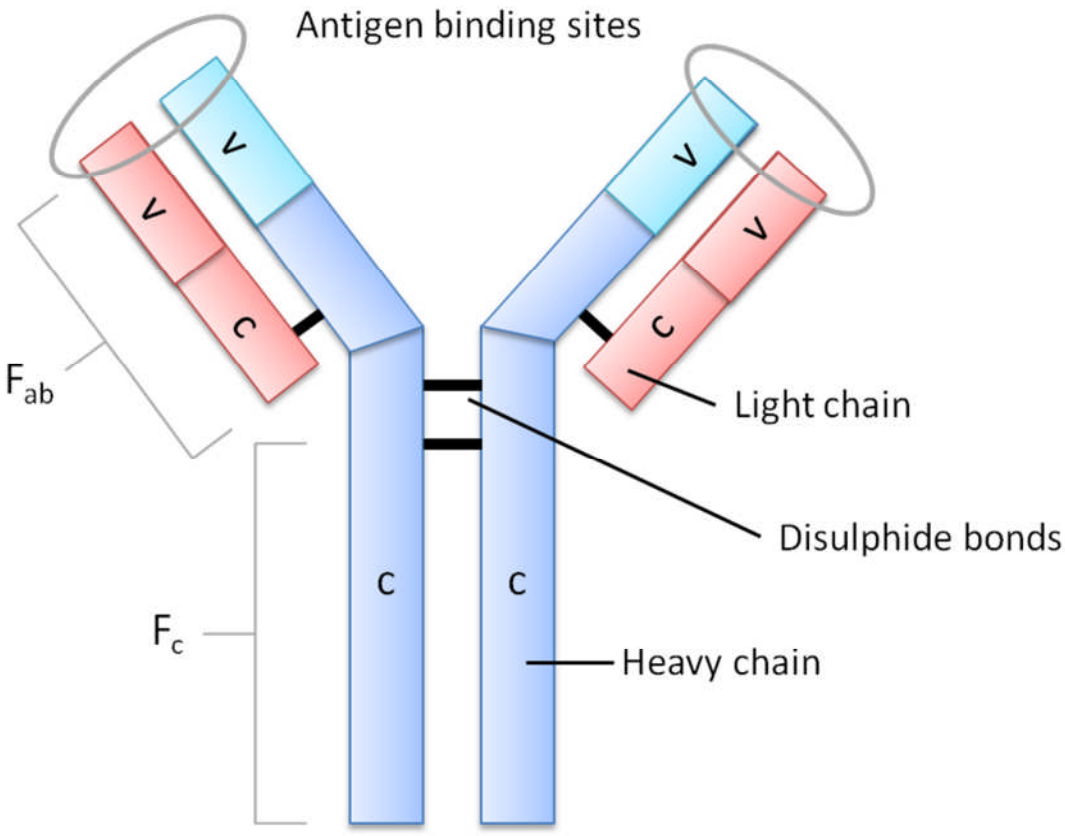

Figure 1.8: Schematic of IgG structure and domains.

Antibodies have been recognised for potential use as biosensor bioreceptors since the late 1980's (Conroy et al., 2009). These "immunosensors", using antibody based biorecognition, have since been developed on a multitude of transducer surfaces to measure a wide range of analytes. A main advantage is the potential for highly selective biosensing, as the antibody undergoes very specific high affinity binding to the analyte of interest (Conroy et al., 2009). High selectivity is particularly the case with monoclonal antibodies, which are derived from one B lymphocyte cell line and so have a single epitope specificity, although these present much higher production costs. Polyclonal antibodies originate from multiple B lymphocyte cell lines and are more commonly used as production involves simple immunisation of the host species, typically sheep or rabbit. Despite broader specificity, or multiple epitope recognition, they are more tolerant to variability in antigen structure, often display higher avidity, and are less expensive (Zourob et al., 2008). Recombinant antibodies, genetically engineered for purpose, are finding

increased use in immunosensor development, as they can be modified to allow better selectivity, size, stability and easier immobilisation onto the transducer surface (Holliger and Hudson, 2005). Strategies for ensuring correct orientation of F_{ab} regions for antigen binding are key to optimising immunosensor performance, with different tethering methods and use of reduced antibody fragments (half antibodies) being evaluated.

1.9.3 Non-antibody binding proteins

Antibody based biosensors exploit the specificity of the immunological reaction between analyte and antibody. However, there is a potential drawback in the clinical setting, where there may be cross reactivity with non-specific antibodies if patients suffer or have been exposed to a similar disease, leading to false positive results (Soledad Belluzo et al., 2011). Improved results have been shown with recombinant antibodies, but also with the use of recombinant proteins. The fusion of DNA sequences encoding antigenic proteins has been used to design new epitopes for superior sensing, as well as the ability to group several of these peptides into one molecule as a highly sensitive bioreceptor. These proteins can be used to construct biosensors to detect antibodies themselves, target proteins, bacteria, viruses and parasitic organisms. They are particularly advantageous in the capacity to engineer particular functional groups onto them such as targeted cysteines, which can facilitate orientation of the bioreceptor *via* thiol targeted linkage to increase sensitivity. Non-antibody binding proteins may also reduce costs, as they are produced by fermentation, with no requirement for an animal host. Bacteriophages, viruses that specifically attach and infect bacteria, may also form the biorecognition element of biosensors, with the recent advent of phage libraries facilitating their use (Meyer and Ghosh, 2010).

1.9.4 Nucleic acids

Genetic analysis is an area of increasing importance since the completion of the human genome project, and has huge implications in the diagnosis and monitoring of genetic disease as well as in detection of DNA damage and interactions. DNA biosensors are consequently gaining considerable interest as a rapid, simple, inexpensive method of gaining sequence-specific genetic information as compared to standard DNA analyses (Wang, 2000). These DNA biosensors are typically based on the use of a single stranded DNA probe immobilised onto a transducer surface, to hybridise specifically to respective base pairs (Katz and Willner, 2003). So called "gene chips" or DNA microarrays allow the multiplex analysis of numerous DNA samples with efficiency and precision by immobilising multiple DNA probes for analysis. The introduction of peptide nucleic acid, synthetic DNA in which the sugar phosphate backbone is replaced with pseudopeptide, imparts DNA biosensors with a high specificity up to single base mismatches, and allows greater freedom of experimental conditions (Wang, 2000). DNA dendrimer nucleic acids as biorecognition elements are also gaining interest, as their branching allows for greater hybridisation to multiple complimentary strands, giving higher signal and greater sensitivity. Advantages of nucleic acid biosensors also include relatively simple construction and the possibility of regeneration for multiple use due to the chemically robust nature of DNA (Millan and Mikkelsen, 1993).

1.9.5 Others

In principle, any molecule capable of recognising a target analyte may be exploited as a bioreceptor in biosensing. Nucleic acid aptamers are DNA or RNA sequences with three-dimensional structures first discovered in 1990, which can specifically bind to target molecules and have immense potential for biosensor medical diagnostics as well as applications including environmental monitoring (Song et al., 2008). Twenty years after discovery, aptamers have been shown to bind with high specificity to a wide range of molecules including proteins, peptides, whole cells, drugs and amino acids. They may also be fabricated readily, are small in size and

cost effective with superior stability (Xiao et al., 2005). Their high affinity is derived from their ability to fold upon binding with their analyte. They are isolated *in vitro* by the Systematic Evolution of Ligands by Exponential Enrichment (SELEX) procedure, and have been dubbed "chemical antibodies" (Xu et al., 2005). However, aptamer technology is still in evolution, with challenges to be overcome including the limited availability of aptamer types and, as yet, poor knowledge of optimal immobilisation techniques onto transducer surfaces.

1.10 Transducer element

The transducer element is used to convert the biological event resulting from the interaction of the bioreceptor with analyte into a measurable signal that may then be read at the signal display (Katz and Willner, 2003). As previously mentioned, biosensors may be classified by their biological recognition element or by the type of transducer used. Types of transducer include optical, electrochemical, mass-based, thermal and piezoelectric. Electrochemical transducers are the oldest and most commonly used.

1.10.1 Optical biosensors

Optical biosensors are advantageous due to their immunity to electromagnetic interference, ability to sense remotely and use of multiple detection in one device (Fan et al., 2008). There are two main types: chromophore-based detection, with the use of fluorescent or absorbent tags, and label-free detection, with the target analyte detected in its natural form. Label-free detection is considered superior, as it negates the costly and time consuming tagging step which can also negatively affect molecular interactions (Cooper, 2002). Within label free optical biosensing, there are a number of detection methods including refractive index (RI) detection, optical absorption and Raman spectroscopy. All of these types of optical biosensors work on the same principle, that of measurement of analyte-bioreceptor

interaction; for example the interaction may change the RI at the sensor surface (Fan et al., 2008). Surface plasmon resonance (SPR) is a type of RI detection optical biosensor that has been extensively investigated for DNA and protein bioreceptors. Surface plasmon resonance is a means of real time detection and is sensitive, but limited penetration confers difficulty in measurement of large molecules such as bacteria, and currently they are not suitable for multiplexed platforms as they can only detect one analyte. SPR equipment is also complex and costly (Homola et al., 1999).

1.10.2 Piezoelectric biosensors

Piezoelectric, or electro-mechanical, transducers act by transforming the physical mass of an analyte into an electrical signal (Janshoff et al., 2000). Examples include quartz crystal microbalances (QCM), surface acoustic wave devices, and atomic force microscopy (AFM). Quartz crystal microbalances consist of an oscillating crystal, in which the frequency decreases in response to a change in mass at its surface due to analyte binding (Muramatsu et al., 1987). These devices have traditionally been used in vacuum deposition and other industrial systems, but are gaining interest for clinical analysis with the use of biorecognition layers coated onto the crystal. QCM-D (dispersion QCM) is a further technique used if the binding analyte is particularly flexible or compressible. Acoustic wave sensor devices have been used for the detection of biological and chemical entities within gas and liquid states. The sensor surface selectively absorbs molecules of interest from within the medium, which changes the amplitude, velocity and surface resonance of the device, all of which may be correlated with analyte concentration (Korotcenkov, 2010). They have been shown to be highly sensitive, and are small and inexpensive to produce. Atomic force microscopy utilises an oscillating cantilever running over the surface of the sample which changes the characteristics of the cantilever when in contact (Ziegler, 2004). The cantilever surface may be modified with a bioreceptor layer as with QCM, to improve selectivity. AFM is highly sensitive, and

has shown promise for the determination of pathogen detection, DNA analysis and tumour marker detection (Lavrik et al., 2004).

1.11 Electrochemical biosensors

Electrochemical sensors are the largest and most developed group of biosensors, with consequently the greatest commercial success in clinical, industrial and environmental fields (Korotcenkov, 2010). General advantages are rapid response times, user friendly application, low cost, and small size with the ability to be easily miniaturised (Zelada-Guillen et al., 2013). Further classification of electrochemical transduction may be divided into amperometric, potentiometric and impedimetric biosensing.

1.11.1 Amperometric sensors

Amperometric biosensors function by the direct measurement of the current produced when a constant potential is applied between two electrodes (Korotcenkov, 2010). The current itself is usually generated by the oxidation or reduction of electroactive species produced by the bioreceptor, commonly an enzyme, in response to the analyte. Alternatively, the inhibition of an enzyme may be exploited in fabrication of an amperometric biosensor (Vakurov et al., 2005). Oxidoreductase and dehydrogenase enzymes often generate electroactive products such as hydrogen peroxide during their catalytic cycle, and are commonly used in amperometric sensing. An example reaction equation for lactate oxidase has already been shown in **Section 1.9.1.** Glucose oxidase is the most frequently used enzyme in amperometry, and forms the biorecognition element of any medical glucose sensor (Wang, 2001). Advantages of amperometric biosensors are a rapid response time for point-of-care diagnostics and excellent sensitivity. However, they can suffer low specificity depending on the potential applied, which if high allows other redox species, particularly in biological fluids, to contribute to the signal

produced and thus give an erroneous reading (Korotcenkov, 2010, Higson, 2012). Amperometric biosensors are also limited in the range of analytes that may be measured as these must be substrates for, or inhibitors of, an enzymatic reaction.

1.11.1.1 Principles of amperometry

The principles of amperometry may be considered in two parts: the mass transfer of analyte to the electrode surface through the bulk solution electrolyte, and electron exchange between the electroactive species and the electrode. Manipulating each part as the rate limiting step allows different information to be obtained e.g. using an applied potential which ensures high electron exchange so mass transfer limits the current is useful for characterisation of complex electrode surfaces (Bard and Faulkner, 2000). The relationship between current and time is described using the Cottrell equation (4):

$$I = n\,F\,A\,C_o\sqrt{\frac{D}{\pi\,t}} \qquad (4)$$

Where I = current in amps, n = number of electrons, F = Faraday constant (95,500 C mol^{-1}), A = area of the electrode in cm^2, C_0 = initial concentration of analyte in the bulk solution, D = diffusion coefficient of species, t = time in seconds

If the solution is stirred thereby removing the rate-limiting step of mass transfer, and no other redox species are present, the current generated is proportional to the analyte concentration and therefore may be determined in unknown samples. The use of a rotating disc electrode for this purpose allows determination of true electron transfer rates. The measurement of current as a function of time is termed chronoamperometry.

The selected enzymes that commonly form part of the bioreceptor of an amperometric biosensor confer their own individual characteristics, but share common principles. Reactions of an enzyme with a single analyte (substrate) and product can be expressed as equation (5) (Wang, 2006):

$$E + S \leftrightarrow ES \rightarrow E + P \quad (5)$$

Where E = enzyme, S = substrate, ES = intermediate complex, P = product

The rate of a reaction catalysed by an enzyme at a known fixed concentration (V) is given by the Michaelis-Menten equation (6):

$$V = \frac{V_m\ [S]}{K_m + [S]} \quad (6)$$

Where K_m = Michaelis-Menten constant, V_m = maximum rate of reaction, S = substrate concentration

K_m is the substrate concentration at which the rate of the reaction is equal to half V_m. **Figure 1.9** shows the relationship between these parameters. The initial rate of reaction increases with substrate, until saturation (an excess of substrate) at which the rate can no longer increase. The plot therefore approaches its asymptote (V_m) as [S] increases. For the purposes of enzyme based biosensors, the highest V_m and lowest K_m are desirable, with low K_m conferring high sensitivity (Wang, 2006).

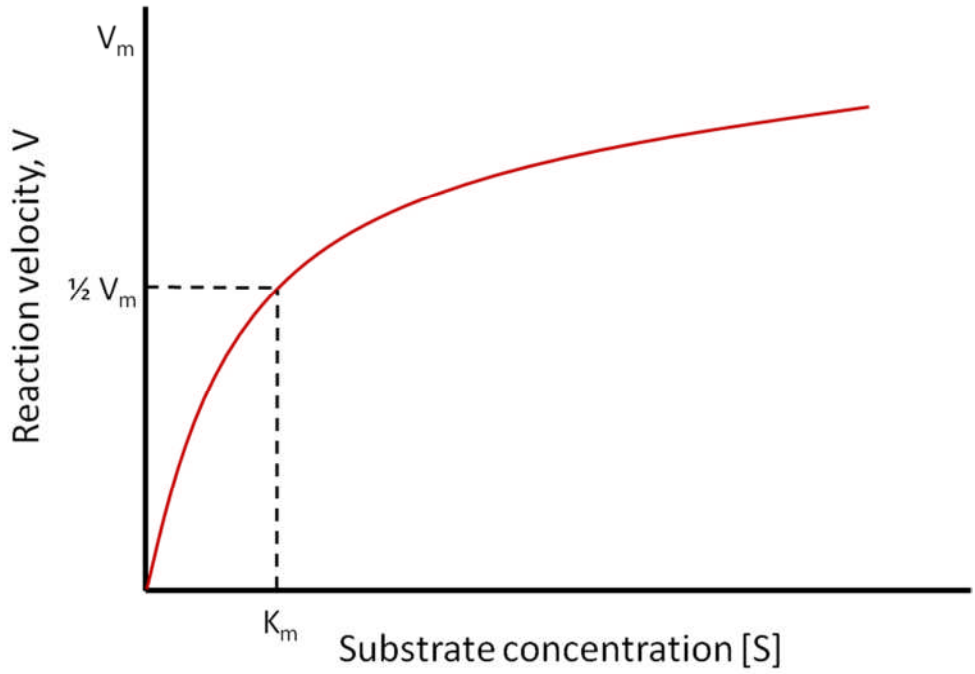

Figure 1.9: Michaelis-Menten enzyme kinetics graph depicting V_m and K_m.

1.11.2 Potentiometric sensors

In potentiometric biosensors the voltage produced is measured when a constant (zero) current flows through the electrochemical cell. Ion selective electrodes are used to measure the potential, by the use of an ion-selective membrane on the electrode which defines the target ion measured (Korotcenkov, 2010). In a manner similar to amperometric sensing, the turnover of analyte by enzymes immobilised on the sensor surface gives rise to a change in concentration of a measurable ion (typically H^+ or NH_4^+). Potentiometry therefore has been used for many decades for the detection of various analytes, or ions directly, and is the basis of the modern pH meter (Zelada-Guillen et al., 2013). Potentiometric biosensors confer excellent selectivity, have broad dynamic ranges and are not destructive (Gerard et al., 2002). They are inexpensive, and readily portable. Potentiometric biosensors have been shown to be useful from a pharmaceutical perspective, to measure penicillin and lysine (Parsajoo et al., 2012). However, they are slow acting, and suffer low sensitivity. They may also be affected by change in pH.

1.11.3 Impedimetric sensors

Electrochemical impedance biosensors detect changes in the electrical field due to a change in capacitance and electron transfer resistance at the working electrode surface arising from analyte-bioreceptor interaction. Simply put, as the concentration of analyte increases, analyte binding to the bioreceptor increases, and subsequently impedance across the electrode surface changes, which is detected at the transducer. Impedance can increase or decrease depending upon the analyte (Daniels and Pourmand, 2007). Impedance biosensors were first described in the 1980's, and lend themselves to the measurement of a wide range of analytes, from small molecules to proteins and up to whole bacteria and viruses (Berggren et al., 2001, Katz and Willner, 2003, Higson, 2012). This is one of the key advantages of impedance sensing over other types of electrochemical transduction; as there is no requirement for electroactive species, there are virtually no limitations on analyte type. They have promising importance in clinical diagnostics, pathogen detection, food quality control and environmental monitoring. Currently, no impedance biosensor has demonstrated widespread commercial success. There are still challenges with reproducibility, non-specific binding, and high limits of detection in many cases (Daniels and Pourmand, 2007, Berggren et al., 2001). However, the growing number of publications within this field shows clear prospects for resolution of these issues, with ongoing improvements in the technology of this rapidly developing technique.

1.11.3.1 Principles of impedance

As described, impedimetric biosensors convert the response from analyte-bioreceptor (typically antibody) binding into a measurable impedance signal, which is proportional to analyte concentration. Impedance is defined as the measure of opposition that a circuit presents to the passage of current when a potential is applied (Chang and Park, 2010). Impedance comprises elements of capacitance and resistance. Capacitance is the ability to store charge after a potential is applied, resistance being the opposition of the material to the flow of current. Electrodes

can act as capacitors, with the capacitance a result of the separation of electrode and electrolyte solution by the immobilised bioreceptor layer. This is known as the dielectric. The dielectric may actually comprise both capacitive and resistive components, which change upon analyte binding, giving the measurable impedance signal. As a sinusoidal potential is applied to the system, charging of the surface dielectric (capacitance) causes a phase shift in the signal wave of current from that of voltage. This is shown in **Figure 1.10**. The ratio of the change in applied voltage and the change in the current of an electrochemical cell is calculated as the impedance (Daniels and Pourmand, 2007).

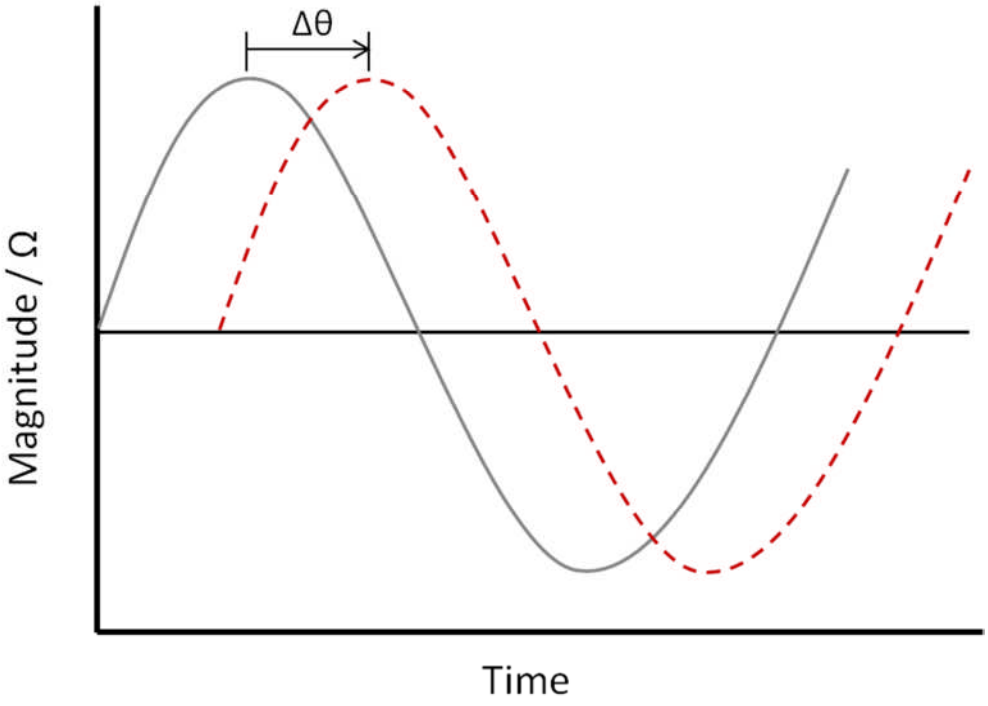

Figure 1.10: The phase shift of impedance. The current (– – – –) shifts from the voltage (————) due to the delay caused by charging of the surface dielectric. The measure of this shift is the phase angle, θ.

The impedance may be calculated using the following equations:

$$V = V_m \sin \omega t \quad (7)$$

Where V = the voltage at a given time, V_m = amplitude in volts, ω = the angular frequency in rad.s^{-1}, t = time in sec

The current, I resulting is given by:

$$I = I_m \sin (\omega t + \theta) \quad (8)$$

Where I = the current at a given time, I_m = maximum current, ω = the angular frequency in rad.s^{-1}, t = time in sec, θ = phase angle

The measurements of impedance are complex, consisting of a real, faradaic component relating to the in-phase resistance of the dielectric, Z', and an imaginary, non-faradaic component relating to the out-of-phase capacitance, Z''. These values may be presented as a function of frequency using a Nyquist plot, seen in **Figure 1.11**. A number of important parameters can be extracted from Nyquist plots including the resistance of the solution (R_s), the charge transfer resistance (R_{ct}), the Warburg impedance (W) and the maximum double layer capacitance (C_{dl}) (Bard and Faulkner, 2000). R_s is the resistance of the solution arising from conductance of ions in the bulk electrolyte solution in an electrochemical cell. It occurs at high frequency (to the left side of the Nyquist plot), when the oscillation is too fast for electron transfer. This parameter is unaffected by analyte binding due to the use of buffered mediators. R_{ct} is the resistance at the electrode surface to electron movement across the bioreceptor layer which occurs at low frequencies, and is changed by analyte binding. Warburg impedance is the frequency dependant diffusion of ions through the bulk electrolyte solution to the electrode interface which retards current flow. It can be controlled or at least minimised by the use of an electroactive mediator such as $Fe(CN_6)^{3-/4-}$ (ferricyanide/ferrocyanide) redox couple, which facilitates electron

transfer (Bard and Faulkner, 2000). The double layer capacitance refers to the capacitance of the dielectric. This phenomenon occurs when ions accumulate at a charged electrode surface in solution, before oppositely charged ions are attracted to form a second layer. It is also affected by analyte binding, with non-uniform bioreceptor layers giving the Nyquist plot its distinctive semi-circular shape and allowing C_{dl} prediction alongside resistive components.

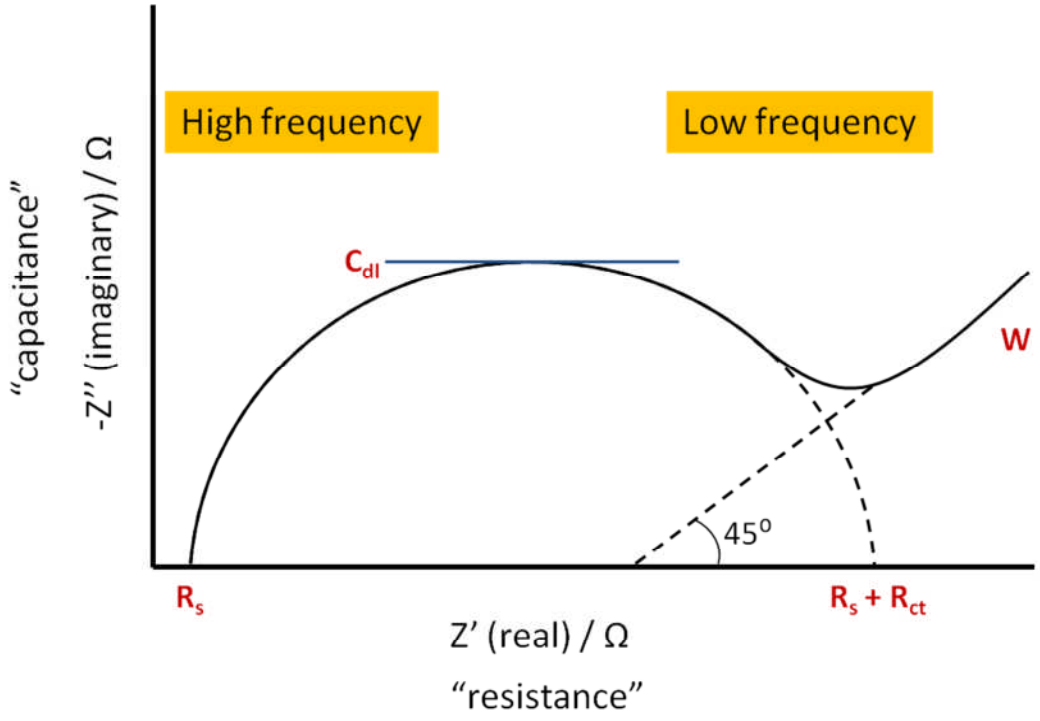

Figure 1.11: Schematic of a Nyquist plot. Nyquist plot showing the real (Z') and imaginary (Z'') elements of impedance. R_s (the solution resistance) and R_{ct} (charge transfer resistance) can be calculated from the Z' axis interception. C_{dl} can be calculated at Z'' max. Warburg impedance is shown as custom by a 45° angle of data at low frequencies.

The most common electrical circuit model used for fitting extracted impedance data is Randles equivalent circuit (Randles, 1947) **(Figure 1.12).** This model arises from faradaic or non-faradaic measurements. In a faradaic process, charge or electrons are transferred across the electrode interface. Non-faradaic processes occur when there is current flow without charge transfer, thus resulting in charge accumulation on a capacitor. Different impedimetric biosensors will show greater

change in the capacitative or resistance aspects of impedance. Capacititive biosensors must comprise a complete covering of the bioreceptor layer over the electrode to prevent electron flow through any gaps, reducing sensitivity (Gebbert et al., 1992). Biosensors not amenable to this due to defects in, or excessive thickness of, the insulating bioreceptor layer can be interrogated as faradaic impedance sensors. The principal response is change in R_{ct}, which varies depending on thickness and polarity of the sensor surface (Malamou and Prodromidis, 2008). Faradaic impedimetric biosensors are excellent choices for immunosensors as large changes in analyte binding give clear shifts in the resistive component of impedance. The use of mediators also reduces the frequency dependence of the response.

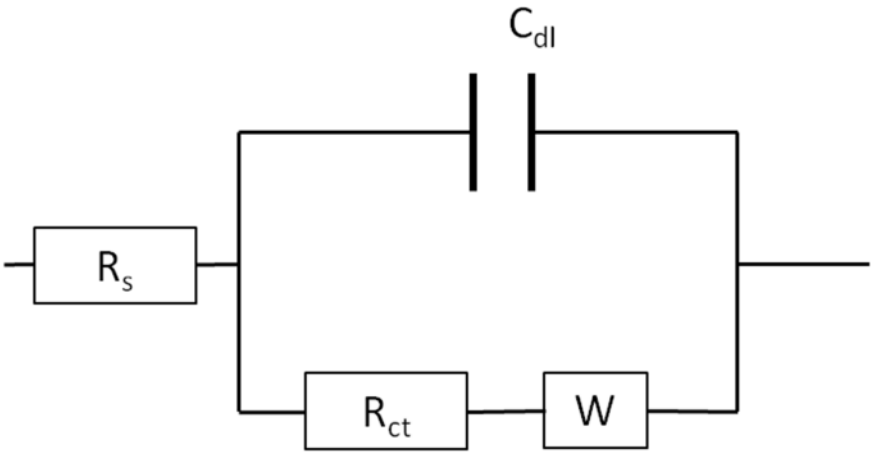

Figure 1.12: Schematic of Randles equivalent circuit. R_s is the resistance of the solution, R_{ct} is the charge transfer resistance, C_{dl} is the charged double layer and W is Warburg impedance.

1.11.4 Voltammetry

Voltammetric techniques involve the application of a potential (E) to an electrode and measurement of the resulting current (I) (Kounaves, 1997). The potential may be varied and the current measured over a period of time, thus voltammetry is usually described as a function of these three parameters: potential, current and time. Voltammetry is considered an active process as the application of potential

forces electrochemical reduction or oxidation of surrounding electroactive species at the electrode surface, changing their local concentration. Its use is extensive, including quantitative determination of inorganic and organic substances, and fundamental studies of redox processes, adsorption processes on surfaces, kinetics of electron transfer and chemical reaction mechanisms (Kounaves, 1997). Advantages include a large linear concentration range, excellent sensitivity and simultaneous determination of multiple analytes.

Cyclic voltammetry (CV) is a widely used voltammetric method, predominantly for the study of oxidation and reduction processes and reaction intermediates. In this technique potential is applied at a working electrode in both forward and reverse directions whilst current is measured. The potential can be cycled in this way several times if required. A CV trace for a bare gold electrode in $Fe(CN)_6^{3-/4-}$ showing the typical redox changes is shown in **Figure 1.13.**

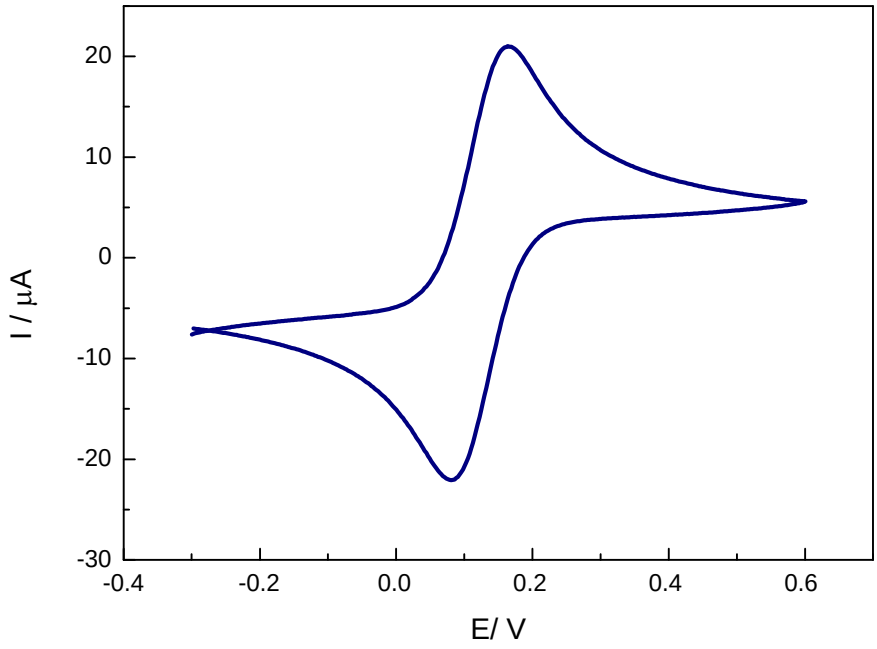

Figure 1.13: A single cyclic voltammetry waveform for a bare gold electrode in the presence of $Fe(CN)_6^{3-/4-}$. Scan rate is 0.1 $V.s^{-1}$.

The forward scan as potential is increased produces a peak current relating to the oxidation potential of the electrochemical species, in this case ferrocyanide. The current degrades as the species concentration depletes at the electrode surface. For this reversible redox couple, reversal of the applied potential then allows re-reduction of species to give another oxidation/reduction peak potential at the reverse polarity. The peaks are usually of a similar shape depending on the complexity of the species. Information regarding redox processes and sensor surface characteristics such as surface roughness can thus be obtained with CV.

1.12 Biosensor translation to clinical practice

Since the first biosensors were described over 40 years ago, there has been tremendous activity towards the development of biosensing devices for applications ranging from food quality control, environmental monitoring and clinical diagnostics and therapeutics. Biosensors particularly lend themselves to clinical use, with 80% of all commercial biosensor devices for medical applications as they are able to provide point-of-care measurements with no requirement for user expertise, additional reagents or specialist equipment (Fracchiolla et al., 2013). This is demonstrated by millions of diabetics worldwide who are able to measure their blood glucose by themselves at home with a glucose biosensor. Biosensors thus potentially have a role in clinics, GP surgeries, ambulances or any decentralised setting. Within the hospital, multiple measurements are possible due to the low cost of biosensors and ease of use, and thus a disease process may be monitored before or after intervention (Higson, 2012).

The use of biosensors for clinical biomarkers is in its infancy, but a rapidly expanding area of interest with huge potential. To date, biosensor technology has been used to detect a number of biomarkers implicated in a variety of disease processes including cancer and infectious diseases (Tothill, 2009). These may be present in blood, urine, cerebrospinal fluid or any other biological fluid of local relevance such as drain fluid. Protein biomarkers are the most extensively developed group, which allow for multiple array sensors with high specificity and sensitivity. Examples of biosensors for medical applications are therefore wide-ranging, and include diagnostic analytes such as hormones, cardiac markers, oncological markers, microorganisms; therapeutic analytes; and those for monitoring and surveillance of disease; all measured by a range of biosensor transducers (Holford et al., 2012, Wang et al., 2013, Kausaite-Minkstimiene et al., 2009, Aboul-Enein et al., 2002, Stringer et al., 2008, O'Regan et al., 2003, Fracchiolla et al., 2013, May et al., 2005, Yuan et al., 2012, Healy et al., 2007, Mohan et al., 2011, Skretas and Wood, 2005, Lenigk et al., 2000). Examples of interest

particularly relating to bowel ischaemia and abdominal sepsis are shown in **Table 1.5.** However despite major progress, commercial electrochemical biosensors are currently only available for glucose, uric acid and cholesterol, with the vast majority of sensors still at an experimental laboratory stage (Higson, 2012). Key limitations to widespread commercial use are requirement for validation of the chosen biomarkers; and ways to improve electrode stability, selectivity, sensitivity, reproducibility and speed of response of the biosensor device are ongoing.

Reference	Analyte	Electrode and bioreceptor	Transducer	Mediator	Biological medium	Limit of detection
(Corcoles et al., 2011)	Lactate, glucose	Carbon electrode Lactate/glucose oxidase and HRP in cellulose ester membrane	Flow cell amperometry	Ferrocene	Real time animal colon	Glucose: 15 mM Lactate: 10 mM
(Krawczyk et al., 1996)	Lactate	Platinum disk electrodes Lactate oxidase-phenylenediamine polymer	Flow injection amperometry	-	Human serum	2 µM
(Yashina et al., 2010)	Lactate	Carbon electrode Lactate oxidase-sol gel	Flow injection amperometry	Prussian Blue	Human venous blood	5×10^{-7} M to 1×10^{-3} M
(Montrose et al., 2013)	Pro-inflammatory monocytes	Gold electrode Antibody-mixed SAM	Impedance	Ferrocene	PBS	1000 to 30,000 cells
(Bergstrand et al., 2008)	Isopeptides (of fibrin)	Antibody-dextran surface	Surface plasmon resonance	-	Human plasma	23 nM to 186 nM
(Liu et al., 2012)	Interferon-γ, TNFα	Gold electrode Aptamer-PEG hydrogel	Voltammetry	Methylene blue	Human venous blood	INF-γ: 0.06 nM TNFα: 0.58 nM
(Pui et al., 2013)	TNFα	Gold electrode Antibody-mixed SAM	Impedance	Ferrocene	Culture media	1 $pg.ml^{-1}$ to 100 $pg.ml^{-1}$
(Qureshi et al., 2010)	CRP, TNFα, Il-6	Gold electrode Antibody-SAM	Capacitative impedance	-	PBS	25 $pg.ml^{-1}$ to 25 $ng.ml^{-1}$
(Ibupoto et al., 2012)	CRP	Gold coated glass Antibody-ZnO nanotubes	Potentiometry	-	PBS	1×10^{-5} $mg.ml^{-1}$ to 1 x 100 $mg.ml^{-1}$
(Bini et al., 2008)	CRP	Gold electrode RNA aptamer-biotin/Avidin	Optical	-	PBS	0.005 ppm
(Huang et al., 2013)	TNFα, MMP-3	Gold nanoparticles Antibody-mixed SAM	Fibre-optic particle plasmon resonance	-	Human synovial fluid	TNFα: 8.22 $pg.ml^{-1}$ MMP-3: 34.3 $pg.ml^{-1}$ (PBS)

(Carrigan et al., 2005)	Il-1	Gold crystal Antibody capture ligands-polymer matrix	Quartz crystal microbalance	-	PBS	25 $ng.ml^{-1}$
(Shao et al., 2001)	LPS	Protein A conjugate-polymyxin B ligand	Quartz crystal microbalance	-	Human plasma	0.05 EU to 0.5 EU
(McCamley et al., 2007)	LPS	Glass substrate-polyimide	Quartz crystal microbalance	-	Saline	1 $pg.ml^{-1}$ to 5 $mg.ml^{-1}$
(James et al., 1996)	LPS	Polymyxin B ligand	Evanescent wave fibre-optic	-	Human plasma	10 $ng.ml^{-1}$
(Iijima et al., 2011)	LPS	Carbon electrode Ferrocene attached polymyxin B and glucose oxidase in BSA membrane	Amperometry	Ferrocene	PBS	50 $ng.ml^{-1}$

Table 1.5: Summary of sepsis biomarkers measured by biosensors to date. A literature search was performed using Science Direct, Web of Knowledge and PubMed databases. The search terms 'Inflammation' and/or 'sepsis' and/or 'bowel ischaemia' and 'biosensor' were used as well as individual analyte names. Articles with emphasis on sepsis biomarker detection using biosensors with an explicitly stated limit of detection were included. BSA, Bovine serum albumin; CRP, C-reactive protein; HRP, Horseradish peroxidase; LPS, Lipopolysaccharide; MMP, Matrix metalloproteinase; PEG, Polyethylene glycol; PBS, Phosphate buffered saline; SAM, Self assembled monolayer; TNFα, Tumour necrosis factor alpha.

Biosensors may be used not only “off-line”, i.e. as disposable sensors using an external sample as in a glucose monitor, but *in vivo*, *via* an implanted sensor *in situ* allowing continuous monitoring, or “on-line” with flow through an incorporated sampling device. These present an added element for development of integrated monitoring (Higson, 2012). Biosensor measurement of biomarkers implicated in anastomotic leak and sepsis has the potential for more sensitive and specific diagnosis, leading to earlier intervention and reducing patient morbidity and mortality postoperatively.

1.13 Project aims

The overall aims of this project were twofold:

i) To identify biomarkers in abdominal fluid which correlate with anastomotic leak and intra-abdominal sepsis.

ii) To develop amperometric and impedimetric biosensors for measurement of the chosen biomarkers for point-of-care diagnostics.

Chapter 2:

Materials and methods

Chapter 2. Materials and methods

2.1 Materials

2.1.1 Inorganic materials

$K_3Fe(CN)_6$, $K_4Fe(CN)_6 \cdot 3H_2O$, H_2O_2 (35 % v/v), Na_2HPO_4, NaCl, KH_2PO_4, KOH, KCl and $FeSO_4 \cdot 7H_2O$ were all purchased from BDH laboratory supplies (Poole, Dorset, UK). H_2SO_4 was supplied by Merck Inc. (Hoddesdon, Hertfordshire, UK). 2-mercaptoethylamine hydrochloride was purchased from Alfa Aesar (Heysham, Lancashire, UK). $LiClO_4$ was obtained from Sigma-Aldrich (Poole, Dorset, UK).

2.1.2 Organic materials

Polyethyleneimine (molecular weight 750,000 Da, 50 % w/v solution), cobalt phthalocyanine (CoPc), lactate, uric acid, acetaminophen, ascorbic acid, newborn calf serum, dimethyl sulfoxide (DMSO), sulfosuccinimidyl 4-[N-maleimidomethyl] cyclohexane-1-carboxylate (sulfo-SMCC) and 2-aminobenzylamine (2-ABA) were all purchased from Sigma-Aldrich (Poole, Dorset, UK). Biotin-N-hydroxysuccimide (biotin-NHS) was purchased from Fluka. NeutrAvidin was supplied by Pierce Biotechnology (Rockford, USA). Ethylenediamine tetraacetic acid (EDTA), tris(hydroxymethyl) aminomethane (Tris) and D-glucose were purchased from BDH (Poole, Dorset, UK).

2.1.3 Enzymes

Glucose oxidase from *Aspergillus niger* Type X-S (GOx), and lactate oxidase from *Pediococcus sp* (LOx) were bought from Sigma Aldrich (Poole, Dorset, UK) as lyophilized powders.

2.1.4 Antibodies

Human TNFα recombinant protein and IgG mouse anti-human TNFα antibody were purchased from eBioscience (Hatfield, UK). Anti-myoglobin IgG antibody was supplied by Micropharm Ltd (Newcastle, UK). Polyclonal antibodies were raised in rabbits against a mixture of *E. coli* strains (*E. coli* 35218, HB101, NCTC10418, DH5a, BL21) and a single strain of *Streptococcus pyogenes (S. pyogenes)* using a custom service offered by GenScript Corp. (Piscataway, New Jersey, USA).

2.1.5 Solvents and buffers

Ethanol and acetonitrile were bought from Thermo Fisher Scientific Inc. (Rockford, USA). Other organic solvents were obtained from Sigma Aldrich (Poole, Dorset, UK), unless otherwise stated. PBS (phosphate buffered saline) tablets were obtained from Oxiod (Hampshire, UK). Standard PBS solution comprised 137 mM NaCl, 2.7 mM KCl, 10 mM Na_2HPO_4 and 2 mM KH_2PO_4. Deionised water produced by a Milli-Q reagent water system was used for all experiments.

2.1.6 Electrodes

Screen printed carbon electrodes for preliminary experiments were kindly donated from Dr Nikolay Pchelintsev, fabricated as part of his PhD work (Pchelintsev and Millner, 2008). Carbon DRP-150 and DRP-710 electrodes pre-impregnated with Prussian Blue, and gold dual working electrode DRP-CX2223AT-CM electrodes were supplied by DropSens (Llanera, Spain).

2.1.7 Commercial kits

L-lactate assay kits (colorimetric) were purchased from Abcam (Cambridge, UK). TNFα ELISA kits (Human and Rat) were purchased from eBioscience (Hatfield, UK). LAL chromogenic endotoxin (LPS) quantification kits were obtained from Thermo

Fisher Scientific Inc. (Rockford, USA). All were used as per the manufacturer's instructions.

2.2 Methods

2.2.1 Animal model of sepsis

2.2.1.1 Ethical approval

The project licence for the caecal ligation and puncture sepsis animal model was granted by the Home Office on 20th August 2012 (Ref: PPL 40/3631). My personal animal licence (Ref: PIL 40/10556) was granted on 28th June 2012, after the required course, examination, and application were completed.

2.2.1.2 Procedure

Male Wistar rats weighing 250 g were used for all experiments, with all animals being maintained under standard laboratory conditions. Animals were acclimatised to the laboratory environment for at least seven days before the start of the experiments. All animals were housed in standard temperature and humidity controlled rooms under a 12:12 light:dark cycle, with free access to food and water throughout the entire experimental period.

All surgical procedures were performed under the use of isofluorane general anaesthesia and using aseptic techniques. The steps outlined are shown in **Figure 2.1.** With the animal in a supine position, the abdomen was shaved and cleaned with ethanol (a). A midline laparotomy incision was made using a no. 15 scalpel blade and then extended with scissors to 3-4 cm to gain entry into the peritoneal cavity (b). The caecum was identified and exteriorised, and the mesentery carefully dissected away (c). The caecum was then ligated at half the distance between the distal pole and the base of the caecum with a 3-0 vicryl tie (d). For caecal puncture,

a 21 gauge needle was used to perform a single through and through puncture midway between the ligation and the tip of the caecum in a mesenteric-to-antimesenteric direction (e). The caecum was then gently compressed to allow extrusion of a small amount of stool, before being placed back in its normal position within the abdomen. The peritoneum, fasciae and abdominal musculature were closed using a mass closure technique with a continuous 4-0 vicryl suture before clips to the skin (f). Sham (control) animals underwent the same procedure, with the caecal ligation and puncture steps omitted (Rittirsch et al., 2009).

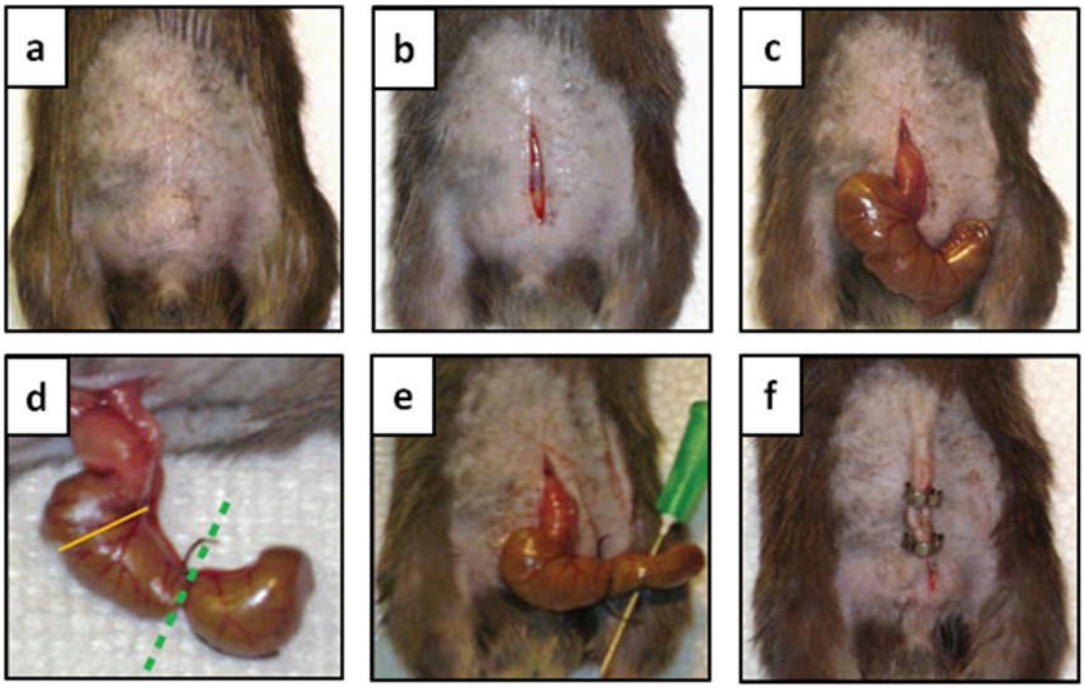

Figure 2.1: Illustration of the caecal ligation and puncture surgical procedure performed. (a) Shaved and disinfected area. (b) Midline laparotomy incision. (c) Exteriorisation of the caecum. (d) Ligation of the caecum (green line) at half the distance between the distal pole and the base of the caecum (yellow line). (e) Mesenteric to antimesenteric needle puncture. (f) Wound closure clips to skin. Adapted from (Rittirsch et al., 2009)

Immediately after surgery each animal received 2.5 ml of subcutaneous warmed normal saline for resuscitation with buprenorphine (0.05 $mg.kg^{-1}$) for postoperative analgesia, and was monitored closely in the recovery environment. Animals were

then transferred back to separate home cages with continued monitoring until the specified time point for sacrifice and sample collection.

2.2.1.3 Collection and storage of samples

At the specified time points the animals were sacrificed as per a Schedule 1 method (CO_2 asphyxiation before dislocation of the neck to confirm death). Re-laparotomy was performed immediately and peritoneal lavage carried out. This consisted of syringing 5 ml of sterile saline solution into the abdominal cavity, gently agitating the fluid around the cavity, then redrawing the fluid back into the syringe. The fluid was then centrifuged at 750 *x g* for 10 min, aliquoted, and frozen at -80 ^{o}C until use (Hendriks et al., 2010).

2.2.2 Patient abdominal drain fluid

2.2.2.1 Ethical approval

Ethical approval from National Research Ethics Service (NRES) committee Yorkshire and the Humber - LeedsEast (Ref: 11/H1306/5) was granted in February 2011, and Research and Development (R&D) permission from the Leeds Teaching Hospitals NHS Trust (Ref: GS10/9674) was granted in April 2011 for patient drain fluid sample collection. Inclusion criteria for selection were: NHS patients undergoing elective surgical bowel resection with anastomosis for benign or malignant disease at Leeds Teaching Hospitals NHS Trust, aged over 18 years, capable of giving consent, and requirement for a surgical drain at operation. Exclusion criteria were: aged < 18 years, patients who did not have a surgical drain as part of their operation, emergency cases, and patients undergoing bowel resection for septic conditions. Informed consent was taken from all participants after the opportunity to read a Patient Information Sheet **(Appendix 8.1)**. All patients were asked to sign a consent form **(Appendix 8.2)** of which a copy was placed in their clinical notes and the study records. Patient samples were collected between April 2011 and October 2012 for a total of 69 patients.

2.2.2.2 Collection and storage of samples

Drain fluid samples were collected intraoperatively directly after access into the abdominal cavity. Samples were subsequently collected from the patient's abdominal drain bag daily at 6.00 am from post-operative day 1 until the routine removal of the drain (as directed by the patient's clinical team, usually 4-5 days post-operation). A unique study number was allocated to each patient and fluid sample, and held securely on a dedicated database. The samples were transported to the laboratory and centrifuged at 3,000 *x g* for 10 min, with the supernatant aliquoted and stored at -20 °C until use (Fouda et al., 2011). Corresponding clinical data were collated including basic patient demographics (age and gender), adjuvant chemo-radiotherapy, type of operation, and adverse outcomes including anastomotic leak.

2.2.3 Electrochemical procedures

All electrochemistry experiments were performed using a three electrode system. Screen printed carbon electrodes (SPCE) that were initially used in preliminary experiments were a gift from Dr Nikolay Pchelintsev, fabricated as part of his PhD work (Pchelintsev and Millner, 2008). When using these electrodes, an external platinum rod counter electrode and a silver/silver chloride (Ag/AgCl) reference electrode were used. The electrodes used primarily in this work were purchased from DropSens (Llanera, Spain) and all consisted of the three electrode system integrated into one sensing chip: DRP-710 and CX2223AT as shown in **Figure 2.2**, and DRP-150. DRP-150 electrodes comprised one carbon working electrode, a carbon counter electrode and a Ag/AgCl reference electrode. DRP-710 electrodes comprised one carbon/Prussian Blue working electrode, a carbon counter electrode and a Ag/AgCl reference electrode. CX2223AT electrodes consisted of dual gold working electrodes, a gold counter electrode and a Ag/AgCl reference electrode. For cyclic voltammetry and chronoamperometric experiments an Eco Chemie B.V Autolab (Utrecht, Netherlands) with GPES4 software control was used, with the current between the working and counter electrodes with respect to the reference

electrode measured. An Eco Chemie B.V. Autolab Type III frequency response analyser (FRA-2) was used for impedance measurements. The basic rig construction showing the three electrode connector configuration with an integrated DropSens electrode and supporting electrolyte is shown in **Figure 2.3**. All electrochemistry work was performed at room temperature under an air atmosphere in a Faraday cage. Where stated, mixing of the electrolyte solution was performed using a magnetic stirrer.

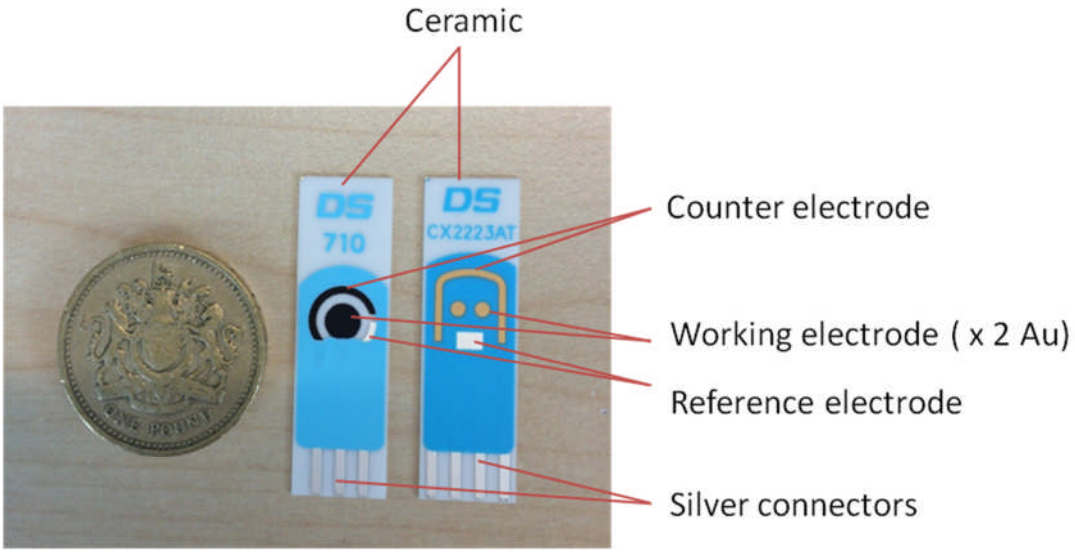

Figure 2.2: DRP-710 and CX2223AT DropSens electrode designs shown with a £1 coin for scale.

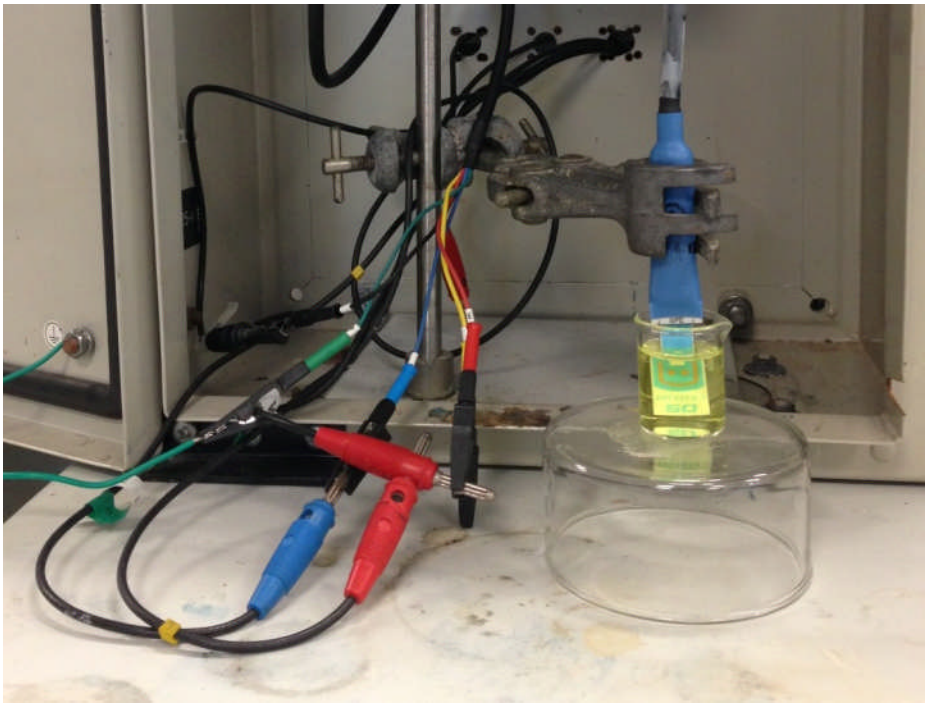

Figure 2.3: Electrochemical rig basic configuration (shown out of Faraday cage). The three electrode connectors can be seen (red, W.E; black, C.E; blue, R.E; N.B green, earth), with the integrated DropSens electrode immersed in electrolyte solution.

2.2.4 Fabrication of lactate biosensors

2.2.4.1 Cobalt phthalocyanine

2.2.4.1.1 Adsorption of cobalt phthalocyanine (CoPc)

Screen printed carbon electrodes courtesy of Dr Nikolay Pchelintsev were incubated in a saturated suspension of CoPc in a 50 °C preheated solution of 10 $mg.ml^{-1}$ PEI (MW 750 kDa) in dH_2O for 1 h. They were then washed in diethylene glycol butyl ether for 3 min, before further washing in 100% ethanol for 3 min (Pchelintsev and Millner, 2008).

2.2.4.1.2 Surface derivation with PEI

Electrodes were incubated in a diethylene glycol butyl ether solution containing 10 $mg.ml^{-1}$ PEI (MW 750 kDa) in dH_2O for 5 min. To allow surface derivation with PEI, the electrodes were mounted to an electrochemical cell also containing 100 mM

$LiClO_4$ electrolyte, and three cyclic voltammetry scans from 0.1 V to 0.9 V at scan rate 100 $mV.s^{-1}$ were run. The modified electrodes were then rinsed in ethanol, before incubation for 3 min in ethanol and 3 min in dH_2O.

2.2.4.1.3 Immobilisation of enzyme

The electrodes were incubated in a 1 $mg.ml^{-1}$ solution of lactate oxidase (LOx) in PBS, pH 7, for 1 h. They were next rinsed briefly with water and immersed in PBS, pH 7.0. The electrodes were incubated a further four times in PBS, pH 7.0, for 5 min duration each time.

2.2.4.1.4 Electrochemical measurements

Chrono-amperometry was performed at +0.6 V potential with respect to the Ag/AgCl reference electrode. Sequential amounts of lactate and/or H_2O_2 were spiked into PBS supporting electrolyte to test for amperometric response. Intensive stirring was applied throughout using a magnetic stirrer.

2.2.4.2 Biotin/avidin

2.2.4.2.1 Biotinylation of enzyme

The LOx enzyme was biotinylated by adding 100 µl of 100 $U.ml^{-1}$ LOx to 18 µL of 10 $mg.ml^{-1}$ biotin-NHS in DMSO, and incubating at room temperature for 30 min with agitation. The solution was added to a 30 kDa cut-off Amicon Ultra centrifugal filter and topped up with PBS. The 30 kDa spin filter was then centrifuged at 11,000 *x g* for 2 min. This was repeated a minimum of three times, each with supernatant discarded. The contents of the filter were then aliquoted and stored at -20 °C until use.

2.2.4.2.2 Polymerisation of electrode surface

The screen printed carbon electrodes and gold CX2223AT DropSens electrodes were mounted to an electrochemical cell containing 10 ml of 100 mM aniline and 100 mM 2-ABA in 1 M HCl. Twenty cyclic voltammetry scans were run from 1.0 V to 0.0 V at a scan rate of 50 $mV.s^{-1}$ to achieve electropolymerisation of the copolymer P(ANI/2-ABA) upon the electrode surface.

2.2.4.2.3 Biotinylation of electrodes and addition of NeutrAvidin

Polymer-coated electrodes were incubated in a 10 $mg.ml^{-1}$ biotin-NHS solution containing 1 mg biotin, 100 µl DMSO and 400 µl PBS for 1 h at room temperature, before rinsing with dH_2O. Electrodes were then incubated with 5 µM NeutrAvidin in PBS for 40 min at room temperature before further rinsing with dH_2O. Incubation with the biotinylated enzyme for 1 h at room temperature was then carried out.

2.2.4.2.4 Electrochemical measurements

Chrono-amperometry was performed at +0.6 V potential. Sequential amounts of lactate were added to PBS to assess amperometric response. Intensive stirring was applied throughout using a magnetic stirrer.

2.2.4.3 Prussian Blue

2.2.4.3.1 Adsorption of PEI

All steps were carried out at 50 °C in closed Eppendorf tubes. The screen printed carbon electrodes, and subsequently DRP-150 electrodes, were first washed in 100% ethanol for 3 min then rinsed with dH_2O for 3 min for surface cleaning. The electrodes were incubated in a 10 $mg.ml^{-1}$ PEI (MW 750 kDa) aqueous solution for 30 min to adsorb PEI. Washing for 3 min in dH_2O was then carried out in order to wash off any weakly bound polymer, before a final rinse with dH_2O. Electrodes

were then incubated in dH_2O for 5 min at room temperature (Pchelintsev et al., 2009).

2.2.4.3.2 Synthesis of surface-confined Prussian Blue

To achieve surface PB synthesis, electrodes were first incubated in 5 mM $K_3Fe(CN)_6$, pH 1, 100 mM KCl, for 5 min to saturate the surface bound PEI-film. Electrodes were then quickly rinsed with 100 mM KCl, pH 1, before immersion into 5 mM $FeSO_4$, pH 1, 100 mM KCl, for 2 h in the dark. The electrodes were next thoroughly washed with copious amounts of dH_2O, dried under a N_2 stream, and left in the dark for 1 h.

2.2.4.3.3 Enzyme immobilisation

The modified electrodes were incubated with 1 $U.\mu l^{-1}$ LOx in PBS, pH 7, 100 mM KCl, for 10 min. They were then carefully rinsed with dH_2O.

2.2.4.3.4 Electrochemical measurements

Chrono-amperometry was performed at 0 V. Lactate was sequentially spiked into PBS, pH 7, 100 mM KCl to assess amperometric response. Intensive stirring was achieved using a magnetic stirrer. The current generated after each lactate addition was taken and used to construct calibration curves.

2.2.4.4 Prussian Blue: modified protocol

2.2.4.4.1 Adsorption of PEI

DRP-710 DropSens electrodes underwent surface cleaning in dH_2O at 50 °C for 3 min. Adsorption of PEI onto the electrode surface was achieved as described in **Section 2.2.4.3.1** by incubating for 30 min in 10 $mg.ml^{-1}$ PEI (MW 750 kDa) aqueous solution at 50 °C. Electrodes were rinsed with dH_2O for 3 min at 50 °C, then further

rinsed with dH_2O, and incubated in dH_2O for 5 min at room temperature. Considerable care was taken to apply reagents exclusively to the working electrode area with no spillage onto the other integrated electrode components.

2.2.4.4.2 LOx immobilisation

The PEI modified electrodes were incubated with LOx in PBS, pH 7, 100 mM KCl at a variety of concentrations (0.31 – 5 U) and incubation times (5 – 40 min) during optimisation. The electrodes were immediately examined electrochemically after being rinsed in dH_2O and dried under an Ar stream.

2.2.4.4.3 Electrochemical measurements

At stages of biosensor assembly, the electrodes were characterised by cyclic voltammetry. This was performed on electrodes in a stirred solution of 10 ml PBS, pH 7, 100 mM KCl between -0.4 and +0.8 V at a scan rate of 100 $mV.s^{-1}$.

Chronoamperometry was used to assess response to lactate. Experiments were performed at 0 V in an electrolyte solution of 10 ml PBS, pH 7, 100 mM KCl which was vigorously stirred throughout. Background current was allowed to stabilise before sequential spiked injections of lactate. The current after each lactate addition was measured and used to construct calibration curves. During interference testing, a single addition of each potential interferent was used. Subsequent lactate spiked experiments were performed in newborn calf serum electrolyte at a range of dilutions in 10 ml PBS, pH 7, 100 mM KCl before drain fluid was used.

2.2.4.5 Drain fluid testing

An autocalibration technique was utilised, in which the current was allowed to reach a steady state (thus generated by the lactate present in the drain fluid sample), before sequential spiked injections of lactate. The concentration of lactate within the original drain fluid was estimated using a kinetic model fitted to calibration curves obtained using the buffer and newborn calf serum experiments.

2.2.4.6 Estimation of kinetic parameters and initial lactate concentration

Chronoamperometric measurements were first scaled so that minimum and maximum values ranged from 0 to 1 using the formula $(I-I_{min})/(I_{max}-I_{min})$ in the case of buffer measurements. Data for each biosensor were then fitted separately using the method of least squares to the Michaelis-Menten kinetic function, Rate= $V_m (S+S_0)/[1-K_m(S+S_0)]$, where S represented the concentration and S_0 was the initial lactate concentration (set to zero in buffer case). Fitted parameters extracted included V_m, representing the maximum rate achieved by the system and K_m, the Michaelis constant which represents the substrate concentration at which the reaction rate is half of V_m.

To estimate the initial concentration of lactate, S_0 in patient drain fluid samples, chronoamperometric measurements were first scaled so that the maximum values ranged up to 1. Data for each biosensor were again fitted separately using the method of least squares to the Michaelis-Menten kinetic function, but with V_m fixed to 1.2 to agree with the best fitted buffer biosensor. Fitted parameters therefore included the initial lactate concentration S_0, and the Michaelis constant K_m adjusted itself to account for differences in the initial current. The first six data points provided the best estimate of initial concentration.

2.2.5 Fabrication of *E. coli* biosensor

2.2.5.1 Gold electrode cleaning

To ensure a reproducible, stable sensor, the gold working electrodes on CX2223AT electrodes were cleaned by being placed in 100% ethanol and sonicated in a water bath for 5 min. They were then rinsed with 100% ethanol, rinsed with dH_2O, and dried under an Ar stream.

2.2.5.2 Polymerisation of electrode surface

A 25 mM solution of tyramine in methanol containing 300 mM NaOH (unless specified) was electro-deposited onto cleaned gold electrodes by cyclic voltammetry. This was achieved using two scans from 0 V to +1.6 V at a scan rate of 100 $mV.s^{-1}$ unless specified. The modified electrodes were then rinsed with dH_2O, before drying under an Ar stream. To equilibrate, the electrodes were incubated in PBS for 30 min, before rinsing with dH_2O and drying under an Ar stream.

2.2.5.3 Reductive antibody cleavage

Twelve millilitres of 2-mercaptoethylamine·HCl (2-MEA) were added to 1 ml of Ar-degassed PBS containing 10 mM EDTA, pH 7.4. Equal volumes of IgG stock (at 8.5 $mg.ml^{-1}$) were added to the 2-MEA/PBS-EDTA and incubated at 37 °C for 90 min (Hermanson, 2008). The reduced IgG was then added to an Amicon Ultra centrifugal filter with a 100 kDa molecular weight cut-off and centrifuged at 11,000 *x g* for 2.5 min to filter off any remaining whole antibody present. The supernatant (half and fragmented IgG) was then added to a 50 kDa cut-off Amicon Ultra centrifugal filter and topped up with Ar-degassed PBS containing 10 mM EDTA, pH 7.4. The 50 kDa spin filter was then centrifuged at 11,000 *x g* for 2.5 min. This was repeated a minimum of three times, each with supernatant discarded (containing IgG fragments) and topped up with PBS-EDTA. The resulting content of the filter was the reduced half IgG antibody which was used immediately. The presence of

half antibody after centrifugation was confirmed by spectrophotometry and SDS-PAGE.

2.2.5.4 Attachment of IgG onto modified electrode surface

One milligram of sulfo-SMCC was added to 50 µl DMSO to dissolve, before addition of 450 µl of Ar-degassed PBS containing 10 mM EDTA, pH 7.4, for a 5 mM solution of sulfo-SMCC. The electrodes were incubated with sulfo-SMCC solution for 1 h at room temperature. The electrodes were then rinsed with dH_2O and dried under an Ar stream. The reduced IgG (as prepared in **Section 2.2.5.3**) was applied to the modified electrode surface and incubated for 1 h at room temperature. The electrodes were then again rinsed with dH_2O and dried under an Ar stream. To equilibrate, the electrodes were incubated in a plentiful volume of PBS for 10 min, before rinsing with dH_2O and drying under an Ar stream.

2.2.5.5 Electrochemical measurements

Electrodes underwent electrochemical interrogation using cyclic voltammetry and electrochemical impedance spectroscopy (EIS) measurements. Electrodes were characterised at construction stages by cyclic voltammetry in the redox mediator $Fe(CN_6)^{3-/4-}$ in PBS at pH 7.0 between -0.3 and +0.6 V at a scan rate of 50 $mV.s^{-1}$. EIS was carried out using an Eco Chemie B.V Autolab Type III frequency response analyser (FRA-2) over a range of frequencies from 25 kHz to 0.25 Hz. The electrolyte $Fe(CN_6)^{3-/4-}$ in PBS at pH 7.0 was used in all EIS experiments (unless stated). The potential was fixed at 0 V relative to the Ag/AgCl reference electrode, with 0.01 mV amplitude. Experiments were initially performed by the addition of increasing concentrations of analyte in PBS, incubated on the completed biosensor surfaces for 30 min before rinsing in dH_2O and drying under an Ar stream before EIS interrogation. Subsequent testing was carried out with analyte spiked into newborn calf serum and drain fluid, before EIS interrogation of neat drain fluid samples. Data were plotted as Nyquist and Bode plots for analysis.

2.2.6 Fabrication of TNFα biosensor

2.2.6.1 Biotinylation of TNFα antibody

To remove the sodium azide present, TNFα IgG (at 0.5 mg.ml^{-1}) was first added to an Amicon Ultra centrifugal filter with a 30 kDa molecular weight cut-off and centrifuged at 11,000 *x g* for 2.5 min. This was repeated three times, each time topping up with PBS. PBS was added to ensure the final volume in the filter was the same as the starting volume i.e. 1 ml. Five hundred micrograms of biotin-NHS was added to 100 µl DMSO to dissolve, before addition of 400 µl PBS for a 1 mg.ml^{-1} solution. To the antibody, 19 µl of this stock solution was then added (5:1 molar ratio, as described in Sigma-aldrich Immunoprobe biotinylation kit) and incubated for 1 hr at room temperature with agitation. The solution was then added to a 30 kDa cut-off Amicon Ultra centrifugal filter and centrifuged at 11,000 *x g* for 2.5 min. This was repeated three times, each with the supernatant discarded and topped up with PBS. The resulting content of the filter was the biotinylated IgG antibody which was aliquoted and stored at 4 °C until use.

2.2.6.2 Modification of electrode surface and electrochemical measurement

Gold CX2223AT electrodes were cleaned and polymer was deposited by electropolymerisation as described in **Sections 2.2.5.1** and **2.2.5.2** respectively. Twenty microlitres of DMSO was added to 0.1 mg of biotin-NHS to dissolve, before addition of 80 µl of PBS for a 1 mg.ml^{-1} solution. The polymerised electrodes were incubated with biotin-NHS solution for 30 min at room temperature. The electrodes were then rinsed with dH_2O and dried under an Ar stream. A stock of NeutrAvidin was prepared at 1 mg.ml^{-1} in dH_2O and 6 µl of this was added to 994 µl PBS before incubation with the biotinylated electrodes for 45 min. The electrodes were then again rinsed with dH_2O and dried under an Ar stream. Specific coupling of NeutrAvidin to biotinylated IgG was achieved with the electrodes incubated with biotin-IgG (as prepared in **Section 2.2.6.1**) for 1 h. After coupling, they were rinsed with dH_2O and dried under an Ar stream. To equilibrate, the electrodes were incubated in a plentiful volume of PBS for 10 min, before again rinsing with dH_2O

and drying under an Ar stream. Electrochemical measurements as described in **Section 2.2.5.5** were carried out.

2.2.7 Colorimetric assay

The methodology for the colorimetric assay was kindly given by Dr Timothy Gibson of ELISHA systems Ltd. (personal communication) based on methods described in the literature (Vojinović et al., 2004). A working reagent of 100 mM phosphate buffer containing 2 $U.ml^{-1}$ horseradish peroxidase (HRP), 0.4 mM 4-aminoantipyrine (4-AAP), and 25 mM phenol-4-sulphonic acid (PSA) was mixed with 100 $U.ml^{-1}$ of lactate oxidase. The assay was performed in a 96 well plate in which 275 µl of the working reagent was added to 25 µl serial dilutions of lactate analyte. The plate was incubated at 25 °C for 15 mins before absorbances were read at 485 nm with a FLUOstar OPTIMA microplate reader (BMG LABTECH, Germany).

2.2.8 Midland blotting

This technique is a novel methodology described by our group (Rushworth et al., 2014). Polymerised electrodes were incubated with 4 $mg.ml^{-1}$ biotin-NHS in PBS, pH 7.0 for 30 min at room temperature in a moist chamber. The electrodes were rinsed three times with dH_2O. StreptAvidin-HRP was diluted to 1:1000 in PBS, pH 7.0 and applied to the modified electrodes for 30 min in the moist chamber. Electrodes were again rinsed with dH_2O. Working solutions of ECL substrate and reagent were prepared as per the manufacturer's instructions and added to the electrode surface. Electrodes were then imaged using a Syngene imager. The electrodes were rinsed with dH_2O and 0.1 % (v/v) Tween-20 was applied for 5 min to remove any non-specific binding. The electrodes were rinsed again with dH_2O. ECL was reapplied and the electrodes reimaged.

2.2.9 Dot blotting

Analyte was applied to a nitrocellulose membrane alongside appropriate controls. After 15 min air drying the membrane was placed into 5 % (w/v) non-fat milk blocking buffer in 10 mM PBS containing 0.1 % (v/v) Tween-20 (PBS-Tween) and incubated for 1 hr at room temperature with agitation. The membrane was then washed in PBS-Tween before incubation with primary antibody in blocking buffer overnight at 4 °C with agitation. The membrane was washed thoroughly in PBS-Tween before three 5 min washes in PBS-Tween. HRP secondary antibody in blocking buffer was then applied for 1 h at room temperature. The membrane was again thoroughly washed in PBS-Tween with three subsequent 5 min washes in PBS-Tween. A final wash in PBS without Tween was performed to remove any traces of the detergent. ECL substrate and reagent were prepared as per the manufacturer's instructions and applied to the membrane, before sandwiching between acetate slides to develop for imaging. A Syngene imager was used for imaging.

2.2.10 Sodium dodecyl sulfate-polyacrylamide gel electrophoresis (SDS-PAGE)

IgG antibody was reduced as described in **Section 2.2.5.3** and samples at different stages of cleavage were added to 5 x non-reducing loading dye consisting of 250 mM Tris, pH 7.6, 10 % (w/v) SDS, 50 % (v/v) glycerol, with a pinch of bromophenol blue. The samples were loaded onto a pre-cast BioRad gel and subjected to electrophoresis in 1 x tris-glycine running buffer at 300 V for approximately 60 min. The gel was then stained with "Instant Blue" for 6 h with agitation, before washing and incubating in dH_2O overnight also under agitation to destain. The gel was imaged using a Syngene imager.

2.2.11 Scanning electron microscopy

Scanning electron microscopy (SEM) was used at different stages of biosensor construction to observe the characteristics of each layer in order to optimise biosensor performance. Electrodes were cut to size using a diamond knife and placed onto an SEM stub. Carbon cement was applied to the exposed edges to allow conduction. The electrodes were observed using a Carl Zeiss EVO© MA 15 SEM machine at the School of Process, Environmental and Materials Engineering (University of Leeds) and a Quanta 200F (FEI) machine at the School of Biomedical Sciences (University of Leeds).

2.2.12 Flow cytometry

Samples were added to equal amounts of 6% BSA in PBS for 30 min. After this time, primary antibody (1:1000) and FITC-secondary antibody (1:1000) were both added simultaneously to each sample. An alternative method was the addition of 1 $mg.ml^{-1}$ propidium iodide (PI) (1:500) added to samples for 15 min. Cells were sorted using a BD-LSRFortessa™ flow cytometer (BD biosciences) and data were analysed using BD FACSDiva software v 3.1 (BD biosciences) available at the School of Biomedical Sciences (University of Leeds). The population of interest was gated, before the addition of counting beads (Invitrogen/Caltag laboratories, Life technologies, UK) for calculation of absolute cell count.

Chapter 3:

Biomarker animal model

Chapter 3. Biomarker animal model

3.1 Introduction

As discussed in **Chapter 1**, a recent shift in focus for diagnosis of abdominal sepsis has been to measure changes in molecules locally at the site of corruption, as biomarkers of septic disease processes that are potentially more sensitive and specific. There is a wealth of potential biomarker targets available, although few which have been formally assessed under controlled conditions and none translated into clinical use for this purpose. From the literature, three potential biomarkers were chosen as representing three different time points in the pathological time course of anastomotic leak that were feasible to be measured by biosensors: lactate, TNFα and *E. coli*. This chapter describes the development and use of a caecal ligation and puncture animal model in assessing each biomarker's suitability in an early diagnostic test for anastomotic leak and abdominal sepsis.

3.1.1 Lactate

Lactic acid (chemical formula $CH_3CH(OH)COOH$) was discovered in 1780 by Swedish chemist Carl Wilhelm Scheele who isolated it from sour milk (Holten et al., 1971). It has two optical forms, L(+) and D(-), of which L(+) is the biological isomer present in the human body. Its molecular weight is 90.08. The three dimensional structure of lactic acid and its chemical formula are shown in **Figure 3.1**. Lactic acid is a weak acid which partially dissociates in water to give the lactate ion ($CH_3CH(OH)COO^-$) and H^+. Under physiological conditions, the pH is higher than the threshold for dissociation (pKa = 3.86) and therefore the majority of lactic acid in the body is present as lactate. This charged form is unable to pass through lipid membranes, unlike the undissociated form. The physiological level of lactate in human plasma is typically 0.3-1.3 mM (Phypers and Pierce, 2006). The terms lactic acid and lactate

are used somewhat interchangeably in the literature. In this work the term lactate is used to mean L(+) lactate.

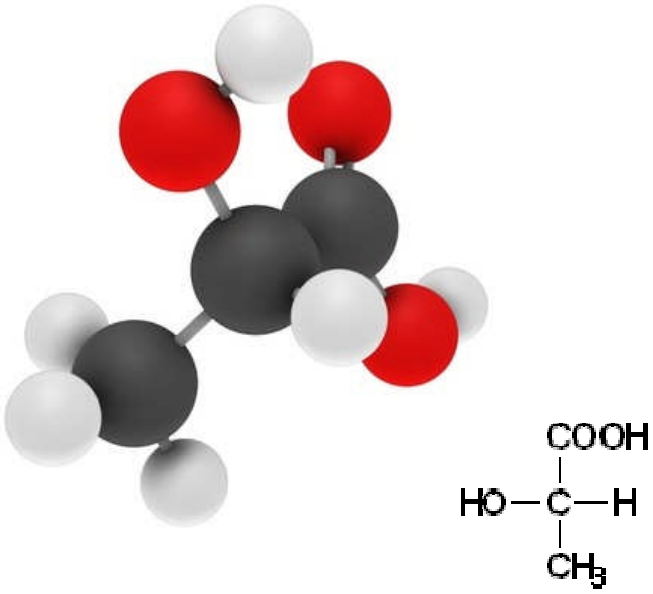

Figure 3.1: Three dimensional structure of lactic acid. Atom colours as CPK standard (black = carbon, red = oxygen, white = hydrogen). Inset: Lactic acid shown as chemical formula. With the loss of H^+ lactic acid becomes lactate.

As discussed in **Section 1.6.2**, under anaerobic conditions, pyruvate cannot be oxidised in the Krebs cycle to generate ATP for cellular energy. Instead, it undergoes fermentation catalysed by lactate dehydrogenase to form lactic acid (Robergs et al., 2004). This allows ATP to continue to be produced, although is a less efficient energy cycle than oxidation of pyruvate under aerobic conditions. Under ischaemic conditions, whether physiological and transitory as in exercise or pathological, anaerobic metabolism dominates leading to increased lactic acid. Raised lactate thus commonly occurs in a wide variety of clinical conditions including multi-organ failure, cancer, drug toxicity, and sepsis which is defined as severe sepsis at lactate levels greater than 4 mM (Nguyen et al., 2004). Sepsis may be caused by anastomotic bowel leak, respiratory infection, pancreatitis and many more disease processes. Lactate can therefore act as a biomarker of ischaemia for a number of disease states.

3.1.2 Tumour Necrosis Factor α

Tumour necrosis factor-alpha (TNFα) is a potent pro-inflammatory cytokine involved in the inflammatory response of the body. TNFα is generated as the precursor transmembrane-TNFα, before processing by TNFα-converting enzyme (TACE) to become the soluble form of TNFα (Horiuchi et al., 2010). Soluble TNFα consists of 157 amino acid residues and is a homotrimer of 17 kDa cleaved monomers arranged in a bell like shape (Locksley et al., 2001). It has a predominantly negative charge at neutral pH as shown in **Figure 3.2**. The activities of TNFα are mediated through its binding to type 1 and 2 TNFα receptors (TNF-R1 and TNF-R2) present on the majority of nucleated cells, to stimulate apoptosis, cell recruitment and proliferation and further cytokine production amongst others *via* phosphorylation of protein kinases and activation of transcription factors (Chowdhury and Bhat, 2009). As discussed in more detail in **Sections 1.6.1** and **1.6.3**, TNFα is a key pro-inflammatory mediator involved in both the physiological response to healing and the pathological states of SIRS and sepsis and autoimmune inflammatory disorders such as Crohn's disease. It is released predominantly by macrophages, at a peak of 2 hours after challenge to LPS administration in one study by Oliver *et al* (Oliver et al., 1993). TNFα has a relatively short half life of 15-18 min (Davies and Hagen, 1997), although in anastomotic leak has been shown to be present in increasing concentrations for a number of days (Fouda et al., 2011, Ugras et al., 2008, Matthiessen et al., 2007, Herwig et al., 2002). Its role in inflammation and sepsis therefore renders TNFα a good candidate for an early biomarker for this application, particularly when in the local abdominal environment to potentially augment specificity.

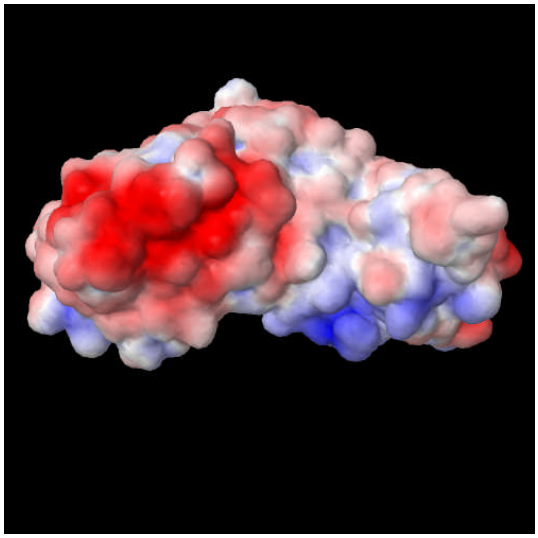

Figure 3.2: Schematic structure of TNFα at pH 7.4. Red is the inherent negative charge and blue is positive charge. PDB ref: 3L9J (Rushworth, 2013)

3.1.3 *E. coli*

Escherichia coli colonise the human gastrointestinal tract shortly after birth and remain coexistent with their host throughout life (Kaper et al., 2004). The human GI tract contains more than 500 types of bacteria, accounting for the average 10^{10}-10^{11} cells per gram that are present in the large intestine alone. *E. coli* is the predominant aerobic organism in this flora and is particularly concentrated in the caecum and large bowel, residing in the mucus covering of the epithelial luminal cells and being shed into the lumen to be excreted in the faeces (Tenaillon et al., 2010). The flora of the GI tract including *E. coli* remains incompletely understood. Traditionally it was considered entirely commensal, but is recently thought to be more mutualistic, particularly with a role in inducing colonisation resistance in the human host (Hooper and Gordon, 2001, Tenaillon et al., 2010). *E. coli* has a number of serotypes, with a total population size estimated to be in the region of 10^{20} in the wild. As well as commensal strains there are several highly adapted *E. coli* clones with specific virulence attributes inciting a broad spectrum of disease to the host depending on the pathotype including enteric/diarrhoeal disease, urinary tract infection and sepsis/meningitis (Kaper et al., 2004). *E. coli* is therefore both a commensal and a pathogen, dependant on the genetic serotype.

E. coli is a rod shaped bacterium approximately 2 µm long and 0.5 µm in diameter with a cell volume of 0.6-0.7 μm^3. Some strains are motile, possessing flagella. In common with all other types of bacteria, *E. coli* have a peptidoglycan cell wall which conveys the cell's rigidity. *E. coli* is a Gram-negative bacterium, characterised by the absence of uptake of ethanol-acetic acid violet stain by the cell wall on Gram staining due to the cell wall being thinner than that of Gram positive cells and its presence in between inner and outer membranes. The outer membrane, consisting of lipopolysaccarides (LPS) and phospholipids, confers to the cell an overall negative charge. The structure of *E. coli* in cross section is shown in **Figure 3.3**.

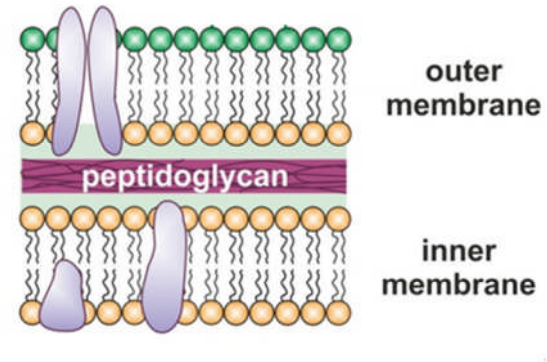

Figure 3.3: Schematic of structure of Gram-negative *E. coli* showing peptidoglycan cell wall between inner and outer membranes. Adapted from (Ahmed et al., 2014)

The peritoneal cavity, in contrast to the lumen of the gastrointestinal tract, is entirely sterile. A breach in the bowel wall caused by perforation of an ulcer or a cancer, or failure of healing of an anastomosis allows spillage of bowel contents including commensal bacteria into this sterile intra-abdominal environment where they may be measured. If unchecked, they progress to infiltration of the vascular system leading to widespread septicaemia and systemic sepsis. Presence in the peritoneal cavity is therefore an early sensitive finding and is a promising biomarker of bacterial sepsis.

3.2 Biomarker measurement

3.2.1 Colorimetric lactate assay

To measure lactate levels in the animal samples, a colorimetric L-lactate assay kit was sourced from Abcam (Cambridge, UK). The assay, which takes a number of hours to perform and requires specialist equipment including a plate reader and operator skill, briefly acts by the lactate present undergoing oxidation by lactate dehydrogenase to generate NAD which then allows reduction of a synthetic substrate to produce coloured formazan crystals. The colour intensity is directly proportional to the initial lactate concentration, which is detected by spectrophotometry at 450 nm. The sensitivity and range are cited as 0.02 mM, and 0.02 mM to 10 mM, respectively. A calibration curve for the kit using the provided lactate standards was performed and is shown in **Figure 3.4**. The coefficient of determination was 0.9905, and the coefficient of variation was 4.515%, showing the excellent concordance of the standards to generate the linear fit with which to calculate lactate in unknown samples.

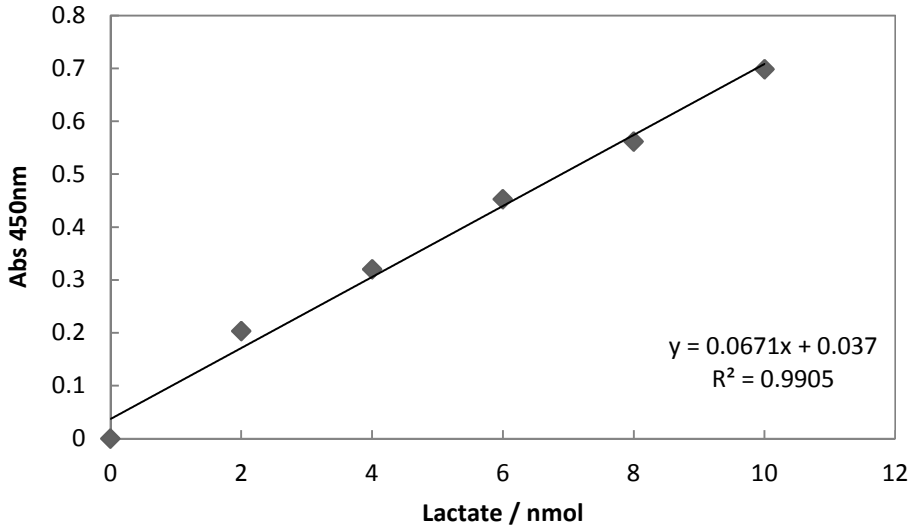

Figure 3.4: Calibration curve with linear fitting from lactate standards in commercial lactate colorimetric assay. Data points given as the mean values, n = 3.

3.2.2 TNFα ELISA

A rat specific TNF alpha ELISA Ready-SET-Go!® was sourced from eBioscience (Hatfield, UK) for TNFα measurement in animal samples. The ELISA acts as a standard antibody ELISA, by the sequential addition into a 96-well plate of an anti-rat TNFα capture antibody, sample (containing TNFα), an anti-rat TNFα biotin detection antibody, Avidin-HRP and a tetramethylbenzidine (TMB) substrate, with meticulous washing in-between each addition to prevent non-specific binding. The intensities of the coloured product are directly proportional to the TNFα concentration in the samples, detected by spectrophotometry at 450nm. The kit is readily available but is very costly, requires a number of reagents and operator skill, and is performed over a period of three days. The sensitivity of the assay is given by the manufacturers as 16 $pg.ml^{-1}$ and the standard curve range from 16 to 2000 $pg.ml^{-1}$. A calibration curve for the kit performed using the included rat TNFα recombinant protein standards in triplicate is shown in **Figure 3.5**. The linear fit had a coefficient of determination of 0.9993, and a coefficient of variation of 2.92%, showing the excellent concordance of the standards and robustness of the assay.

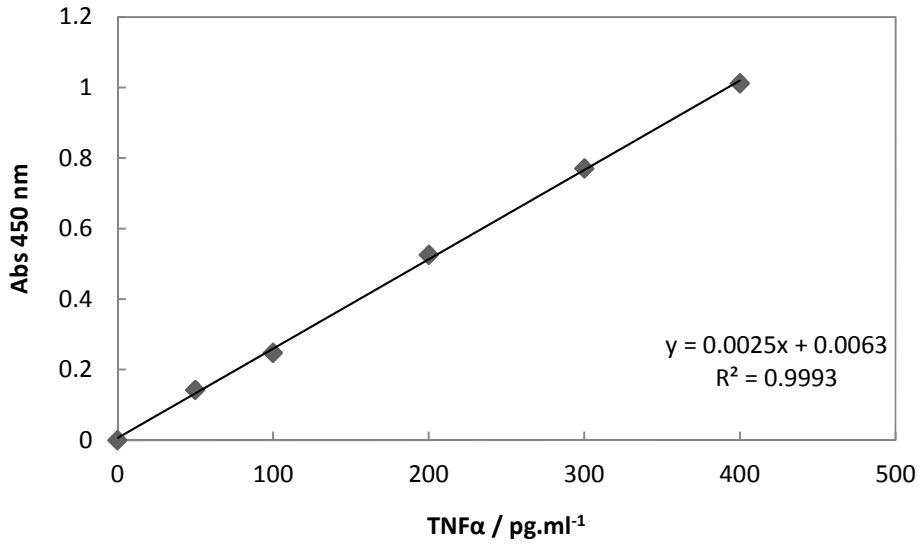

Figure 3.5: Calibration curve with linear fitting from rat TNFα recombinant protein standards in commercial rat TNFα ELISA kit. Data points given as the mean values, n = 3.

3.2.3 Colorimetric *E. coli* LPS assay

After an extensive literature search no commercial assays for measurement of *E. coli* in biological samples were found suitable for purpose, particularly highlighting the importance of development of new bacterial tests as in this work. A colorimetric lipopolysaccaride (LPS, also known as endotoxin) assay kit was therefore sourced and utilised, with LPS being a component of the Gram-negative bacterial cell wall as discussed in **Section 3.1.3** and therefore a surrogate marker for *E. coli*. An LAL chromogenic endotoxin quantitation kit for measurement of LPS was obtained from Thermo Fisher Scientific Inc. (Rockford, USA). The kit acts by the presence of LPS/endotoxin catalysing the activation of a proenzyme, factor C, in modified *Limulus* Amebocyte Lysate (LAL). This activated proenzyme then catalyses the lysis of yellow coloured p-nitroaniline from the colourless synthetic peptide substrate Ac-Ile-Glu-Ala-Arg-pNA, with the activation rate directly proportional to the sample LPS concentration. The colour intensity is detected by spectrophotometry at 405-410 nm. The sensitivity of the assay is given as 0.1 $EU.ml^{-1}$ (approx. 0.01 ng.ml-1). A calibration curve for the assay using the included *E. coli* LPS standards is shown in **Figure 3.6**. The linear fit had a coefficient of determination of 0.9927, and a coefficient of variation of 6.506%, demonstrating the good concordance of the standards to the linear standard curve for use.

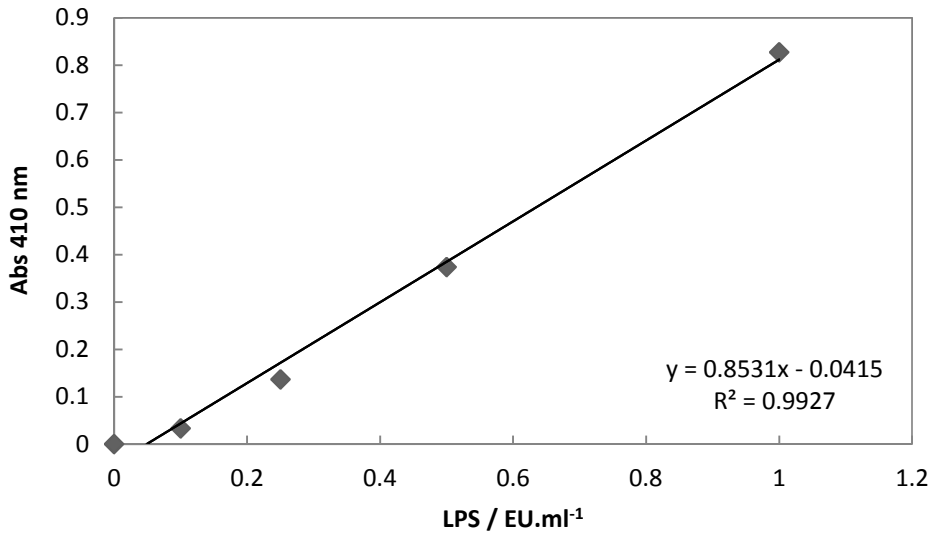

Figure 3.6: Calibration curve with linear fitting from *E. coli* LPS standards in commercial LPS colorimetric assay kit. Data points given as the mean values, n = 3.

3.3 Animal model protocol

3.3.1 Refinement of protocol

3.3.1.1 Refinement part A: Sham *vs.* caecal ligation and puncture *vs.* caecal ligation

The use of caecal ligation and puncture (CLP) as the gold-standard animal model in sepsis research has been discussed in **Chapter 1**. However, its use for measurement of sepsis biomarkers in the peritoneal cavity has so far been limited and no definitive procedure or sampling time intervals in this context have been determined. The initial protocol for identifying biomarkers in the abdominal environment correlating with abdominal sepsis as a translation to humans was therefore first optimised. Type of procedure was initially varied. Sham *vs.* caecal ligation and puncture (CLP) or caecal ligation alone (CL), were examined, as although CLP is described as the gold standard, it was considered that for peritoneal measurement of biomarkers it may be over sensitive compared to systemic serum measurement. Caecal ligation alone was tested as potentially representing a more sensitive change in biomarker at the sampling times. Sampling times of 6 hours and

24 hours were initially chosen based on the limited previous studies available and expected peak biomarker increases, with the expectation that lactate would increase in sepsis induced animals first at 6 hours, followed by TNFα, with *E. coli* predominantly raised at 24 hours. The initial protocol tested, refinement of protocol part A, is shown as a flow diagram in **Figure 3.7**. Three animals (male Wistar rats) were used in each of the three arms of the study of sham *vs.* CLP *vs.* CL at each of the two time points, totalling 18 animals. Three animals in each group were considered acceptable at this refinement stage to give adequate results to optimise the procedure without unnecessary sacrifice as discussed with the veterinary officer overseeing the work. The protocol used throughout is given in detail in the **Methods Section 2.2.1.2**.

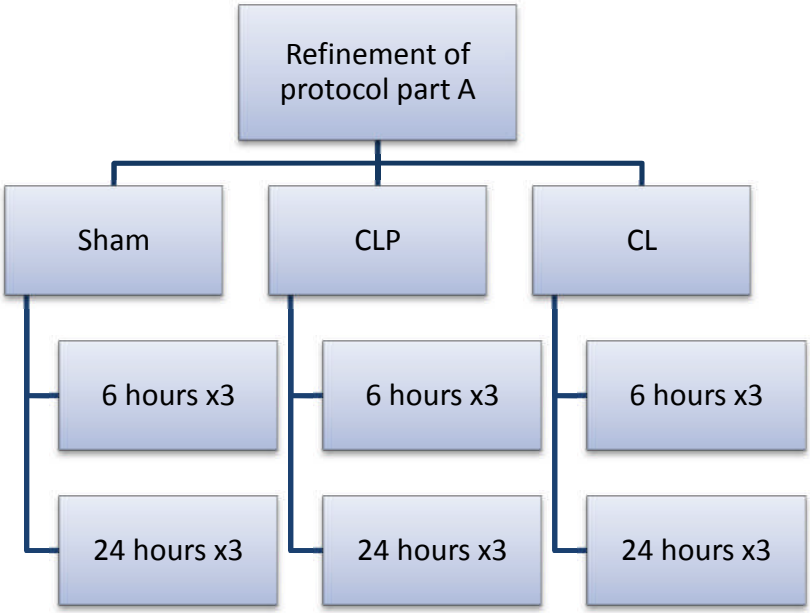

Figure 3.7: Flow diagram of refinement of protocol part A of animal biomarker sepsis model.

The results for lactate are shown in **Figure 3.8**. **Figure 3.8A** shows no significance between sham and CLP or sham and CL at 6 hours sampling after procedure using a Kruskal-Wallis statistical test with Dunn's post test. Data are shown as lactate in µmol calculated from the dilution of 5 ml saline peritoneal lavage used during

sampling. This 5 ml lavage dilution was subsequently factored into each biomarker measurement throughout the work. **Figure 3.8B** shows significance between sham and CLP at 24 hours, p = 0.0036. CL showed no significance compared to sham. The results were unexpected as we had anticipated that lactate would be highest in CLP or CL with most significance compared to sham animals at the earlier time point of 6 hours compared to 24 hours. It was observed that lactate levels were higher in all groups at 24 hours compared to 6 hours, but proportionally higher in CLP at 24 hours than sham or CL. Lactate biomarker rise from the ischaemic insult therefore is shown at a later time than expected, although this was still in agreement with the scant literature on animal models measuring lactate and the human data discussed in **Chapter 1.**

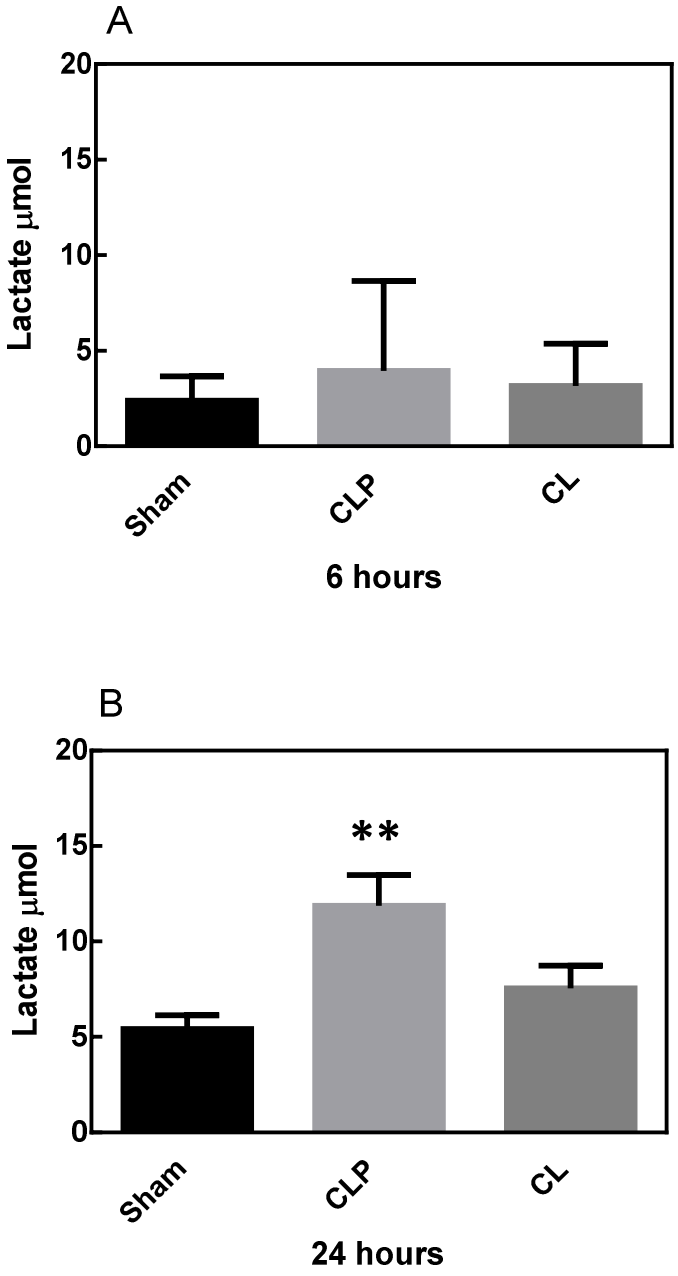

Figure 3.8: Lactate results from refinement of protocol part A. (A) Lactate at 6 hours. No significance between sham and CLP or CL. (B) Lactate at 24 hours. Significance between sham and CLP, p = 0.0036. Data are all mean ± S.D for n = 3. **, p < 0.01; Kruskal-Wallis with Dunn's post test.

Figure 3.9 shows the results of TNFα measurement at 6 and 24 hours for sham, CLP and CL groups. At 6 hours **(Figure 3.9A)** and 24 hours **(Figure 3.9B)** there were no significant differences between sham and CLP or sham and CL using Kruskal-Wallis with Dunn's post test. The CLP group showed higher TNFα levels than CL or sham

at both time points however, and would be expected to reach significance compared to sham when powered appropriately. Interestingly TNFα levels of CLP animals were highest at 6 hours compared to 24 hours although this was increased by one very large value in the CLP group at 6 hours on inspection of the raw data, as evidenced by the large standard deviation seen. This does correlate with the known pathophysiology of TNFα as an early released cytokine with peak rise at 2 hours post insult in one study (Oliver et al., 1993) and with a short half life. However studies in the literature have measured abdominal TNFα in animal models at varying time intervals between 2 - 72 hours with significance, and human studies show significance of TNFα abdominal measurement from 24 hours. Later sampling time points are likely to be more useful in translation to clinical practice where an anastomotic leak is commonly diagnosed on day five and clinically useful early measurement would demonstrate high biomarker levels on days 1-4. A trend of increasing biomarker over this period of time would also be more clinically relevant than a very early measurement in which biomarkers may be globally raised after an operative insult or very variable patient to patient, not necessarily progressing to a complication.

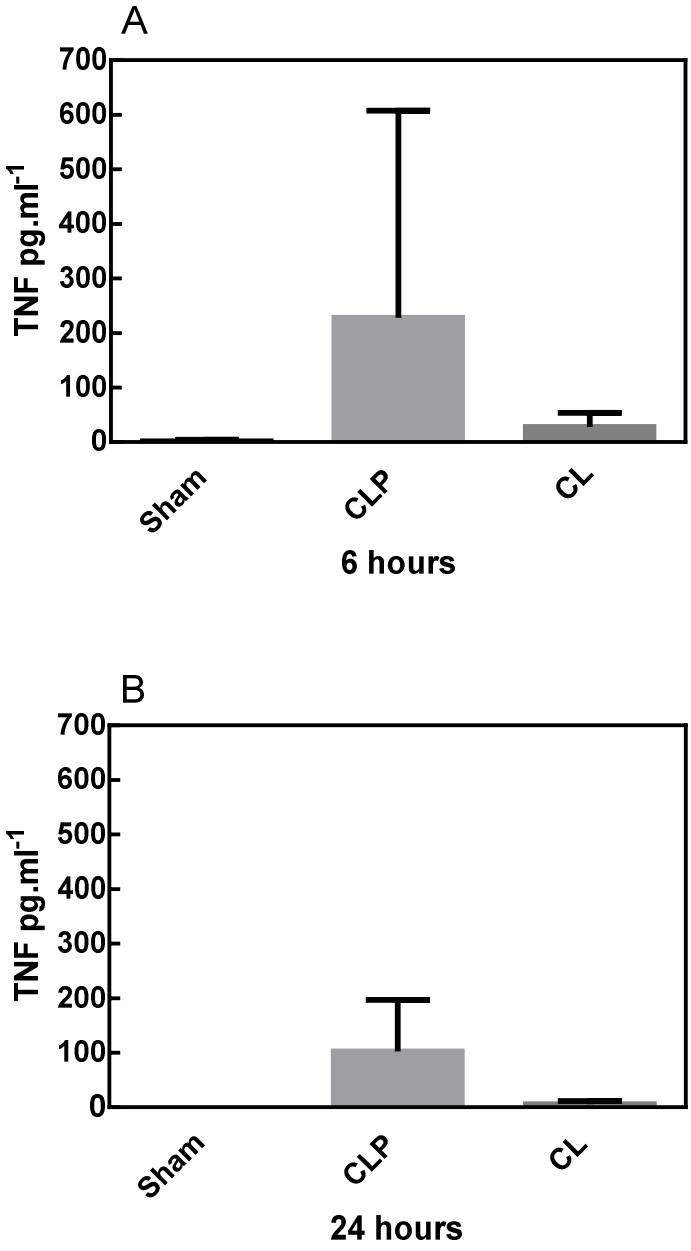

Figure 3.9: TNFα results from refinement of protocol part A. (A) TNFα at 6 hours. No significance between sham and CLP or CL. (B) TNFα at 24 hours. No significance between sham and CLP or CL. Data are mean ± S.D for n = 3. Kruskal-Wallis with Dunn's post test.

E. coli was not measured at either refinement stage A or B due to the difficulty in timely sourcing of an accurate commercial test outlined in **Section 3.2.3.** Based on lactate and TNFα results, sham *vs.* CLP was chosen for the final protocol as CL results for both biomarkers were only marginally higher than sham, particularly for

TNFα. From the provisional results the sampling time points were extended to greater than 24 hours as it appeared that lactate particularly may have peak concentrations later than first expected. With the use of drains explored in refinement of the protocol part B, multiple sampling time points would be feasible without increasing animal numbers and this was subsequently investigated.

3.3.1.2 Refinement part B: Use of drains

The second refinement of the animal sepsis model protocol, part B, explored the use of drains in the animals. This would allow an increased number of time points to be sampled without the requirement for increased animal numbers to be sacrificed and potentially give more meaningful comparison with the human drain fluid data. A flow diagram for the refinement part B is shown in **Figure 3.10**. Sampling time points were initially kept at 6 and 24 hours so direct comparison could be made with the samples from part A, ensuring the use of drains did not affect the results in any way. Three animals were again assigned to each group, totalling six animals as sampling would be performed at 6 and 24 hours on the same animals *via* their drains.

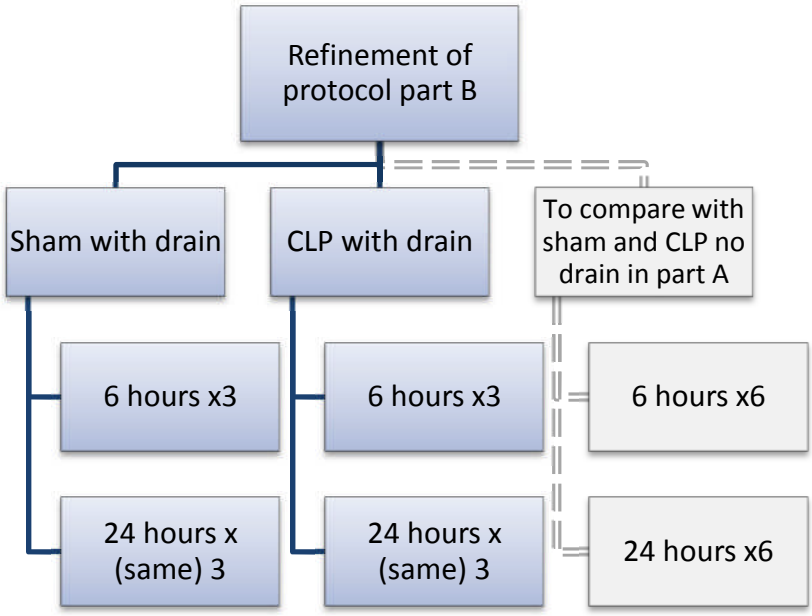

Figure 3.10: Flow diagram of refinement of protocol part B of animal biomarker sepsis model.

The procedure was carried out again as described in the **Methods Section 2.2.1.2**, with the addition before closure of the abdomen of a sterile Robinson's drain inserted through the abdominal wall into the abdominal cavity as used in humans. The drains were tunnelled through the subcuticular tissues to exit through the scruff of the rats to minimise biting/scratching of the drain and potential harm to the animal. They were then sutured in place and sterile tape was placed over the end of the drain to seal it. Initially two rats underwent drain insertion to assess feasibility, one after CLP and one after sham. The rats tolerated the drains well, with neither being able to access the drain position to chew or scratch it and appearing comfortable when observed in their home cages. The drain fluid sampling at relevant time points consisted of attaching a syringe to the drain, lavaging the abdominal cavity with up to 5 ml sterile saline and withdrawing back on the syringe to obtain the sample. Unfortunately both animals tolerated this poorly and were under undue distress, even before lavage could be carried out. The animals also appeared in pain during the attempted sampling despite the standard analgesia being given. Logistically the drain sampling was also very difficult and less than 0.5 ml of fluid could be obtained. For these reasons the use of drains was abandoned with no further animals undergoing this process.

3.4 Final animal model protocol

The final optimised animal model protocol used is shown as a flow diagram in **Figure 3.11**. As elucidated from the refinement in part A, sham *vs.* CLP was used. Unfortunately the use of drains was abandoned from assessment in part B, therefore the interval and number of sampling times was carefully considered to give the relevant data required without the unnecessary sacrifice of animals. Two sampling times were consequently chosen as 24 and 36 hours based on the previous animal and human literature and the results from the optimisation studies in part A. The subsequent comparison to human samples at which collection was daily from 24 hours was also considered. To again ensure use of the minimum number of animals required for statistically significant results, a power calculation

was performed by the named animal facility statistician, with 20 animals calculated as being required for each group for significance of biomarker results. Thus 80 animals in total were required for the final protocol. It should be noted that some groups include 21 animals due to the inclusion of data from the optimisation studies where stated.

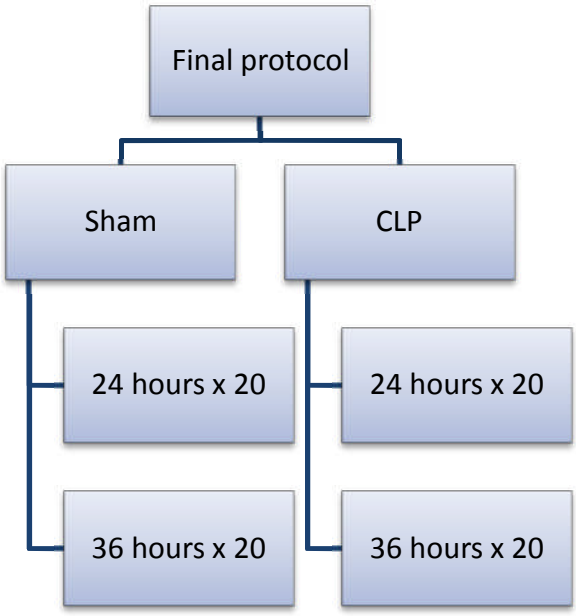

Figure 3.11: Flow diagram of optimised final animal biomarker sepsis model.

3.4.1 Lactate biomarker

Lactate levels in the abdominal fluid of sham and CLP animals were measured using the lactate colorimetric kit as before. Results at 24 and 36 hours are shown in **Figure 3.12**. Animals are shown as individual data points, with median values illustrated using the black line. The interrupted red line represents the cut off values for best combined sensitivity and specificity which is discussed later in **Section 3.4.5.** A Mann Whitney U non-parametric statistical test was used to compare groups in all cases unless stated. At both 24 hours **(Figure 3.12A)** and 36 hours **(Figure 3.12B)**, CLP lactate levels were significantly higher compared to sham, with maximum significance reached for each, therefore validating lactate as a useful biomarker in abdominal sepsis. In contrast to levels at 6 hours seen during

the refinement stages, the lactate levels at 24 and 36 hours were both higher and also relatively static, suggesting a lactate peak which continues for some time after an ischaemic insult and sepsis, presumably as a result of the ongoing pathological process. The difference between the sham and CLP medians at each time point is greater at 36 hours suggesting that lactate in sepsis does increase later than originally anticipated. The lactate level in a septic process may thus continue over time to diverge from sham levels that are marginally raised as a result of the normal operative insult, although as different animals were used at each time point, trends in individuals could not be evaluated. Using the animal model, lactate is therefore shown to be an excellent biomarker of sepsis.

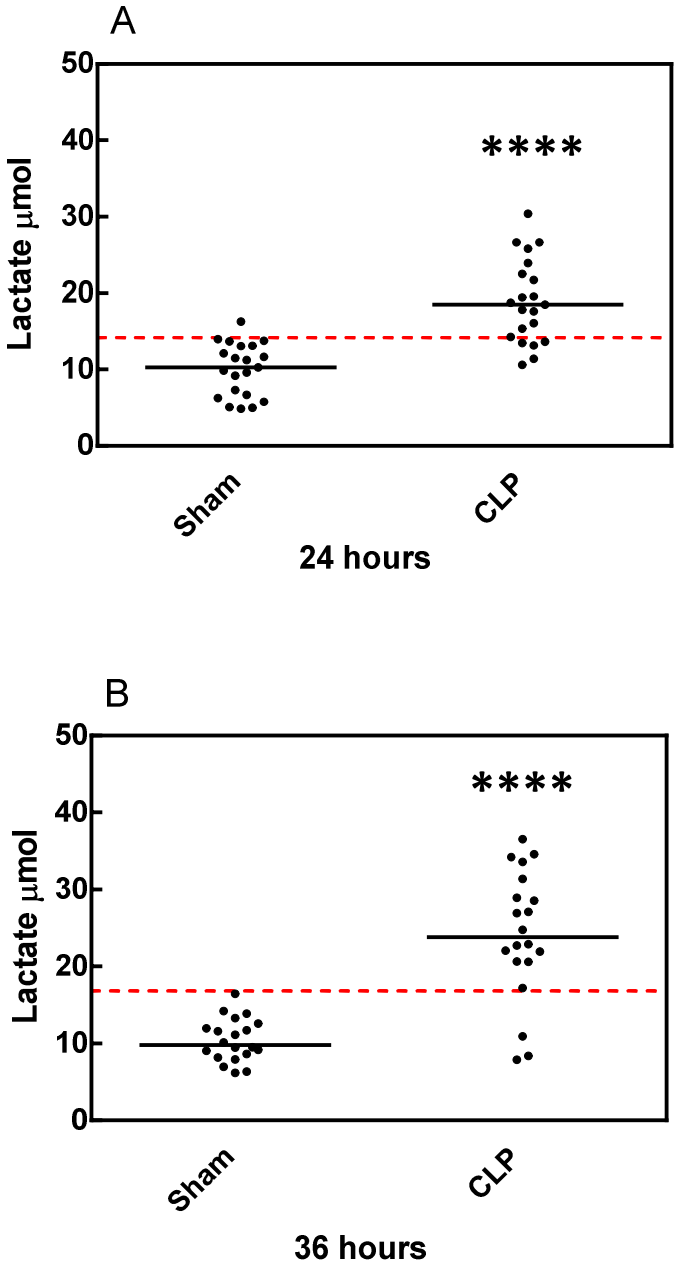

Figure 3.12: Lactate results from final animal model protocol. (A) Lactate at 24 hours, 21 animals per group. Significance between sham and CLP, p = <0.0001. Cut off value >14.12. (B) Lactate at 36 hours, 20 animals per group. Significance between sham and CLP, p = <0.0001. Cut off >16.85. Data are all individual points with median. ****, p < 0.0001; Mann Whitney U test

3.4.2 TNF biomarker

TNFα levels of sham and CLP animals were measured using the rat specific ELISA kit at 24 and 36 hours. **Figure 3.13** shows the results, with again median (black line) and cut off values (interrupted red line) included. TNFα levels were significantly higher in CLP animals compared to sham at 24 hours **(Figure 3.13A)** and 36 hours **(Figure 3.13B)**, demonstrating that TNFα as well as lactate is a good biomarker of abdominal sepsis shown by the model. TNFα at 36 hours was of greater significance than at 24 hours, despite the previously noted 6 hourly levels being higher. It was noted however that the 6 hour group included one very high result from the 3 animals which increased the mean and gave a large standard deviation, and so was unreliable to draw conclusions from. Using the powered data, TNFα appeared more significantly raised in CLP at 36 hours than 24 hours as was previously anticipated. There were a large number of very low TNFα values seen in both sham and CLP groups and at both time points which again raised the hypothesis of repeated measurements over time in an individual being more clinically meaningful than arbitrarily at one time point, as a trend in values may then be seen to increase from baseline.

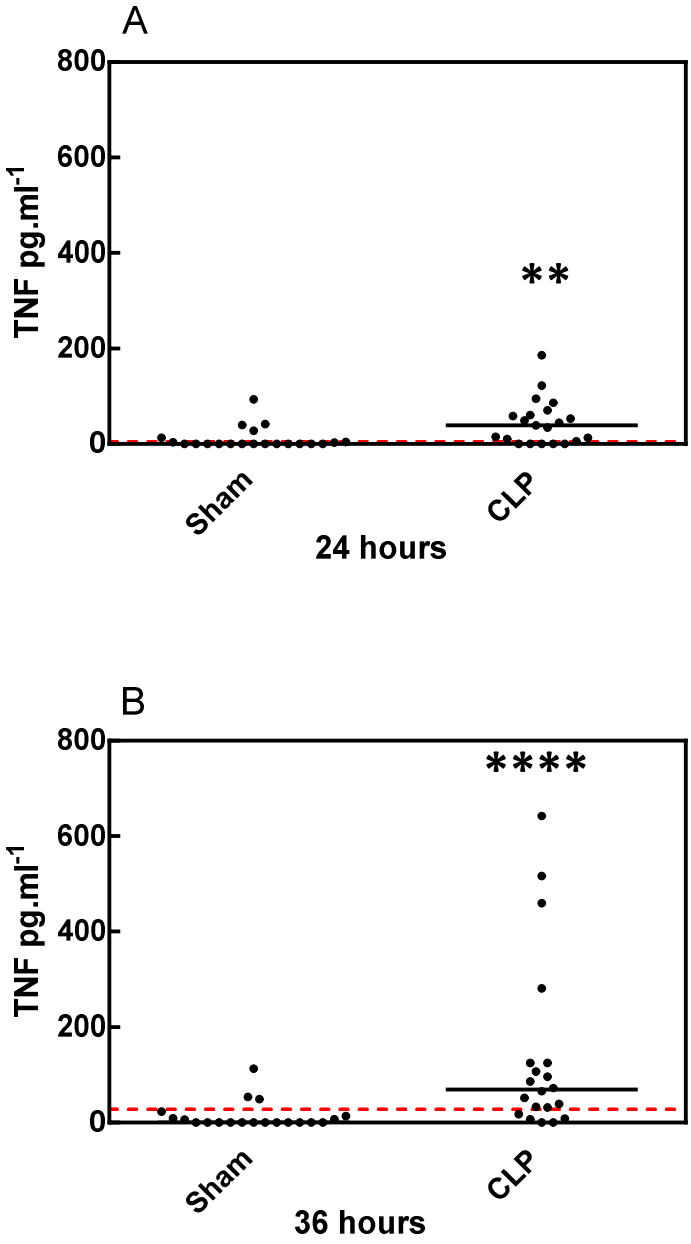

Figure 3.13: TNFα results from final animal model protocol. (A) TNFα at 24 hours, 21 animals per group. Significance between sham and CLP, p = 0.0018. Cut off value >4.953. (B) TNFα at 36 hours, 20 animals per group. Significance between sham and CLP, p = <0.0001. Cut off value >27.47. Data are all individual points with median. **, p < 0.01; ****, p < 0.0001; Mann Whitney U test.

3.4.3 *E. coli* biomarker

As there was no readily available or suitable commercial kit to measure *E. coli*, an LPS colorimetric kit was used with LPS a surrogate marker of *E. coli*, it being a component of the Gram-negative bacterial cell wall, as discussed in **Section 3.2.3.** The results of abdominal LPS measurement in sham *vs.* CLP animals at 24 and 36 hours are shown in **Figure 3.14**. Statistical tests used and data presented are as used for lactate and TNFα. In similarity to the other biomarkers, LPS was significantly higher in CLP compared to sham at both time points, validating its use as a biomarker for abdominal sepsis with potential clinical translation to humans. Greater significance was seen at 24 hours compared to 36 which was unexpected, although only marginally greater, and the CLP median at 36 hours was higher than that at 24 hours. Due to the difficulty in sourcing a suitable bacterial test, LPS was not measured at 6 hours during the optimisation stages and so was not available for comparison although based on knowledge of the pathological sepsis process, detectable *E. coli*/LPS would be a late event after frank perforation enabling luminal contents into the abdominal cavity. The time points measured are therefore likely to be representative and are in any case both significant.

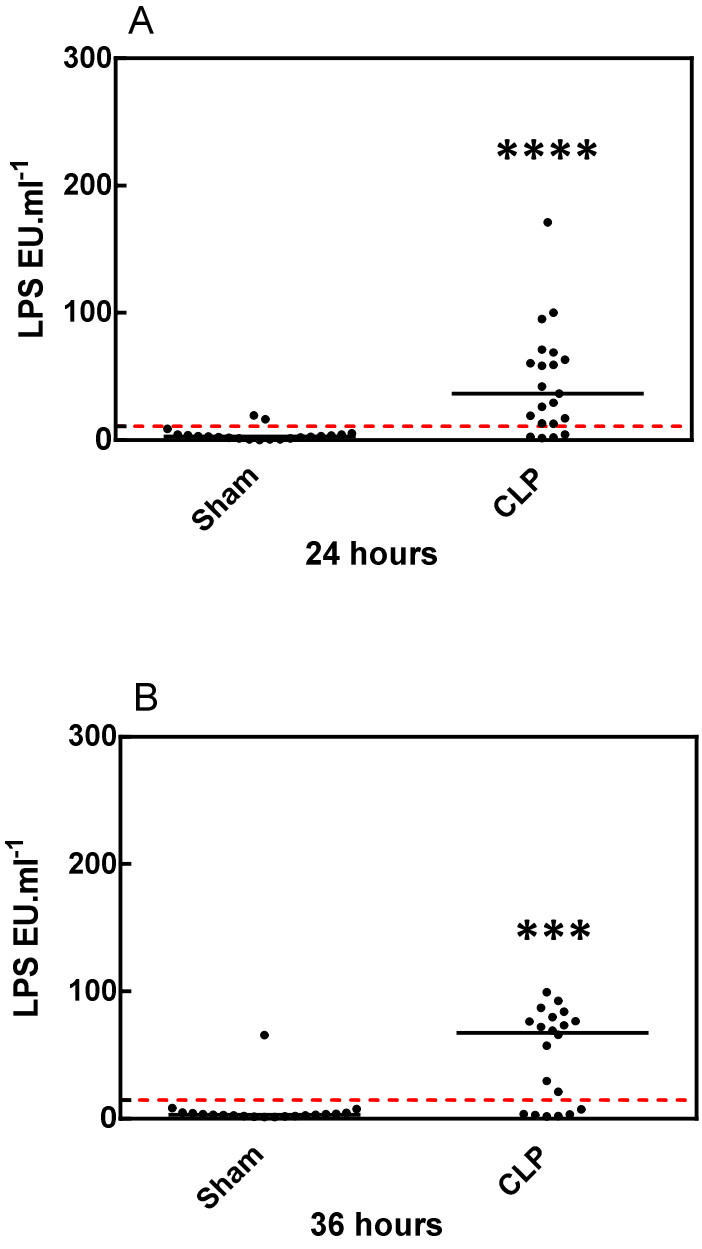

Figure 3.14: LPS (*E. coli*) results from final animal model protocol. (A) LPS at 24 hours, 21 animals per group. Significance between sham and CLP, p = <0.0001. Cut off value >10.79. (B) LPS at 36 hours, 20 animals per group. Significance between sham and CLP, p = 0.0001. Cut off value >14.69. Data are all individual points with median. ***, p < 0.001; ****, p < 0.0001; Mann Whitney U test.

3.4.4 Photographs of sham and CLP animal models at re-laparotomy

The biomarker results have been shown, with all three tested biomarkers showing significance at both time points in CLP *vs.* sham and therefore all demonstrating suitability as biomarkers of abdominal sepsis. Representative photographs of the gross pathophysiological processes induced in the model are shown in **Figure 3.15**. In **Figure 3.15A** the caecum appears healthy and normal at re-laparotomy after 36 hours in a sham model where the bowel was removed from the peritoneal cavity and immediately replaced during operation. **Figure 3.15B** shows a picture of the abdominal contents after 24 hours in a CLP animal. The caecum is clearly abnormal and necrotic, both in the abnormal purple colour seen and a gross increase in size. The corruption is still relatively localised however, with small bowel appearing normal (superior to the caecum in the photograph) and no overt peritoneal cavity pus or faecal matter. **Figure 3.15C** is of a CLP animal after 36 hours at re-laparotomy. There is now evidence of gross generalised sepsis, with necrosis of the caecum as before as well as involvement and contamination of the small bowel with the caecum adherent to it. The images are not dissimilar to those of patients with gross abdominal corruption (see anastomotic leak, **Figure 1.2**) and thus the animal model chosen does appear to accurately represent human abdominal sepsis in order to translate to patient data as the literature suggests.

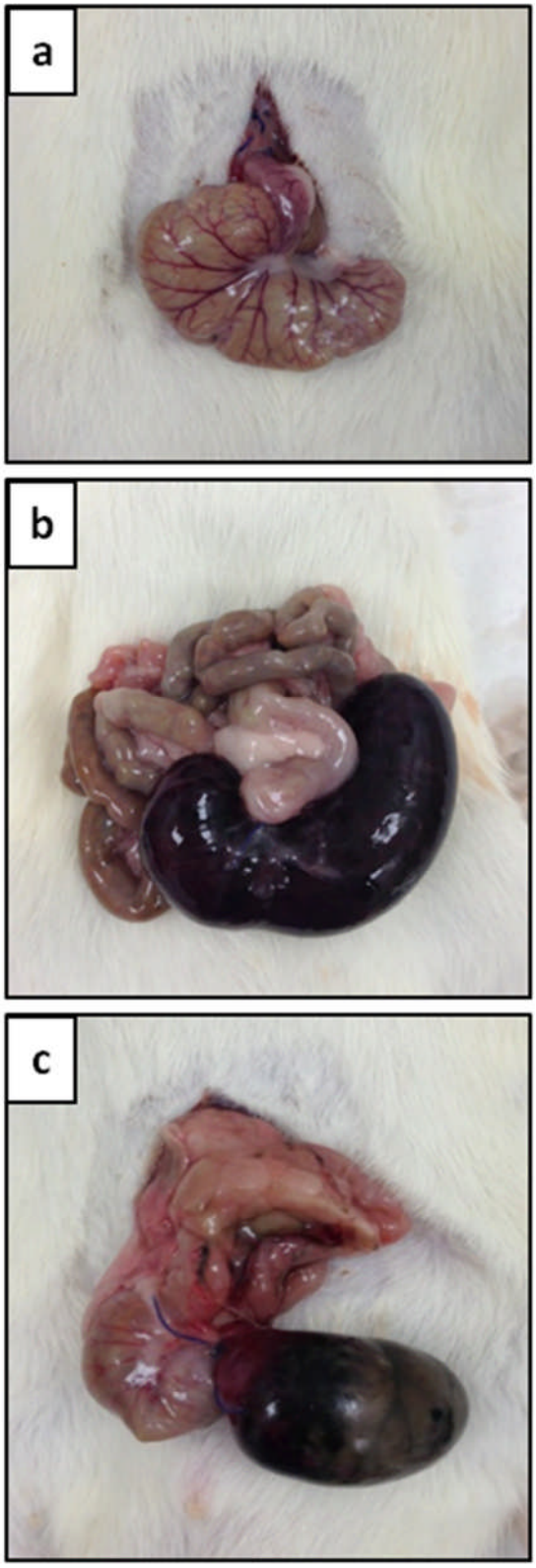

Figure 3.15: Photographs at re-laparotomy in animal model. (A) Sham at 36 hours, the bowel looks normal and healthy. (B) CLP at 24 hours, the necrotic focus at the caecum is well visualised. The small bowel appears unaffected. (C) CLP at 36 hours. The necrotic ligated caecum is again present, which has now adhered to the small bowel (shown detached). There is evidence of gross septic insult involving the whole bowel.

3.4.5 Receiver operating characteristic analysis

Receiver operating characteristic (ROC) analysis was developed in the 1950's for signal detection analysis in technical sciences and has since found increasing use in the development of clinical laboratory tests (Greiner et al., 2000). ROC curves are used as a measure of diagnostic accuracy of markers or tests either independently or in combination, and are presented as a plot of sensitivity as the y-coordinate versus 1-specificity or false positive rate as the x-coordinate, for each of the possible cut off values (Zweig and Campbell, 1993). The cut off value used depends upon the individual requirements of the test as higher cut off values lead to decreased sensitivity but increased specificity and vice versa. The area under the curve (AUC) is a combined measure of sensitivity and specificity. AUC is a measure of the overall performance of a diagnostic test and is interpreted as the average value of sensitivity for all possible values of specificity. A value of 0.5 (50%) shows no predictive ability, with a value of 1.0 (100%) indicating perfect accuracy. There is evidence to suggest human and non-human *i.e.* animal subject ROC curves are very similar, although this is largely based on psychological studies such as memory research (Alsop, 1998). For the purposes of this work, comparison of actual biomarker levels in the animal model are unlikely to directly translate to human patients, meaning data such as cut off points are not strictly useful. However, as a comparative indicator between each biomarker and combination of biomarkers ROC analysis has a role in demonstrating how accurate and valid each biomarker has the potential to be in the clinical setting.

ROC curves for all three biomarkers evaluated at each of the two time points are shown in **Figure 3.16**. The respective AUC values are shown for each. All the AUC values are relatively high, showing that each biomarker at the sampling times measured has the potential for high diagnostic accuracy in a test for sepsis. The highest AUC value was 0.9229, shown in **Figure 3.16A** for lactate at 24 hours suggesting this biomarker and time point would give the optimum discriminatory power. Lactate at 36 hours showed the second highest AUC at 0.8975 **(Figure**

3.16B), thus lactate is shown to be the most accurate biomarker overall as expected from the previous data in **Section 3.4.1**. The lowest AUC was 0.7653 in TNFα at 24 hours **(Figure 3.16C)**. This was however still moderately high and potentially useful in clinical translation.

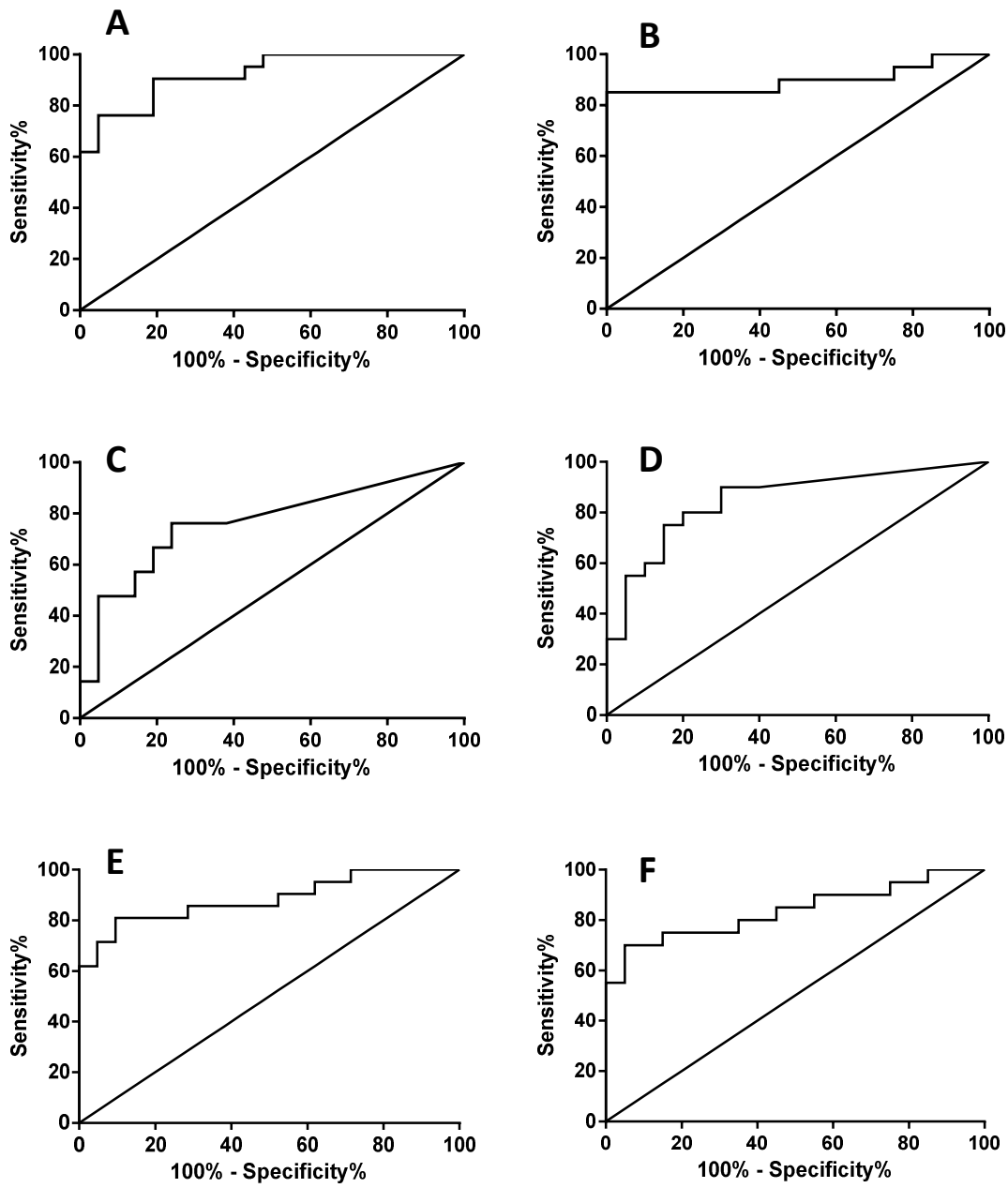

Figure 3.16: ROC curves for lactate, TNFα and LPS (*E. coli*) biomarkers at 24 and 36 hours in animal sepsis model. The area under the curve (AUC) value is given. (A) Lactate 24 hours, AUC = 0.9229. (B) Lactate 36 hours, AUC = 0.8975. (C) TNFα 24 hours, AUC = 0.7653. (D) TNFα 36 hours, AUC = 0.8500. (E) LPS 24 hours, AUC = 0.8844 (F) LPS 36 hours, AUC = 0.8375.

Table 3.1 shows the paired optimal sensitivity and specificity (%) for each biomarker at each time point, as well as the respective cut off values, standard error and 95% confidence interval. Analysis of combinations of biomarkers in pairs and as a combination of all three was also derived. Lactate alone gave the highest specificity at both time points, 95.24% at 24 hours and 100% at 36 hours. In a clinical application, the specificity of a diagnostic test for anastomotic leak and sepsis would be considered more important than sensitivity as the ability to correctly exclude patients without anastomotic leak and sepsis, and therefore not subject them to a reoperation or intervention needlessly, is of principle concern. A relatively low sensitivity would be acceptable as patients with initially false negative results would be subsequently picked up on repeated testing and treated. The highest specificity with any biomarker combination was 95% seen with lactate and LPS at 36 hours, with moderately high sensitivity at 85%. The advancing technology of biosensors in multi-array sensing, *i.e.* the ability to measure a number of biomarkers simultaneously on one chip, lends itself to use for this type of application.

Table 3.1: Combined ROC curve data analysis for individual and combined biomarkers at 24 and 36 hours. Included values are cut off values, sensitivity, specificity, standard error and 95% confidence interval (CI).

Time Interval	Biomarker	Cut off value	Sensitivity (%)	Specificity (%)	Std Error	95% CI
24 hours	Lactate	>14.2	76.19	95.24	0.0929	0.580 to 0.944
	TNF	>4.953	76.19	76.19	0.0929	0.580 to 0.944
	LPS	>10.79	80.95	90.48	0.0857	0.642 to 0.978
	Lactate/TNF	>14.2 and >4.953	90.48	71.43	0.0641	0.779 to 1.030
	Lactate/LPS	>14.2 and >10.79	95.24	85.71	0.0465	0.861 to 1.043
	TNF/LPS	>4.953 and >10.79	90.48	66.67	0.0641	0.799 to 1.030
	Lactate/TNF/LPS	>14.2, >4.953, >14.69	95.24	61.90	0.0465	0.861 to 1.043
36 hours	Lactate	>16.85	85	100	0.0779	0.697 to 1.003
	TNF	>27.47	75	85	0.0945	0.565 to 0.935
	LPS	>14.69	70	95	0.102	0.499 to 0.901
	Lactate/TNF	>16.85 and >27.47	85	85	0.0798	0.694 to 1.007
	Lactate/LPS	>16.85 and >14.69	85	95	0.0798	0.694 to 1.007
	TNF/LPS	>27.47 and >14.69	85	80	0.0798	0.694 to 1.007
	Lactate/TNF/LPS	>16.85, >27.47, >10.79	85	80	0.0798	0.694 to 1.007

3.5 Discussion

The data presented in this chapter show the optimisation of an animal model of sepsis in order to validate potential biomarkers of anastomotic leak and sepsis. Three biomarkers were chosen from the available literature as having potential to be raised in an anastomotic leak and sepsis pathological course at three different time points, and with feasibility to be the target of a biosensor application; lactate, TNFα and *E. coli*.

Initially, existing commercial assays to measure each of the biomarkers were sourced. There was no suitable available assay for *E. coli* and therefore a kit for LPS used as a surrogate marker to *E. coli* was utilised. The animal protocol used was first optimised as there was little available data on the measurement of biomarkers in abdominal cavity fluid in existing animal models of sepsis. The model was therefore first optimised to sham (control) animals *vs.* caecal ligation and puncture (CLP) or caecal ligation (CL) alone. Caecal ligation and puncture showed significance in biomarkers compared to sham and so was used in the final animal model protocol, with CL discounted. The use of drain insertion was explored in order to increase the sampling time points without increasing animal number. Unfortunately this was not tolerated by the animals and did not yield enough abdominal fluid sample to be feasible. The final animal model therefore comprised sham *vs.* CLP at two sampling times of 24 and 36 hours based on the previous animal and human literature and results from the optimisation studies. Twenty animals were required in each group as given by a power calculation. There was a statistically significant difference between sham and CLP at each of the two time points sampled for all of the biomarkers tested ($p < 0.05$). Lactate showed the most significant differences at both 24 and 36 hours ($p < 0.0001$).

Receiver operating characteristic analysis was performed to assess potential diagnostic accuracy of each biomarker, although caution in drawing conclusions in

relation to translation to human clinical data was exercised. Area under the curve (AUC) values were relatively high for all biomarkers (AUC > 0.7653) proving their suitability in a diagnostic application. Lactate at 24 hours demonstrated the greatest discriminatory power with the highest AUC value of 0.9229. Using combined sensitivity and specificity values lactate again demonstrated the highest specificity of 95.24% at 24 hours and 100% at 36 hours. When in combination lactate together with LPS showed the highest specificity of 95% at 36 hours sampling time, with retained moderately high sensitivity at 85%. All three biomarkers tested therefore were shown using an animal model to be suitable candidates for an early diagnostic test for anastomotic leak and sepsis.

Chapter 4:

Amperometric biosensors for the detection of lactate

Chapter 4. Amperometric biosensors for the detection of lactate

4.1 Introduction

Lactate biosensors are commonly enzymatic, and utilise immobilised lactate dehydrogenase or lactate oxidase (LOx) (Romero et al., 2008). The oxidases are the most widely used family of enzymes for electrochemical applications, imparting high selectivity (Boccola et al., 2011). As previously discussed in **Section 1.9.1** lactate oxidase catalyses the conversion of lactate to pyruvate and hydrogen peroxide, of which the hydrogen peroxide product can be detected amperometrically *via* an oxidative or reductive current signal (Lipska et al., 2006). The use of amperometry is ideal for a lactate biosensor as the enzymes catalysing the lactate reaction to form hydrogen peroxide are readily available.

The amperometric lactate biosensors fabricated in this chapter all utilised lactate oxidase immobilised onto a polymer surface. Two distinct methods of construction were evaluated using techniques developed for the fabrication of glucose biosensors. The first comprised polyethyleneimine (PEI) polymer immobilised onto a carbon electrode, before lactate oxidase was added directly *via* electrostatic binding (Pchelintsev and Millner, 2008, Pchelintsev et al., 2009). Redox mediators were added or electrodes with commercially pre-impregnated mediators were used. This scheme is shown in **Figure 4.1**. The second surface was constructed using an electro-deposited co-polymer of aniline and 2-aminobenzylamine (P(ANI/2-ABA)) onto gold and carbon electrodes before immobilisation of biotinylated lactate oxidase *via* NeutrAvidin onto biotin-functionalised pendant amine groups of the copolymer (**Figure 4.2**). This chapter describes the work and resulting data from investigations into the most favourable sensing surface for lactate biosensors, and subsequent optimisation and validation of the chosen

sensor in real patient drain fluid samples compared to a commercial enzyme-based assay. Methods used for characterisation and interrogation of the biosensor include cyclic voltammetry, chronoamperometry and colorimetric testing.

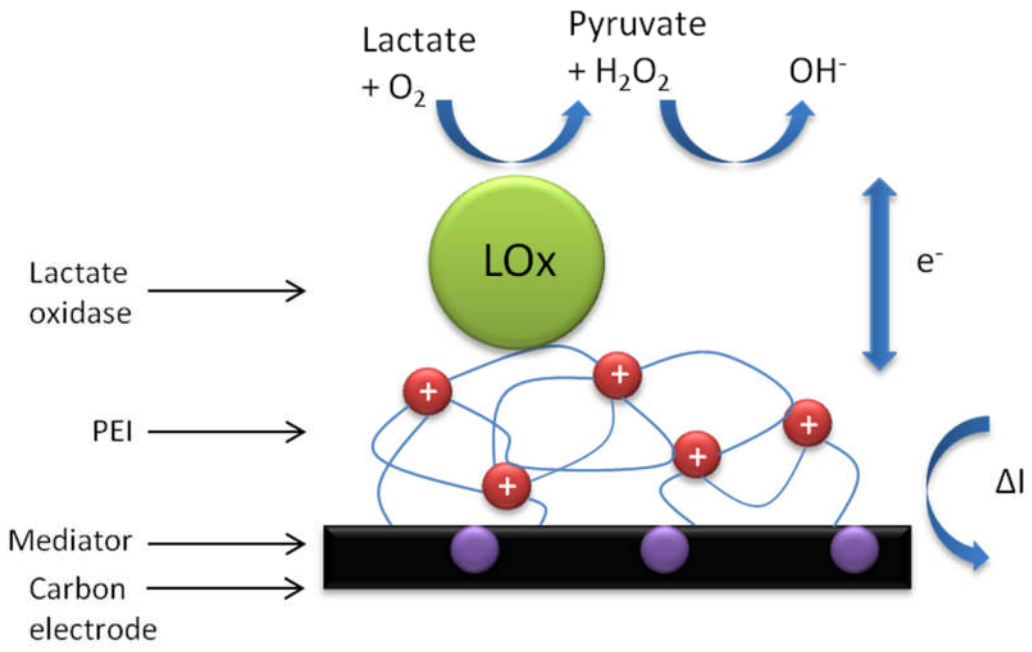

Figure 4.1: Schematic showing immobilisation of lactate oxidase onto a PEI polymer surface on a carbon electrode with presence of mediator. The reaction mechanism is also shown.

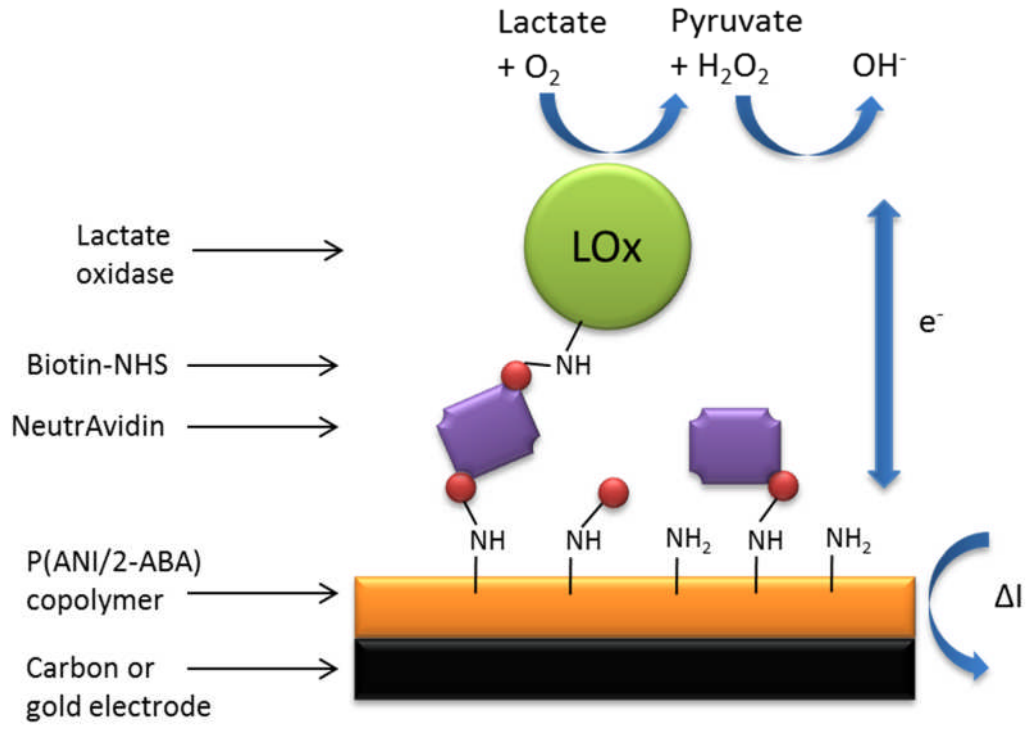

Figure 4.2: Schematic showing immobilisation of biotinylated lactate oxidase onto a biotinylated P(ANI/2-ABA) polymer surface *via* NeutrAvidin with a gold or carbon electrode. The reaction mechanism is shown.

4.2 Cobalt phthalocyanine mediated biosensors

The initial methodology used for fabrication of the lactate biosensor utilised cobalt phthalocyanine (CoPc) mediator with immobilised PEI polymer and lactate oxidase onto screen printed carbon electrodes. CoPc is a common mediator for the oxidation of thiols and hydrogen peroxide, the product of interest, which acts to reduce the working potential required by shuttling electrons to the electrode surface, thus reducing or eliminating interfering redoxing compounds. The method described, of surface doping of CoPc by simple adsorption rather than the standard blending into the electrode surface layers during screen printing, has been shown to result in lower amounts required, reducing cost and manufacturing time whilst maintaining electrode sensitivity for measurement of glucose and acetylcholine (Pchelintsev and Millner, 2008).

The polymer PEI was used as it has numerous secondary amine groups for binding to the electrode surface and for enzyme immobilisation which may be covalent or electrostatic. In this case PEI was ideal due to its strong positive charge in aqueous solution enabling subsequent electrostatic binding of the negatively charged (neutral pH) lactate oxidase with high avidity. Optimisation of PEI molecular weight and adsorption time has previously been evaluated (Pchelintsev et al., 2009), as well as a new approach described for PEI immobilisation. This used a one-step electro-oxidative covalent coupling to the carbon electrode surface based on its random coil structure anchoring the molecule but also leaving free amine groups distal to the surface for further binding (Pchelintsev and Millner, 2008). Moreover, PEI is inexpensive and readily commercially available, and screen printed carbon electrodes also confer low cost and potential for mass production. The methodology used describes CoPc doping of the electrode surface through simple hydrophobic adsorption during incubation at 50 °C, before electro-polymerisation of PEI using cyclic voltammetry and electrostatic binding of lactate oxidase to construct the complete lactate biosensor.

4.2.1 Cyclic voltammetry mediated electro-deposition of polymer onto the screen printed carbon electrode

After CoPc doping, screen printed carbon electrodes were first incubated in a diethylene glycol butyl ether solution containing 10 $mg.ml^{-1}$ PEI (MW 750 kDa) in dH_2O for 5 min to allow equilibration of the PEI between the electrode surface and the bulk solution. PEI was then covalently bound to the screen printed carbon electrode surface using cyclic voltammetry (CV). The electrodes were mounted to an electrochemical cell also containing 10 ml of 100 mM $LiClO_4$ as supporting electrolyte, and three CV scans were run from 0.1 V to 0.9 V at scan rate 100 $mV.s^{-1}$. The modified electrodes were then rinsed in ethanol, before incubation for 3 min in ethanol and 3 min in dH_2O to remove any weakly bound PEI. **Figure 4.3** shows a typical cyclic voltammogram of electro-polymerisation of PEI onto a screen printed carbon electrode *vs.* an external Ag/AgCl reference electrode. The three successive scans **(Figure 4.3 a-c)** show each scan cycle decreasing in current as each layer of PEI formed on the surface sequentially reduced the charge transfer across the electrode with surface passivation.

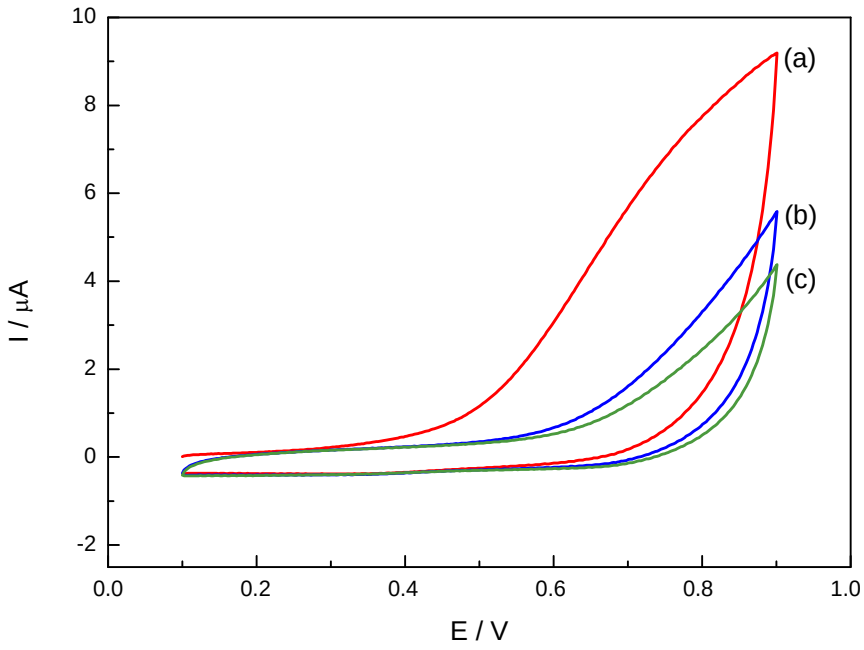

Figure 4.3: Successive cyclic voltammograms showing electro-polymerisation of PEI onto a CoPc modified screen printed carbon electrode. Scans were performed from 0.1 V to 0.9 V at a scan rate of 100 $mV.s^{-1}$ with the potential applied *vs.* a Ag/AgCl reference electrode. Scans (a), (b), and (c) show the sequential decrease in current as polymer is formed on the surface.

4.2.2 Chronoamperometric interrogation of CoPc/PEI modified biosensors

For the immobilisation of lactate oxidase, the CoPc/PEI modified electrodes were incubated in a 1 $mg.ml^{-1}$ solution in PBS, pH 7, for 1 h. They were next rinsed briefly with dH_2O and immersed in PBS, pH 7.0, before incubation a further four times in PBS, pH 7.0, for 5 min to remove weakly bound enzyme. Once the sensors were fully constructed, they were interrogated using chronoamperometry driven by GPES Autolab software. A three electrode configuration was used as described in **Section 2.2.3**, with screen printed carbon working electrodes, and an external platinum counter electrode and Ag/AgCl reference electrode, in a PBS electrolyte medium. The electrodes were first interrogated with spiked additions of hydrogen peroxide into the electrolyte in order to observe electron transfer in isolation from the enzymatic mechanism (**Figure 4.4**). Lactate was then spiked into solution, to test the system in entirety (**Figure 4.5**).

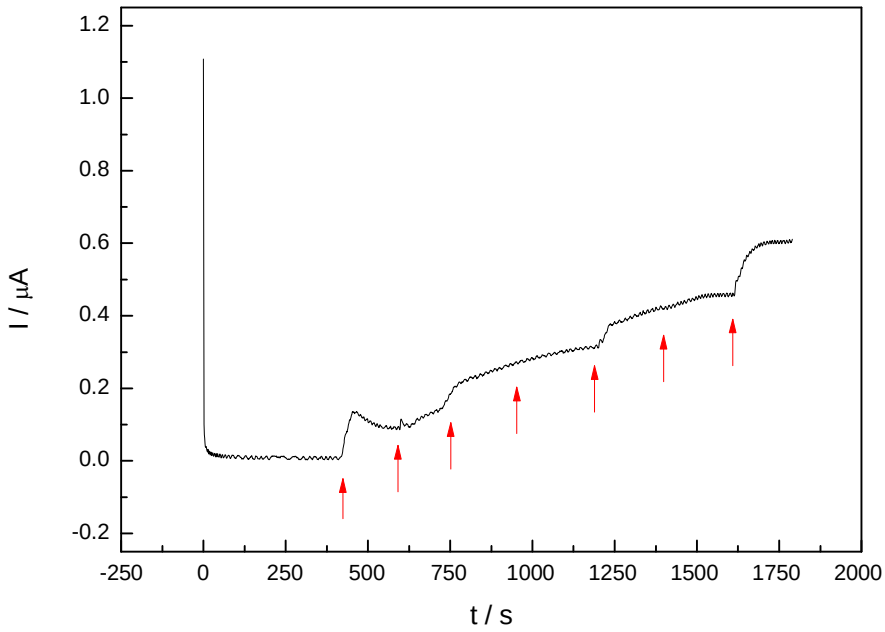

Figure 4.4: Time-current plot for one CoPc/PEI modified electrode after immobilisation of 1 mg.ml^{-1} LOx upon successive additions of 0.1 mM H_2O_2 (shown by arrows) in PBS, pH 7. Current was measured at +0.6 V with constant stirring.

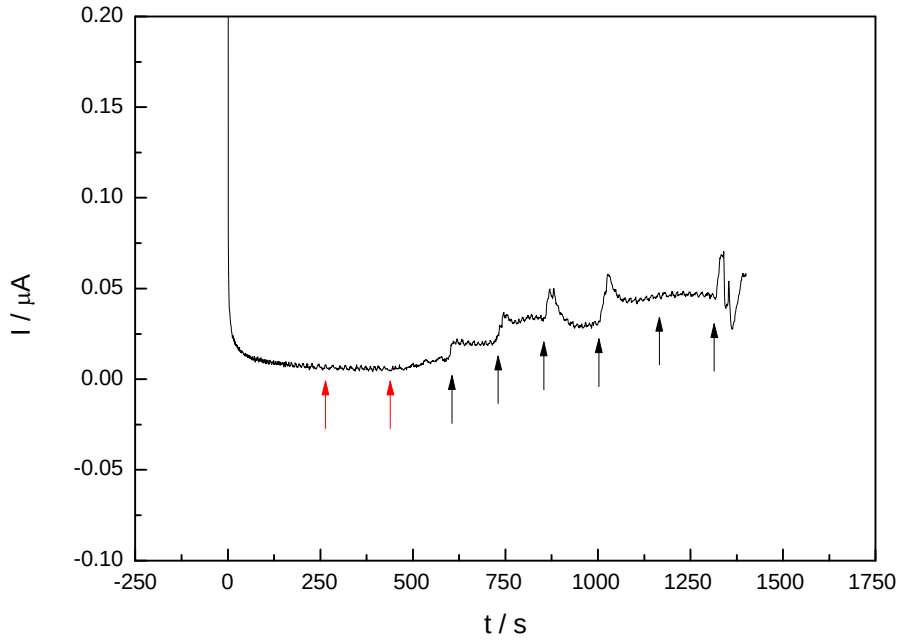

Figure 4.5: Characteristic time-current plot for one CoPc/PEI modified electrode after immobilisation of 1 mg.ml^{-1} LOx upon successive additions of 0.1 mM lactate (red arrows) and 0.3 mM lactate (black arrows) in PBS, pH 7. Current was measured at +0.6 V with constant stirring.

Interrogation with hydrogen peroxide additions did give appropriate corresponding increases in current showing that electron transfer across the electrode was occurring. However, this was generally seen to be an inconsistent, erratic response, and was very poorly reproducible between electrodes. This is reflected in the data shown as only single electrode measurements. Spiked additions of lactate during interrogation did not show any amperometric response in any electrode tested. The variability between the traces generated was also again very high and inconsistent. To attempt to increase enzyme sensitivity, CoPc/PEI modified electrodes were incubated with a range of lactate oxidase concentrations (1 mg.ml^{-1} to 10 mg.ml^{-1}), and interrogated with a range of lactate additions (0.1 mM to 5 mM). **Figure 4.6** shows a time-current plot for an electrode incubated with 5 mg.ml^{-1} lactate oxidase and interrogated with spiked additions of 1 mM lactate. There was some amperometric response as lactate was added, but not uniformly in

order to generate a calibration curve, and not reproducibly using other electrodes. Other electrodes tested for the ranges given gave no response (data not shown).

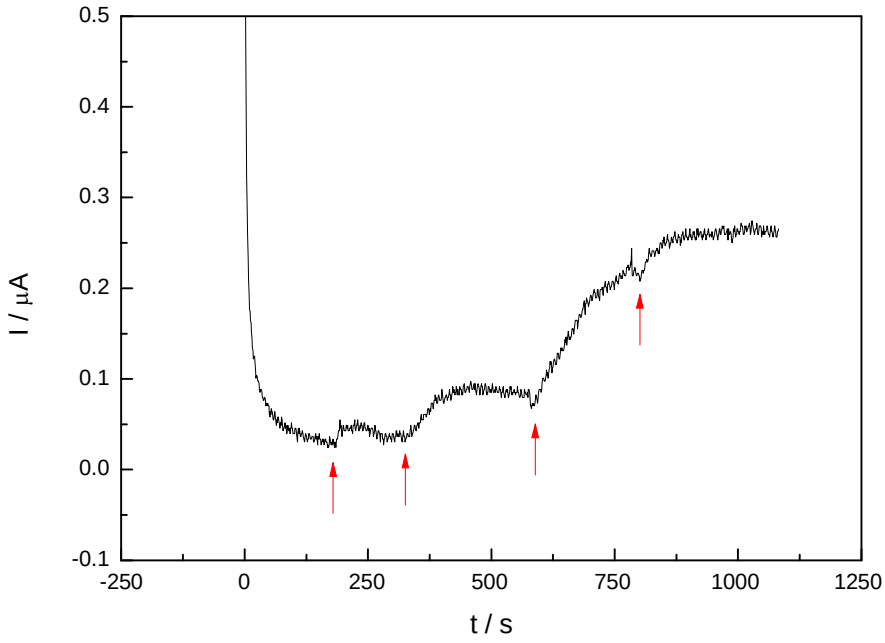

Figure 4.6: Time-current plot for one CoPc/PEI modified electrode after immobilisation of 5 mg.ml^{-1} LOx upon successive additions of 1 mM lactate (shown by arrows) in PBS, pH 7. Current was measured at +0.6 V with constant stirring.

As there had been a degree of direct amperometric response to hydrogen peroxide it appeared that the enzyme component of the biosensor was not functioning, thus accounting for the inconsistent and poor results with lactate interrogation. Two hypotheses were considered. First, that the enzyme may not have bound to the electrode during its incubation, potentially as a result of the methodology being reliant on relatively weak electrostatic binding. Second, that the enzyme itself may have suboptimal activity. The activity of the enzyme was believed to be the fundamental issue to first be addressed before considering other biosensor construction strategies using LOx as the same problems would occur. Therefore, to first determine viability of the lactate oxidase enzyme, a colorimetric assay was performed in order to test LOx function in isolation from the electrical components of the system.

4.3 Colorimetric assay to test activity of lactate oxidase

The colorimetric assay methodology used to test functionality of lactate oxidase was kindly provided by Dr Timothy Gibson of ELISHA systems Ltd. (personal communication) based on methods described in the literature (Vojinović et al., 2004). The protocol was followed as described in the **Methods** section. Hydrogen peroxide generated by oxidation of lactate catalysed by lactate oxidase was reduced by horseradish peroxidase (HRP) which subsequently co-oxidised 4-aminoantipyrine (4-AAP) and phenol-4-sulphonic acid (PSA) producing strongly coloured quinone-imine dye. The colour intensity was directly proportional to the initial lactate concentration, which was detected by spectrophotometry at 485 nm. Using this application the viability and activity of the lactate oxidase enzyme in isolation was assessed.

Figure 4.7 shows the lactate calibration curve for the colorimetric assay using lactate oxidase. The data showed excellent linear fit and reproducibility between tests. From these results it was concluded that there was adequate activity of the lactate oxidase enzyme, at least when in isolation from the biosensor system. The poor success of the CoPc/PEI/LOx lactate biosensor in response to lactate was thus potentially due to weak binding of the enzyme to the working electrode. Therefore, other methodologies for immobilisation of the enzyme that featured stronger binding techniques were next considered.

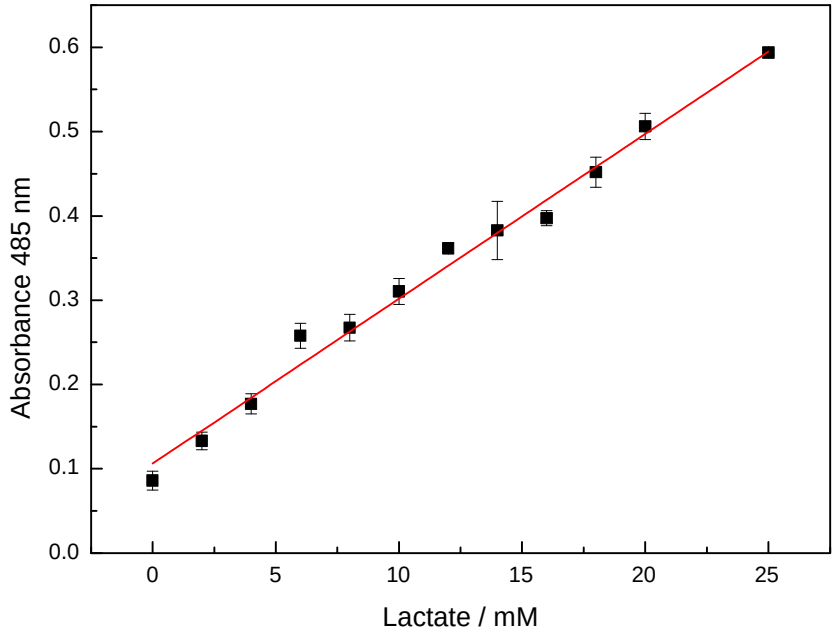

Figure 4.7: Calibration curve from the colorimetric assay for detection of lactate using lactate oxidase in the presence of HRP, 4-AAP, and PSA. Linear fitting of mean ± S.D (n = 10) with ( ) linear regression line of best fit.

4.4 Biotin-Avidin constructed biosensors

Avidin is a glycoprotein found in its native form in egg white. It is tetrameric, with four identical subunits with which to bind biotin with high affinity and specificity. The dissociation constant (K_d) is in the order of 10^{-15} M, and thus is one of the strongest protein-ligand non-covalent bonds known to date (Wilchek et al., 2006). Synthetic avidin is available as modified forms of native avidin, such as NeutrAvidin which is a deglycosylated version and shows reduced non-specific binding. Since its discovery in the 1970's, the biotin-avidin complex has been exploited in many biological applications (Kresge et al., 2004, Guesdon et al., 1979). Developments including the ability to biotinylate antibodies and other surfaces has consequently rendered it an important method of immobilisation for biotechnological applications (Wilchek et al., 1986).

A biotin-avidin system was therefore employed to improve the enzyme immobilisation step in sensor construction, as enzyme immobilisation to the electrode surface would be more definitive. As shown in **Figure 4.2**, both the enzyme and the electrode surface were biotinylated before NeutrAvidin was applied to the sensor surface to bind both biotin molecules, thus forming a robust organised layer. The electrode surface was first coated with a conducting co-polymer of aniline and 2-aminobenzylamine (P(ANI/2-ABA)) using CV, to permit subsequent binding of NHS-biotin to the free pendant amine groups. This technique has previously been used in the Millner laboratory for construction of impedance immunosensors and reviewed for use with amperometric biosensors (Millner et al., 2009).

4.4.1 Cyclic voltammetry mediated electro-deposition of copolymer onto gold and screen printed carbon electrodes

A 1:1 monomer mix of aniline and 2-ABA was made to a concentration of 100 mM each in 1 M HCl. This was electro-polymerised onto screen printed carbon electrodes and custom-made gold CX2223AT DropSens electrodes using CV in which 20 scans were run from 1.0 V to 0.0 V at a scan rate of 50 $mV.s^{-1}$. Both gold and carbon electrodes were tested for comparison using this method. Gold DropSens electrodes were employed additionally as these had previously been used to generate sensors successfully using biotin-NeutrAvidin tethering methodology (Caygill, 2012). The screen printed carbon electrodes were again used in combination with external platinum counter and Ag/AgCl reference electrodes. The DropSens electrodes contain integrated gold counter and Ag/AgCl reference electrodes.

Figure 4.8 presents cyclic voltammograms for electro-polymerisation of polyaniline onto gold (**Figure 4.8A**), and carbon (**Figure 4.8B**), showing electrodes over 20 cycles (overlaid). The distinctive patterns reflected the different working electrode

materials onto which the polymer was layered, although common to both was the clear increase in conductivity of the surface as each cycle of potential was applied and the polymer layer increased. This is characteristic of polyaniline, a so called 'conducting' polymer, as these polymers are able to form electroactive species by the presence of partially filled molecular orbitals overlapping to allow free electron movement through their matrix (Gerard et al., 2002). In **Figure 4.8A**, the gold electrode shows the monomers deposit in three oxidative states (at approx 0.25, 0.5, 0.8 V) and one reduced state (approx 0.55 V). In **Figure 4.8B**, the screen printed carbon electrode is more complex with three oxidative states at approximately 0.3, 0.6, 0.9 V and two reduction states at approx 0 and 0.4 V. Due to carbon being a comparably poorer conductor than gold the peaks were seen to be wider and achieved much lower currents overall.

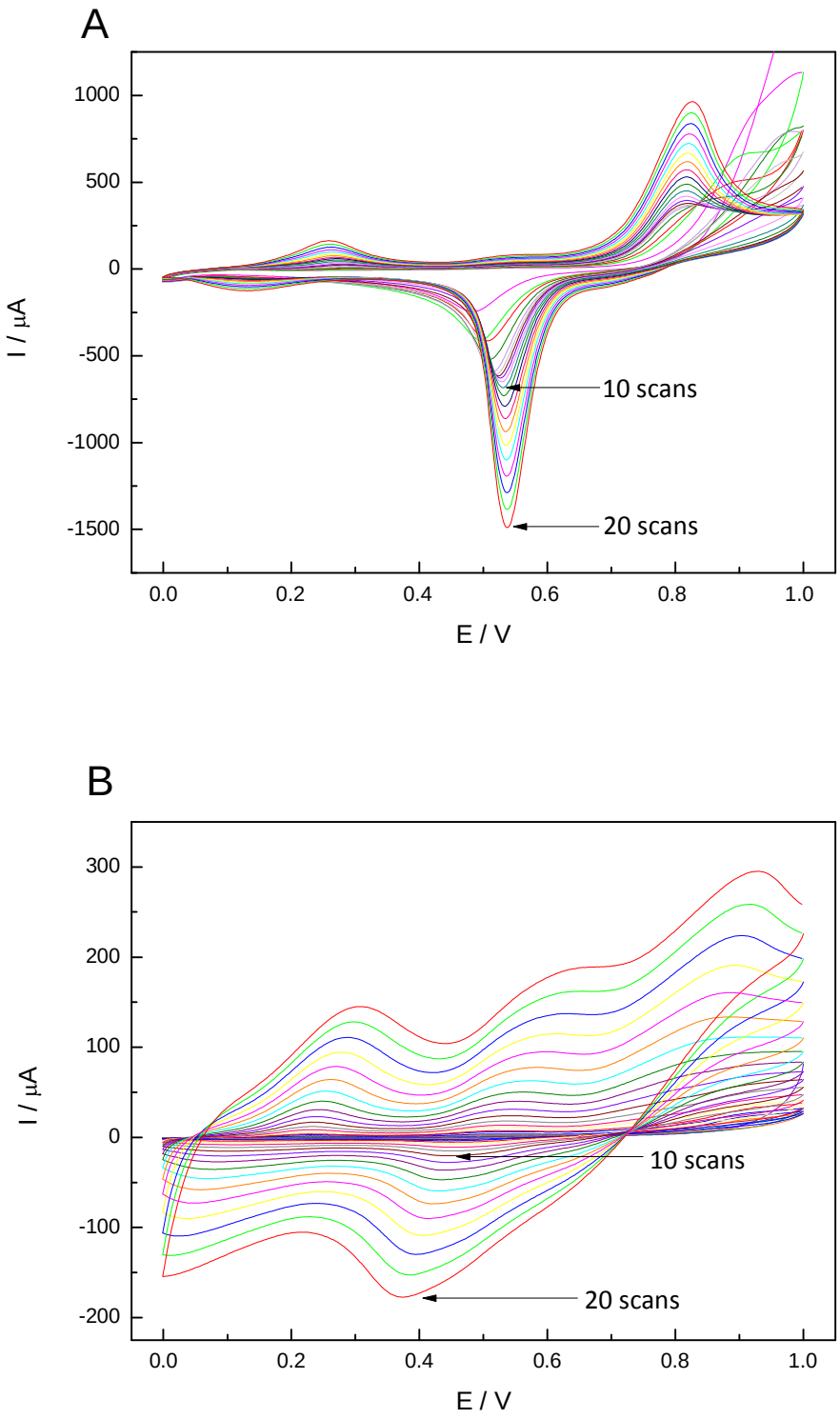

Figure 4.8: Cyclic voltammograms showing electro-polymerisation of P(ANI/2-ABA) copolymer onto (A) bare gold electrode (B) screen printed carbon electrode. Scans were performed from 1.0 V to 0.0 V at a scan rate of 50 $mV.s^{-1}$ with the potential applied *vs.* a Ag/AgCl reference electrode. Scans 10 and 20 are indicated to demonstrate the increased conductivity as the polymer is formed on the surface.

4.4.2 Chronoamperometric interrogation of biotin-avidin modified biosensors

The modified electrodes were biotinylated by incubation in a 10 $mg.ml^{-1}$ biotin-NHS solution for 1 h. Electrodes were then incubated with 5 µM NeutrAvidin in PBS for 40 min ready for enzyme immobilisation. Lactate oxidase was first biotinylated with 10 $mg.ml^{-1}$ biotin-NHS for 30 min, before unbound biotin was removed by the use of 30 KDa cut-off Amicon Ultra centrifugal filtration as described in the **Methods** section. Incubation with the biotinylated enzyme onto the electrode surface for 1 h at room temperature was then carried out for complete sensor construction. Chronoamperometry was used to interrogate electrodes with sequential spiked additions of lactate into PBS electrolyte at +0.6 V. **Figure 4.9** shows amperometric responses on modified gold (A) and screen printed carbon electrodes (B) respectively.

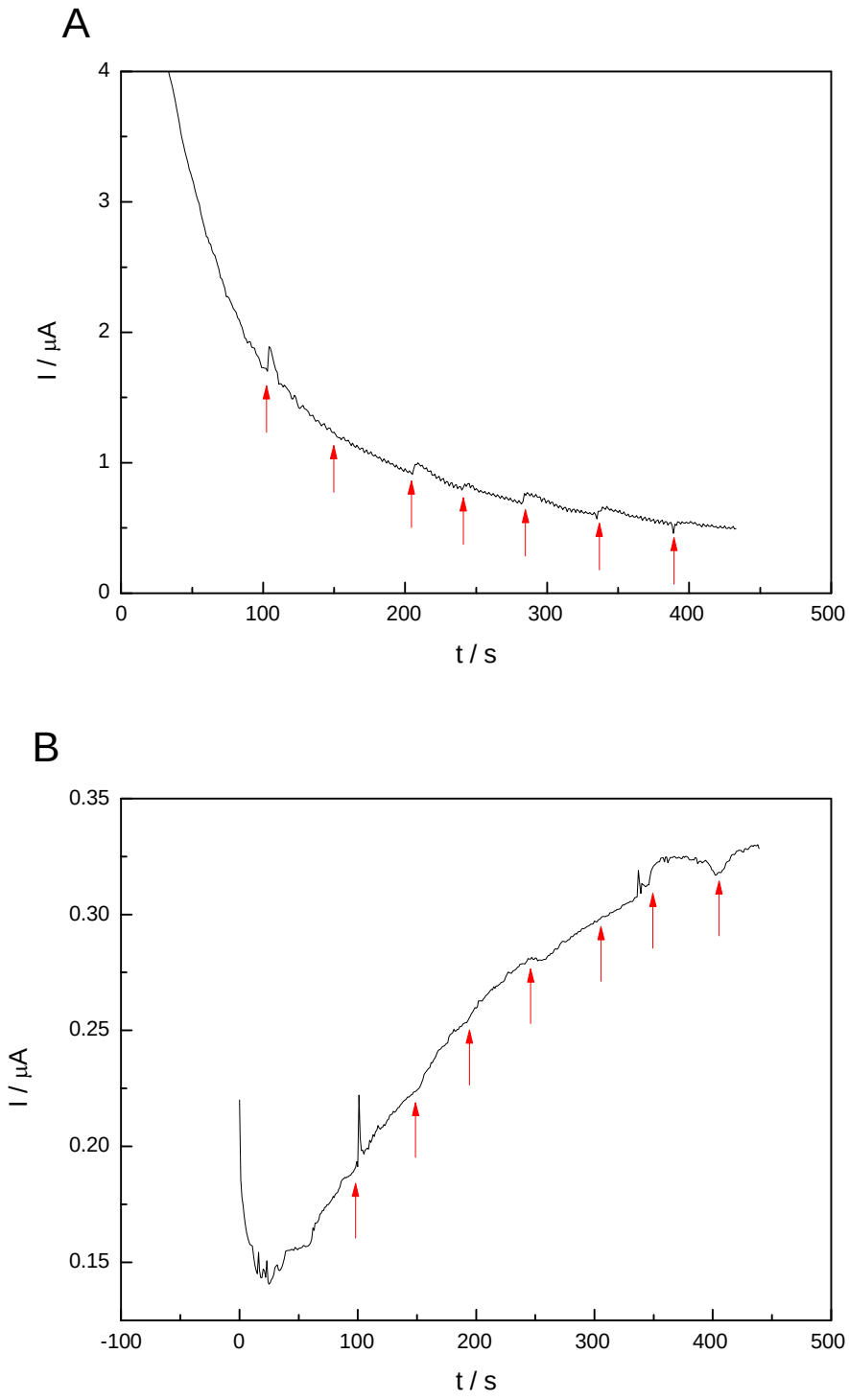

Figure 4.9: Time-current plots of P(ANI/2-ABA)/biotin-avidin modified electrodes for (A) gold electrode (B) carbon electrode. 0.1 mM lactate was added sequentially (shown by arrows). The current was measured at +0.6 V and pH 7 with constant stirring.

There was some response of both gold and carbon electrodes to lactate additions, more so seen with gold, but not of a uniform, consistent nature in order to produce calibration curves. Neither gold nor carbon electrodes gave any reproducibility, with repeats of each (not shown) showing lesser or no response at all to lactate.

Hypotheses for inability to produce an appropriate response to lactate were loss of enzyme during the biotinylation process, denaturation or deactivation of enzyme during biotinylation or when immobilised on the electrode surface, enzyme not bound to the sensor surface, or poor electron transfer across the electrode due to the polymer layer although this copolymer surface has been successful with other bioreceptors as discussed (Caygill, 2012). To attempt to elucidate a potential cause, the modified electrodes were incubated with reagents from the colorimetric assay and lactate **(Section 4.3).** This did not show a colour change; therefore the enzyme initially appeared to be inactive on the electrode surface. However, biotinylated enzyme in solution was then added to the colorimetric reagents and lactate and also did not demonstrate a colour change, suggesting that the enzyme was deactivated by the biotinylation methodology, or lost during filtration removal of unbound biotin. To test the conducting system in isolation, modified electrodes were interrogated with spiked additions of hydrogen peroxide **(Figure 4.10).**

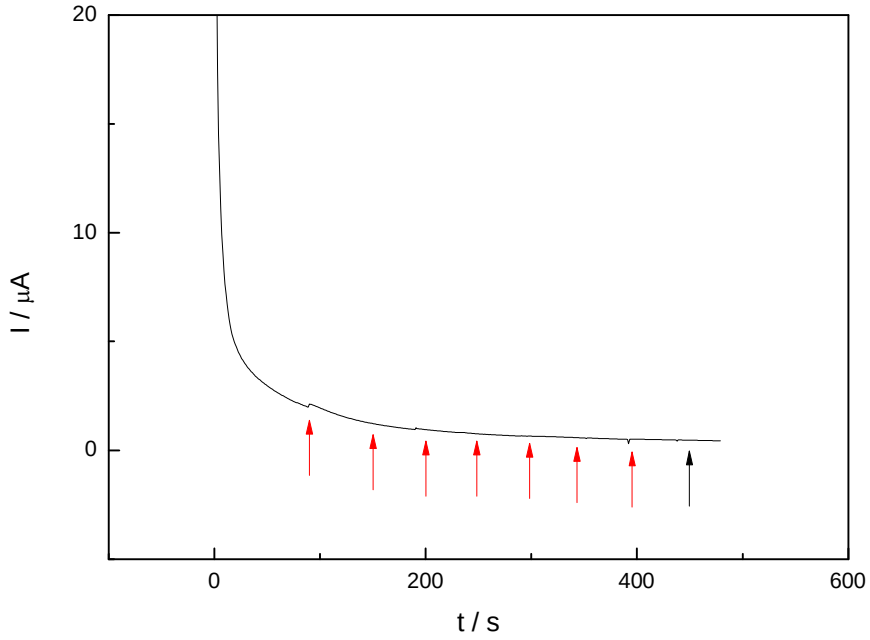

Figure 4.10: Time-current plot of one P(ANI/2-ABA)/biotin-avidin modified gold electrode upon successive additions of 0.1 mM H_2O_2 (red arrows) and 0.2 mM H_2O_2 (black arrows) in PBS, pH 7. Current was measured at +0.6 V with constant stirring.

There was virtually no response seen with repeated testing and when using modified screen printed carbon electrodes. It was therefore clear that there was also a direct problem with electrical conduction using this fabrication method as well as an issue with enzyme inactivation during biotinylation. An alternative method of immobilisation of enzyme and biosensor construction was therefore sought.

4.5 Prussian Blue mediated biosensors

The use of Prussian Blue (PB) as a mediator to allow low potential, selective detection of hydrogen peroxide has found wide use in the biosensor field since it was first described by Karyakin in 1995 (Rullier et al., 1998). A dense redox active layer is usually prepared by electrochemically depositing Prussian Blue on an electrode surface. Crucially it is the reduction of hydrogen peroxide, rather than its

more common oxidation, as with CoPc mediator, that is measured at the PB sensor. The reduction of hydrogen peroxide can be detected at potentials below 0 V, therefore allowing the high specificity and sensitivity to be retained, as interfering redox reactions are avoided (Nesbakken et al., 2001, Ricci and Palleschi, 2005).

Electrochemical synthesis of PB on electrode surfaces is now well established (Vo-Dinh and Cullum, 2000, Conroy et al., 2009, Rullier et al., 1998), but this strategy suffers from several disadvantages including high expense due to complex fabrication methods, and difficulty in further layer formation for deposition of enzymes. Recent interest has been in development of PB chemical synthesis without the costly requirement for an electrochemical step, and to provide an activated surface for facilitation of subsequent enzyme immobilisation. Methods include carbon ink doping (O'Halloran et al., 2001), adsorption of PB polymer (Zhao et al., 2005) and dendrimer supported PB synthesis (Bustos et al., 2005). A novel methodology for the non-electrochemical synthesis of PB on the surface of screen printed carbon electrodes which can be followed by electrostatic immobilisation of enzymes was recently described by our group (Pchelintsev et al., 2009). In this work the anion-exchange properties of the PEI polymerised surface were exploited in simultaneous Prussian Blue and glucose oxidase deposition for glucose measurement.

To construct lactate biosensors using PEI and PB as a mediator, PEI polymer was first immobilised on the surface of screen printed carbon electrodes by simple absorption during incubation in a 10 $mg.ml^{-1}$ PEI (MW 750,000 Da) aqueous solution for 30 min. After incubation the electrodes were washed in dH_2O to remove any weakly bound polymer. Prussian Blue was then formed by incubation with 5 mM $K_3Fe(CN)_6$, pH 1, 100 mM KCl to bind ferrocyanide anions within the film, before further condensation with Fe (III) cations from $FeSO_4$, pH 1, 100 mM KCl to form PB crystals on the sensor surface. Importantly this methodology allowed the PEI positive charge to become partially restored during PB synthesis, allowing

electrostatic binding of lactate oxidase in a further incubation step for complete fabrication of the sensor before amperometric interrogation.

4.5.1 Chronoamperometric response of PEI/PB modified biosensors to H_2O_2

To first test the conducting system independently of the enzyme, the biosensors were interrogated with spiked additions of hydrogen peroxide into a 10 ml PBS, pH 7, 100 mM KCl supporting electrolyte medium. A typical plot is seen in **Figure 4.11A**. It can be seen that there was a uniform response of increase in current upon each successive addition of H_2O_2, showing that the electrical components of the biosensor were functioning. Of note, the current is shown as becoming increasingly more negative as the hydrogen peroxide is reduced, not oxidised, as facilitated by the Prussian Blue mediator. **Figure 4.11B** shows a respective calibration curve generated from calculating the average of each current step. The results show good linear correlation, and are entirely consistent with work shown previously (Pchelintsev et al., 2009).

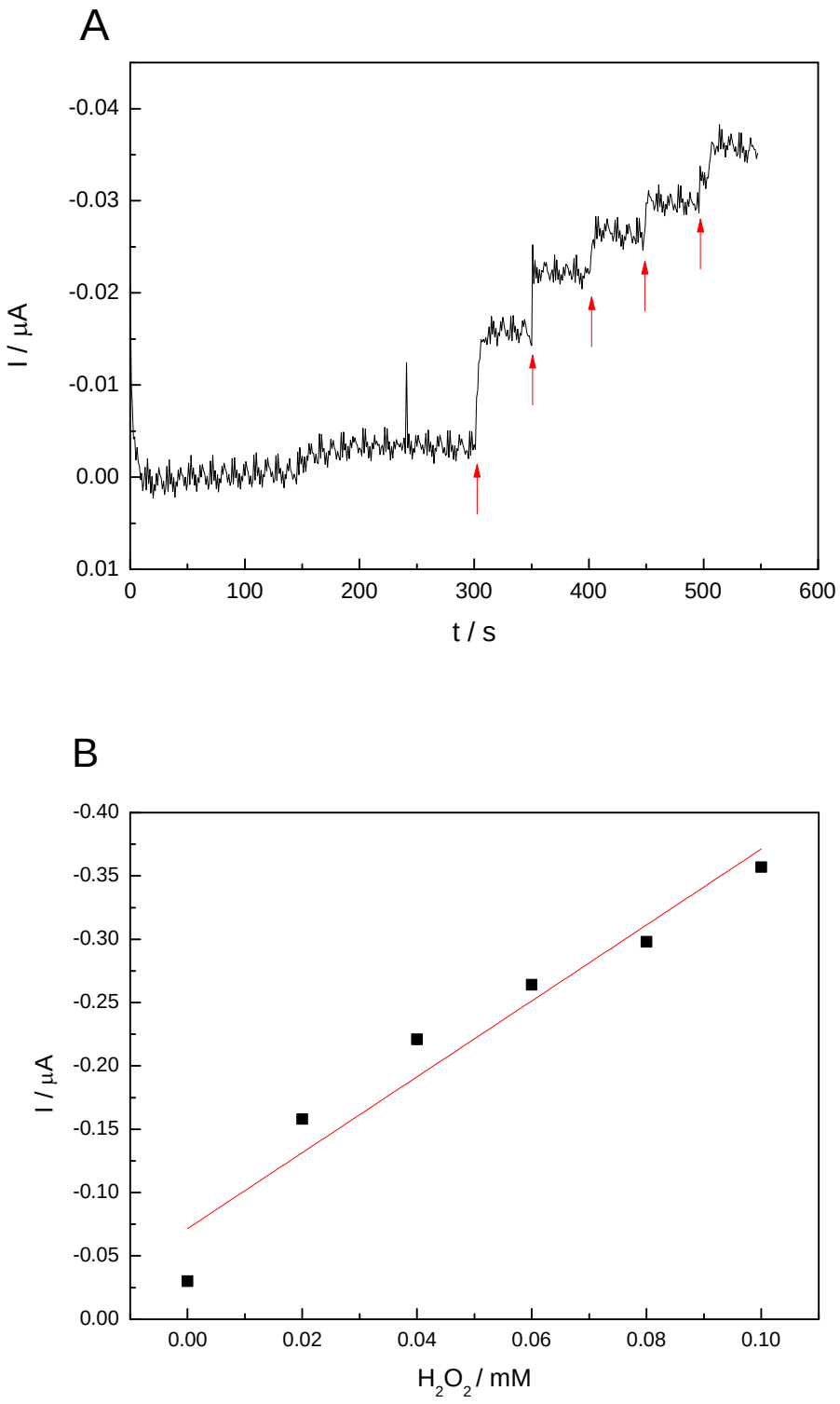

Figure 4.11: Plots from PEI/PB modified SPCE after immobilisation of 1 U.ml^{-1} LOx. (A) Time-current plot of successive additions of 0.02 mM H_2O_2 (shown by arrows) in PBS, 100 mM KCl. The current was measured at 0 V with constant stirring. (B) Respective lactate calibration curve for H_2O_2 additions with linear fitting, n = 1.

4.5.2 Chronoamperometric interrogation of PEI/PB modified biosensors

As there was initial success with a uniform response seen to H_2O_2, PEI/PB modified screen printed carbon electrodes were then interrogated with additions of lactate spiked into 10 ml PBS, pH 7, 100 mM KCl. As shown in **Figure 4.12A**, the PEI/PB modified biosensors were successfully able to show a response to lactate by measurement of the reduction of H_2O_2. Repeated SPCE were then interrogated, and a calibration curve for a series of four electrodes was produced, seen in **Figure 4.12B**. However, the SPCE's proved to be very variable, with only approximately 40% of electrodes tested yielding a response to lactate. Despite normalisation of data, the electrodes included in the calibration curve also showed large variation in standard deviation; therefore if a modified electrode was able to show a response to lactate, it was not in a uniform, reproducible way and so would not be suitable for the anticipated diagnostic use in a commercial application.

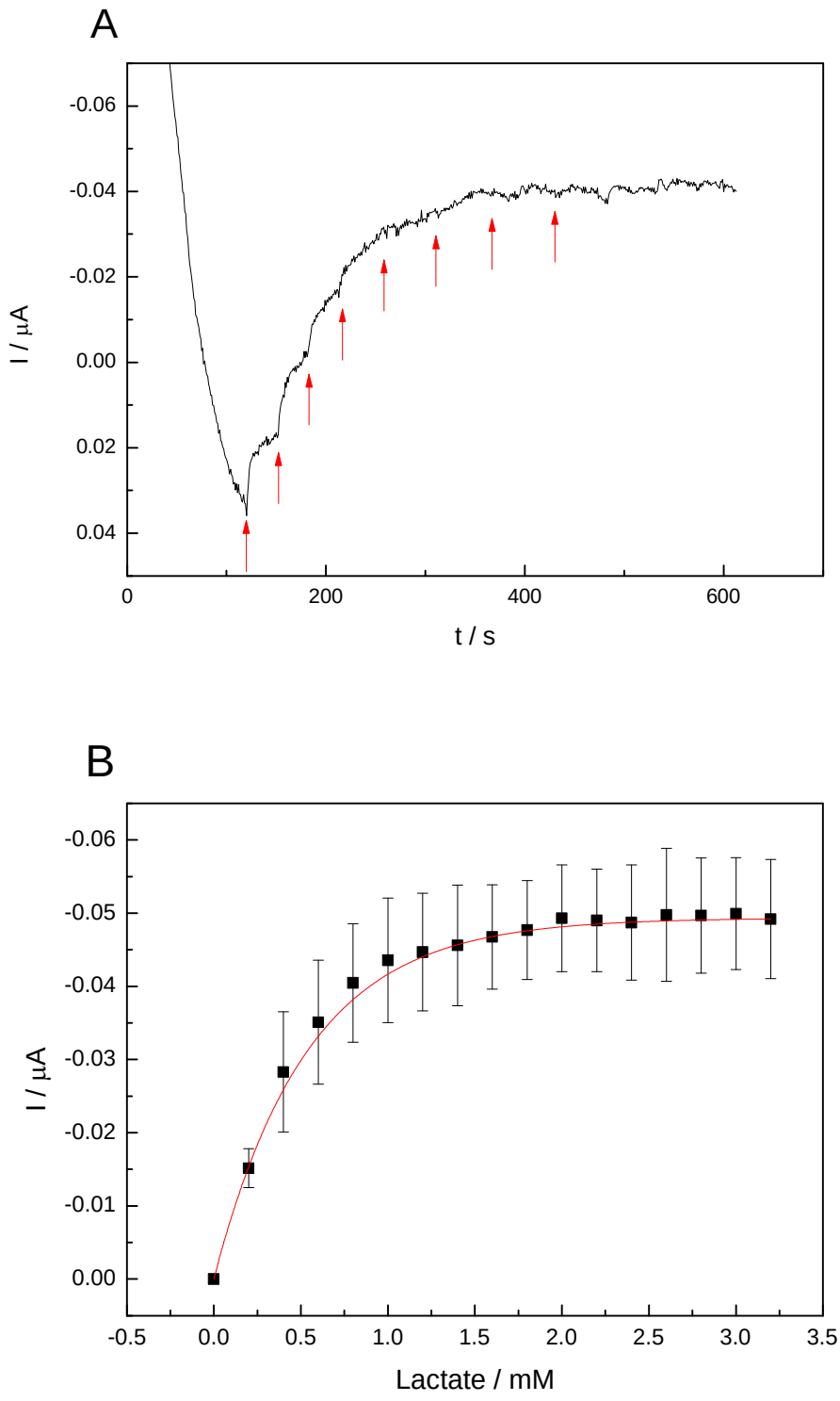

Figure 4.12: Plots from PEI/PB modified SPCE after immobilisation of 1 U.µl^{-1} LOx. (A) Time-current plot of successive additions of 0.2 mM lactate as shown by the arrows. The current was measured at 0 V with constant stirring. (B) Respective lactate calibration curve for PEI/PB modified electrodes. Points are mean ± S.D. for n = 4

4.5.3 Optimisation of enzyme immobilisation onto PEI/PB modified biosensors

Despite the observed sensor-to-sensor variability, attempts were made to optimise the biosensor fabrication methodology specifically for lactate oxidase enzyme to try to improve sensitivity, by testing at different enzyme concentrations, and for different incubation times on the electrode surface. Calibration curves for each of these parameters tested respectively are shown in **Figure 4.13.** A 1 $U.\mu l^{-1}$ enzyme concentration appeared to give the most linear calibration curve, as did the shortest incubation time of 10 minutes. However these results were irreproducible between electrodes with only n = 1 thus produced for each parameter tested, and therefore the results could not be considered meaningful. A fundamental issue with the biosensor construction to yield such lack of response (in the majority of biosensors interrogated) or at best show poor reproducibility between electrodes was considered. Since the same methodology using glucose oxidase to measure glucose had previously been successful, the electrodes themselves were examined in more detail. The screen printed carbon electrodes that had been donated were unfortunately in suboptimal condition, with the majority scratched including over the working electrode surface as they had been stored poorly. This was felt to be a principal reason for the variability seen when interrogating the sensors, and for the inability to construct biosensors that showed a response to lactate in all cases. Alternative carbon electrodes were therefore sourced. Commercial gold electrodes from DropSens had previously been used by our group (Caygill et al., 2012). DropSens DRP-150 carbon electrodes were subsequently purchased for further work.

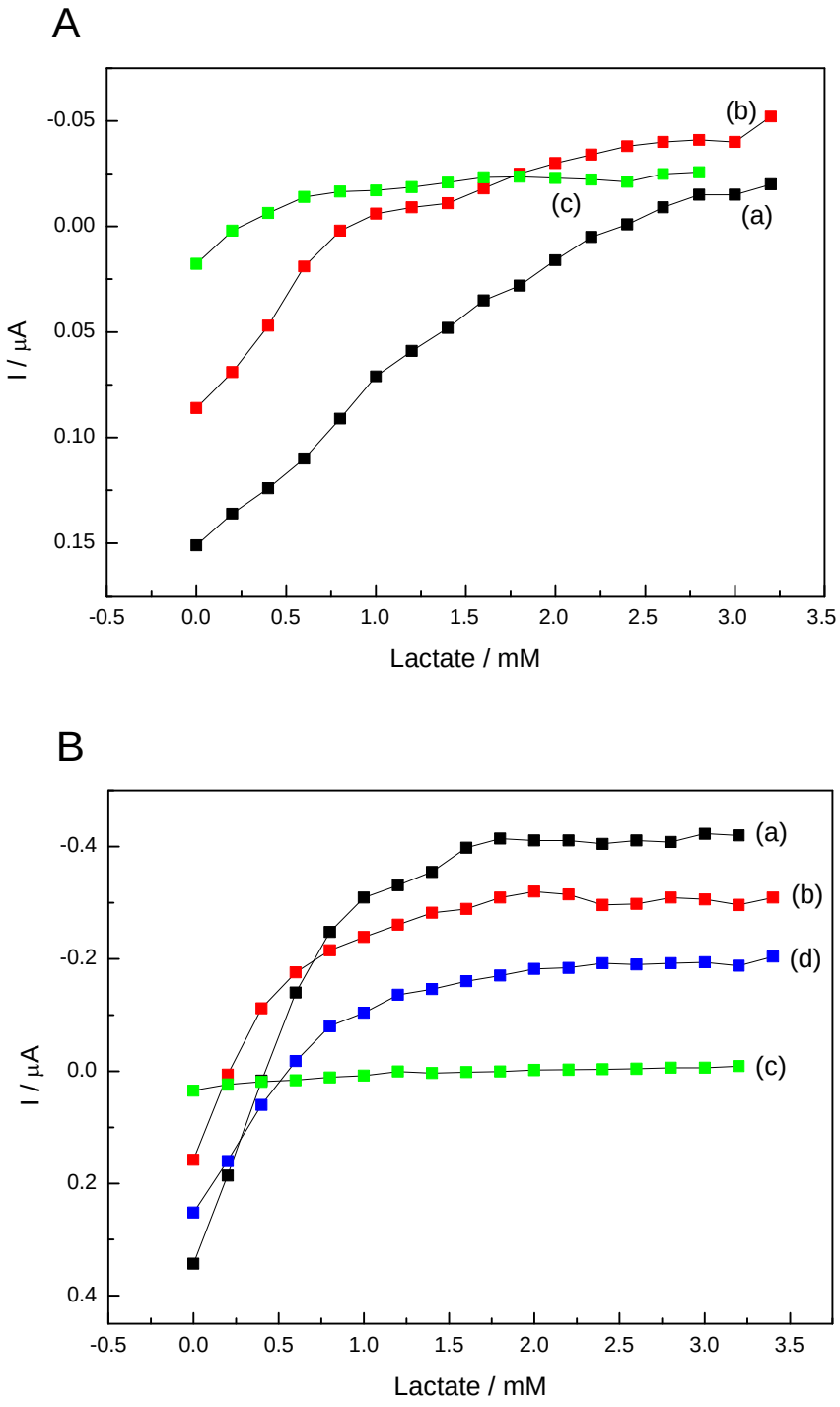

Figure 4.13: Lactate calibration curves for PEI/PB modified SPCEs in response to spiked additions of 0.2 mM lactate after immobilisation at a range of (A), LOx concentrations and (B), LOx incubation times. In (A), LOx concentrations were: (a) 1 U.µl^{-1}, (b) 0.5 U.µl^{-1}, (c) 0.1 U.µl^{-1}. In (B), LOx incubation durations were: (a) 10 min, (b) 20 min, (c) 30 min, (d) 60 min.

4.5.4 Chronoamperometric interrogation of DropSens carbon electrodes

DRP-150 carbon electrodes purchased from DropSens were tested using the same fabrication methodology as in **Section 4.5** onto the new electrode surface. These commercial electrodes consist of carbon working and counter electrodes and a Ag/AgCl reference electrode. Gold working electrode variants of these electrodes had been successfully used by our group in the construction of impedimetric viral detection biosensors (Caygill et al., 2012). In particular the electrodes were found to improve reproducibility in the previous studies, as the integrated three electrode system onto one transducer base negated the variation found in positioning of the working and external counter and reference electrodes. **Figure 4.14** shows a typical time-current plot for a PEI/PB modified DRP-150 DropSens electrode with spiked additions of lactate.

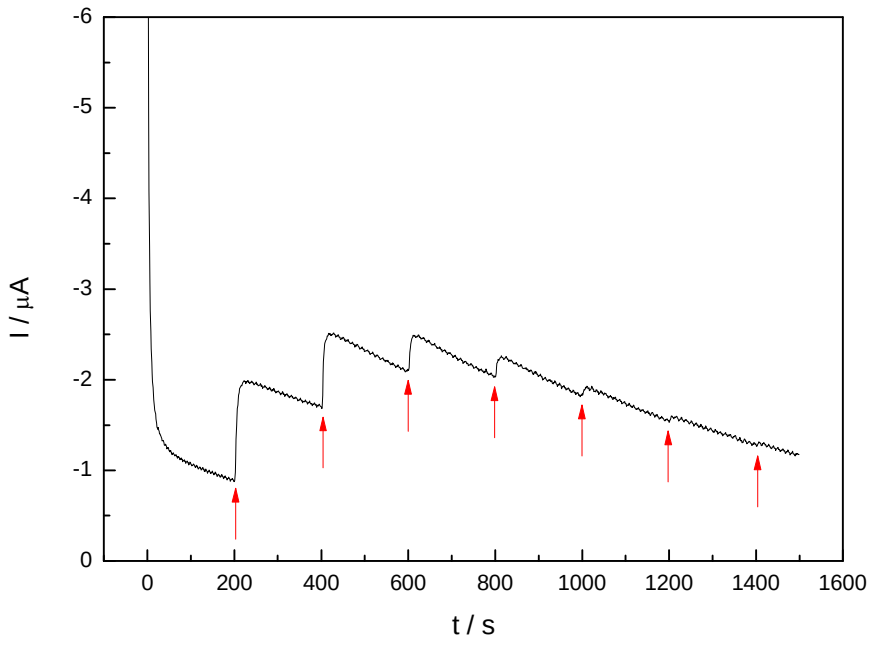

Figure 4.14: Time-current plot for one PEI/PB modified DRP-150 electrode upon successive additions of 0.1 mM lactate (shown by arrows) in PBS, pH 7, 100 mM KCl. Current was measured at 0 V with constant stirring.

The increase in current in response to spiked lactate additions was clearly seen and this was reproducible in 100% of the electrodes tested, confirming that the poor

quality of the screen printed carbon electrodes was almost certainly the reason for the variability in their function seen previously. However, the response with DropSens electrodes, although reproducible, gave the characteristic appearance of current decreasing after the initial rise that can be seen after each lactate addition. There also appeared a general saturation effect after approximately four additions of 0.1 mM lactate in which there was still a modest increase in current, but in which it persistently drifted towards the baseline. This appearance was seen in all of the electrodes interrogated, and was also seen when biosensors fabricated with glucose oxidase were tested with additions of glucose, and therefore was not specific to lactate oxidase (data not shown). It was hypothesised that the DropSens electrode surface may have conferred different characteristics to that of the SCPE's and have lead to incomplete formation of Prussian Blue during fabrication. The absence or minimal amount of PB mediator would account for the initial increase in current seen in response to lactate, which was then unable to be sustained as electron transfer was reduced and therefore the rate limiting step. To investigate this further, SEM was performed on DRP-150 electrodes to characterise the electrode surface at different stages of sensor construction.

4.5.5 SEM to characterise the surface of DropSens carbon electrodes at stages of PEI/PB biosensor construction

Scanning electron microscopy was performed using a Zeiss EVO© MA 15 SEM at the School of Process, Environmental and Materials Engineering, University of Leeds, to assess the sensor surface at stages of construction. **Figure 4.15** shows the roughness of the bare DropSens electrode surface (A), which continued to be very irregular after polymer deposition (B). It was therefore unlikely that Prussian Blue crystals would have been able to form evenly on this surface to act as a mediator, accounting for the decrease in current seen after each initial response to lactate additions in **Figure 4.14**. In view of this, DropSens carbon electrodes with pre-impregnated Prussian Blue (DRP-710) were purchased and were used throughout

the rest of the work in this chapter, since reproducibility was more likely to be found resulting from DropSens' own quality control.

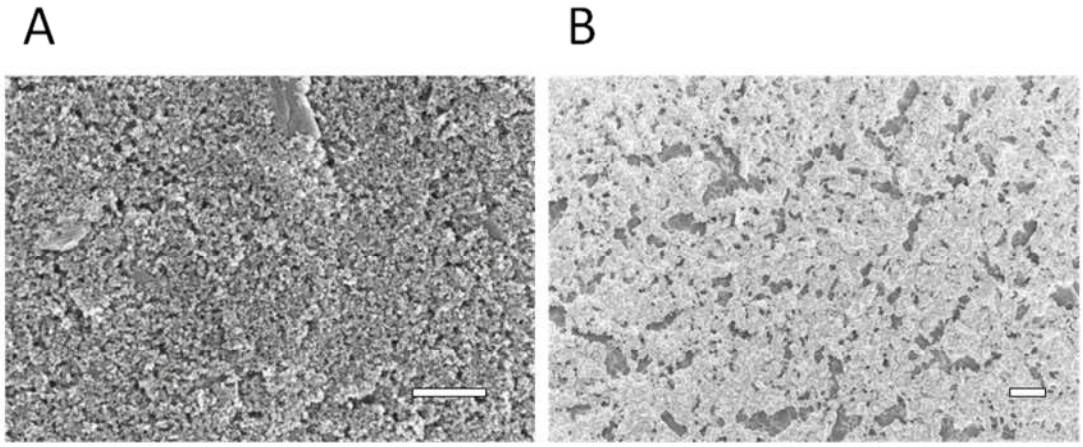

Figure 4.15: Scanning electron microscopy images. (A) bare DRP-150 carbon electrode, (B) after incubation with 10 mg.ml^{-1} PEI (MW 750,000 Da) for 30 min. Scale bars are 1µm (A) and 20µm (B).

4.6 Adapted Prussian Blue mediated sensor construction

4.6.1 Cyclic voltammetry of DRP-710 biosensor construction and analyte detection

First, bare DRP-710 DropSens electrodes were interrogated with cyclic voltammetry in 10 ml PBS, pH 7, 100 mM KCl at a range of scan speeds, the results of which are shown in **Figure 4.16**. Similar characteristic peaks were seen with each scan speed trace, with a cathodic, or positive, current observed at approximately 0.4-0.2 V due to the reduction of species leading to increase in current and electron transfer rate. As the redox species was reduced at the electrode surface, its concentration reduced to zero. According to Fick's first law of diffusion, this leads to a diffusion gradient from the electrode surface extending into the bulk electrolyte solution and the mass transfer of species becomes the rate limiting step, with subsequent cathodic current peak decrease. The current thus approaches a new equilibrium plateau until the voltage is reversed. On reversal of voltage there is a second peak

as species are re-oxidised, yielding an anodic current. Again, the redox species depletes in concentration at the electrode surface, limiting peak negative current on return to the original potential. The peak currents are seen to be higher on increasing the scan rate, as at faster voltage scan rates the charge passed per unit time is greater, hence an increase in current, whilst the total amount of charge remains the same. This effect is described by the Randles-Sevcik equation.

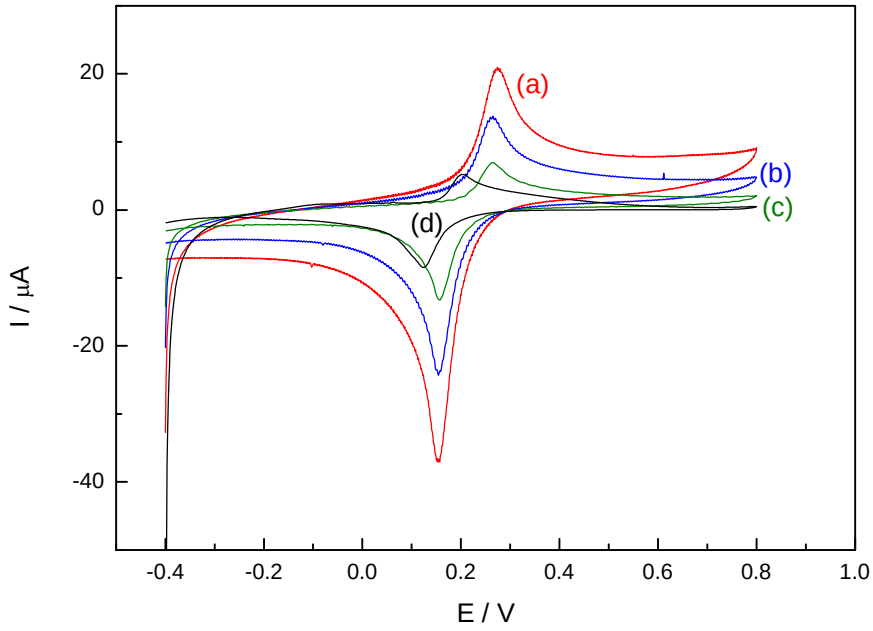

Figure 4.16: Cyclic voltammetry of bare DRP-710 PB carbon electrodes in in 10 ml PBS, pH 7, 100 mM KCl at a range of scan rates. (a) 100 $mV.s^{-1}$, (b) 50 $mV.s^{-1}$, (c) 20 $mV.s^{-1}$, (d) 10 $mV.s^{-1}$.

Cyclic voltammetry was then performed on bare DRP-710 DropSens carbon electrodes, after modification with PEI, and after further modification with lactate oxidase as described in the methodology **Section 2.2.4.4** to show changes in surface characteristics. The resulting cyclic voltammograms are shown in **Figure 4.17**. Characteristic differences in oxidation and reduction peaks demonstrated the altered electrochemical properties of the electrode as layers were added to the biosensor surface. Small redox peaks at 0.18 V and 0.07 V observed at the bare carbon electrode (a) were almost certainly attributable to the oxidation and reduction of printing ink contaminants within the carbon electrode surface from

the commercial fabrication process. After the PEI polymer layer was deposited on the electrode, two larger (477% and 620% compared to those in trace (a)) redox peaks were seen, showing the increased conductivity attributable to the polymer (b). When LOx was added, the redox peaks were then decreased by 26% and 28% respectively, in (c). This was likely to be due to the insulating effect of the enzyme.

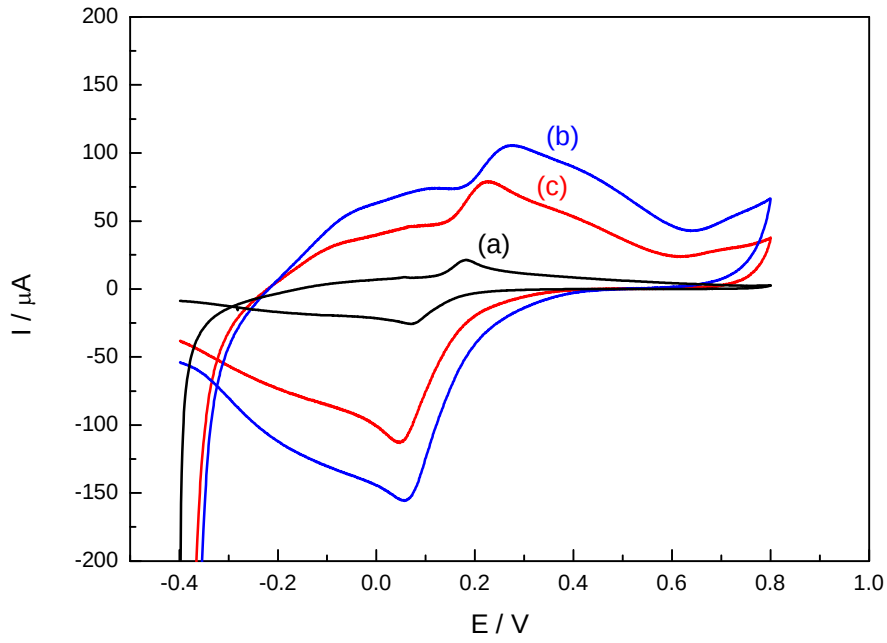

Figure 4.17: Cyclic voltammograms of PEI/LOx modified DRP-710 PB electrodes at stages of construction. Overlay data are: (a) bare DRP-710 electrode, (b) modified with PEI electrode, (c) modified with PEI and LOx electrode. All interrogations were performed in PBS, pH 7, 100 mM KCl, at 100 $mV.s^{-1}$

Figure 4.18 shows the cyclic voltammograms recorded for the fully constructed biosensor in PBS, pH 7, 100 mM KCl, without lactate **(1)**, and with 10 successive additions of 0.1 mM lactate at each cycle **(2-11)**. The oxidation peak current (at approx 0.3 V) was sequentially increased with each addition, pertaining to the production of hydrogen peroxide from the enzymatic reaction as outlined previously. The reduction peaks (at approx 0.16 V) also increased each time lactate was added; indicating the hydrogen peroxide product then underwent electrocatalytic reduction as mediated by Prussian Blue. Thus biosensors fabricated onto pre-impregnated PB DropSens DRP-710 electrodes were shown to respond to

lactate additions in a reproducible uniform manner using cyclic voltammetry before chronoamperometric interrogation.

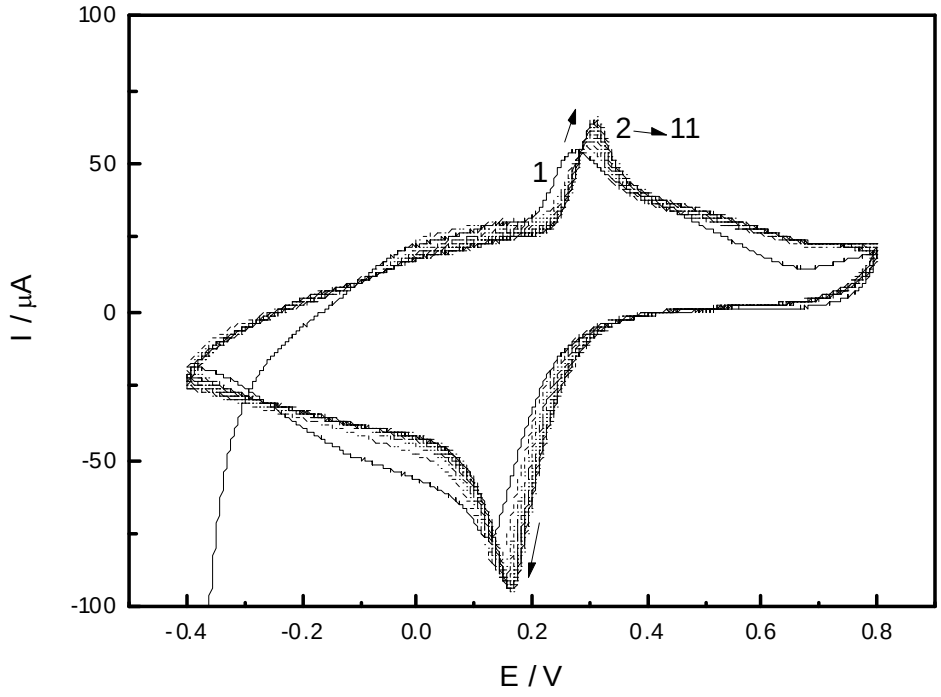

Figure 4.18: Cyclic voltammograms of one PEI/LOx modified DRP-710 PB electrode in response to sequential additions of 0.1 mM lactate in PBS, pH 7, 100 mM KCl, at 100 mV.s^{-1}. Data show: 1) without lactate, and 2) - 11) upon lactate additions.

4.6.2 Chronoamperometry of DRP-710 pre-impregnated Prussian Blue carbon electrodes

Chronoamperometry was used to interrogate modified PEI/LOx DRP-710 electrodes. In these experiments, a constant potential of 0 V was applied before sequential additions of 0.2 mM lactate were added to 10 ml PBS, pH 7, 100 mM KCl supporting electrolyte. **Figure 4.19** shows the typical chronoamperometric response of a modified electrode in which lactate was added at regular intervals. The corresponding change in current at each lactate addition is clearly seen as a uniform, stepwise increase. In contrast to the SPCE's this was again entirely reproducible in every electrode tested, but unlike the DropSens DRP-150 electrodes the current was maintained until the following spiked lactate addition without

drifting towards the baseline. The PB mediator component of the biosensor was thus functioning, facilitating electron transfer across the electrode from reduction of H_2O_2, and avoiding the rate limitation and current drift previously seen with the DRP-150 electrodes.

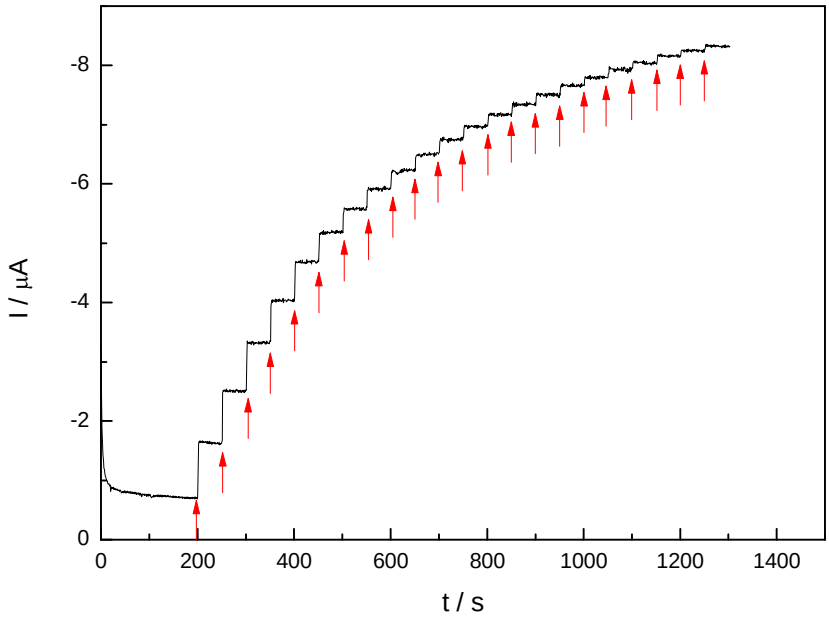

Figure 4.19: Characteristic time-current plot for one PEI/LOx modified DRP-710 PB electrode upon successive additions of 0.2 mM lactate (shown by arrows) in PBS, pH 7, 100 mM KCl. Current measured at 0 V with constant stirring.

Figure 4.20 shows the consequent calibration curve for a series of 5 electrodes (mean ± standard deviation). The initial linear range demonstrated good reproducibility and obeyed Michaelis-Menten enzymatic kinetics as shown in **Figure 4.20** (inset). However, as electrodes reached saturation, there was greater variability between electrodes, and the enzyme kinetic model was less well adhered to. It has been suggested that the apparent K_m value of immobilised LOx may be increased by the formation of multiple layers of enzyme with polymer or chitosan onto electrodes (Pchelintsev et al., 2009). Overall, an 85% reproducibility over the linear range was achieved for biosensors manually fabricated in the laboratory. Ultimately for a commercial clinical application, automated manufacturing methods such as the use of a biomolecule compatible printer e.g. Biodot, will be utilised for

biosensor construction to greatly decrease variability between electrodes and adhere to the European requirements for POC medical devices (Caygill et al., 2012).

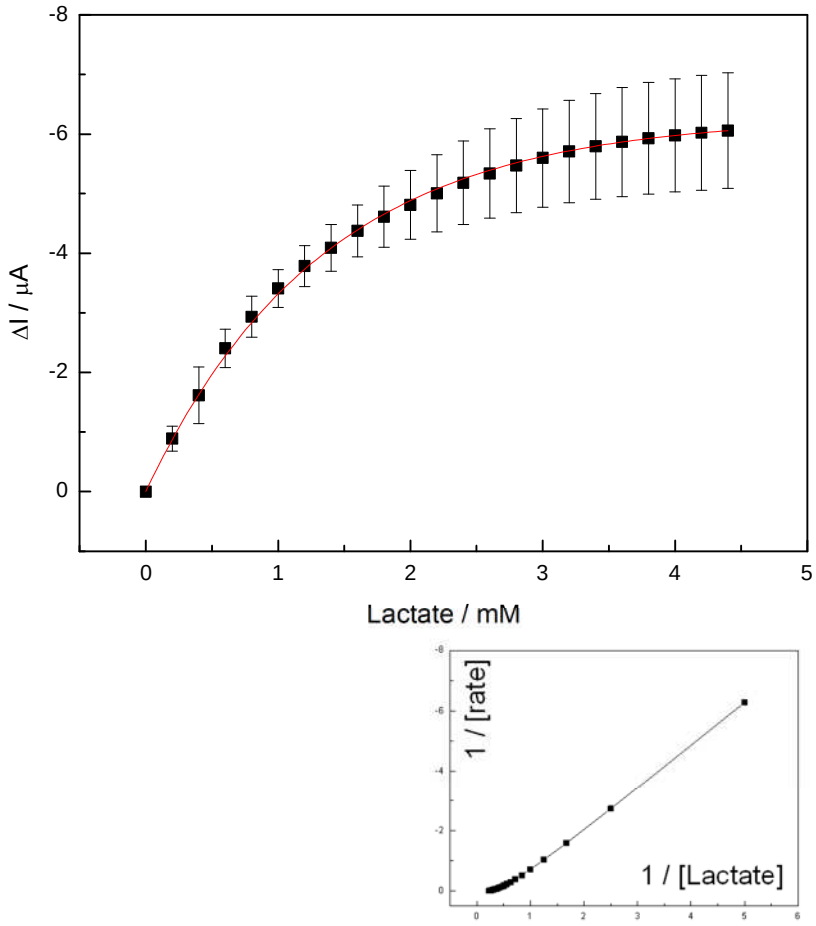

Figure 4.20: Lactate calibration curve for PEI/LOx modified DRP-710 PB electrodes (mean ± S.D. for n = 5). Inset: Derived Lineweaver-Burk plot of lactate calibration data.

4.6.3 Optimisation of enzyme immobilisation

The use of Prussian Blue to catalyse hydrogen peroxide reduction for oxidase enzyme based sensors, as well as the use of a PEI scaffold, has largely been evaluated using glucose oxidase as this is a common model enzyme for any amperometric biosensor development due to its high stability and importance of natural substrate (Ricci and Palleschi, 2005, Pchelintsev et al., 2009). To ensure optimal activity of the working biosensor with immobilised lactate oxidase, the

chronoamperometric response after varying the concentrations of enzyme used and enzyme incubation times was assessed. In **Figure 4.21**, the effect of varying the concentration of LOx (0.31 – 5 U) during preparation is shown. At the highest (5 U) and lowest (0.31 U) concentrations, the chronoamperometric response was distinctly inferior to that with mid range concentrations (2.5 U, 1.25 U, 0.63 U). It was hypothesised that at high concentrations, a dense enzyme layer was formed which impeded electron transfer to the electrode. Low concentrations, in contrast, may be insufficient to drive the reaction to full capacity with optimal K_m. The three mid range concentrations were comparable in response, therefore the middle value was considered optimal and used in all subsequent experiments.

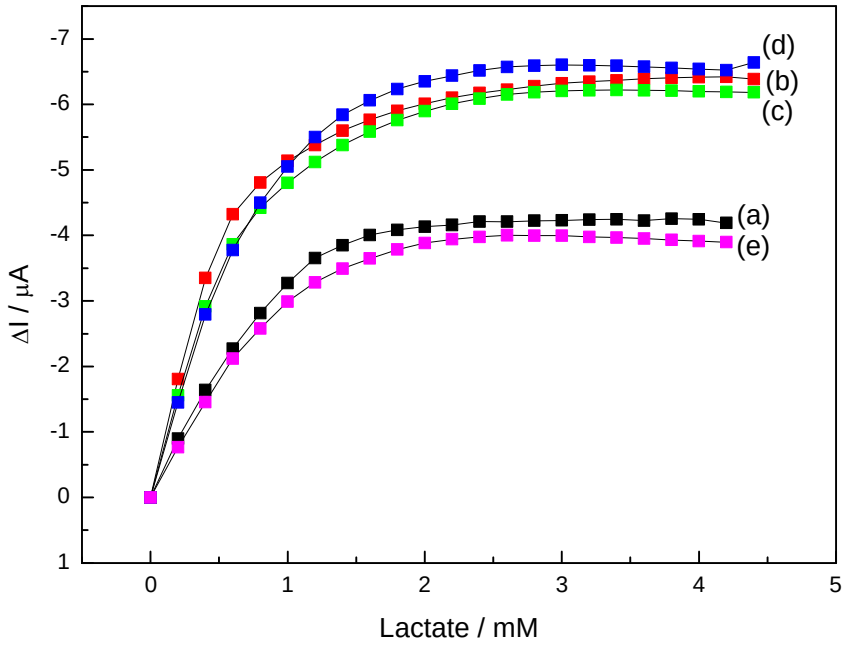

Figure 4.21: Lactate calibration curves for PEI/LOx modified DRP-710 PB electrodes after immobilisation at a range of LOx concentrations. Data show concentrations at: (a) 5 U, (b) 2.5 U, (c) 1.25 U, (d) 0.63 U, (e) 0.31 U. Sequential additions of 0.2 mM lactate into PBS, pH 7, 100 mM KCl were used throughout, current measured at 0 V with constant stirring.

The length of time LOx was incubated on the working electrode surface before rinsing and interrogation was also evaluated and the results are shown in **Figure 4.22**. An increasing length of time appeared to enhance the chronoamperometric

response, until 40 min when the response began to decline. At 5 min duration this was particularly apparent, with the poor response seen potentially as a result of too little enzyme available for immobilisation. The optimal LOx parameters for the biosensor methodology were therefore determined to be 1.25 U per electrode for 20 min immobilisation, and were used in all successive experiments.

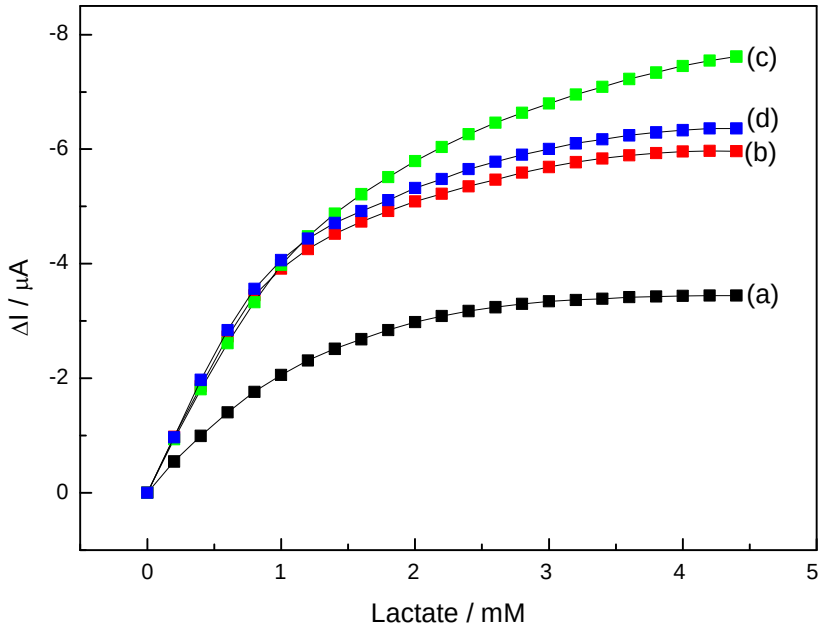

Figure 4.22: Lactate calibration curves for PEI/LOx modified DRP-710 PB electrodes after immobilisation at a range of LOx incubation times. Data show incubation times of: (a) 5 min, (b) 10 min, (c) 20 min, (d) 40 min. Sequential additions of 0.2 mM lactate into PBS, pH 7, 100 mM KCl were used throughout, current measured at 0 V with constant stirring.

4.6.4 Interference testing

The ability of Prussian Blue mediator to allow detection of hydrogen peroxide by its reduction at 0 V is fundamental, as it may avoid, or at least greatly reduce, the common problem of electrochemical interferences in which at higher potentials other compounds undergo redox reactions and add to current signal. The chronoamperometric response of the biosensor to successive additions of 0.2 mM lactate and potential interferents into a stirred solution of 10 ml PBS, pH 7, 100 mM KCl is shown in **Figure 4.23**. Lactate response was lesser at (f) than (a) due to the

approaching lactate substrate saturation of the LOx enzyme as seen in **Figure 4.19**. Ascorbic acid, a common interferent present in blood, produced some response (b), which was 9.6% of the response seen with an equivalent lactate concentration. The physiological level of ascorbic acid in blood is 50-200 µM, therefore only the upper threshold meeting the concentration tested (Halliwell and Gutteridge, 1990). Uric acid, acetaminophen (paracetamol) and glucose, which may also be found within human blood samples, showed no observable change in current at points (c), (d) and (e) respectively. The biosensor therefore showed high selectivity, which is of great importance for translation into use with clinical samples such as blood.

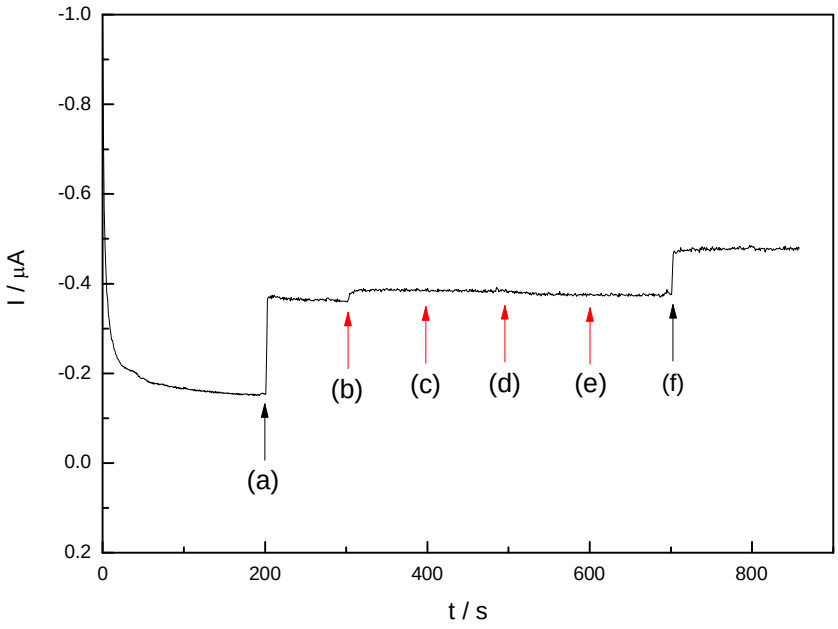

Figure 4.23: Effect from possible interferents in lactate biosensors. A time-current plot obtained at a PEI/LOx modified DRP-710 PB electrode after additions of 0.2 mM of each analyte: (a) and (f) lactate, (b) ascorbic acid, (c) uric acid, (d) acetaminophen, (e) glucose; as shown. Current measured at 0 V with constant stirring.

4.6.5 Testing in newborn calf serum

Newborn calf serum was used as an intermediary to testing on patient drain fluid in order to ascertain dilutions yielding measurable signal, since it was likely that large proteins or other components of drain fluid may interfere with the enzyme or

overall biosensor performance. Chronoamperometric interrogation of different dilutions (10, 20, 30, 40%) of newborn calf serum in PBS, pH 7, 100 mM KCl was conducted at PEI/LOx modified DropSens DRP-710 PB electrodes by applying a potential of 0 V and spiking with sequential additions of lactate as before. All solutions were vigorously stirred in all experiments. Overlay results of the calibration curves generated are shown in **Figure 4.24**. All of the newborn calf serum dilutions generated currents that were at least 83% smaller that those obtained at electrodes placed in 100% PBS, pH 7, 100 mM KCl. This was hypothesised to have been due to the increased viscosity of the serum impeding mass transport and electron transfer or non-specific binding of serum proteins to the electrode masking access to the enzyme active sites. It can be seen that at 10% (v/v) serum the signal was greatest, with a large decrease in current at a higher concentration of 20% (v/v) serum. Dilutions of 30% (v/v) and 40% (v/v) sera gave very low signals, indistinguishable from background. Therefore all patient drain fluid samples were diluted to 10% with PBS, pH 7, 100 mM KCl before being tested and analysed.

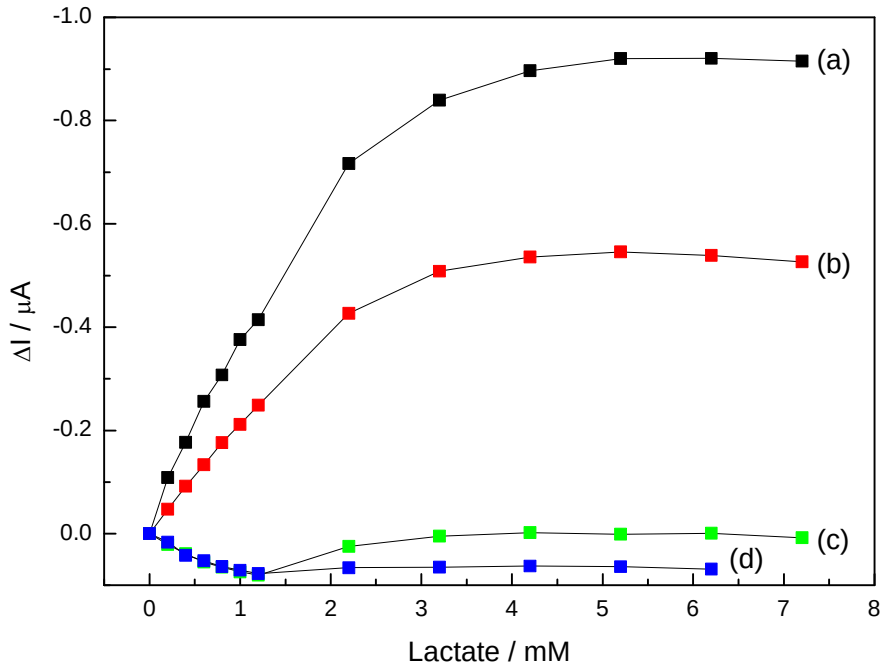

Figure 4.24: Lactate calibration curves for PEI/LOx modified DRP-710 PB electrodes in a range of dilutions of newborn calf serum in PBS, pH 7, 100 mM KCl. Data show newborn calf serum concentrations at: a) 10%, b) 20%, c) 30%, d) 40%. Sequential additions of 0.2 mM and 1 mM lactate were used throughout, current measured at 0 V with constant stirring.

4.6.6 Testing in patient drain fluid samples

A ten patient cohort was chosen from the drain fluid samples collected as described in **Section 2.2.2**, of which five patients underwent an uneventful post operative course and five patients suffered an anastomotic leak (AL). Groups were matched for basic patient demographics e.g. age, gender, type of operation, chemo-radiotherapy etc. As discussed in the **Methods** section the samples were collected intraoperatively, and from the patient's abdominal drain bag daily at 6.00 am from post-operative day one until the routine removal of the drain. Samples were then transported to the laboratory and centrifuged at 3,000 *x g* for 10 min, with the supernatant aliquoted and stored at -20 °C until use.

4.6.6.1 Commercial lactate kit results

To validate the fabricated lactate biosensor results on patient drain fluid samples, the samples were first tested using the commercial kit used for the animal samples **(Section 3.2.1).** The drain fluid samples of all ten patients for each post-operative day (POD) were tested in triplicate with the commercial colorimetric kit. The mean value of each triplicate was then used to calculate the lactate level for that sample using the standard calibration curve (also shown in **Chapter 3**). It should be noted that all patients had a post-operative day one sample, but on subsequent days this was not the case as drains were removed on differing days. The sample range for the patient cohort was day zero to day seven. The mean ± standard deviation lactate level results for each post-operative day in AL and non-AL patients are shown in **Figure 4.25**.

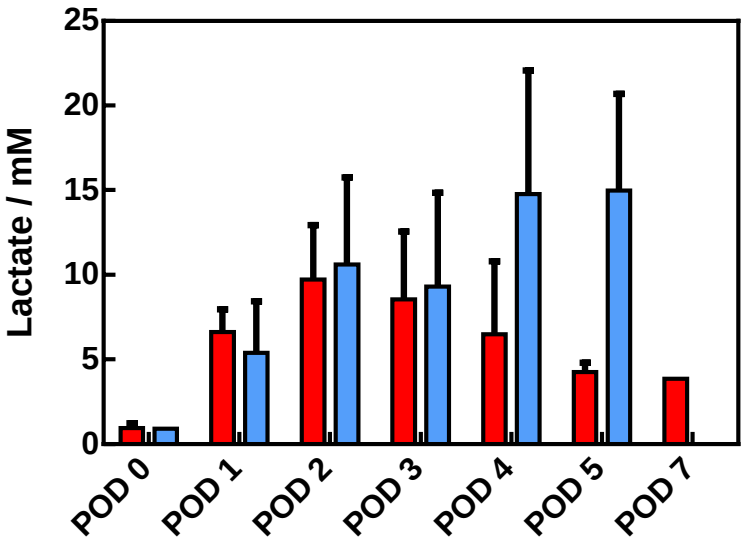

Figure 4.25: Commercial colorimetric lactate kit tested on patient samples. Data are mean ± S.D. of the five AL patients' (red) and the five non-AL patients' (blue) drain fluid samples on each post-operative day (POD).

It can be seen that the lactate levels were very variable between the AL and non-AL groups in all post-operative days. There was no statistical difference between groups in any post-operative day using a non-parametric statistical test (Mann

Whitney U). Reasons that the patient results did not show a clear statistically significant increase in lactate in AL compared to non-AL as in the animal model work **(see Chapter 3)** were thought in part to be attributable to the small sample sizes tested. The leak rate for AL is approximately 10%, therefore only a small number of anastomotic leak samples were able to be collected in the given time frame and tested, a total of five AL patients out of 69. The standard deviation of the results is also shown to be very large, showing the wide variation in lactate between individual patients. This is highlighted further in **Figure 4.26**. This raises the hypothesis that measurement of an individual patients' lactate trend over time may be more important than an arbitrary cut off value, although it is not possible to show here with the small dataset used. Future work with larger multicentre data sets is required. Biosensors lend themselves to serial testing due to low cost and simple POC use.

It was also hypothesised that the collection methodology of taking room temperature drain fluid from the sampling bag at 24 hour intervals was suboptimal, and samples were not therefore representative of lactate levels in the abdomen. Studies have shown that in as little as 30 minutes lactate levels in blood at room temperature vary due to ongoing glycolytic pathways (Seymour et al., 2011). This has future implications for the commercial development of sampling devices to the biosensors such as the use of microdialysis catheters to deliver "fresh" samples to an external biosensing component at the bedside and immediate refrigeration to reduce sample degradation.

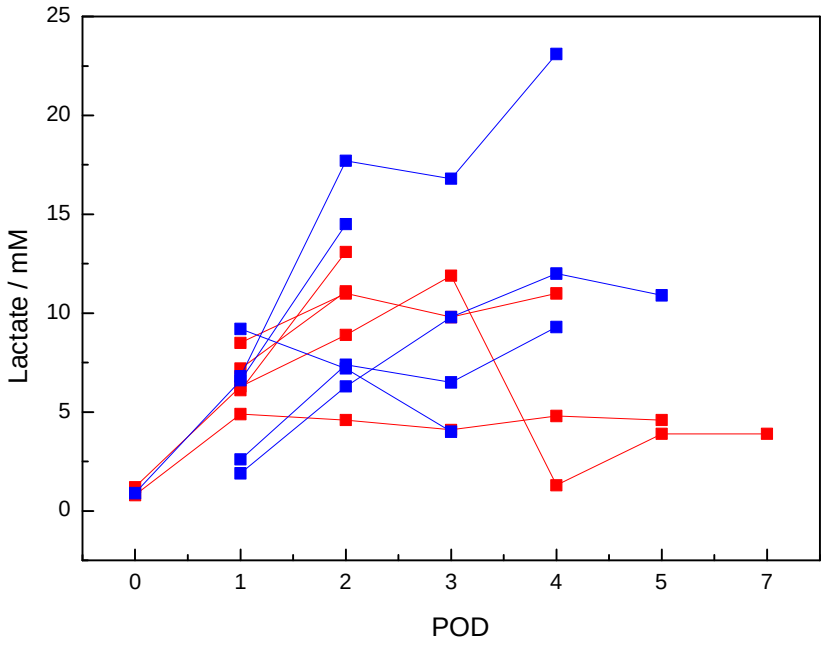

Figure 4.26: Plots of individual patients' drain fluid lactate levels as measured by the commercial colorimetric kit. Again AL patients are represented in red, non-AL in blue.

4.6.6.2 Osmolarity testing

As the drain fluid samples were so variable in viscosity and colour despite centrifugation, attempts to standardise them included measurement of osmolarity which was carried out by the pathology laboratory at the Leeds Teaching Hospitals NHS Trust. A table of osmolarity results for each post-operative day one sample is shown in **Table 4.1**. The osmolarity values differed little between samples and so further standardisation tests were not pursued. For proof of concept for validation of the constructed biosensors however, the drain fluid samples were still of use.

Table 4.1: Table showing the osmolarity of each patient drain fluid sample. Patients 1-5 are AL, patients 6-10 non-AL

Patient sample	Osmolarity ($Osmol.kg^{-1}$)
1	291
2	294
3	283
4	277
5	290
6	290
7	242
8	288
9	285
10	278

4.6.7 Drain fluid testing using biosensors

Drain fluid samples from post-operative day one were tested using the fabricated lactate biosensors, as each patient had a sample from this day, and the literature suggests ischaemic biomarker changes are present this early in the anastomotic leak pathophysiological process (Pedersen et al., 2009b). An auto calibration technique was used, in which each stirred 10% diluted patient sample was interrogated by chronoamperometry at 0 V with spiked additions of lactate added as previously. However, the current was allowed to reach a steady state for longer than with buffer and serum samples before spiked lactate additions, this being the current generated by the lactate inherently present in the sample. **Figure 4.27** shows a typical data set. Each patient sample was interrogated in triplicate as shown by the overlaid data in **Figure 4.27A**. The data were then normalised in order to construct calibration curves as shown in **Figure 4.27B.** The calibration curves show the excellent reproducibility between the electrodes tested in triplicate for each sample but were not otherwise useful, as normalising the data in this case deducts the current generated by the lactate within the sample, not a baseline to zero the background noise. Mathematical modelling was used to derive the lactate level in each patient sample, as described below.

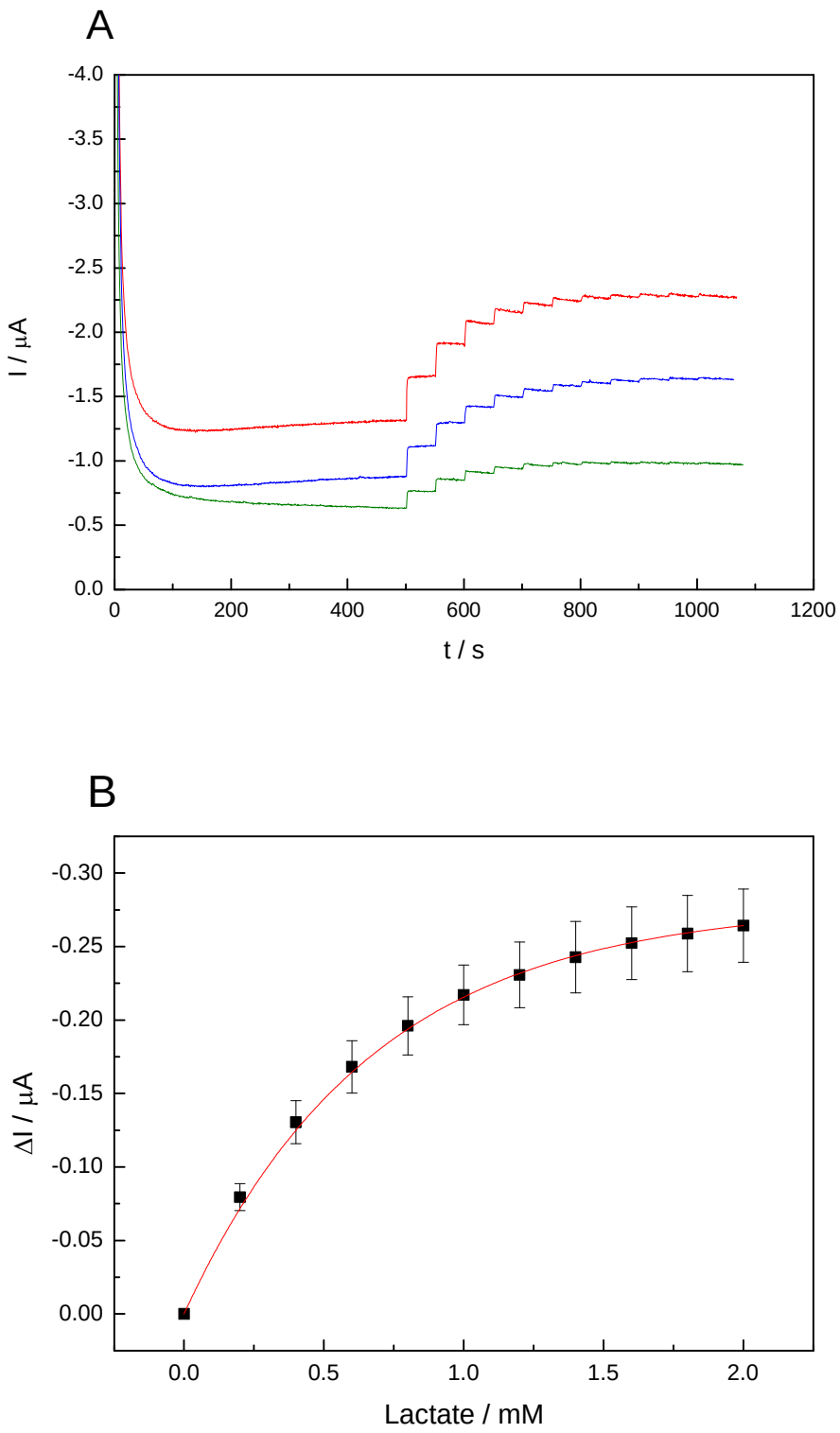

Figure 4.27: Plots from PEI/LOx modified DRP-710 PB electrodes in patient drain fluid samples. (A) Overlay of triplicate time-current plots for upon successive additions of 0.2 mM lactate in 10% drain fluid in PBS, pH 7, 100 mM KCl. Current measured at 0 V with constant stirring. (B) Respective normalised lactate calibration curve. Points are mean ± S.D. for n = 3.

4.6.8 Mathematical modelling of biosensor results in drain fluid

As outlined in **Section 2.2.4.6** recorded drain fluid sample currents were fitted by the method of least squares to Michaelis-Menten enzyme kinetics, where the initial amount of lactate was a free parameter. V_{max} was fixed to agree with the results of buffer and serum experiments (V_{max} = 1.2). The resulting values of K_m and S_0 (initial lactate concentration) are shown in **Table 4.2**. Data were adjusted for the 10 fold dilution to give the true value of lactate in each sample.

Table 4.2: Resulting K_m and S_0 of each patient drain fluid sample tested with lactate biosensors. Data fitting was by the method of least squares to Michaelis-Menten enzyme kinetics, with V_{max} fixed to agree with buffer and serum experimental results.

Patient sample	K_m	S_0 (mM)
1	4.79	6.83
2	4.40	8.17
3	4.49	7.14
4	3.98	6.78
5	4.86	11.85
6	5.44	18.24
7	4.89	13.96
8	3.99	8.32
9	3.06	2.86
10	4.86	6.77

4.6.9 Comparison of constructed lactate biosensor results to results of commercial colorimetric kit

Figure 4.28 shows the biosensor results *vs.* the commercial colorimetric kit results for the cohort of ten samples, with intercept set to 0. The biosensor standard deviations were larger than those of the kit, illustrating the greater variability between manually constructed biosensors compared to a commercially produced kit. Biosensor results were on average 49% higher than kit results, thought to be due to the possibility of interference. A Spearman's rank order statistical test was

performed to determine the relationship between the patient samples as measured by the biosensor and commercial kit. There was a strong, positive correlation between the biosensor and commercial kit results for each patient, which was statistically significant (r_s = 0.891, p = 0.001). The constructed biosensor therefore was shown to be validated and working in real time clinical samples. In the literature as discussed in **Section 1.6.2,** Pedersen *et al* found statistically significant increases in lactate in patients who developed anastomotic leak (7 mM), compared to those with an uneventful post operative course (3 mM) (Pedersen et al., 2009b). The fabricated lactate biosensor is capable of showing this difference. A Bland-Altman plot was also created using the same data to show the differences between measurements from each of the biosensor and commercial kit, as a function of the average of the two measurements of each sample. The resulting plot is shown in **Figure 4.28** (inset). The bias was relatively high at 3.089, showing some discrepancies between the two methods. However the 95% limits of agreement were narrow, and show the biosensor results were consistently higher than those of the commercial kit as already discussed, accounting in some part for the degree of bias seen. The differences observed between results from each method were lowest at the middle range lactate values. The lactate biosensor is therefore already potentially clinically applicable, as a non-invasive, promising method for early detection of anastomotic leak.

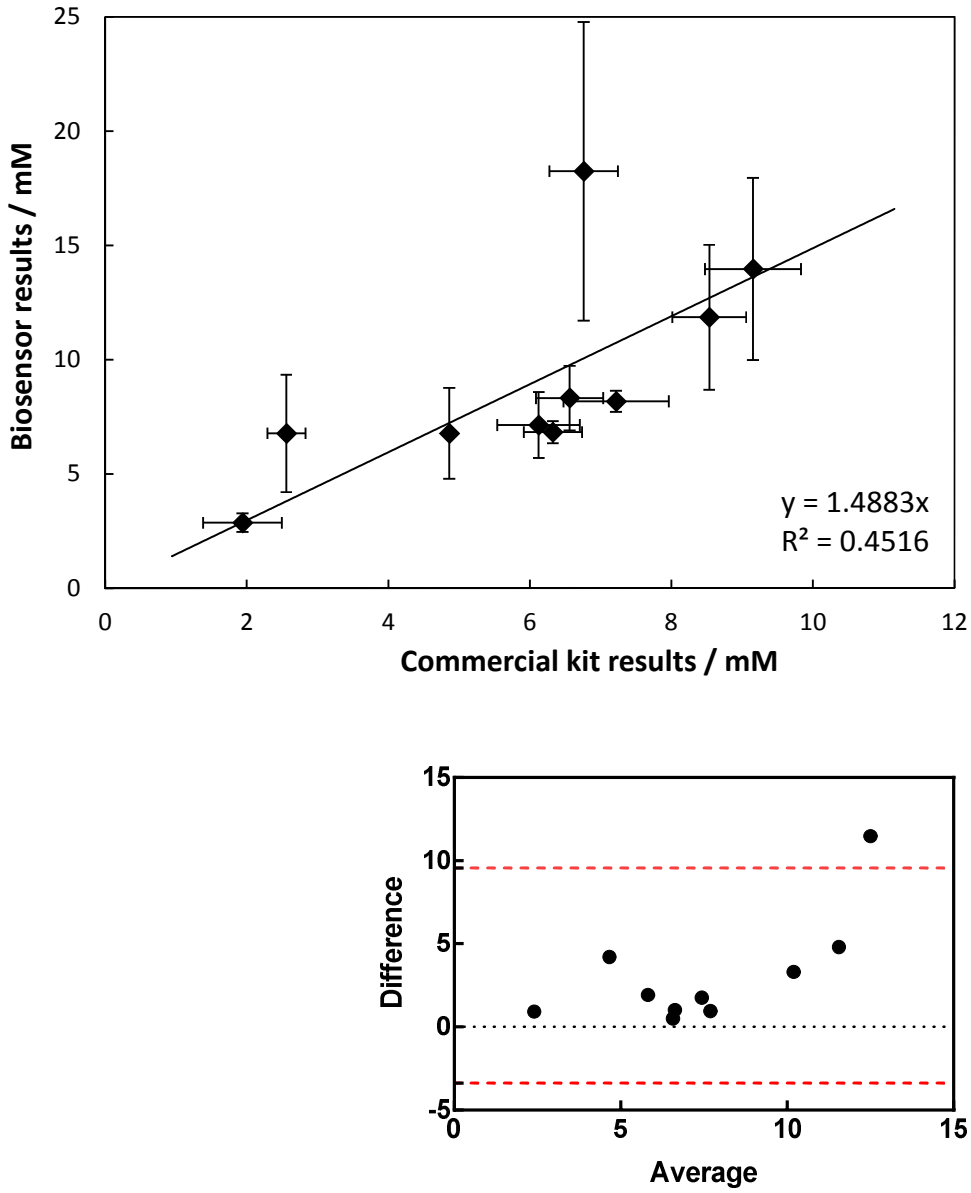

Figure 4.28: Biosensor results *vs.* commercial kit results (mean ± S.D., n = 3) of all ten patient drain fluid samples. Linear fitting with intercept = 0. Inset: Bland-Altman plot of the same data. Average bias was 3.089, with 95% limits of agreement shown by the red dotted lines (-3.379 to 9.557).

The biosensor *vs.* commercial kit patient lactate results were divided into those from the AL group and those from the non-AL group, shown in **Figure 4.29**. Interestingly, the AL group (A) consisted of the samples yielding the middle range lactate results, and showed excellent linear concordance. The non-AL group (B) results consisted of outliers at extremes of high and low lactate levels and showed much poorer concordance between the biosensor and the kit. The error bars were

significantly larger for this group. Despite the small sample size and therefore difficulty in drawing conclusions from comparing the groups, it was thought that patients without anastomotic leak may have very variable amounts of lactate compared to those who suffer an anastomotic leak, which in the samples tested consistently showed raised levels of lactate. As previously mentioned, this may indicate that the trend in an individual patient's lactate levels is more important than a single arbitrary value. The immediate collection of samples from the locality of the anastomosis, as opposed to collection from drain bags containing up to 24 hr old fluid is also paramount, *via* a flow cell sampling device delivery to external biosensors at the bedside or other methods which would yield more accurate real-time results as a continuation of this work.

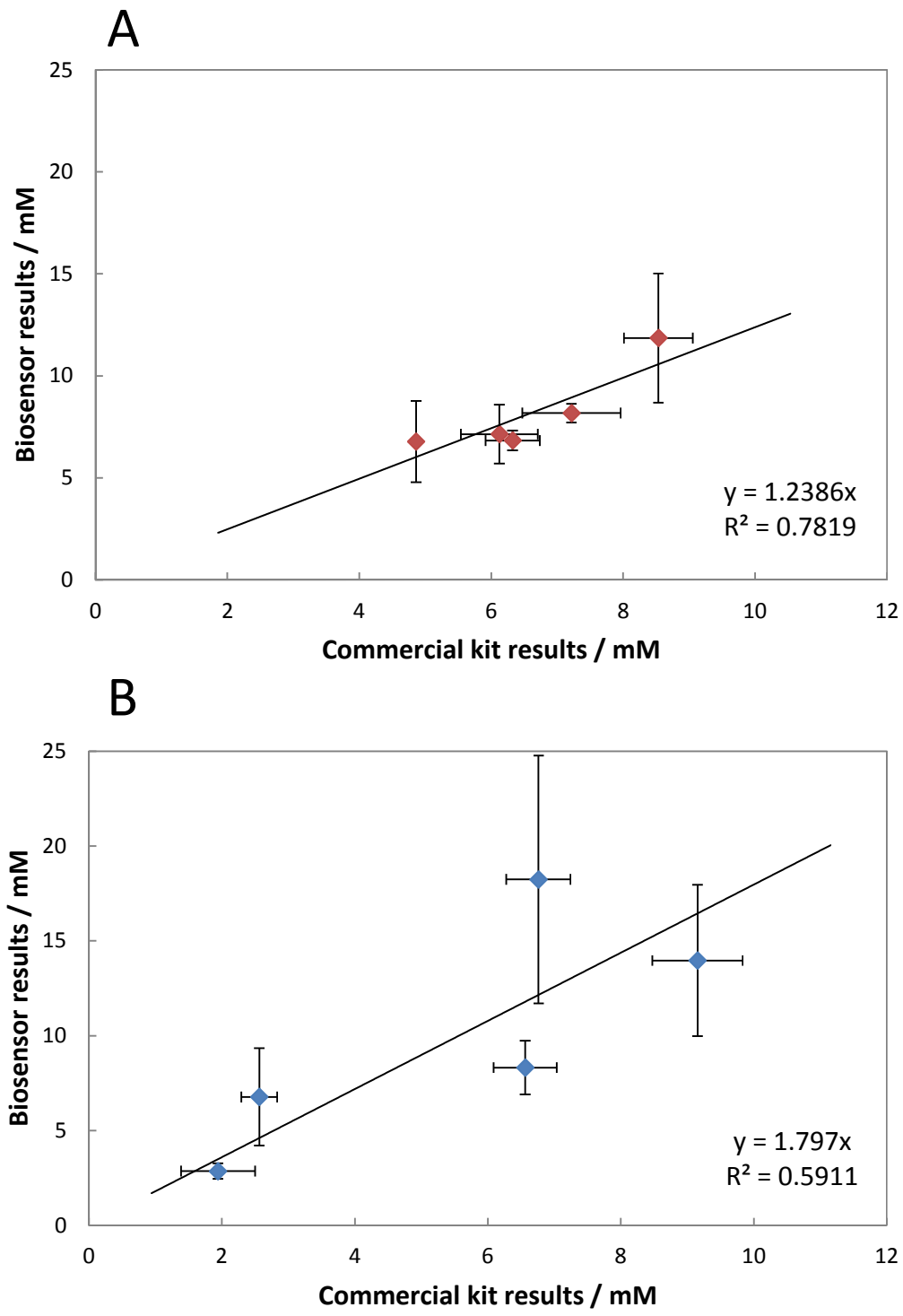

Figure 4.29: Biosensor results vs. colorimetric kit results (mean ± SD, n = 3) of patient drain fluid samples. Shown separately as AL group (A) and non-AL group (B).

4.7 Discussion

In this chapter, initial methodologies applied to lactate biosensor testing were largely unsuccessful, or inconsistent and unable to generate calibration curves. The first methodology tested utilised CoPc as a mediator, with PEI polymer allowing electrostatic binding of lactate oxidase to the screen printed carbon working electrode surface. The methodology had previously been reported successfully using glucose oxidase by our group. Poor results, however, were obtained during chronoamperometric interrogation of the sensor, despite attempts to optimise the methodology by varying enzyme and lactate concentrations. The time-current plots generated using hydrogen peroxide spiked into buffer were marginally superior to those using lactate, suggesting a problem with enzyme activity, and/or with binding of the enzyme to the electrode surface. A colorimetric assay was therefore used to assess activity of the lactate oxidase enzyme in isolation. This data demonstrated excellent linear response of the enzyme in the range 0 to 25 mM lactate. Consequently, a methodology incorporating a biotin/avidin system was next chosen for testing, in order to ensure adequate tethering of the enzyme to the electrode. This methodology however proved again largely unsuccessful on gold and carbon electrodes. Biotinylated enzyme in solution and on the constructed sensor surface was subjected to the same colorimetric assay reagents used previously, to assess whether the enzyme was still viable and active. No colour change response in either case indicated that the enzyme had been denatured or deactivated during biotinylation, accounting for the lack of response during chronoamperometric interrogation. A poor electrochemical response was also noted with hydrogen peroxide spiked additions, therefore the methodology failed from both enzymic and electrical system components.

A simple adsorption methodology for biosensor construction previously developed by our group was then evaluated, utilising Prussian Blue mediator formed onto a PEI polymer surface on screen printed carbon electrodes. An excellent response to chronoamperometric interrogation with spiked H_2O_2 was initially seen, with a

calibration curve generated entirely consistent with the published work from predecessors. Response to lactate additions likewise proved successful, although with only approximately 40% of the screen printed carbon electrodes yielding a response and with large variation seen between electrodes, despite attempts to optimise LOx concentration and incubation duration. Due to the poor quality of the stored SPCE's a commercial electrode alternative was sourced. The DropSens electrodes purchased incorporated a three electrode system onto one transducer base which was thought to also omit the variation seen when positioning the external counter and reference electrodes in proximity to the working electrode, and the positioning of the working electrode itself. The initial DropSens electrodes interrogated, DRP-150, showed excellent, reproducible response to lactate. However the current was subsequently seen to fall quickly after each lactate addition, hypothesised to be due to incomplete formation of Prussian Blue during fabrication. SEM was performed on bare DRP-150 electrodes and after PEI deposition to characterise the surface. Both surfaces were shown to be very rough, and it was unlikely that the Prussian Blue mediator was being formed correctly. DRP-710 electrodes with pre-impregnated Prussian Blue were subsequently used in experimental work. Cyclic voltammetry was initially utilised to characterise the biosensor at different stages of construction. Modified DRP-710 electrodes subsequently showed excellent, reproducible response to lactate in a uniform stepwise fashion in accordance with Michaelis-Menten enzyme kinetics, allowing calibration curves to be generated. Optimisation using a variety of enzyme concentrations and incubation times was achieved and testing with common interferents present in biological samples demonstrated the high selectivity of the constructed sensor in buffer. Chronoamperometric interrogation in newborn calf serum was subsequently used as an intermediary to determine required dilutions, before testing on patient abdominal drain fluid samples. Compared to buffer, NCS was found to yield much lower signal overall. This was likely to be due to the presence of large proteins inhibiting mass diffusion to the surface and blocking enzyme active sites. A 10% dilution was found to yield greatest signal, which by fortuitous advantage was the dilution at which the samples were within the linear range of the biosensor.

Ten patient drain fluid samples were selected for testing from the cohort collected; five patients whom had a normal uncomplicated post-operative course and five patients who suffered an anastomotic leak. Samples were first tested using a commercial colorimetric kit, in order to then validate the biosensor results. The lactate levels measured by the kit between AL and non-AL groups in all post-operative days were very variable, with no statistical difference between groups in any post-operative day using a Mann Whitney U non-parametric statistical test, in contrast to results seen in **Chapter 3** in the animal model. This was felt to be predominantly due to the small sample size as well as variability in samples although attempts to standardise the samples including measurement of osmolarity were not useful. Use of the drain fluid results was still however valid as a proof of principle for the constructed lactate biosensor.

Biosensors were constructed and tested on post-operative day one drain fluid samples using an autocalibration technique, with mathematical modelling of results based on parameters elicited during initial buffer and NCS experiments. Results were generated using the method of least squares to give biosensor results for each patient sample. Biosensor results were compared with those of the commercial kit, and were found to be significantly similar using a Spearman's rank correlation, r_s = 0.891, P = 0.001. Interestingly the five AL results were shown to have consistently high lactate levels and showed excellent concordance between the biosensor and kit. The non-AL results consisted of high and low outliers and showed poor correlation, raising the hypothesis that in practice an individual patient's lactate trend may be more useful than one arbitrary value. The fabricated biosensor is however shown to work in real patient samples, as an initial proof of concept diagnostic test. Lactate biosensors in the literature are well described, but there appear to be none with evidence of authentication using real-life patient samples.

The work in this chapter has produced a robust lactate biosensor validated on real patient drain fluid samples as a potentially valuable clinical test for monitoring

ischaemia for sensitive, early detection of anastomotic leak and sepsis (Hirst et al., 2013). Future work involves the testing of larger patient data sets to determine sampling accuracy and unequivocally show statistically higher lactate levels in AL patients *vs*. non-AL as shown in the animal model. Attainment of superior reproducibility with commercial fabrication methods such as *via* Biodot robotic printing should also be investigated in order to decrease electrode to electrode variability for POC testing. Stability testing is first paramount before proceeding to any commercial clinical application.

Chapter 5:

Impedimetric biosensors

Chapter 5. Impedimetric biosensors

5.1 Introduction

5.1.1 *E. coli* biosensor design

Strategies for the measurement of bacteria by biosensors have previously included targeting a variety of surface antigens on the membrane of whole bacteria such as LPS, peptidoglycan and glycoprotein to act as biorecognition elements (Ahmed et al., 2014). Measurement of whole bacteria is most commonly accomplished in biosensing by using polyclonal antibodies as bioreceptors; this has the advantage of higher sensitivity as false negatives are lower due to the greater range of antigen recognition and a positive result. Monoclonal antibodies increase specificity, but this is less relevant for the detection of anastomotic leak, where any bacterial type or *E. coli* strain present in the peritoneal cavity should yield a positive result to prompt further investigation and management.

Impedimetric immunosensors were fabricated for whole *E. coli* using custom-made IgG antibodies (Genscript, USA). A mixture of common GI commensals was kindly donated by Mr John Wright, Senior Biomedical Scientist, School of Molecular and Cell Biology, University of Leeds for use as analyte and for antibody manufacture. These comprised *E. coli* strains 35218, HB101, NCTC10418, DH5a, and BL21 which were used in a mixed solution. The protocols chosen were based on methods previously developed to successfully construct impedance biosensors using IgG bioreceptors to detect virus and protein (Caygill et al., 2012, Billah et al., 2010). After optimisation, the *E. coli* biosensors were all constructed as seen in the schematic in **Figure 5.1**. Reduced half antibody was bound to polytyramine polymer coated gold electrodes using sulfo-SMCC cross linker as shown. The functional amine groups on polytyramine allowed cross-linking to available -SH

groups of reduced antibody after heavy chain cleavage at the hinge region by the mild reductant 2-MEA for optimal analyte recognition.

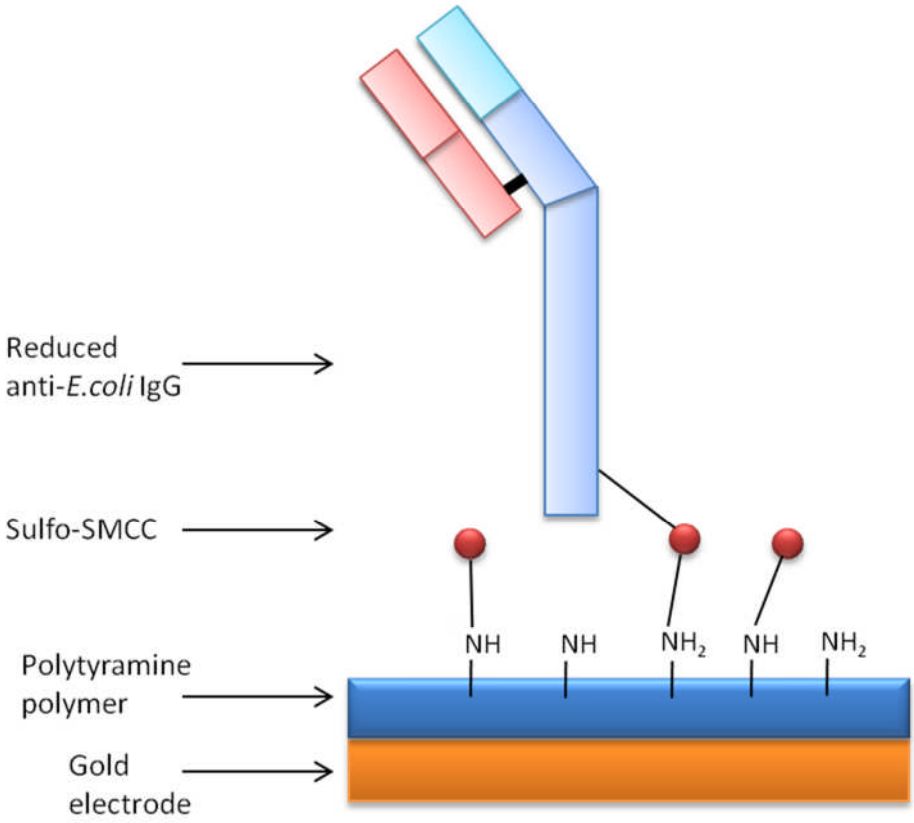

Figure 5.1: Schematic showing immobilisation of reduced *E. coli* IgG onto a polytyramine polymer surface *via* a sulfo-SMCC crosslinker. Schematic is not to scale, and IgG may be orientated other than shown.

5.1.2 TNFα biosensor design

Human TNFα recombinant protein and IgG mouse anti-human TNFα antibody were both purchased from eBioscience (Hatfield, UK). The necessity for collection in live animal models renders the availability of TNFα and its antibody difficult and only in small concentrations and volumes. It was anticipated that the methodology of reductive antibody cleavage with 2-MEA and subsequent removal of remaining 2-MEA by centrifugal filtration used with *E. coli* immunosensor construction would decrease the concentration of TNFα antibody to below a feasible working level on the sensor surface. The concentration of *E. coli* antibody using this method

decreased by approximately 400 fold. The use of biotinylated whole antibody bound *via* NeutrAvidin to a biotin-tagged amine group of polytyramine on gold electrodes had previously been used with some success to detect viruses (Caygill, 2012), and negates the requirement for filtration and subsequent dilution. The smaller size of TNFα analyte compared to whole bacteria and virus also lends itself to binding to whole antibody without encountering problems with spacing and orientation. A schematic of the methodology used for construction of TNFα immunosensors is shown in **Figure 5.2**.

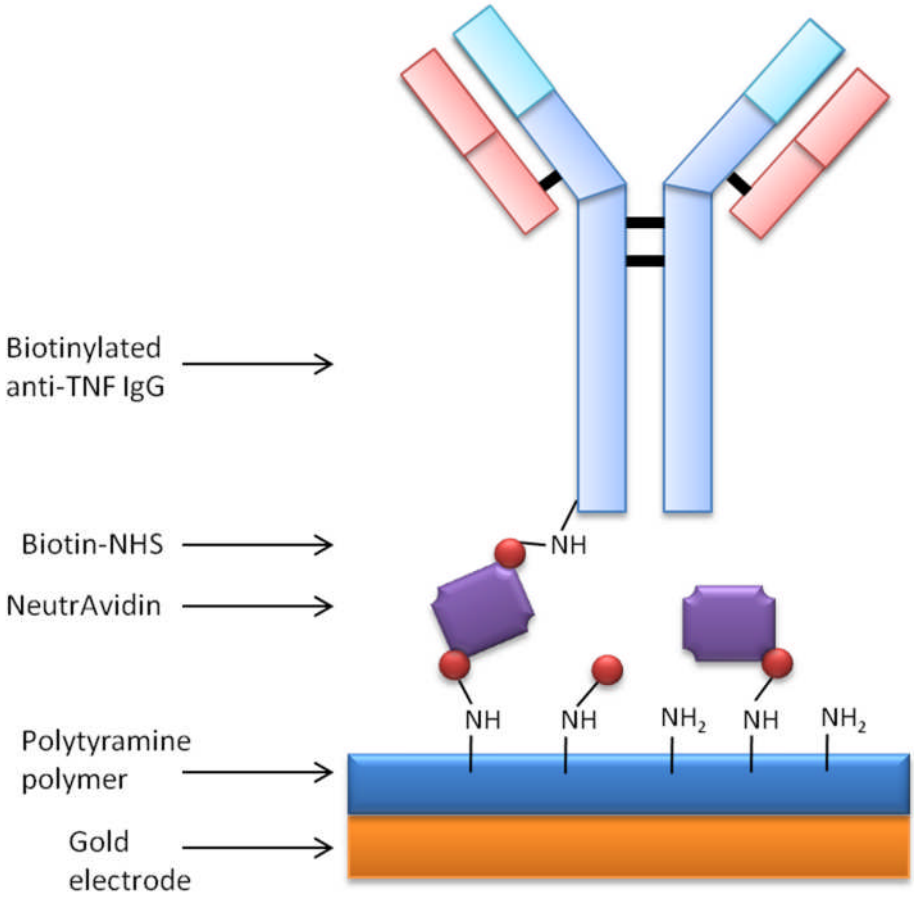

Figure 5.2: Schematic showing immobilisation of TNFα IgG onto a polytyramine polymer surface *via* biotin-NeutrAvidin. Schematic is not to scale, and IgG may be orientated other than shown.

This chapter describes polymer optimisation and subsequent construction of immunosensors for *E. coli* and TNFα detection using half and whole antibodies

respectively. Optimisation of each sensor was achieved in buffered solutions before validation in patient drain fluid samples as used in **Chapter 4** in comparison to commercial methodologies. Cyclic voltammetry, electrochemical impedance spectroscopy (EIS), Midland blotting, SDS-PAGE, SEM, dotblotting and flow cytometry were used to characterise the individual sensors and their components.

5.2 Optimisation of polymer deposition onto gold DropSens electrodes

5.2.1 Cyclic voltammetry mediated electro-polymerisation of an array of polymers

Traditionally polymers are well known for their insulating properties. Recently, a range of conducting polymers has emerged and gained popularity in biosensing due to properties of rapid electron transfer and ability to immobilise biomolecules as bioreceptors for specific analyte detection. Conducting polymers are so named as they allow free movement of electrons through their lattice structure due to the formation of electroactive species from the overlap of partially filled molecular orbitals. These polymers include polyaniline, used in preliminary experiments to develop amperometric lactate biosensors in **Chapter 4**. Cyclic voltammetry is commonly used for synthesis of conducting polymers on surfaces due to its simplicity, reproducibility and ability to take place at room temperature (Gerard et al., 2002, Ates, 2013). Formation of a polymer layer occurs by oxidative coupling, with monomers of the polymer becoming oxidised to form a cation radical followed by coupling to form di-cations. The cyclic repetition of this process forms a polymer layer on the electrode surface, the thickness of which is then finely controlled by variation of current with time or potential.

The choice of polymer for immunosensor construction was first considered, before testing the chosen range of polymers in different supporting media and varying the

potential at CV. Polyaniline was previously not successful in preliminary experiments developing amperometric lactate sensors and was used with variable success in other projects (personal communication). Tyramine however, has been found to be an ideal monomer as it can be electro-polymerised onto an electrode surface, to which bioreceptor can then be immobilised *via* a crosslinker through free amino groups on the polymer surface. Although a poorly conducting polymer, its assembly occurs in a similar way to that of conducting polymers, with monomer oxidation and formation of a cation radical and dimerisation to form a smooth oligomeric polytyramine film. Importantly, the layer formed is self-limiting and typically only 10-100 nm thick, therefore allowing efficient diffusion (Ismail and Adeloju, 2010). Advantages also cited for non or poorly conducting polymers are reduced interference and reduced fouling at the electrode surface. Tyramine has been used in amperometric sensing (Situmorang et al., 1998) and has been shown to successfully immobilise IgG in immunosensor construction for glucose detection (Tsuji et al., 1990). It has recently been shown to be a promising scaffold for immunosensing projects and so was used for initial experimental testing (Ahmed et al., 2013). The dissolving solution with each of two forms of tyramine (tyramine and tyramine hydrochloride) was varied as this was inconsistent in the literature, with tyramine showing poor solubility into aqueous solutions. A 3:1 mix of tyramine:phloretic acid was also tested. Phloretic acid (3-(4-hydroxyphenyl)propanoic acid) possesses no amino groups for subsequent bioreceptor attachment but was included in the mixture with tyramine to potentially reduce non-specific binding. Polytyramine has a positive charge in solution, and as mentioned both *E. coli* and TNFα are negatively charged. Therefore, non-specific binding may be of particular concern with immunosensors for these analytes. Phloretic acid conveys a negative charge which would potentially negate this effect. The range of potential scanned was also a varying parameter. **Figure 5.3** shows the overlaid cyclic voltammograms for each polymer electro-deposition after cleaning of DropSens gold CX2223AT electrodes in ethanol in a water bath using sonication. The scan rate was consistent at 100 $mV.s^{-1}$ and two scans were performed as per previous work (Ahmed et al., 2013). Other parameters were as shown in the legend. The modified electrodes were then

rinsed with dH_2O, before drying under an Ar stream. To equilibrate, the electrodes were incubated in PBS for 30 min, before rinsing with dH_2O and drying under an Ar stream.

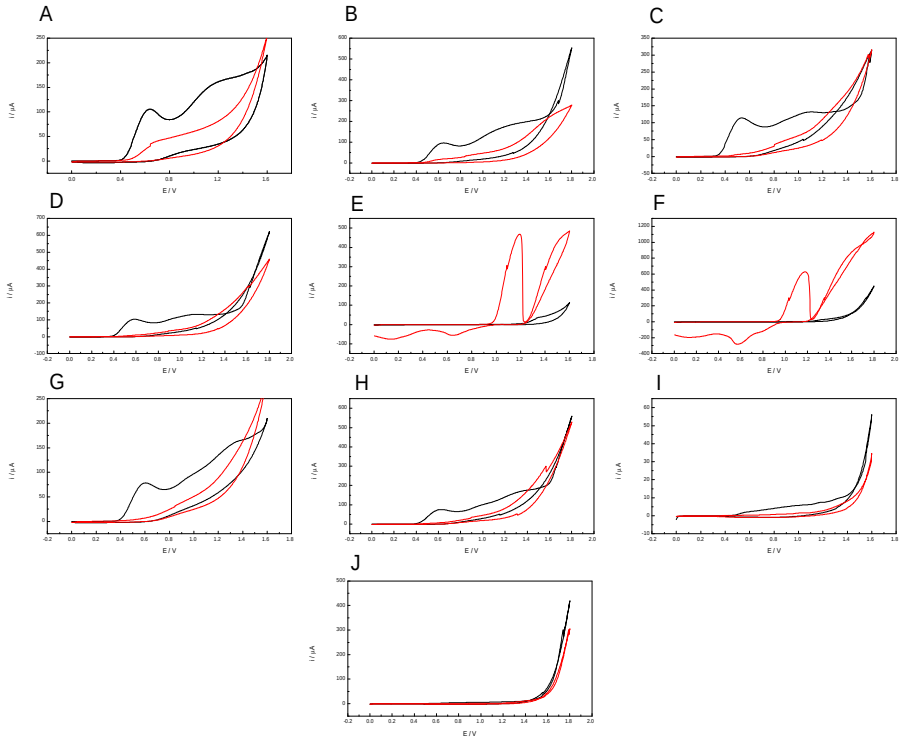

Figure 5.3: Cyclic voltammograms of electrochemical deposition of polymers onto gold DropSens electrodes varying range of potential and polymer type. In all cases, scan one is shown in black, scan two is shown in red. Scan rates were all 100 $mV.s^{-1}$. A, electro-deposition with 0.025 M tyramine in methanol/0.3 M NaOH 0-1.6 V; B, 0.025 M tyramine in methanol/0.3 M NaOH 0-1.8 V; C, 0.025 M tyramine.HCl in methanol/0.3 M NaOH 0-1.6 V; D, 0.025 M tyramine.HCl in methanol/0.3 M NaOH 0-1.8 V; E, 0.025 M tyramine.HCl in PBS 0-1.6 V; F, 0.025 M tyramine.HCl in PBS 0-1.8 V; G, 0.025 M tyramine and phloretic acid (3:1) in methanol/0.3 M NaOH 0-1.6 V; H, 0.025 M tyramine and phloretic acid (3:1) in methanol/0.3 M NaOH 0-1.8 V; I, 0.025 M tyramine and phloretic acid (3:1) in PBS 0-1.6 V; J, 0.025 M tyramine and phloretic acid (3:1) in PBS 0-1.8 V. N.B. Figures not scaled to display differences in characteristics of each trace.

It can be seen that for each set of parameters tested there are varying characteristic traces, although in the majority of cases as expected there is a

reduction in current from the first cycle to the second due to the increasing passivation of the electrode from the poorly conducting polytyramine film formed. Cyclic voltammograms from polymers dissolved in PBS **(E, F, I, and J)** were found to be quite markedly different from their direct counterparts in methanol/NaOH, with tyramine.HCl in PBS at each potential range **(E and F)** showing polymer deposition in two distinct oxidative states during the second scan. Tyramine and phloretic acid mix in PBS **(I and J)** showed particularly low oxidation and reduction of polymer, with very 'flat' traces. Tyramine **(A and B)** and tyramine.HCl **(C and D)** in methanol/NaOH showed equivalent traces. Therefore the presence of hydrochloride did not appear to affect the deposition of polytyramine onto the electrode surface. Tyramine and phloretic acid mixture in methanol/NaOH **(G and H)** also gave similar cyclic voltammograms, demonstrating that the dissolving medium caused a major effect on electro-deposition of polymer regardless of the polymer concentration and variant used. The range of potential from 0-1.6 V or 0-1.8 V did not appear to have any great effect on CV deposition.

5.2.2 Electrochemical impedance spectroscopy of an array of polymer surfaces

The electrochemical impedance spectroscopy (EIS) of each electro-polymerised electrode was then carried out using an Eco Chemie B.V Autolab Type III frequency response analyser (FRA-2) over a range of frequencies from 25 kHz to 0.25 Hz with potential fixed at 0 V and 0.01 mV amplitude. The supporting electrolyte $Fe(CN_6)^{3-/4-}$ in PBS at pH 7.0 was used in all cases. Cleaned bare gold and un-cleaned bare gold electrodes were included for comparison. Data are shown in **Figure 5.4** overlaid as a Nyquist plot, with a further magnification panel for clarity. As discussed in **Section 1.11.3**, Nyquist plots show impedance data comprised of the imaginary (-Z") *vs.* real impedance (Z') of a circuit taken from the respective capacitance and resistance of the cell. In **Figure 5.4**, the bare cleaned and uncleaned gold electrodes showed very small semicircles as expected, implying very low electron transfer resistance to the redox species in the electrolyte.

Interestingly, the spectra for tyramine.HCl in PBS **(E and F)** were comparable to the bare gold and so were not deemed suitable for further investigation. In each polymer interrogated except tyramine in methanol/NaOH **(A and B)**, the capacitance and resistance was higher in the 0-1.6 V than the 0-1.8 V group. Tyramine in methanol/NaOH for both range of potentials **(A and B)** showed the greatest electron transfer resistance of any of the parameters tested.

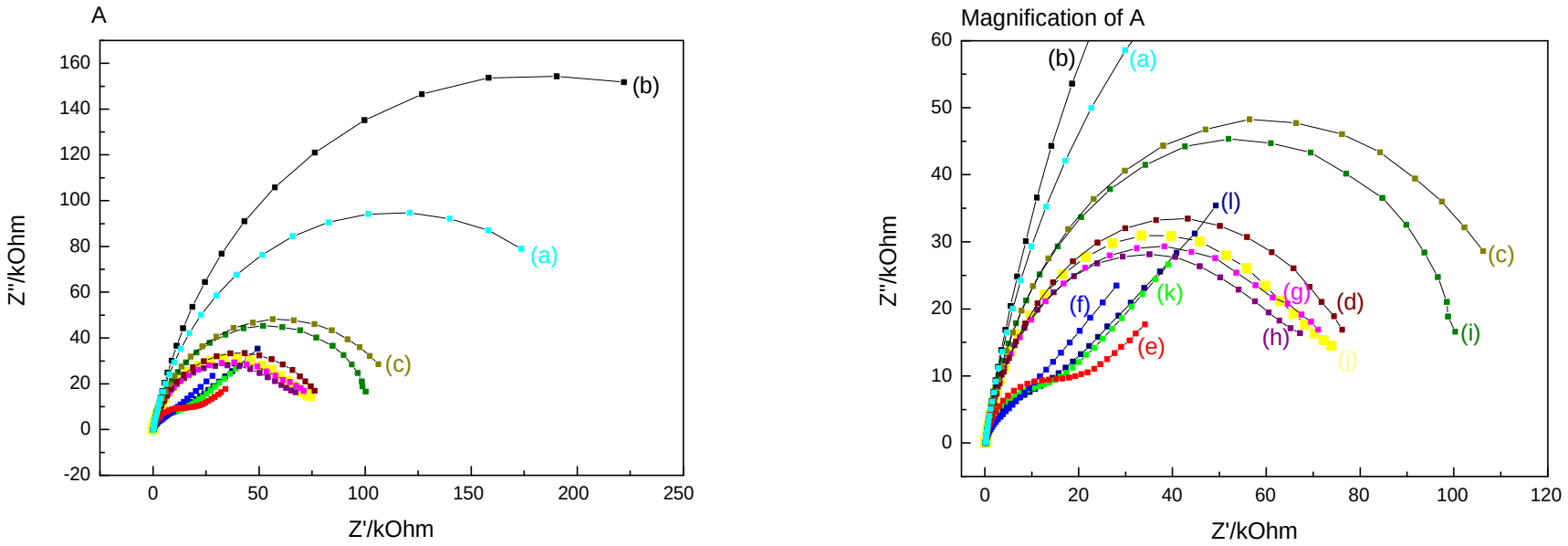

Figure 5.4: Nyquist plots showing impedance of a range of polymers and potentials. Data were obtained in a redox mediator of $Fe(CN_6)^{3-/4-}$ in PBS at pH 7.0 across a frequency range of 0.1 Hz to 25 kHz at an applied sinusoidal voltage of 0 V. Sequential profiles are: (a) 0.025 M tyramine in methanol/0.3 M NaOH 0-1.6 V; (b), 0.025 M tyramine in methanol/0.3 M NaOH 0-1.8 V; (c), 0.025 M tyramine.HCl in methanol/0.3 M NaOH 0-1.6 V; (d), 0.025 M tyramine.HCl in methanol/0.3 M NaOH 0-1.8 V; (e), 0.025 M tyramine.HCl in PBS 0-1.6 V; (f), 0.025 M tyramine.HCl in PBS 0-1.8 V; (g), , 0.025 M tyramine and phloretic acid (3:1) in methanol/0.3 M NaOH 0-1.6 V; (h), 0.025 M tyramine and phloretic acid (3:1) in methanol/0.3 M NaOH 0-1.8 V; (i), 0.025 M tyramine and phloretic acid (3:1) in PBS 0-1.6 V; (j), 0.025 M tyramine and phloretic acid (3:1) in PBS 0-1.8 V; (k), Cleaned bare gold; (l) Uncleaned bare gold

5.2.3 Cyclic voltammetry of an array of polymer surfaces

To characterise the behaviour of the range of polymers further, cyclic voltammetry was performed using the redox mediator $Fe(CN_6)^{3-/4-}$ in PBS at pH 7.0 between -0.3 and +0.6 V at a scan rate of 50 $mV.s^{-1}$. The voltammogram for bare cleaned gold **Figure 5.5i** is presented for comparison, with the trace shown characteristic of the oxidation and reduction of $Fe(CN_6)^{3-/4-}$ on the bare gold surface through which current was free to flow.

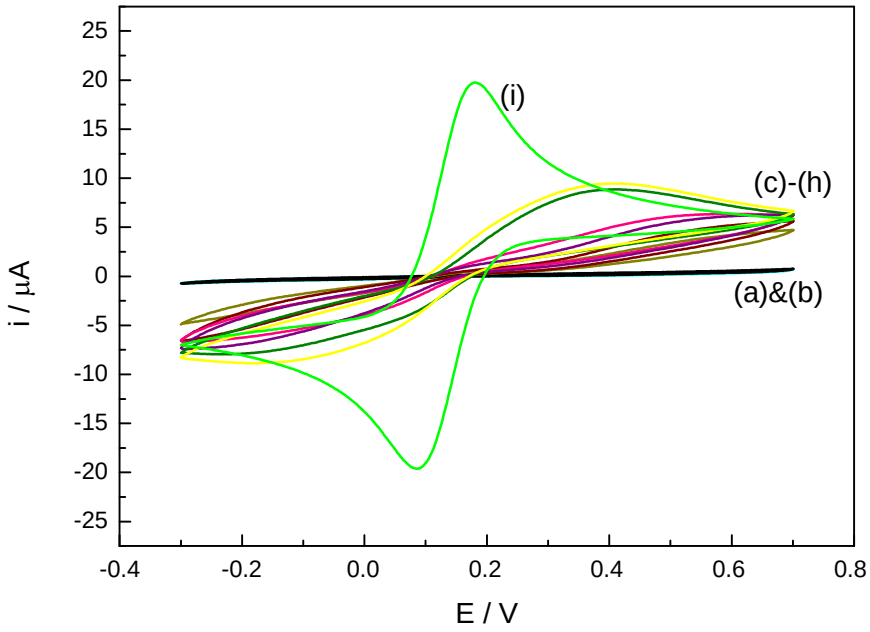

Figure 5.5: Cyclic voltammograms of a range of polymers and potentials. (a) 0.025 M tyramine in methanol/0.3 M NaOH 0-1.6 V; (b), 0.025 M tyramine in methanol/0.3 M NaOH 0-1.8 V; (c), 0.025 M tyramine.HCl in methanol/0.3 M NaOH 0-1.6 V; (d), 0.025 M tyramine.HCl in methanol/0.3 M NaOH 0-1.8 V; (e), , 0.025 M tyramine and phloretic acid (3:1) in methanol/0.3 M NaOH 0-1.6 V; (f), 0.025 M tyramine and phloretic acid (3:1) in methanol/0.3 M NaOH 0-1.8 V; (g), 0.025 M tyramine and phloretic acid (3:1) in PBS 0-1.6 V; (h), 0.025 M tyramine and phloretic acid (3:1) in PBS 0-1.8 V; (i) Cleaned bare gold.

After electro-polymerisation of polytyramine onto the electrodes with all parameters tested, the charge peaks seen with cyclic voltammetry in **Figure 5.5** decreased for both the anodic and cathodic current as compared to bare gold. This is consistent with the polymers causing a surface passivation, preventing the flow of

electrons between the working and counter electrodes and limiting the redox reaction of the redox mediator. Again, tyramine in methanol/NaOH **Figure 5.5 (a) and (b)** traces were distinctly separate from the other conditions tested and were found to be especially insulating. The other polymers and respective dissolving solutions and potentials gave equivalent cyclic voltammetric traces.

5.2.4 Midland blots of an array of polymer surfaces as a technique for availability of amine groups on the sensor surface

To demonstrate the availability of amine groups on the polymers for bioreceptor tethering in order to construct full biosensors, the Midland blot technique was used. Midland blotting is a novel methodology described by our group (Rushworth et al., 2014) in which biotin-NHS, then streptavidin-HRP is applied to the modified electro-polymerised electrodes before addition of enhanced chemiluminescence substrate (ECL) and subsequent imaging. HRP catalyses the oxidation of luminol and causes chemiluminescent light emission. Thus a light signal is seen in the presence of amine groups bound to biotin-NHS, which may be quantified. **Figure 5.6** shows the data for Midland blot analysis of the full range of polymers and conditions tested. Images are of superimposed electrodes and false coloured as captured, and include panels imaged after the application of Tween-20 to remove any non-specific binding. Appearances were largely unchanged after Tween-20 washing. Bare cleaned and uncleaned gold electrodes were included for comparative controls. Tyramine and tyramine.HCl in methanol/NaOH showed a strong presence of available amine groups, with tyramine.HCl in PBS not showing any amines above that of the bare gold controls. Interestingly, a tyramine and phloretic acid mixture in PBS indicated the presence of amine groups much more definitively than that of the polymer mix in methanol/NaOH. This was however still less than shown with single agent tyramine as expected, as it is known that the phloretic acid does not contribute available amine groups on its surface.

The optimal polymer and polymerisation conditions to provisionally take forward in construction of *E. coli* and TNFα immunosensors were found to be 0.025 M tyramine in methanol/0.3 M NaOH 0-1.6 V, due to excellent electron transfer resistance on EIS and passivation of the surface demonstrated *via* cyclic voltammetry indicating a good deposition layer of polymer, and the clear availability of amine groups shown on Midland blot analysis.

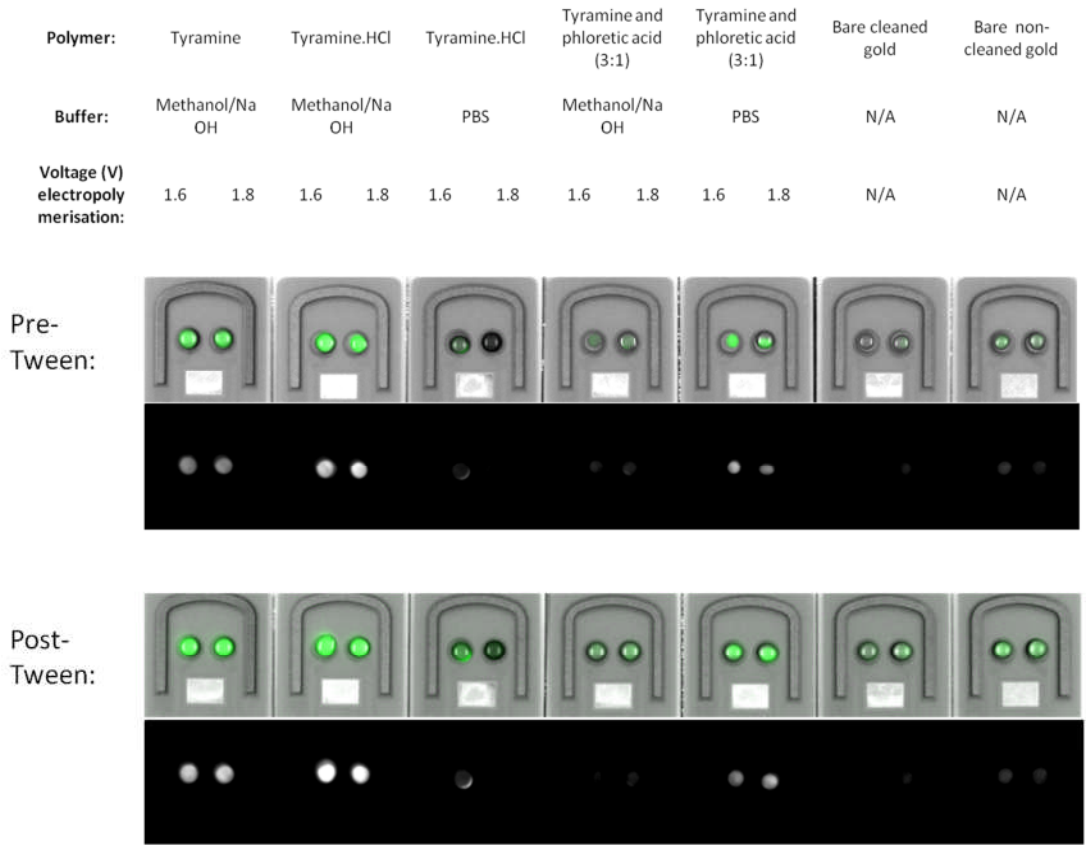

Figure 5.6: Midland blot analysis to characterise range of polymers and potentials for the presence of surface amine. The polymer types in dissolving buffers and potentials are shown. The top panels are superimposed images with the electrodes, bottom panels are as imager captured, pre and post-Tween-20 washing (to remove non-specific bound antibody) as shown.

5.2.5 Scanning electron microscopy of polymer surfaces

Modified electrodes with the chosen polymer (0.025 M tyramine in methanol/0.3 M NaOH) were observed by scanning electron microscopy (SEM) using a Quanta

200F (FEI) machine within the Faculty of Biological Sciences (University of Leeds). This was to ensure the polymer gave an even, smooth layer after electro-deposition in contrast to the known rough bare gold electrodes. It can be seen in **Figure 5.7** that this appears to be the case, with the polymerised modified electrode, **Figure 5.7(A)**, appearing much smoother than that of **Figure 5.7(B)**, the bare gold electrode. This is of importance in order to present a relatively flat surface to facilitate further binding of crosslinkers and orientated antibody in the fully constructed biosensors and therefore is ideal.

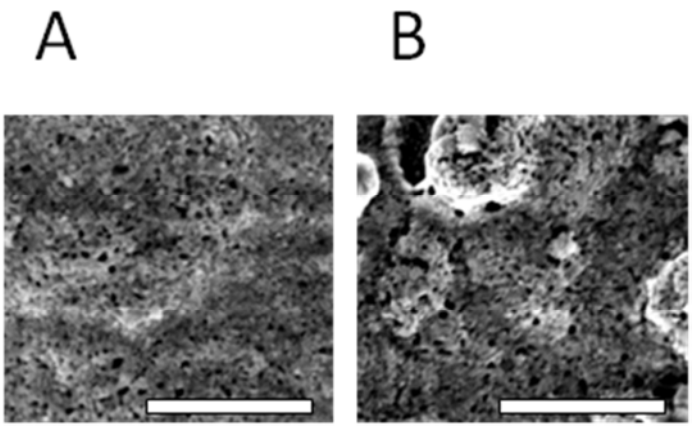

Figure 5.7: Scanning electron microscopy images. A is after deposition of tyramine in methanol/NaOH 0-1.6 V, compared to B, bare gold electrode. The scale bars are 2 µm.

5.3 *E. coli* biosensor

5.3.1 Dot blotting as a technique to show specific *E. coli* analyte to anti-*E. coli* binding

Before any biosensor construction, the specificity of *E. coli* to its antibody was examined in isolation using dot-blotting. As described in **Section 2.2.9**, *E. coli* and *S. pyogenes*, a Gram-positive bacteria which causes throat and skin infections, as a control, were spotted onto nitrocellulose membrane and then probed with anti-*E. coli* antibody. Spots with no primary antibody were also tested as controls. HRP-

secondary antibody (donkey anti-rabbit) was then applied before ECL reagent addition and imaging in a Syngene imager to capture any chemiluminescence, indicating specific analyte-antibody binding. Data are shown in **Figure 5.8**. There was almost no response in spots without primary antibody, showing that non-specific binding of secondary antibody was not present. Likewise, there was very little response in the spot containing *S. pyogenes*, demonstrating specificity, with lack of binding of the anti-*E. coli* antibody to other bacteria. *E. coli* probed with anti-*E. coli* antibody showed a strongly positive dot-blot response, therefore the analyte-antibody binding is shown to be excellent, as well as specific.

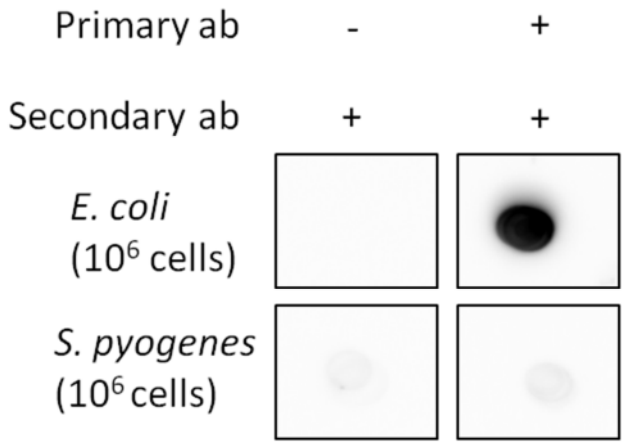

Figure 5.8: Dotblot to show anti-*E. coli* to *E. coli* analyte specific binding. S. pyogenes was used as a negative control. Primary antibody was native *E. coli* antibody at 1:1000 dilution, secondary antibody was 1:5000 donkey anti-rabbit HRP.

5.3.2 Reductive cleavage of *E. coli* antibody

The anti-*E. coli* IgG antibody and that of controls (anti-*S. pyogenes*) were reduced to half antibodies by cleavage of the disulphide groups in the hinge region by 2-MEA as described by Hermanson (Hermanson, 2008). This leaves free sulphydryl groups for binding to crosslinkers and other molecules. The antibody solutions were then exchanged into PBS buffer to remove 2-MEA, remaining whole antibody and smaller antibody fragments with the use of Amicon Ultra spin columns as described in **Section 2.2.5.3.** The resulting half antibody was used immediately to prevent the

re-formation of whole antibody. This relatively gentle method of reduction to generate half antibody is important for orientation, as antibody randomly immobilised on the sensor surface *via* other reactive groups on fragments from a variety of reductive processes may be inaccessible to analyte due to steric hindrance. The free –SH generated by hinge region reduction in this methodology can be used to bind the half antibody in a more orientated fashion, with the antibody recognition site freely available to improve accessibility for analyte and therefore improved analyte recognition and a superior biosensor (Billah et al., 2010).

5.3.2.1 SDS-PAGE gel

To demonstrate the reduction of antibody and subsequent filtration to leave half antibody, the protein composition at each stage of antibody processing was analysed using non-reducing SDS-PAGE. The data are shown in **Figure 5.9**. It can be seen that the native antibody sample in **lane 1 (and 1b)** contained proteins at 150 kDa, and therefore comprised whole IgG as expected. Samples in **lanes 2 and 2b** show the protein composition to be predominantly at 75 kDa, indicating the 2-MEA had reduced the sample to predominantly half antibody. There was still some presence of protein at 150 kDa however, illustrating the gentle reductive nature of 2-MEA which did not reduce all the antibody present, and protein at 50 kDa and 25 kDa indicative of reduction to heavy and light chain fragments. **Lanes 3 and 4** show protein content after centrifugal filtration at 100k and 50k respectively. The filtration process should replace 2-MEA with PBS buffer and remove any non-reduced whole and fragmented antibody. **Lanes 3b and 4b** show the identical process, but at higher relative concentrations to those in **lanes 1, 1b, 2 and 2b**. In these **lanes (3b and 4b)** the remaining presence of half antibody at 75kDa is seen, showing that the reduction and filtration process worked successfully. Using spectroscopy the half antibody after this process was found to be at a concentration of 0.0214 $mg.ml^{-1}$, which has been shown to be in the range of the optimum concentration for use on bacterial immunosensors (Ahmed et al., 2013).

This optimum concentration is much lower than anticipated, but thought be due to higher concentrations of antibody decreasing sensitivity of the biosensor, likely as a result of steric hindrance on the surface. The half antibody used on the completed biosensor surface was therefore maintained at this concentration.

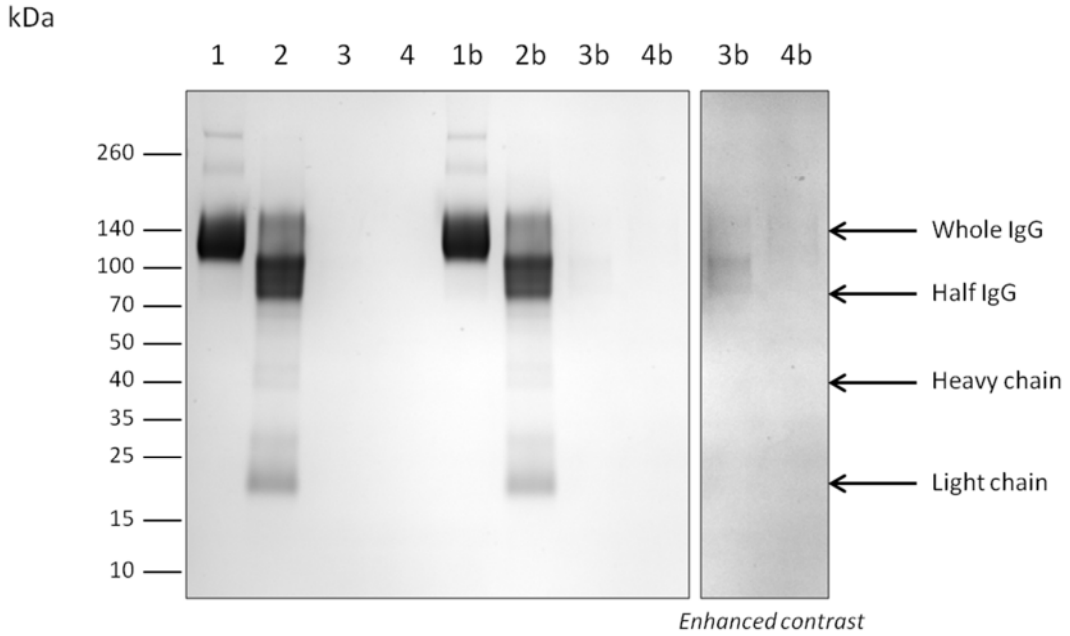

Figure 5.9: Non-reducing SDS-PAGE gel of reduced *E. coli* IgG samples. Lane 1 contains native *E. coli* antibody (8.468 mg.ml^{-1}), lane 2 is antibody after incubation with 2-MEA, lane 3 after 100k filtration, and lane 4 after 50k filtration. Lanes 1-4 show comparable concentrations of antibody at different stages of reduction and filtration, with lanes 1b-4b showing higher comparable concentrations of filtered contents compared to native and post 2-MEA, and at enhanced contrast.

5.3.3 Cyclic voltammetry mediated electro-deposition of polytyramine onto gold working electrode

Once polymer and antibody were optimised, the biosensor construction was commenced. As described in **Section 5.2**, the chosen polymer comprised a 25 mM solution of tyramine in methanol containing 300 mM NaOH. The polymer was applied onto cleaned gold electrodes using cyclic voltammetry with two scans from 0 V to +1.6 V at 100 mV.s^{-1}. The modified electrodes were then rinsed with dH_2O, before drying under an Ar stream and equilibrated by incubation in PBS for 30 min

before again rinsing with dH_2O and drying under an Ar stream. The resulting cyclic voltammograms of the two scans are shown overlaid in **Figure 5.10**. As previously seen, the second cycle achieves a lower current than the first indicating the passivation of the surface due to the layer formation of the non-conducting polymer. The voltammograms generated were consistent throughout all experiments.

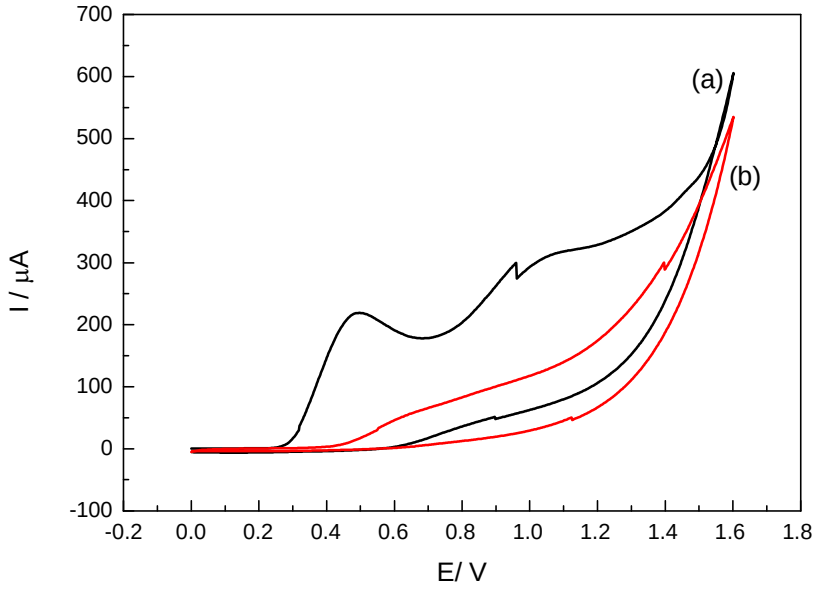

Figure 5.10: Cyclic voltammograms of electrochemical deposition of 0.025 M tyramine in methanol containing 0.3 M NaOH. Scan rate was 100 $mV.s^{-1}$. (a) is the first scan, (b) is the second scan, showing the increased insulation as polymer layers were added.

5.3.4 Cyclic voltammetry of *E. coli* biosensor construction steps

The different stages of *E. coli* immunosensor construction were evaluated using cyclic voltammetry in the redox mediator $Fe(CN_6)^{3-/4-}$ to show the changes in profiles as layers were added to the surface and thus altered the electrochemical properties. The CV data is shown in **Figure 5.11**. The overlaid scans show the bare cleaned gold electrode in trace **(a)** which is characteristic of the oxidation and reduction of $Fe(CN_6)^{3-/4-}$ with free diffusion of electrons generating current. Trace **(b)** shows the comparably smaller redox peaks generated after electro-deposition

of polytyramine on the electrode surface. This increased insulation is attributable to the layer of non-conducting polymer formed on the surface. After addition of sulfo-SMCC cross-linker and anti-*E. coli* IgG **(c)**, the anodic and cathodic current peaks were shown to marginally increase indicating less passivation than that seen with polymer.

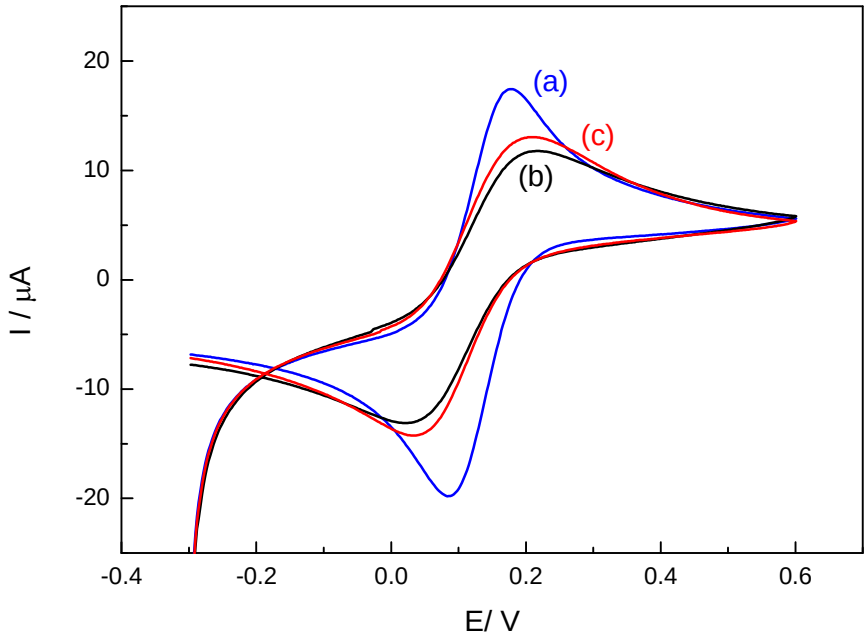

Figure 5.11: Cyclic voltammograms at different biosensor construction steps. (a) cleaned bare gold electrode, (b) after electro-polymerisation of polytyramine, (c) after sulfo-SMCC crosslinker and anti-*E. coli* IgG immobilisation. Scan rate 50 mV.s^{-1} in redox mediator $Fe(CN_6)^{3-/4-}$.

5.3.5 Electrochemical impedance spectroscopy of *E. coli* biosensor in buffer

5.3.5.1 Interrogation of *E. coli* biosensor

After construction of functional *E. coli* immunosensors, electrochemical impedance spectroscopy (EIS) was carried out using an Eco Chemie B.V Autolab Type III frequency response analyser (FRA-2) over a range of frequencies from 0.25 Hz to 25 kHz in $Fe(CN)_6^{3-/4-}$ at a voltage of 0 V for interrogation. Experiments were performed by the incubation of increasing concentrations of *E. coli* analyte in PBS

on the electrode surface for 30 min, rinsing in dH_2O and drying under an Ar stream before interrogation using EIS between each addition. The concentration of *E. coli* applied was 0 and 10^4 - 10^8 cells ml^{-1}, as previous systems were shown to have limits of detection of 10^6 particles ml^{-1} (Yang et al., 2004). Data were analysed as a Nyquist plot as shown in **Figure 5.12**. The data clearly show the increase in impedance as greater concentrations of *E. coli* were incubated on the constructed immunosensor surface, as demonstrated by the increasing gradients of the partial semi-circles. The constructed *E. coli* biosensors were therefore successful at detecting *E. coli* in buffered solution.

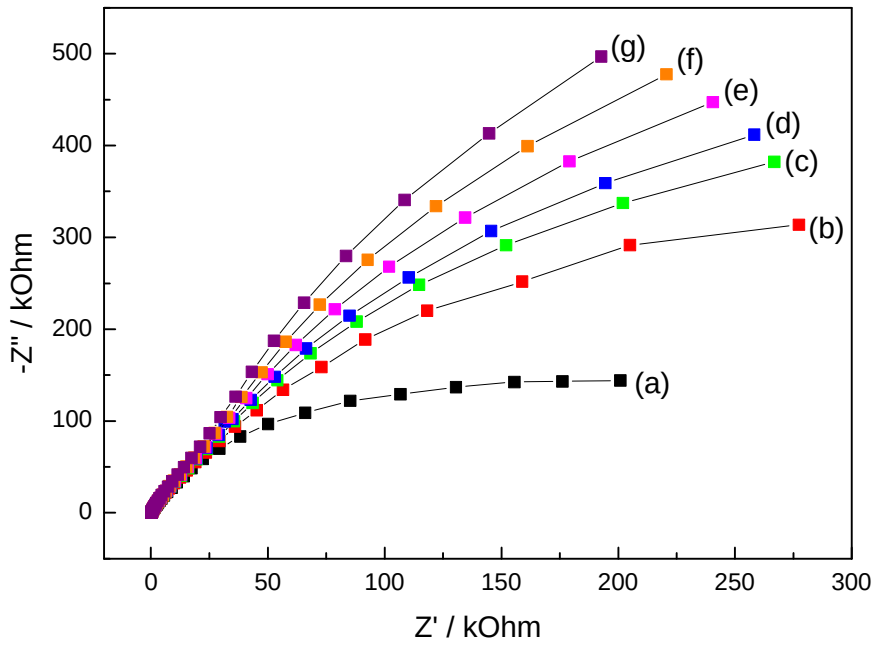

Figure 5.12: Nyquist plots showing impedance of *E. coli* biosensors after *E. coli* addition. Data were obtained in a redox mediator of $Fe(CN)_6^{3-/4-}$ in PBS at pH 7.0 across a frequency range of 0.25 Hz to 25 kHz at an applied sinusoidal voltage of 0 V. Sequential profiles are: (a) cleaned bare gold electrode with electro-polymerised tyramine in methanol/NaOH, (b) fully constructed anti-*E. coli* biosensor with no analyte, (c)-(g) 10^4 to 10^8 *E. coli* cells ml^{-1} respectively.

To demonstrate specificity, a negative control immunosensor was conducted in parallel using antibodies against *S. pyogenes*. Analyte incubation, concentrations and EIS parameters were identical to those of the *E. coli* onto anti-*E. coli*

immunosensor experiments. Nyquist plot data are shown in **Figure 5.13**. In both **Figure 5.12 (a)** and **Figure 5.13 (a)** the bare cleaned gold electrodes with immobilised polymer show equivalent impedance semi-circles demonstrating the comparable starting points for both biosensors. As analyte was added, there was some increase in impedance seen in **Figure 5.13**, but this was minimal, demonstrating the selectivity of the fabricated immunosensor to *E. coli*.

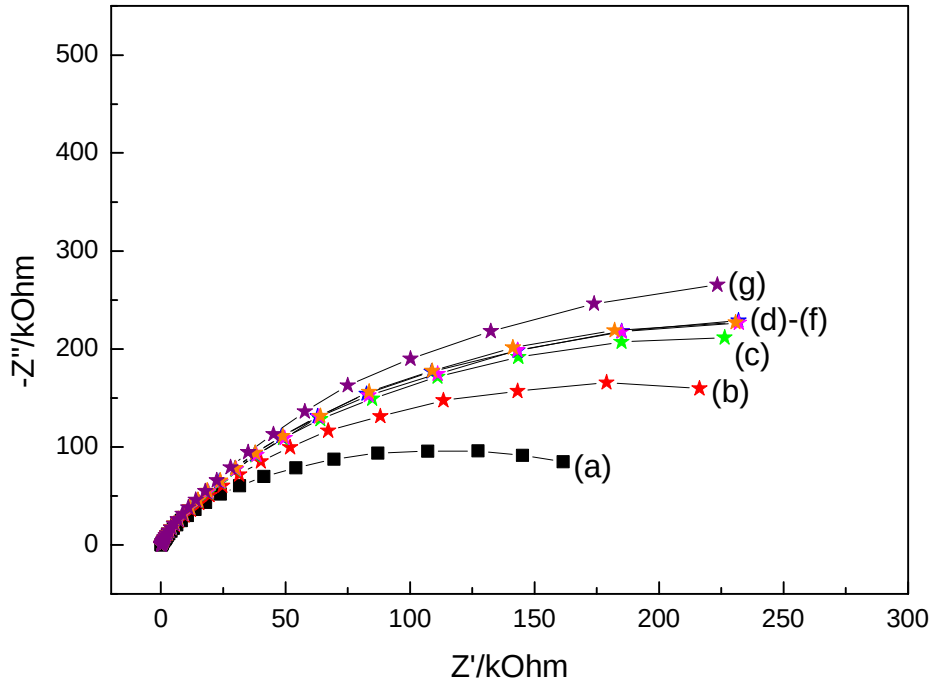

Figure 5.13: Nyquist plots of impedance spectra recorded with S. pyogenes biosensor as control. Redox mediator and parameters as in **Figure 1.12** were used. Sequential profiles are: (a) cleaned bare gold electrode with electro-polymerised tyramine in methanol/NaOH, (b) fully constructed anti-*S. pyogenes* biosensor with no analyte, (c)-(g) 10^4 to 10^8 *E. coli* cells ml^{-1} respectively.

5.3.6 *E. coli* biosensor calibration curves in buffer

For each Nyquist plot data for each electrode, the charge transfer resistance (R_{ct}) was determined, as modelled to Randles equivalent circuit detailed in **Section 1.11.3.1.** Randles equivalent circuit modelling has been used in previous work and was found to fit the data generated in this study well (Caygill et al., 2012). It is a useful method for facilitating the comparison of two sets of data, as it only uses one

parameter of impedance i.e. the capacitance or the resistance. As in previous work Randles equivalent circuit was modified to simplify C_{dl} to a constant phase element, CPE, with assumption of full passivation of the electrode indicating CPE was capacitive, and the removal of Warburg impedance due to the lack of diffusion of the redox mediator $Fe(CN)_6^{3-/4-}$ because of inhibition of electron flow across the modified electrodes. Upon analyte binding, the double layer increased in thickness, thus decreasing capacitance and blocking the flow of redox species across the double layer, omitting Warburg impedance (Caygill, 2012).

Data shown in **Figure 5.14** are thus derived from the Nyquist plots modelled to a modified Randles equivalent circuit. The experiments demonstrate that the fabricated *E. coli* immunosensors successfully detected *E. coli*, as the R_{ct} increased across the electrode-solution interface upon increasing concentrations of *E. coli* due to the binding of the *E. coli* cells to the sensor surface **(Figure 5.14a).** The negative control of *E. coli* to anti-*S. pyogenes* conducted in parallel **(Figure 5.14b)** shows minimal binding to the sensor surface, with no real increase in R_{ct} on increasing analyte concentration seen, thus confirming high specificity. The limit of detection was shown to be 10^4 cells ml^{-1} when data were corrected for non-specific binding. The standard deviations seen in **Figure 5.14** for n = 5 were relatively small, particularly for the control data, showing high concordance between sensors and robustness in buffered solution.

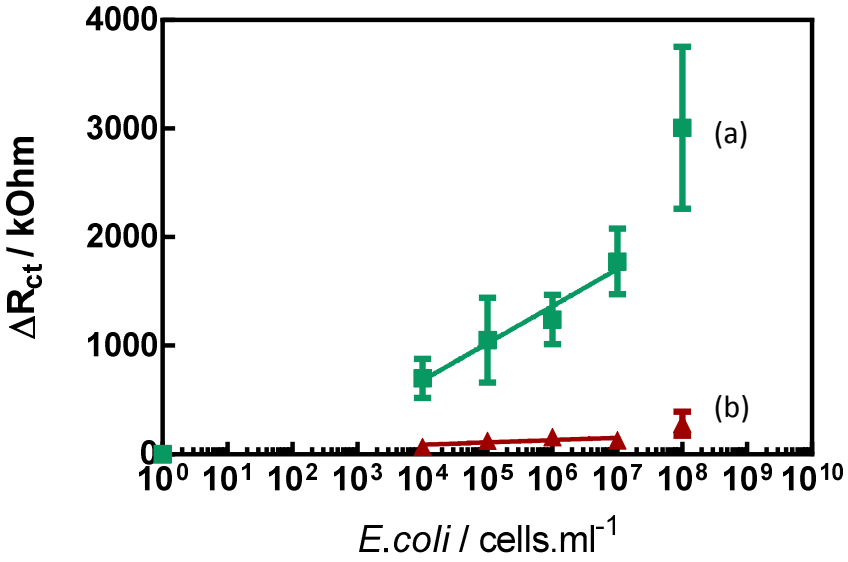

Figure 5.14: R_{ct} of biosensors after additions of *E. coli* analyte. Each set of biosensors were exposed to increasing concentrations of *E. coli* analyte, the impedance read and the R_{ct} determined. Data shows binding for (a) *E. coli* to anti-*E. coli* IgG, and negative control of (b) *E. coli* to anti-*S. pyogenes* IgG, in all cases where mean ± S.D has been calculated for n = 5. LOD is 10^4 cells ml^{-1}. Linear fitting with GraphPad Prism v.5 was used.

5.3.7 Biological media dilution optimisation of *E. coli* biosensor

5.3.7.1 R_{ct} of *E. coli* biosensors with *E. coli* spiked into a range of dilutions of newborn calf serum

After proof of concept and optimisation in buffer, newborn calf serum (NCS) was again utilised as an intermediary to testing on patient drain fluid samples as shown in **Section 4.6.5**; this time to generate a biologically comparable calibration curve to calculate concentrations of analyte from biosensor R_{ct} values as well as optimising dilutions of drain fluid samples. Increasing concentrations of *E. coli* analyte (10^3 – 10^7 cells ml^{-1}) each in dilutions of 10, 20, 40, 60 and 90% (v/v) newborn calf serum in PBS were incubated on a modified electrode surface for 30 min before rinsing in dH_2O and drying under an Ar stream. EIS was then performed between each *E. coli* addition under parameters used previously in $Fe(CN)_6^{3-/4-}$. R_{ct} results for each NCS dilution are shown in **Figure 5.15**. A striking feature common to all plots were the much higher R_{ct} values generated than those seen in buffer, with data in **Figure 5.15**

B in particular in the region of 30x higher. Specific anti-*E. coli* biosensors **(a)** compared to anti-*S. pyogenes* controls **(b)** for each given NCS dilution were also seen to behave unpredictably, with 10% dilutions showing higher R_{ct} in controls than with specific antibody. Data were repeated which served to show entirely different R_{ct} plots on each occasion, therefore representative data for each antibody and NCS dilution are shown. These appearances were thought to be attributable to a high level of non-specific binding of serum proteins and other substances, although this was not observed in a proportional way from dilution to dilution, nor still higher as expected in specific compared to controls. Newborn calf serum was thus discounted for use in an equivalent media calibration curve to the patient drain fluid samples for calculation of *E. coli* using EIS.

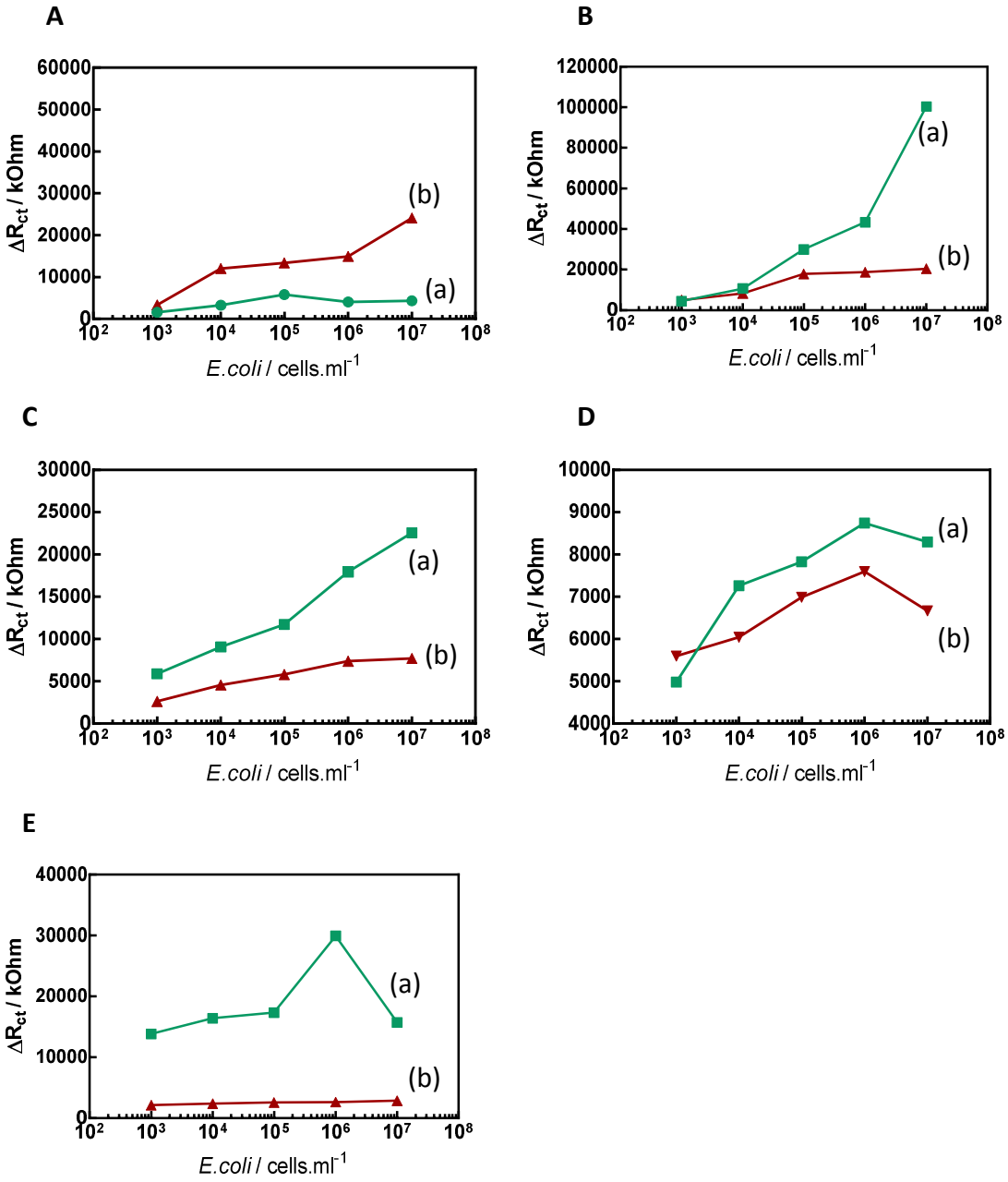

Figure 5.15: R_{ct} of biosensors after additions of *E. coli* analyte in newborn calf serum. Each set of biosensors were exposed to increasing concentrations of *E. coli* analyte in a range of dilutions of newborn calf serum. Data in A shows binding in 10% NCS; B, 20% NCS; C, 40% NCS; D, 60% NCS; E, 90% NCS. In all cases, data shown is (a) *E. coli* to anti-*E. coli* IgG, and negative control of (b) *E. coli* to anti-*S. pyogenes* IgG.

5.3.7.2 R_{ct} of *E. coli* biosensors with *E. coli* spiked into a range of dilutions of patient drain fluid diluents

To overcome the issues seen with non-specific binding in newborn calf serum, a novel approach recently described for EIS measurement of prostate specific antigen (PSA) in human plasma was experimentally tested. Chornokur *et al* used a real patient sample with known low concentration of PSA diluted 1000x with PBS as a "diluent" for all other experiments (Chornokur et al., 2011). This was found to reduce non-specific binding and thus maintain sensitivity and specificity. To evaluate this, a selected patient drain fluid sample containing comparably low levels of bacterial cells (14,205 cells ml^{-1} measured by flow cytometry, see **Section 5.3.11**) was diluted 1000x with PBS and used as a diluent. Two concentrations of *E. coli* analyte (10^3 and 10^6 cells ml^{-1}) were spiked into 10, 50, and 90% patient "diluents" before interrogation with EIS under previous parameters. Data are shown in **Figure 5.16**. In contrast to the experiments in NCS, the R_{ct} values were consistently comparable to those of buffer, allowing a consistent graphical scale to be used to show results. Specific anti-*E. coli* biosensors showed higher R_{ct} values compared to anti-*S. pyogenes* controls in 10% diluent, but were found to be equivalent at higher dilutions in agreement with previous work shown in **Section 4.6.5** where 10% drain fluid samples were ultimately used.

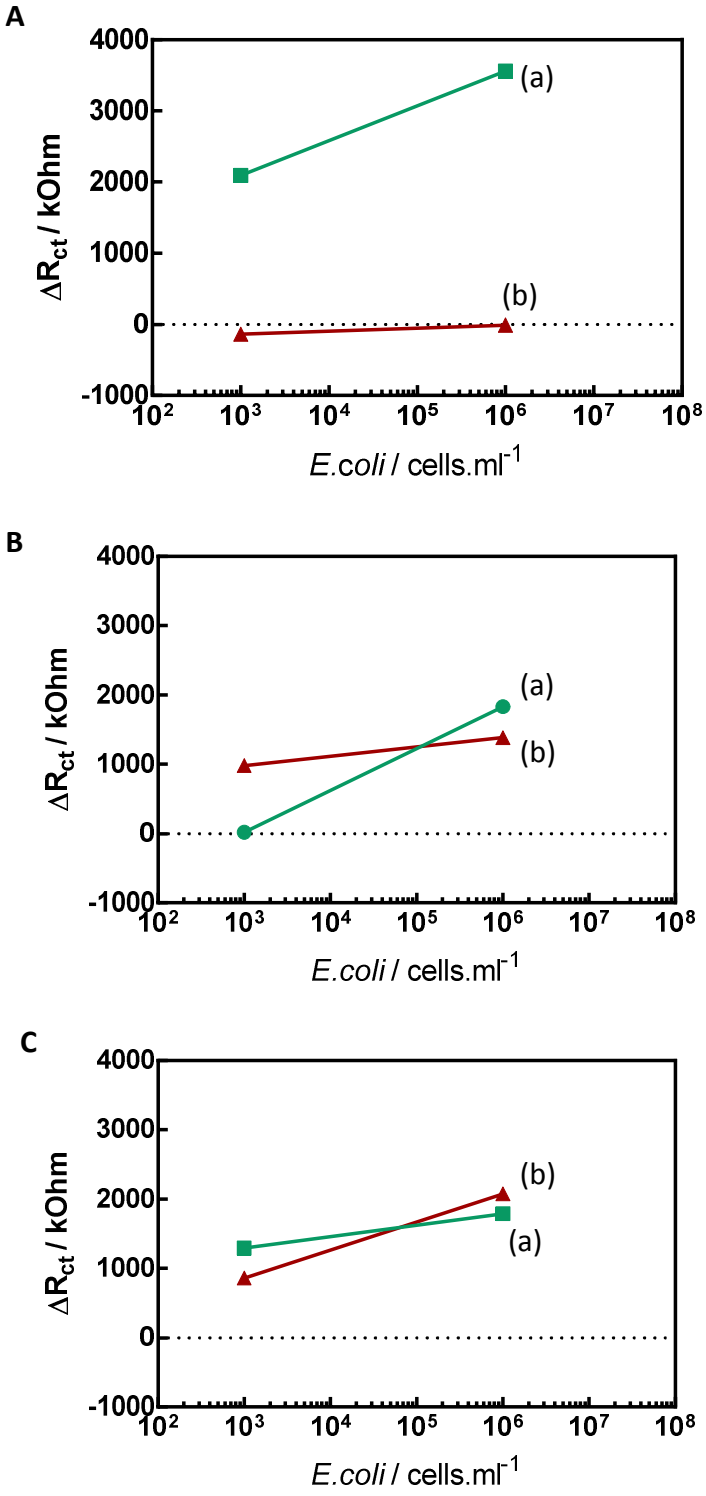

Figure 5.16: R_{ct} of biosensors after additions of *E. coli* analyte in patient diluent. Each set of biosensors were exposed to increasing concentrations of *E. coli* analyte in a range of dilutions of patient drain fluid acting as diluent. Data in A shows binding in 10%; B, 50%; C, 90%. In all cases, data shown is (a) *E. coli* to anti-*E. coli* IgG, and negative control of (b) *E. coli* to anti-*S. pyogenes* IgG.

Despite only being demonstrated at two *E. coli* concentrations, the R_{ct} results in 10% diluents showed the same trend as those previously seen in buffered solutions. This is demonstrated more clearly with a bar chart shown in **Figure 5.17**. The proportional R_{ct} increase from 10^3 to 10^6 cells ml^{-1} in buffer and 10% diluent shows a clearly similar trend, as compared to higher diluents. A 10% diluent was therefore used for further experiments in development of *E. coli* calibration curves.

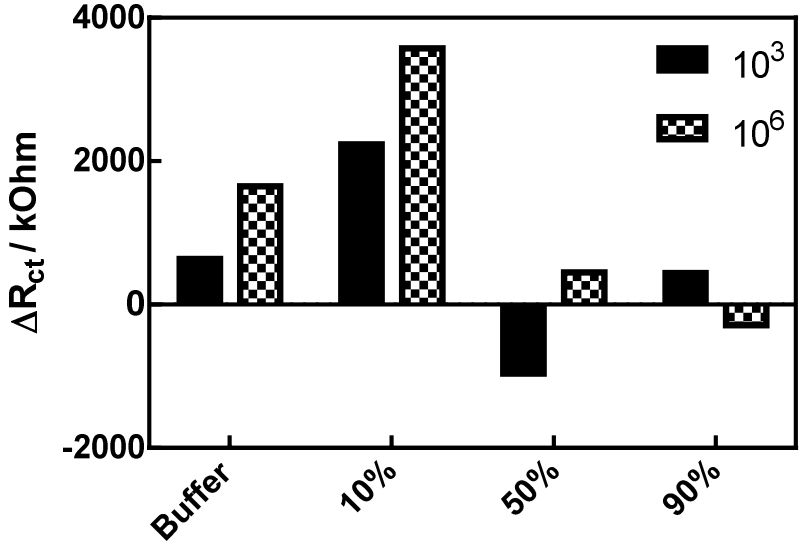

Figure 5.17: Bar chart showing overall ΔR_{ct} at two *E. coli* concentrations in buffer and 10%, 50% and 90% patient drain fluid "diluents".

5.3.8 *E. coli* biosensor calibration curves in patient diluent

Once the dilution of patient drain fluid sample "diluent" was established as 10%, EIS was repeated using spiked *E. coli* analyte at a larger range of concentrations (10^3 – 10^7 cells ml^{-1}) into 10% diluent for n = 5. Again, specific anti-*E. coli* biosensors were compared to anti-*S. pyogenes* controls and EIS parameters were as previously. The corresponding R_{ct} data is shown in **Figure 5.18**. It can be seen that R_{ct} values were higher in both specific and controls compared to results in buffer, which was hypothesised as being due to a degree of non-specific binding which was not

unexpected in these biological samples. The lower level of detection remained 10^4 cells ml^{-1}. The data were corrected for this non-specific binding by specific **(a)** minus control **(b)** at each *E. coli* concentration to generate calibration curve **(c)**. This calibration curve was ultimately used to calculate *E. coli* concentration in the ten patient drain fluid samples subsequently measured by the constructed immunosensors for validation of their operational capacity.

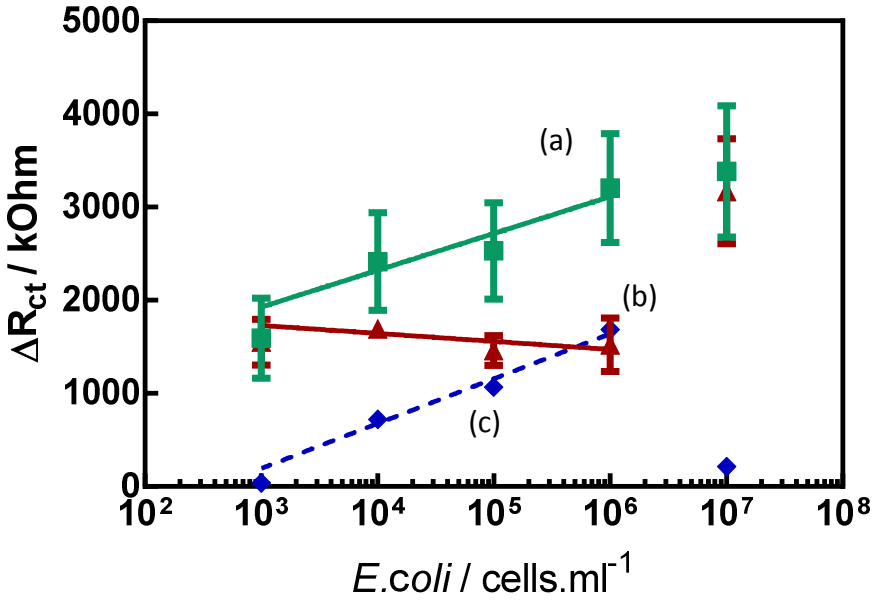

Figure 5.18: R_{ct} of biosensors after additions of *E. coli* analyte spiked into 10% patient drain fluid diluent. Each set of biosensors were exposed to increasing concentrations of *E. coli* analyte in 10% patient drain fluid diluent, the impedance read and the R_{ct} determined. Data shows binding for (a) *E. coli* to anti-*E. coli* IgG, and negative control of (b) *E. coli* to anti-*S. pyogenes* IgG, in all cases where mean ± S.E has been calculated for n = 5. LOD is 10^4 cells.ml^{-1}. Linear fitting with GraphPad Prism v.5 was used. Calibration curve (c) is specific (a) minus control (b) for each *E. coli* concentration.

5.3.9 Testing in patient drain fluid samples

The same post-operative day (POD) one drain fluid samples from ten patients described and used in **Section 4.6.6** for validation of the amperometric lactate biosensors were used to validate the *E. coli* biosensors. As outlined in **Sections 2.2.2** and **4.6.6,** five of these patients underwent an uneventful post operative course and five patients suffered an anastomotic leak (AL), with groups matched for basic demographics and operation type etc. Samples were collected daily from patient's abdominal drain bags at 6.00 am and supernatant stored at -20 °C until use after centrifugation at 3,000 *x g* for 10 min. Each drain fluid sample was diluted to 10% (v/v) as optimised, before testing in triplicate with EIS interrogation in $Fe(CN)_6^{3-/4-}$ with parameters as previously, using an applied potential of 0 V and frequency range 0.25 Hz to 25 kHz. Each drain fluid sample was also interrogated with a control using anti-*S. pyogenes* biosensors. The R_{ct} data for all ten patient samples is shown in **Figure 5.19.** As before, patients 1-5 are AL and 6-10 are non-AL. The dotted red line corresponds to the mean average of the control results for all patients, as this was found to be inconsistent when plotted individually and therefore not reliant. Interestingly, patient four had three negative R_{ct} results when the data were normalised. Standard deviation error was low except in this patient and patient nine, demonstrating good concordance between electrodes for each patient sample.

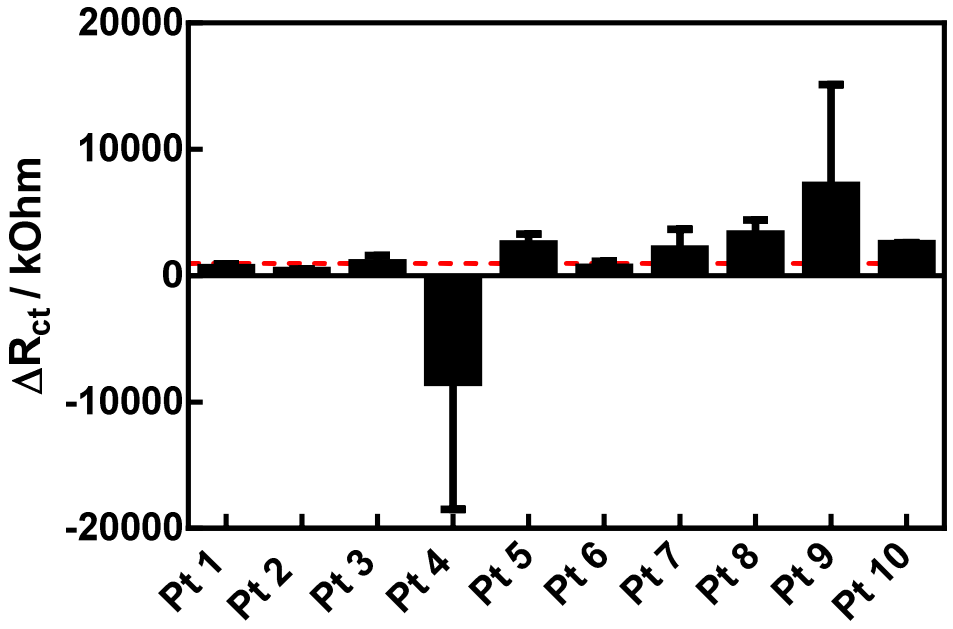

Figure 5.19: R_{ct} of biosensors tested on 10% patient drain fluid samples. Each biosensor was exposed to patient samples at 10% dilution as optimised. Data are shown as mean ± S.D calculated for n=3. An average control of each drain fluid sample on an anti-*S. pyogenes* biosensor is shown by the red dotted line.

Using the R_{ct} values for each patient in triplicate, results were then inputted into the equation given by the calibration curve in **Figure 5.18** to give mean and standard deviation values of *E. coli* concentration in each sample. Data are shown after results from commercial methods used to validate the biosensor results.

5.3.10 Commercial bacterial assay results

5.3.10.1 Commercial lipopolysaccaride assay

To validate the *E. coli* impedance biosensor results on patient drain fluid samples, the LPS commercial kit used for the animal samples was again utilised **(Section 3.2.3),** with LPS being a component of the Gram-negative bacterial cell wall and therefore a surrogate marker of *E. coli.* A limitation of this method for validation purposes was the possibility of other Gram-negative bacteria being present in the samples tested leading to higher LPS levels being measured than those of *E. coli*

measured by the biosensors. However, it was considered that the increase would be proportional and so although not ideal, would still be a suitable test for validation of the biosensors. Firstly the "in-house" *E. coli* analyte dilutions used during interrogation of the constructed *E. coli* biosensors were tested in triplicate with the commercial LPS assay. This was in order to provide a further calibration curve for the assay result conversion of LPS in EU.ml^{-1} to *E. coli* (and other Gram-negative bacteria) in cells.ml^{-1} for a more direct comparison with the *E. coli* biosensor results. Although it was not strictly necessary for the validation assay to use the same units as the biosensors as they would be plotted on opposite graph axes, it was considered a useful adjunct. The results are shown in **Figure 5.20.** The calibration curve is of sigmoid form, with the linear range steepest between 10^4 and 10^6 *E. coli* cells ml^{-1}, which correlates with the range shown by the *E. coli* biosensors. The assay results were also shown to be concordant between triplicates, with the kit giving consistent results.

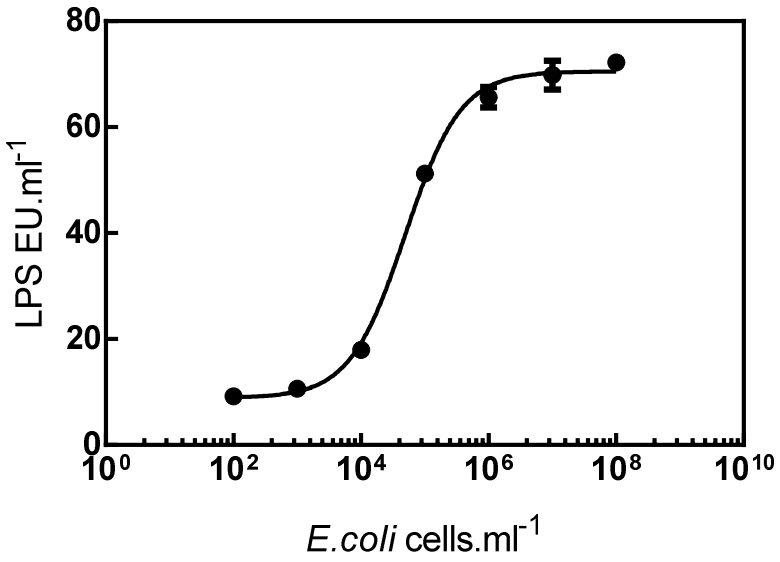

Figure 5.20: Calibration curve generated by *E. coli* analyte at concentrations 10^2 – 10^8 cells ml^{-1} as measured by the commercial LPS colorimetric assay kit. Data points are mean ± S.D for n = 3.

The commercial LPS assay kit was then performed on the drain fluid samples of all ten patients on post-operative day one samples in triplicate. However, the LPS assay was found to be unsuitable for purpose on the patient drain fluid samples. This was due to the drain fluid samples retaining a high degree of colour upon kit application and therefore interfering with the absorbance readings. This was not an issue with the colourless *E. coli* standards and in-house samples, with the colorimetric lactate kit due to the high sample dilutions used, or with the animal samples. The TNFα commercial kit used was also an ELISA in which sample colour is irrelevant.

Figure 5.21 shows photographs of the 96-well plates during the LPS commercial kit assay application immediately after addition of samples including kit standards and patient drain fluid samples. In **A**, drain fluid samples were added undiluted. A wide variability in colour in wells can be seen, which clearly would affect the corresponding absorbance readings. Many of the well samples were measured as the maximum absorbance reading by the spectrophotometer, and therefore were clearly affected. This was corroborated with the method recommended by the kit for determination of whether the sample inherent colour was affecting the results, which was strongly positive. To attempt to negate this problem the drain fluid samples were diluted to 1:10 and 1:50 with endotoxin free water as per the kit instructions for dilution. The 96-well plates containing the diluted samples are shown in **B**. It can be seen that the 1:10 samples remain affected by colour, but the 1:50 dilutions, at least by eye, appear to be colourless.

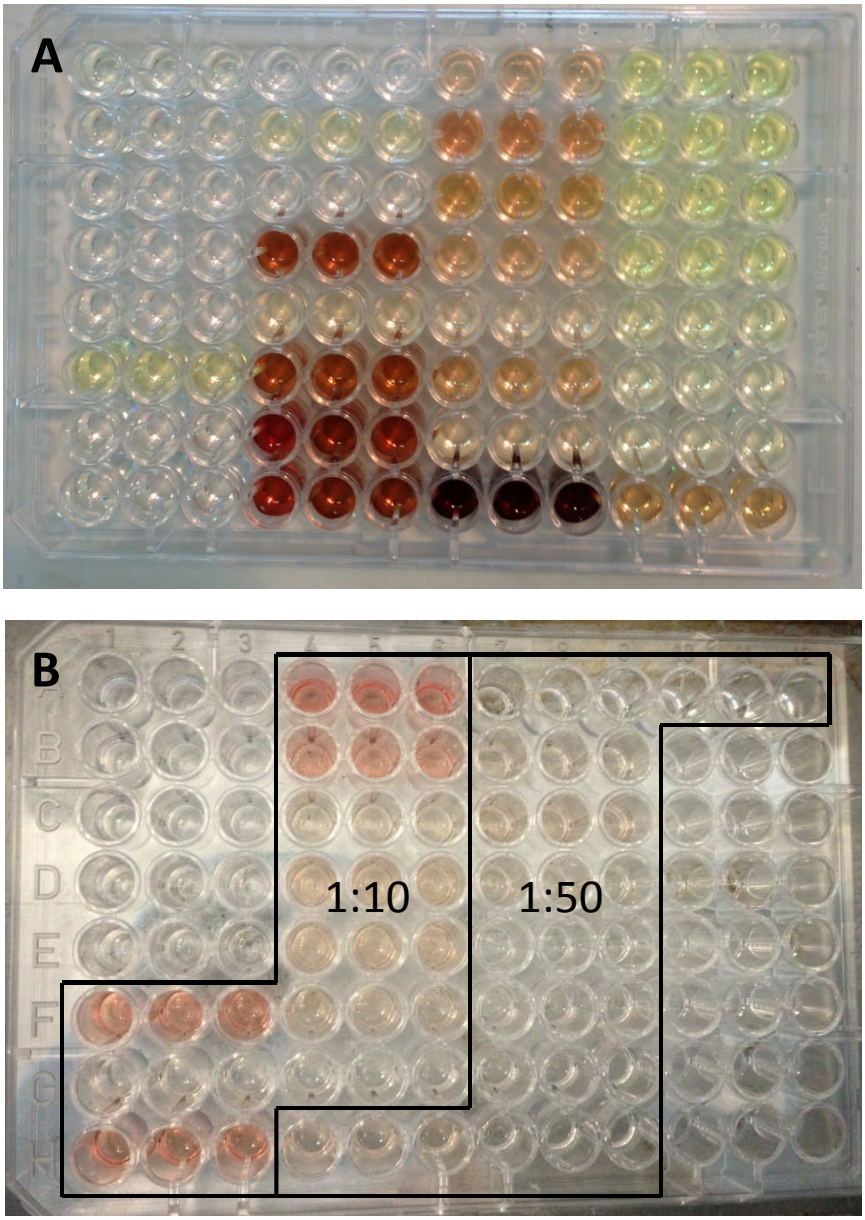

Figure 5.21: Photographs of 96-well plates immediately after sample addition during the commercial LPS colorimetric assay kit. In A, samples are undiluted. In B, sample dilutions are 1:10 and 1:50 as shown. Samples are in triplicate (left to right) in all cases, for each of ten patient samples.

The drain fluid samples of all ten patients for post-operative day one were then again tested in triplicate with the commercial kit at a dilution of 1:50 as optimised. The mean value of each triplicate was then used to calculate the LPS level for that sample using the standard calibration curve (shown in **Chapter 3**). Results are shown in **Figure 5.22**. As with the lactate assay results, there was no statistical difference in LPS concentration between the AL and non-AL group using a non-

parametric Mann Whitney U test (p = 0.9444). The potential reasons for the variability in patient samples and lack of statistical significance between AL and non-AL groups compared to the animal model have previously been discussed in **Section 4.6.6.1,** although the issue of colour interference could not be discounted as an important factor leading to error in the samples. The commercial LPS kit was therefore abandoned as a validation to the *E. coli* immunosensors due to the lack of reliability and alternative comparison validation methods were sought.

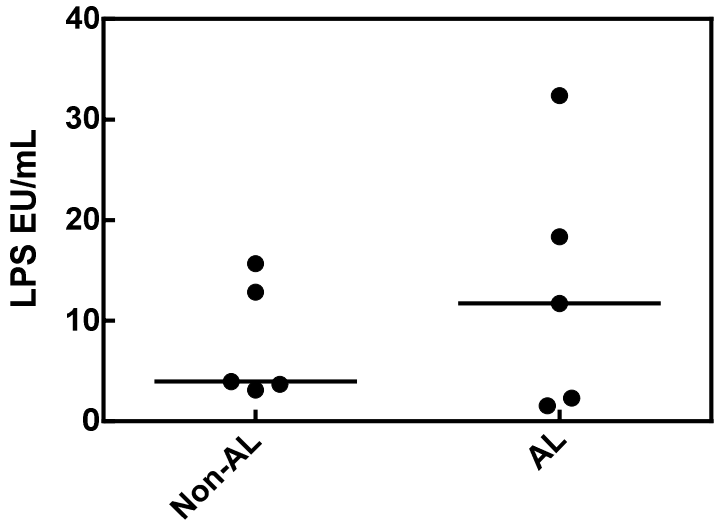

Figure 5.22: Post operative day one patient samples as measured by the kit in 5 non-AL vs. 5 AL patients with median shown. There was no significant difference between the two groups (Mann Whitney U, p = 0.9444).

5.3.11 Flow cytometry as an alternate validation technique

Flow cytometry was chosen as an alternative validation technique for measurement of *E. coli* in drain fluid samples as the inherent colour of the samples would not cause interference, and the technique was readily available, although requiring sample preparation and use of equipment. As detailed in the **Methods**, the ten chosen drain fluid samples were each added to equal amounts of 6% (v/v) BSA in PBS for 30 min before addition of rabbit anti-*E. coli* primary antibody and FITC-

secondary antibody (donkey anti-rabbit). Cells were sorted using a BD-LSRFortessa™ flow cytometer (BD biosciences) and data were analysed using BD FACSDiva software. Initial optimisation included gating of the population of interest using unlabelled samples **(Figure 5.23A),** primary and FITC-secondary antibody **(Figure 5.23B),** and FITC-secondary antibody only **(Figure 5.23C).** Unfortunately the population was unable to be gated for *E. coli* as there was a high degree of non-specific staining with the FITC-secondary antibody, as seen in **Figure 5.23C** compared to **A** and **B** in the area seen as pink coloured staining.

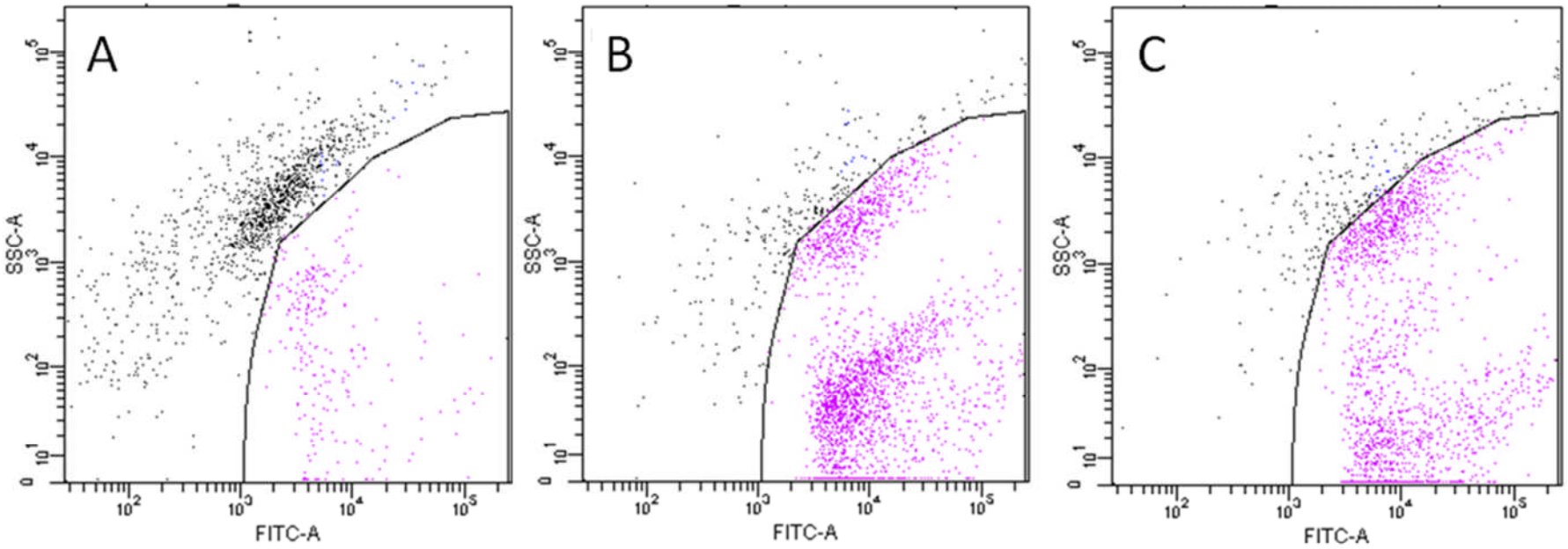

Figure 5.23: Flow cytometry dotplots showing optimised gate of population of interest *E. coli* bacteria. A shows results from unlabelled samples, **B** is *E. coli* primary antibody with FITC-secondary antibody, **C** is secondary antibody only.

Alternative methods therefore to characterise bacterial cell count using flow cytometry were with the addition of 1 $mg.ml^{-1}$ propidium iodide (PI) to samples. PI acts by staining all the DNA present in a sample, therefore again a limitation of this technique was the lack of specificity to *E. coli* from other bacteria and any other DNA containing material in the samples. However, the concentration of "total bacteria" (all DNA containing material), *i.e.* degree of PI staining should be proportional to that of *E. coli* concentration, as the levels of bacteria in samples should be either high or low both as a total and individually by the nature of the sample. Measurement of the total cell number may therefore still act as a validation technique for *E. coli* measured by the constructed biosensors when graphically represented on opposite axes, with each individual sample being plotted as high or low by both techniques in a linear trend.

After PI addition, counting beads were added to the samples according to the manufacturer's instructions. A representative dotplot is shown in **Figure 5.24** for patient one. Numbers of events were measured in the gated area of interest after optimisation of gating using unlabelled samples containing beads (data not shown). Calculations were then made using the beads as reference for absolute cell count in each sample.

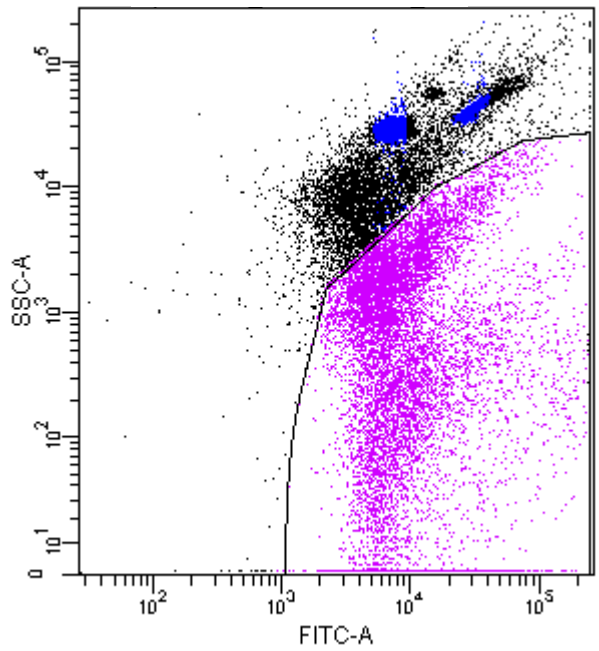

Figure 5.24: Example flow cytometry dotplot for patient one after PI staining. The gated area containing the population of interest is shown in pink. The counting beads are shown by the two blue areas.

5.3.12 Comparison of constructed *E. coli* biosensor results to results of flow cytometry

The results of each of the ten chosen patient drain fluid samples measured by the fabricated *E. coli* biosensor *vs.* total cell number by flow cytometry are shown in **Figure 5.25**. The data show two clear outliers at the high and low limits of measurement which were omitted in **Figure 5.25B** to show the good concordance between the two tests for the remaining eight samples. Interestingly, the cell numbers of *E. coli* measured by the biosensor were magnitudes higher than those measuring total cell numbers by flow cytometry. This was an unexpected finding and was not fully understood but a tentative explanation may be simply the disparity in type of methodologies used. To characterise statistically, a Spearman's rank order test was performed which showed significant correlation between the biosensor and flow cytometry results for each sample (r_s = 0.9273, p = 0.0003). Therefore as hypothesised despite a mismatch in units measured, proportionally

the results are concordant. Despite the limitations in finding a suitable validating commercial test, the results therefore show the constructed *E. coli* immunosensors to be working in real patient samples. As mentioned, the problems encountered in finding a robust validation methodology serves to highlight the need for a rapid, inexpensive, point-of-care *E. coli* test such as a biosensor and this work provisionally shows this as a promising early diagnostic method for anastomotic leak.

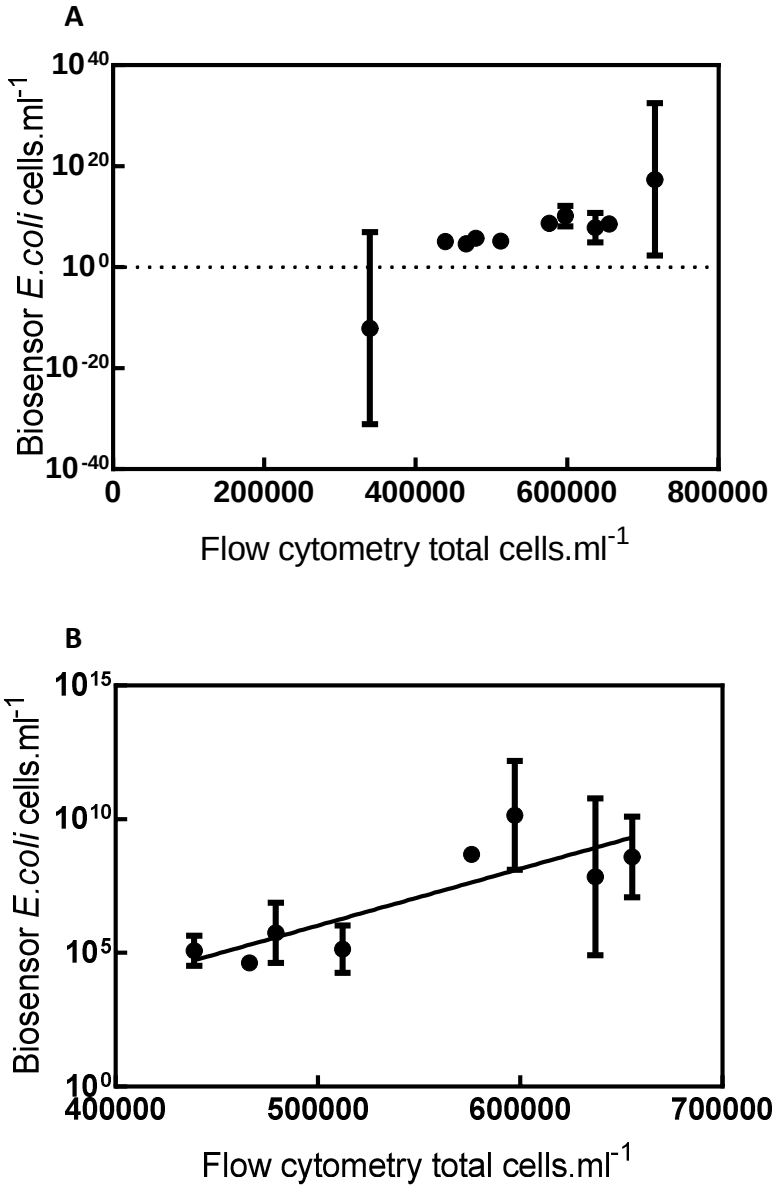

Figure 5.25: Biosensor results (mean ± SD, n = 3) *vs.* flow cytometry results of ten patient drain fluid samples. B shows data of 8 patient samples with two outliers from **A** excluded.

5.4 TNFα biosensor

5.4.1 Dot blot as a technique to show specific TNFα analyte to anti-TNFα binding and biotinylation of anti-TNFα

As with *E. coli* biosensor fabrication, initial experiments used dot blotting to examine the specificity of TNFα analyte to anti-TNFα binding. The successful biotinylation of anti-TNFα was also shown using this technique. TNFα and myoglobin as a control were spotted onto nitrocellulose membrane before the addition of primary antibody anti-TNFα, HRP-secondary antibody and ECL with imaging in a Syngene imager. **Figure 5.26(a)** shows no response with either analyte when primary antibody was absent to confirm the lack of non-specific secondary antibody binding as a control. In **Figure 5.26(b)**, there was a strongly positive response of TNFα to anti-TNFα compared to myoglobin control confirming selective binding. **Figure 5.26(c)** shows no response of analyte with native anti-TNFα and StreptAvidin-HRP, a positive response is only seen of TNFα and biotinylated anti-TNFα with StreptAvidin-HRP **(Figure 5.26(d))** confirming the successful biotinylation of anti-TNFα and specificity of analyte to biotinylated antibody binding.

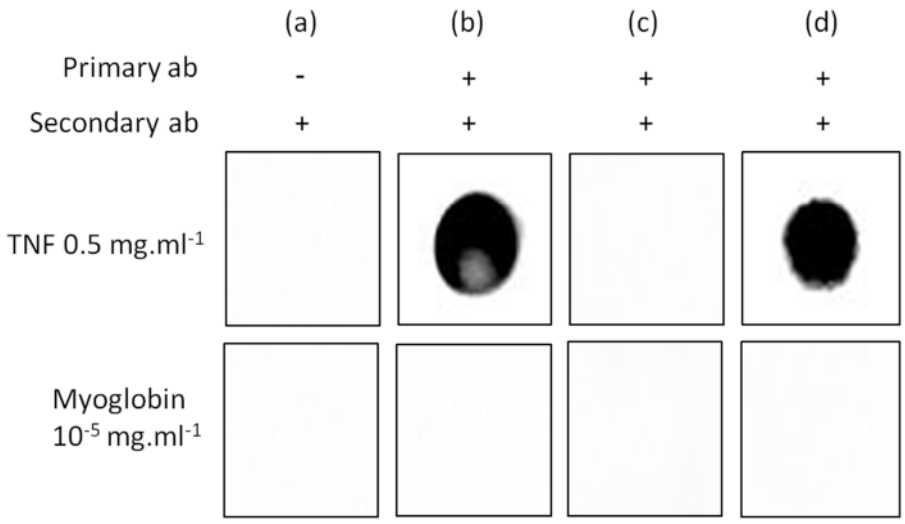

Figure 5.26: Dot blot to show native anti-TNFα to TNFα analyte specific binding, and presence of successfully biotinylation of anti-TNFα to analyte binding. Myoglobin was used as a negative control. In (a) there is no primary antibody, to demonstrate specificity of binding. (b) shows appropriate staining with 1:1000 native anti-TNFα primary antibody and 1:5000 anti-mouse HRP secondary antibody. (c) is a negative control of native anti-TNFα primary antibody with 1:1000 StreptAvidin HRP. (d) shows appropriately staining 1:1000 biotinylated anti-TNFα primary antibody with 1:1000 StreptAvidin HRP, thus showing specific biotinylation of antibody.

5.4.2 Cyclic voltammetry of TNFα biosensor construction steps

Cyclic voltammetry was performed on cleaned bare CX2223AT gold electrodes, after modification with 25 mM tyramine in methanol containing 300 mM NaOH, biotin-NeutrAvidin addition, and then biotinylated IgG anti-TNFα antibody to characterise the changes in surface layers electrochemically. Parameters were a scan rate of 50 $mV.s^{-1}$ between -0.3 and +0.6 V in the redox mediator $Fe(CN_6)^{3-/4-}$ in PBS at pH 7.0. The overlaid results of the cyclic voltammograms are shown in **Figure 5.27**. Traces in **(a)** and **(b)** are equivalent to those shown with *E. coli* biosensors in **Section 5.3.4** as the sensor construction was identical to this level. Traces **(c)** and **(d)** demonstrate further reduction in redox peaks respectively, as the added constructed biosensor layers increased the insulating properties of the electrode surface, with prevention of flow of electrons from the working to counter electrodes and limitation of the redox reaction of the electrolytic solution.

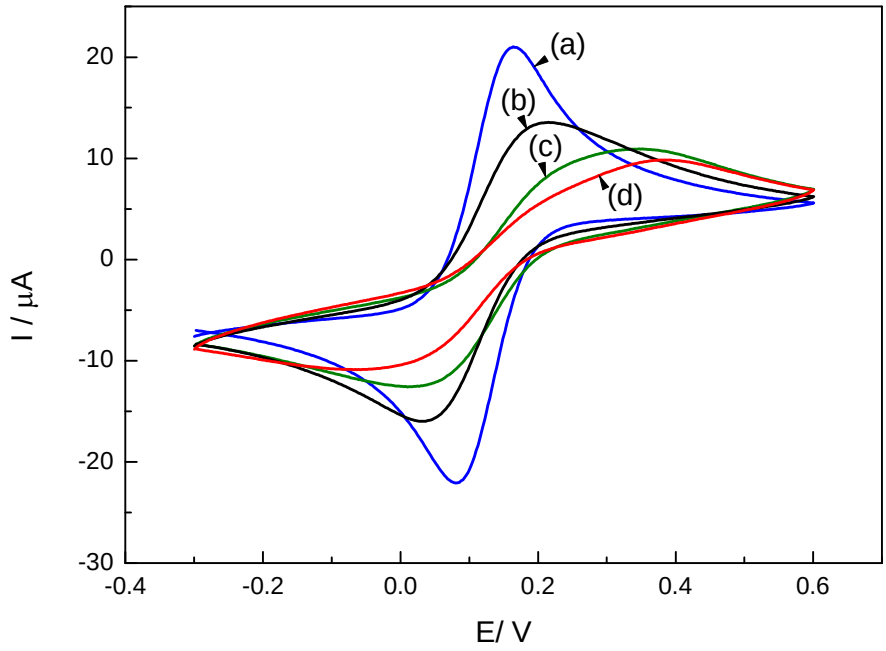

Figure 5.27: Cyclic voltammograms at different TNFα biosensor construction steps. (a) cleaned bare gold electrode, (b) after electro-polymerisation of polytyramine, (c) after biotin-NeutrAvidin addition, (d) after 100% anti-TNFα IgG immobilisation. Scan rate 50 mV.s^{-1} in redox mediator $Fe(CN_6)^{-3/-4}$.

5.4.3 Optimisation of constructed TNFα sensor

Electrochemical impedance spectroscopy (EIS) was performed on the fully constructed TNFα biosensors. As before, an Eco Chemie B.V Autolab Type III frequency response analyser (FRA-2) was used over a range of frequencies from 0.25 Hz to 25 kHz at a voltage of 0 V in redox mediator $Fe(CN)_6^{3-/4-}$. Increasing concentrations of TNFα analyte in PBS (range of 1 pg.ml^{-1} to 1 µg.ml^{-1}) were incubated on the completed electrode surface for 30 min before rinsing and drying and performing EIS between each analyte addition. Data are shown as a Nyquist plot in **Figure 5.28**. Data in **(a)**, **(b)** and **(c)** are EIS for cleaned bare gold electrode with polytyramine, with biotin-NeutrAvidin, and with biotinylated IgG anti-TNFα antibody respectively. The increase in impedance at each of these stages of biosensor construction is evident and corroborates the CV findings of increased passivity as electrode surface layers are formed. The impedance shown after TNFα incubation however, did not increase upon increasing concentrations of the analyte

as expected **(Figure 5.28c-g).** The Nyquist plots show very high impedance at each TNFα concentration as well as for the fully constructed sensor with no analyte, with a high gradient of partial semi-circle shown. It was hypothesised that the impedance may already be at a maximum or capacity level at sensor fabrication which was unable to be increased further by additional analyte binding. Strategies for exploring this further included testing with a different polymer solution, and varying the scan rate of the electro-polymerisation process, IgG antibody concentration and widening the TNFα concentration range.

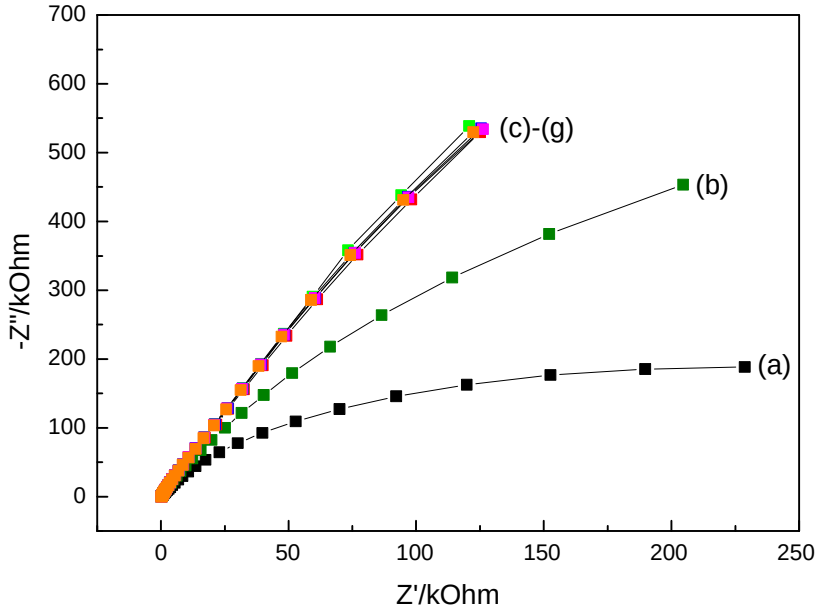

Figure 5.28: Nyquist plots showing impedance of TNFα biosensors after TNFα addition. Data were obtained in a redox mediator of $Fe(CN_6)^{3-/4-}$ in PBS at pH 7.0 across a frequency range of 0.25 Hz to 25 kHz at an applied sinusoidal voltage of 0 V. Sequential profiles are: (a) cleaned bare gold electrode with electro-polymerised tyramine in methanol/NaOH at scan rate 100 $mV.s^{-1}$, (b) after biotin and NeutrAvidin immobilisation, (c) fully constructed biosensor after addition of biotinylated anti-TNFα with no analyte, successive TNFα analyte incubations at: (d) 1 $pg.ml^{-1}$, (e) 100 $pg.ml^{-1}$, (f) 10 $ng.ml^{-1}$, (g) 1 $\mu g.ml^{-1}$.

Phloretic acid was evaluated in **Section 5.2** during polymer optimisation. Although not able to contribute amino groups for attachment and therefore tested in combination with tyramine, phloretic acid conveys a negative charge which was considered potentially useful in the presence of non-specific binding of the negatively charged TNFα to positively charged tyramine in solution. The polymer mix in PBS was shown to demonstrate good impedance with more available amine groups shown by Midland blot than in methanol/NaOH. Experiments were therefore performed with electro-deposition of 0.025 M tyramine and phloretic acid (3:1) polymer mix in PBS using two scans from 0 V to +1.6 V at a rate of 100 $mV.s^{-1}$ before full TNFα sensor construction using previous parameters. Nyquist plots at sensor construction and after TNFα analyte incubation are shown in **Figure 5.29**. The overall impedance was seen to be much lower than that of using tyramine alone, with a more pronounced semi-circular plot shape for each measurement. However, the same pattern was seen whereby impedance increased over sensor construction but was static on addition of increasing concentrations of TNFα. Appearances were thought to be due to lower levels of biotin-NeutrAvidin-IgG binding due to decreased availability of amino groups on the polymer sensor surface.

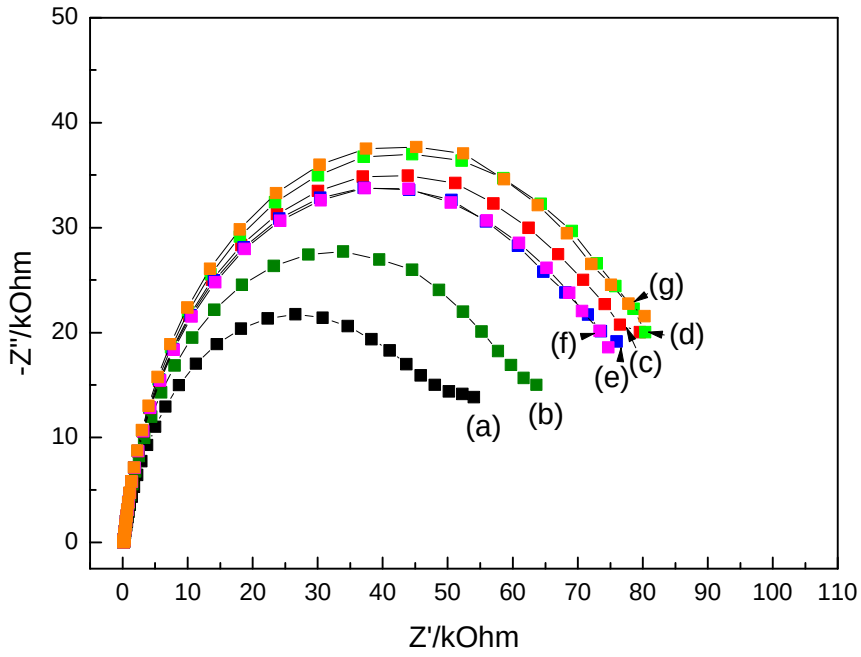

Figure 5.29: Nyquist plots showing impedance of TNFα biosensors after TNFα addition using tyramine/phloretic acid polymer. Data were obtained in a redox mediator of $Fe(CN_6)^{3-/4-}$ in PBS at pH 7.0 across a frequency range of 0.25 Hz to 25 kHz at an applied sinusoidal voltage of 0 V. Sequential profiles are: (a) cleaned bare gold electrode with electro-polymerised tyramine/phloretic acid in methanol/NaOH at scan rate 100 $mV.s^{-1}$, (b) after biotin and NeutrAvidin immobilisation, (c) fully constructed biosensor after addition of biotinylated 100% anti-TNFα with no analyte, successive TNFα analyte incubations at: (d) 1 $pg.ml^{-1}$, (e) 100 $pg.ml^{-1}$, (f) 10 $ng.ml^{-1}$, (g) 1 $\mu g.ml^{-1}$.

Coverage of polymer upon a sensor surface is known to be controlled by either the concentration of the monomer in the forming solution, by the number of scans and/or by the scan rate (Pournaras et al., 2008). The concentration of tyramine and its supporting media was already optimised (Ismail and Adeloju, 2010, Ahmed et al., 2013), and was shown to demonstrate good impedance and amino group availability on polymer testing in **Section 5.2**. Scan number has also been evaluated in bacterial impedance biosensors, with two scans leading to polymer coverage on the surface without increasing capacitance as more than two scans has been shown to do (Ahmed et al., 2013). Increasing the scan rate from 100 $mV.s^{-1}$ to 200 $mV.s^{-1}$ was also shown by authors to reduce the thickness of the polymer layer and decrease the resulting impedance (Ahmed et al., 2013). 0.025 M tyramine in

methanol containing 0.3 M NaOH was therefore electro-deposited onto cleaned gold electrodes using two scans from 0 V to +1.6 V at a rate of 200 $mV.s^{-1}$. The resulting CV traces are seen overlaid in **Figure 5.30**. Compared to a scan rate of 100 $mV.s^{-1}$ **(Figure 5.10)** the currents generated in both cycles were much higher, indicating the lesser insulation of the surface as a consequence of a thinner polymer layer formed. The passivity from scan one to scan two was also correspondingly less than that seen with the slower scan rate.

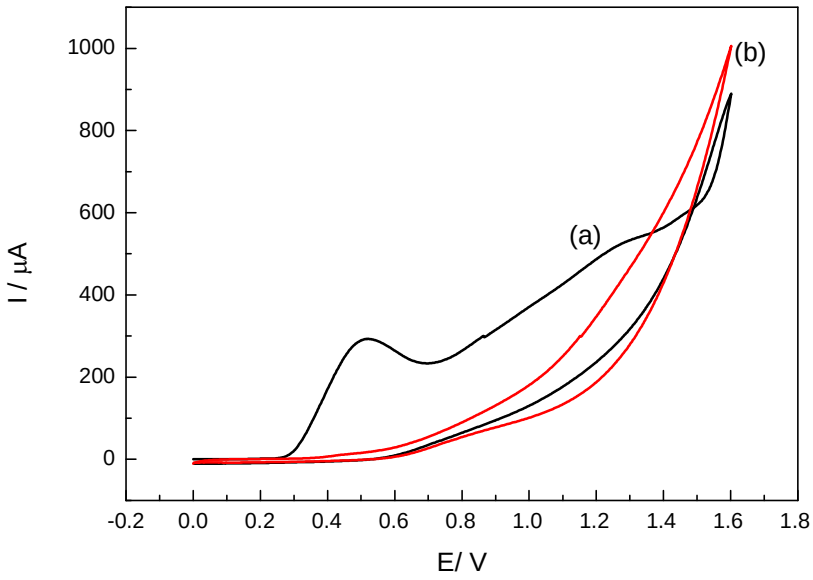

Figure 5.30: Cyclic voltammograms of electrochemical deposition of 0.025 M tyramine in methanol containing 0.3 M NaOH. Scan rate was 200 $mV.s^{-1}$. (a) is the first scan, (b) is the second scan, showing increased insulation.

After electro-polymerisation of tyramine at an increased scan rate of 200 $mV.s^{-1}$, TNFα biosensors were constructed identically to previously described. EIS was then performed after each biosensor construction step and after each TNFα addition as before. The corresponding Nyquist plots can be seen in **Figure 5.31**. The overall impedance is approximately half of that seen with the lower polymerisation scan rate, indicating that altering this parameter did decrease the polymer layer size and the subsequent impedance, particularly apparent in the plots from the biosensor

construction steps. The Nyquist plots after TNFα addition were more distinct than when previously seen overlapping, although still in close proximity and with the highest concentration of TNFα **(g)** not in increasing order of impedance as the other concentrations demonstrate. As this was an improvement, the increased scan rate was used in all successive experiments.

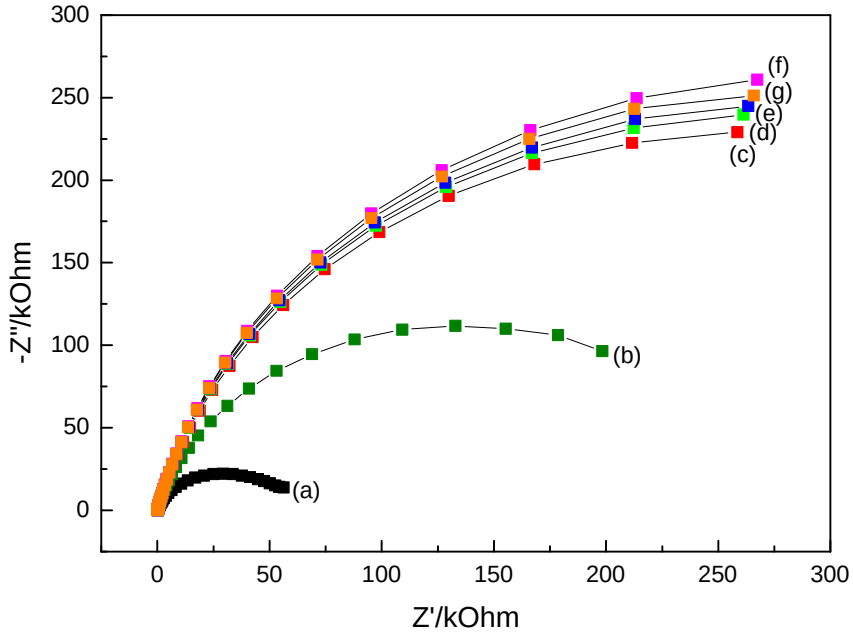

Figure 5.31: Nyquist plots showing impedance of TNFα biosensors after TNFα addition with increased scan rate of 200 mV.s^{-1}. Data were obtained in a redox mediator of $Fe(CN_6)^{3-/4-}$ in PBS at pH 7.0 across a frequency range of 0.25 Hz to 25 kHz at an applied voltage of 0 V. Sequential profiles are: (a) cleaned bare gold electrode with electro-polymerised tyramine in methanol/NaOH at scan rate 200 mV.s^{-1}, (b) after biotin and NeutrAvidin immobilisation, (c) fully constructed biosensor after addition of biotinylated anti-TNFα with no analyte, successive TNFα analyte incubations at: (d) 1 pg.ml^{-1}, (e) 100 pg.ml^{-1}, (f) 10 ng.ml^{-1}, (g) 1 µg.ml^{-1}.

The concentration of anti-TNFα was previously discussed in **Section 5.1.2**, as the commercial availability of the antibody from live animal models was at low concentration and volume. A whole antibody methodology was therefore used for TNFα biosensor fabrication to reduce antibody processing with the aim of maintaining concentration. Antibody processing involved the removal of sodium

azide by centrifugal filter replacement into PBS with an unknown loss of antibody, and biotinylation which bound unknown quantities of antibody onto the sensor surface. It was anticipated that the concentration of anti-TNFα from the purchased 0.5 $mg.ml^{-1}$ was therefore considerably lower on the constructed biosensor surface, although this was too low to be measured by conventional means such as spectrophotometry. Despite this, the logical premise that a higher antibody concentration on the sensor surface would improve sensitivity has been shown to be inaccurate as lower concentrations may reduce steric hindrance to improve analyte binding **(see Section 5.3.2.1)**. The concentration of anti-TNFα was therefore varied to explore whether sensor sensitivity could be improved. Anti-TNFα antibody was immobilised onto sensor surfaces at 10% and 1% of the total (unknown) concentration. Electro-polymerisation of tyramine was performed at 200 $mV.s^{-1}$ as optimised in the previous section, with all other parameters remaining as previously. EIS was performed on fully constructed sensors and after addition of two TNFα concentrations **(Figure 5.32).** The impedance was shown to be proportionally lower, but with no discrimination between the biosensors and after analyte incubation. Therefore antibody concentration was used at the highest concentration, i.e. “neat” after biotinylation, in all further experiments.

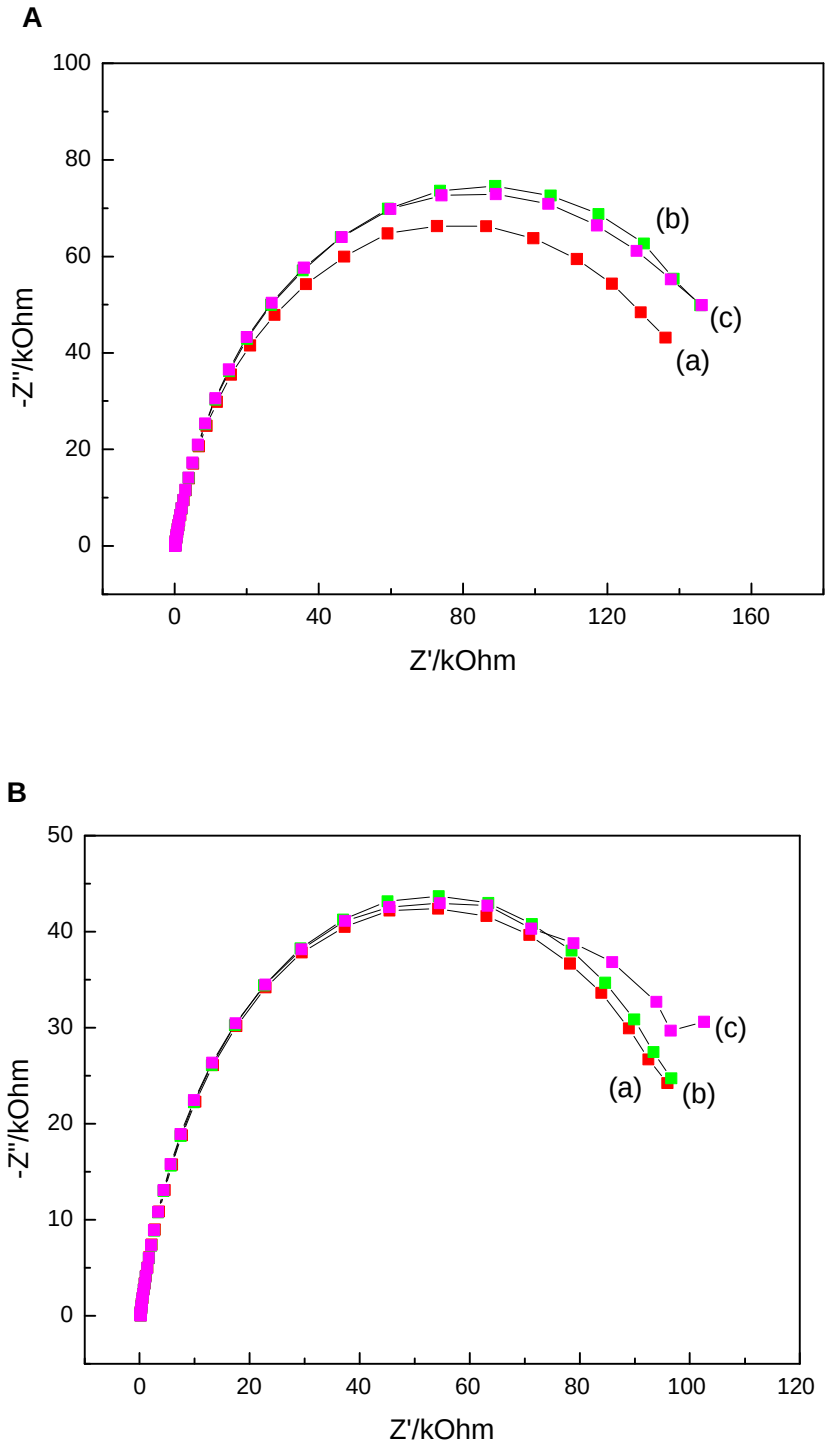

Figure 5.32: Nyquist plots showing impedance of TNFα biosensors after TNFα additions at A, constructed with 10% anti-TNFα and B, with 1% anti-TNFα. Data were obtained in a redox mediator of $Fe(CN_6)^{3-/4-}$ in PBS at pH 7.0 across a frequency range of 0.25 Hz to 25 kHz at an applied sinusoidal voltage of 0 V. Sequential profiles are: (a) cleaned bare gold electrode with electro-polymerised tyramine in methanol/NaOH at scan rate 200 $mV.s^{-1}$, biotin and NeutrAvidin immobilisation, and biotinylated anti-TNFα with no analyte; and successive TNFα analyte incubations at: (b) 1 $pg.ml^{-1}$, (c) 10 $ng.ml^{-1}$.

Lastly, the range of concentrations of TNFα was increased in the optimisation experiments. The range initially tested was consistent with given concentrations in the literature potentially useful for clinical assessment (Pui et al., 2013). However the Nyquist plots seen with this range were very close together suggesting poorer biosensor sensitivity than anticipated. A wider range of TNFα concentrations was therefore tested to determine if the impedance data seen would be more distinct from one another. This would indicate a potentially less sensitive biosensor, but would confirm the biosensor functionality. The data in **Figure 5.33** shows Nyquist plots for constructed biosensor steps **(a)**, **(b)**, and **(c)**, and at two TNFα concentrations of 10 $ng.ml^{-1}$ **(d)**, and 0.5 $mg.ml^{-1}$ **(e)**. The 10 $ng.ml^{-1}$ TNFα plot is consistent with that shown previously (where it was one of the higher concentrations tested). It is clear that the impedance increased greatly when sensors were incubated with the very high concentration of 0.5 $mg.ml^{-1}$ TNFα. The biosensors were thus working, but at lower sensitivities than initially examined.

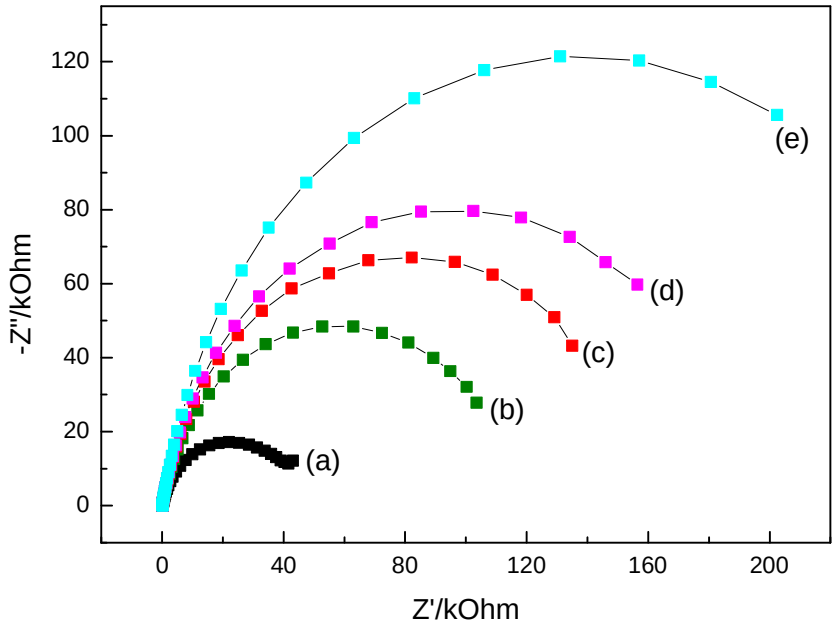

Figure 5.33: Nyquist plots showing impedance of TNFα biosensors after range of TNFα additions. Data were obtained in a redox mediator of $Fe(CN_6)^{3-/4-}$ in PBS at pH 7.0 across a frequency range of 0.25 Hz to 25 kHz at an applied sinusoidal voltage of 0 V. Sequential profiles are: (a) cleaned bare gold electrode with electro-polymerised tyramine in methanol/NaOH at scan rate 200 $mV.s^{-1}$, (b) after biotin and NeutrAvidin immobilisation, (c) fully constructed biosensor after addition of biotinylated 100% anti-TNFα with no analyte; successive TNFα analyte incubations at: (d) 10 $ng.ml^{-1}$, (e) 0.5 $mg.ml^{-1}$.

5.4.4 Interrogation of TNFα biosensor with optimised fabrication parameters in buffer

After optimisation steps, TNFα immunosensors were constructed using the elicited parameters, namely with electro-deposition of 0.025 M tyramine in methanol containing 0.3 M NaOH at scan rate 200 $mV.s^{-1}$, with 100% antibody after removal of sodium azide and biotinylation. Electrochemical impedance spectroscopy (EIS) was performed on the fully constructed TNFα biosensors with, as before, an Eco Chemie B.V Autolab Type III frequency response analyser (FRA-2) over a range of frequencies from 0.25 Hz to 25 kHz at a voltage of 0 V in redox mediator $Fe(CN)_6^{3-/4}$. Increasing concentrations of TNFα analyte in PBS with a wider range of 1 $pg.ml^{-1}$ to

100 µg.ml^{-1} were incubated on the completed electrode surface for 30 min before rinsing and drying and impedance read between each analyte addition.

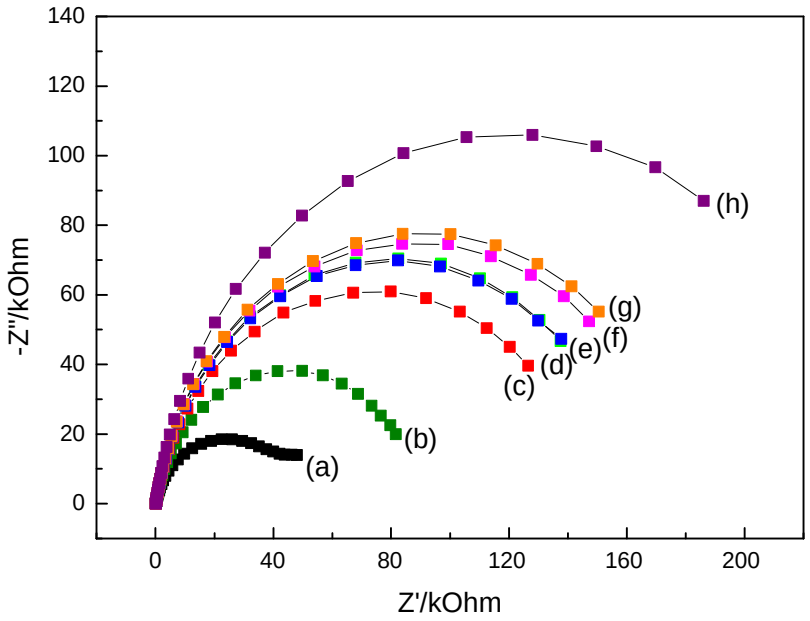

Figure 5.34: Nyquist plots showing impedance of TNFα biosensors after range of TNFα additions. Data were obtained in a redox mediator of $Fe(CN_6)^{3-/4-}$ in PBS at pH 7.0 across a frequency range of 0.25 Hz to 25 kHz at an applied sinusoidal voltage of 0 V. Sequential profiles are: (a) cleaned bare gold electrode with electro-polymerised tyramine in methanol/NaOH at scan rate 200 mV.s^{-1}, (b) after biotin and NeutrAvidin immobilisation, (c) fully constructed biosensor after addition of biotinylated 100% anti-TNFα with no analyte; successive TNFα analyte incubations at: (d) 1 pg.ml^{-1}, (e) 100 pg.ml^{-1}, (f) 10 ng.ml^{-1}, (g) 1 µg.ml^{-1}, (h) 100 µg.ml^{-1}.

Nyquist plot data for the experiments are shown in **Figure 5.34**. The plots show clearly increasing impedance at sensor construction stages **(a)**, **(b)**, and **(c)**, and at sequentially greater concentrations of TNFα, with the exception of the two lowest concentrations, **(d)** 1 pg.ml^{-1} and **(e)** 100 pg.ml^{-1}, which are seen to overlay. The specificity was examined using a negative control constructed immunosensor with anti-myoglobin IgG antibody. Experiments were conducted in parallel, with 0.53 mg.ml^{-1} anti-myoglobin biotinylated under the same conditions as anti-TNFα, and subjected to EIS after identical preparation and TNFα additions. **Figure 5.35** shows the corresponding Nyquist plot data. The impedance shown for the bare cleaned

gold electrodes with electro-polymerised tyramine in methanol/NaOH and after biotin and NeutrAvidin immobilisation were comparable in both the specific **(Figure 5.34a and b)** and control **(Figure 5.35a and b)** experiments. At greater concentrations of TNFα analyte the Nyquist plots demonstrated correspondingly higher impedances with the control antibody **(Figure 5.35)**, indicating poor specificity and a high degree of non-specific binding.

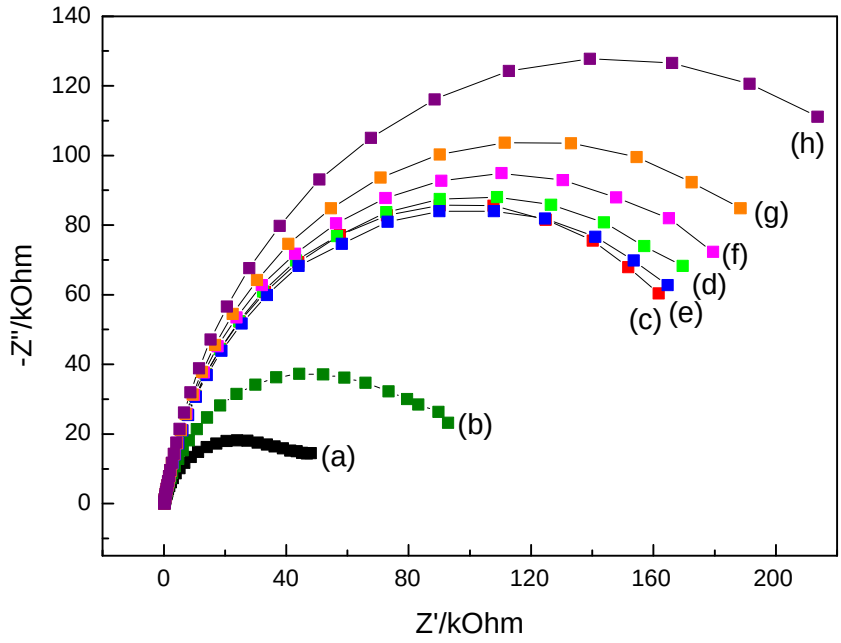

Figure 5.35: Nyquist plots showing impedance of anti-myoglobin biosensors after range of TNFα additions. Data were obtained in a redox mediator of $Fe(CN_6)^{3-/4-}$ in PBS at pH 7.0 across a frequency range of 0.25 Hz to 25 kHz at an applied sinusoidal voltage of 0 V. Sequential profiles are: (a) cleaned bare gold electrode with electro-polymerised tyramine in methanol/NaOH at scan rate 200 $mV.s^{-1}$, (b) after biotin and NeutrAvidin immobilisation, (c) fully constructed biosensor after addition of biotinylated anti-myoglobin with no analyte; successive TNFα analyte incubations at: (d) 1 $pg.ml^{-1}$, (e) 100 $pg.ml^{-1}$, (f) 10 $ng.ml^{-1}$, (g) 1 $\mu g.ml^{-1}$, (h) 100 $\mu g.ml^{-1}$.

The charge transfer resistance (R_{ct}) values of the specific and control TNFα biosensor impedance data were derived, as modelled to Randles equivalent circuit which was used previously in **Section 5.3.6** for *E. coli* immunosensor data analysis. The R_{ct} data are shown in **Figure 5.36**. The results show that there was increasing

R_{ct} upon successively higher TNFα concentrations indicating an appropriate increase in binding to the sensor surface, expected to be binding of analyte **(Figure 5.36a)**. However, an almost equivalent increase in R_{ct} was also seen with the control anti-myoglobin sensors **(Figure 5.36b).** Thus the TNFα biosensors demonstrated a high degree of non-specific binding to the sensor surfaces. Interestingly the highest concentration of TNFα tested (100 $\mu g.ml^{-1}$) did show a difference between specific and controls, and this raised the question of whether the tested TNFα concentrations were still too low for the relatively insensitive biosensor, with 100 $\mu g.ml^{-1}$ as the limit of detection. Higher concentrations of TNFα measured by constructed TNFα to anti-TNFα sensors are thus potentially able to show higher change in impedance vs. controls and this may still translate to clinical application.

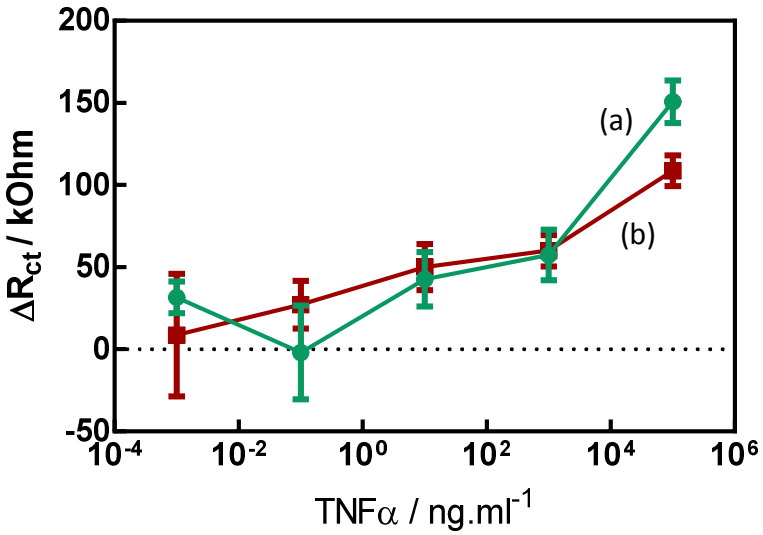

Figure 5.36: R_{ct} of biosensors after additions of TNFα analyte. Each set of biosensors were exposed to increasing concentrations of TNFα analyte, the impedance read and the R_{ct} determined. Data shows binding for (a) TNFα to anti-TNFα IgG, and negative control of (b) TNFα to anti-myoglobin IgG, in all cases where mean ± S.D has been calculated for n = 3.

5.4.5 Commercial TNFα ELISA kit assay as a validation for TNFα biosensor

The constructed TNFα biosensors were unfortunately not completed to testing in the ten patient drain fluid sample cohort and therefore did not require validation of

results using a commercial assay. However, for ongoing work and to investigate any significant differences between TNFα levels in anastomotic leak (AL) and non-AL groups at each post-operative day (POD), a human TNF alpha ELISA Ready-SET-Go!® was purchased from eBioscience (Hatfield, UK). The kit was identical to that used for the animal samples in **Section 3.2.2**, but with antibody and substrate specific to human, not the previously used rat equivalents. The sensitivity of the human assay is given by the manufacturers as 4 $pg.ml^{-1}$, with standard curve range 4–500 $pg.ml^{-1}$.

All ten patients' drain fluid samples at each post-operative day were tested in triplicate with the commercial kit. The mean value of each triplicate was then used to calculate the TNFα level for that sample using the standard calibration curve (not shown). As with the commercial lactate kit, but not with the LPS kit due to its limitations as discussed, all the available drain fluid samples for the ten patient cohort were measured, although as previously noted each patient did not have all subsequent daily samples after POD one. This was due to variable drainage amounts, and the drains being removed on differing days. The mean ± standard deviation TNFα level results for each post-operative day in AL and non-AL patients are shown in **Figure 5.37**. The TNFα levels for each group were very variable, with high standard deviations seen at each POD. Using a Mann Whitney U statistical test, there were no significant differences in TNFα levels between AL and non-AL groups at any post-operative day although there was a trend towards increased AL TNFα levels particularly at days 3 and 4. This could infer that TNFα is an informative biomarker at a later time interval, as also suggested by the corresponding animal model in which there was greater significance between groups at 36 hours than 24 **(Section 3.4.2)**. The patient results were not unexpected however given the lack of significance already seen with the other biomarkers using these samples. Reasons for this have previously been discussed, with hypotheses considered including the small sample cohort, and wide variation between individual patients i.e. high S.D; meaning an individual's biomarker levels as a trend over time may be more relevant clinically than an imposed cut off value. The results are useful as a validation test

when the TNFα biosensors are completed and able to be performed on all the patient samples in future work.

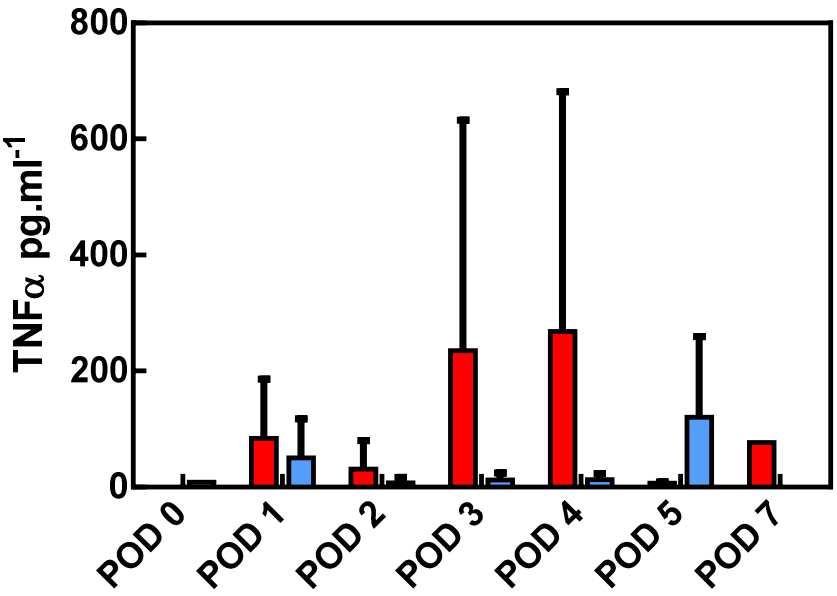

Figure 5.37: Commercial TNFα ELISA kit tested on patient samples. Data are mean ± S.D. of the five AL patients' (red) and the five non-AL patients' (blue) drain fluid samples on each post-operative day (POD).

5.5 Discussion

This chapter describes the work undertaken in development and optimisation of two impedimetric biosensors to *E. coli* and TNFα, with ultimate validation of *E. coli* biosensors shown to be working in patient drain fluid samples.

Studies began on optimisation of the polymer surface which would attach the respective antibodies for sensor recognition *via* crosslinkers and biotin/NeutrAvidin for both biosensors. A range of polymers chosen based on recent group success with tyramine (Ahmed et al., 2013) were tested including a tyramine/phloretic acid mixture in a variety of supporting media. The range of potential scanned was also a

varying parameter. Data were examined using cyclic voltammetry, electrochemical impedance spectroscopy, Midland blot and SEM. The polymer 0.025 M tyramine in methanol/0.3 M NaOH 0-1.6 V was chosen as being most suitable for biosensor construction as it demonstrated excellent electron transfer resistance on EIS, passivation of the surface as shown by cyclic voltammetry indicating a good deposition layer of polymer, and clear availability of amine groups shown on Midland blot analysis. SEM confirmed an even, relatively smooth electrode surface after electro-deposition of the polymer to facilitate further binding of crosslinkers and orientated antibody in the fully constructed biosensors. This polymer was therefore taken forward in all further experiments except where stated.

Impedimetric *E. coli* biosensor construction was the first to be addressed. To initially confirm specific *E. coli* to anti-*E. coli* binding a dot blot was performed which showed excellent specific binding compared to an alternate Gram-positive bacterial control. The methodology for *E. coli* sensor construction utilised cleaved half antibody attached to the polymerised gold electrode surface *via* a sulfo-SMCC crosslinker. SDS-PAGE was able to show the antibody reductive technique using 2-MEA was successful, before biosensors were fully constructed with the half antibody elicited from the method. Cyclic voltammetry was performed on the biosensors during construction and characteristic changes in redox peaks were seen, illustrating the changes in surface morphology altering the electrochemical properties upon addition of each biosensor layer. With these promising results, EIS was performed on *E. coli* biosensors *vs. S. pyogenes* biosensors as controls. The immunosensors were successfully able to show specific detection of *E. coli* to a limit of detection of 10^4 cells ml^{-1} in buffered solutions. However to fully demonstrate specificity, *E. coli* biosensors should also be interrogated with *S. pyogenes* analyte. The promising results in buffer did not translate to good performance when moving into newborn calf serum, previously used in lactate sensor experimentation as an intermediary to determine required dilutions before testing on the ten patient drain fluid sample cohort used previously. It was hypothesised that this was due to a high level of non-specific binding of serum proteins and other substances, and

NCS was not considered suitable for this application. From the literature, an alternative physiological media using diluted own samples as a "diluent" were assessed with which the issues with non-specific binding were greatly reduced. A dilution factor of 10% was found to be optimum for the drain fluid samples from EIS experiments in this medium and a calibration curve constructed for subsequent patient sample use. One of the key issues faced with the *E. coli* biosensor work was the lack of suitable commercial test with which to validate the biosensor results. This highlights the importance of this work in the development of new bacterial tests. The colorimetric LPS kit, used previously as a surrogate marker of *E. coli* in the animal samples, was found to be unsuitable in the patient samples as it gave erroneous results due to the colour inherent in the patient samples, despite attempts at dilution. The kit was therefore abandoned and an alternative validation with flow cytometry was used which was successful. Biosensor results for each of the post-operative day one patient drain fluid samples were compared to those from flow cytometry and found to be statistically significant using a Spearman's rank correlation, $r_s = 0.9273$, $p = 0.0003$. Therefore, despite the limitations in finding a suitable validating commercial test, the results showed the constructed *E. coli* immunosensors to be working in real patient samples as an initial proof of concept diagnostic test.

The TNFα impedimetric biosensors had many more limitations. Initially, as with the *E. coli* sensor experiments, dot blots were performed which demonstrated specific binding compared to controls and also successful biotinylation of anti-TNFα antibody. The construction stages of the TNFα biosensor which involved electro-deposition of tyramine polymer before biotin/NeutrAvidin attachment of whole antibody to form the biological recognition element of the impedimetric sensors were again investigated using cyclic voltammetry. The redox peaks shown by CV at the stages of sensor construction were sequentially reduced, as each layer added onto the electrode increased the insulation of the surface demonstrating the change in surface characteristics. Initial impedance of the fully constructed TNFα biosensors was seen to be very high, with consequent additions of TNFα analyte

seemingly not able to increase the impedance further. Strategies for reducing the initial impedance of the sensors were therefore explored, with increased scan rate to 200 $mV.s^{-1}$ from 100 $mV.s^{-1}$ during electro-deposition of tyramine polymer onto the electrode surface proving to be the most successful, in creating a thinner polymer layer on the surface to reduce impedance by approximately half. Optimisation of type of polymer, anti-TNFα concentration, and TNFα analyte concentration were also examined with little improvement in sensitivity. Using the optimised parameters EIS was performed on TNFα biosensors *vs.* biotinylated anti-myoglobin controls in buffered solutions. The constructed immunosensors were successfully able to show increasing impedance over sensor construction stages and with sequentially increased concentrations of TNFα, with the exception of the two lowest TNFα concentrations which overlaid. Unfortunately the data were equivalent using a negative control, therefore demonstrating non-specific binding and poor specificity. The corresponding R_{ct} data showed this more clearly. At the highest concentration of TNFα tested (100 $\mu g.ml^{-1}$) with the biosensors there was however a difference between specific and controls raising the hypothesis that the sensor may be relatively insensitive to the levels of TNFα predicted and this highest level tested may be the limit of detection. Further work aims to first perform experiments using TNFα biosensors with higher concentrations of TNFα analyte *vs.* controls to examine the sensitivity and specificity for proof of principle before strategies to improve both.

Despite not achieving TNFα biosensor testing in patient samples, the ten patient drain fluid samples used for validation in the lactate and *E. coli* work were tested using a commercial TNFα ELISA kit, a human version of that used on the animal samples as a future validation TNFα test. In similarity to the other biomarkers in the patient samples there were no significant differences in TNFα levels between AL and non-AL groups at any post-operative day. Again, there was seen a wide variation between individual patients in the small cohort tested. The TNFα levels in the AL groups were generally higher than those of the non-AL groups, although in the order of 1 000 000 times lower than the TNFα concentration at which the

biosensors were able to show a difference between specific and controls (100 $\mu g.ml^{-1}$). The sensitivity of the TNFα biosensors is therefore paramount for any clinical application and will be the focus of future work.

Chapter 6:

General discussion

Chapter 6. General discussion

6.1 General discussion

Anastomotic leak is a catastrophic surgical complication, leading to high morbidity and mortality. Diagnosis is currently difficult due to the insidious presentation, and current diagnostic tests lack sensitivity and specificity. The aims of this work were to show proof-of-principle for an early diagnostic test of anastomotic leak and intra-abdominal sepsis with two objectives. Firstly, to identify local biomarkers correlating with anastomotic leak and intra-abdominal sepsis using an animal model, and secondly, to construct and optimise biosensors to the chosen biomarkers, with ultimate validation in real clinical samples compared to commercially available assays.

One of the fundamental aspects of this work was the measurement of biomarkers locally at the anastomotic site as opposed to systemically. As discussed in **Chapter 1**, during anastomotic leak and the development of abdominal sepsis there are early local molecular changes, with increase and decrease of a number of ischaemic, inflammatory and bacterial biomarkers (Komen et al., 2008). These biomarkers can be utilised as a diagnostic tool by monitoring their real time levels, which show greater sensitivity and specificity due to the locality of measurement (Komen et al., 2008). The available literature on local biomarkers of anastomotic leak and abdominal sepsis was assessed, and three potential biomarkers chosen as representing three time points in the pathophysiological course of anastomotic leak, namely lactate, TNFα and *E. coli*. To evaluate these biomarkers, a small animal model of intra-abdominal sepsis using caecal ligation and puncture (CLP) *vs.* sham controls was developed. CLP is considered the gold standard animal model in sepsis research and has been in use for a number of years (Rittirsch et al., 2009,

Dejager et al., 2011), but crucially, few studies have measured biomarkers directly in peritoneal fluid.

Available methodologies such as ELISA for the detection of sepsis biomarkers require specialist equipment, user proficiency and are time consuming and expensive. The use of biosensors for measurement of clinical biomarkers is in its infancy, but is a rapidly expanding area of interest with great potential. There are currently no commercially available biosensors for anastomotic leak or septic complications although a small number have been assessed at the laboratory stage, predominantly measuring markers in plasma, blood and buffered solutions, as summarised in **Table 1.5**. The key advantages of biosensors for this purpose include point-of-care testing, low cost, no requirement for specialist equipment and ease of use, which allow for repeated testing and monitoring of biomarker trends over time – a particular advantage for anastomotic leak which presents on an evolving spectrum for which a single value is less useful.

Using the small animal model, all three biomarkers were found to be significantly raised in septic animals compared to sham controls at 24 and 36 hours. The time intervals chosen were based on the available literature and initial optimisation studies at which 6 hours appeared too early for even lactate to increase. However, sepsis is an evolving pathology in which anticipated peaks for each biomarker were at different, overlapping time intervals, thus it was unfortunate that for practical reasons, measurement of a greater number of time points in the animal model was not achievable. As there were no available commercial assays for *E. coli*, LPS (lipopolysaccharide) was used as a surrogate marker, as an LPS kit was available. LPS was thought to be clinically valid for this purpose as the presence of any gram negative bacteria in the sterile peritoneal cavity would be indicative of a leak. The inadequacy of *E. coli* assays was also an issue when comparing the *E. coli* biosensor results with a commercial validation, and flow cytometry had to be requisitioned. Comparison of the data from the animal model with that of the literature is

challenging due to the paucity of studies using biomarkers measured in the abdomen, and the dissimilarity in technique and animal type in the studies available. However, from the limited evidence in the literature it appears that my findings are consistent. For example, in a similar study using CLP *vs.* sham, the mean peritoneal levels of TNFα in mice was 35 $pg.ml^{-1}$ at 24 hours (Ebong et al., 1999), comparable to my experimental data in which the median was 39 $pg.ml^{-1}$ at the same time interval; both of which were significantly higher than sham controls. Ebong's group reported no detectable TNFα in the systemic circulation at any time point. Such data, when taken with logical extrapolation from other sepsis models, supports the use of my three chosen biomarkers as being representative of anastomotic leak.

After validation of the biomarkers using the animal model, three biosensors were constructed to lactate, TNFα and *E. coli*. Amperometric lactate biosensors were ultimately constructed using lactate oxidase on a screen printed carbon electrode with pre-impregnated Prussian Blue mediator *via* a PEI polymer surface. Preceding this, a number of methodologies were unsuccessful in generating a robust amperometric signal and were discounted, with a switch to commercial electrodes and isolated enzyme testing required during optimisation in buffer. In newborn calf serum (NCS), used as an intermediary to patient drain fluid, a range of dilutions spiked with lactate were assessed to evaluate that yielding greatest signal. Fortuitously, a 10% (v/v) dilution was found to both produce optimal signal, and bring the lactate levels into the linear range of the biosensor when testing in the patient abdominal samples. The biosensor and commercial assay results of the patient abdominal samples were significantly concordant, demonstrating proof-of-principle for use as a clinical diagnostic test. The biosensor results were all higher than those of the commercial kit, with a range of 3-18 mM for the biosensors compared to 2-9 mM with the kit. Despite interference testing showing good selectivity, this was likely to be due to non-specific binding of proteins in the samples increasing the amperometric signal. Non-specific binding is a significant issue with biosensors in biological media and a common obstacle in translation

from laboratory work in buffered solutions to measurement in clinical samples. Levels of lactate in patient abdominal fluid from other clinical studies in the literature show lower lactate levels, although not incomparable, with one study showing a lactate of 7 mM after anastomotic leak, and 3 mM in non-AL patients, using an alternative methodology (Pedersen et al., 2009b). The developed biosensor is therefore comparable to other studies, although non-specific binding needs to be further investigated with comparison to controls. A drawback of the lactate biosensor methodology is the requirement for a dilution step, as a fundamental advantage of biosensors is their instantaneous, "in-field" use with no requirement of additional reagents. As a commercial application, ways to facilitate this could include the addition of a pre-filled tube of diluent solution with each biosensor kit, which is added to the sample before measurement. The complex mathematical modelling used would also require automation with data fitting algorithms, as adopted in commercial glucose sensors. The biosensor preparation time, although greatly simplified by the use of pre-impregnated Prussian Blue mediator, is an aspect which would require consideration when up scaling to a commercial level. The lactate oxidase enzyme is relatively expensive, and an alternative source or in-house production would need to be investigated to bring the lactate biosensors to market with a feasible per unit cost.

E. coli and TNFα immunosensors were constructed using half antibodies and whole antibodies respectively, with immobilisation onto polytyramine coated gold electrode surfaces *via* chemical cross linkers. Initially a range of polymers were evaluated to optimise for type, as well as potential and scan rate during electro-deposition onto the electrode surface. Polytyramine was found to yield greatest electron transfer resistance and availability of amine groups after characterisation by CV, EIS, SEM and Midland blotting (Rushworth et al., 2014), in keeping with other biosensor work of this nature (Ahmed et al., 2013). During optimisation, isolated analyte and antibody binding was successfully confirmed using dot blotting, and later construction was verified using CV and EIS. Reductive cleavage of IgG to

half antibodies using 2-MEA for *E. coli* sensor fabrication was verified with SDS-PAGE analysis.

The *E. coli* immunosensors showed excellent detection of *E. coli* compared to an *S. pyogenes* control with a limit of detection of 10^4 cells ml^{-1} in buffer. The methodology for construction was based on previous immunosensor work where successful detection of virus and bacteria were shown (Ahmed et al., 2013, Caygill et al., 2012). Therefore significant optimisation had already been accomplished, and the *E. coli* sensors required little initial optimisation. However, upon progression to testing in NCS, the *E. coli* sensors showed variability and inconsistent data compared to controls at a range of NCS dilutions. This was thought to be attributable to a high level of non-specific binding of serum proteins and other substances within the NCS. For the *E. coli* sensors this stage was of great importance, in order to generate calibration curves to calculate *E. coli* concentrations in patient samples using a comparable media to the samples themselves. A recent novel approach described for an immunosensor detecting prostate specific antigen (PSA) in human plasma using a "diluent" of real sample with known low concentrations of analyte diluted 1000x with PBS was found to negate this effect, to allow generation of meaningful calibration curves (Chornokur et al., 2011). Application of this strategy using spiked *E. coli* into a patient drain fluid sample with low bacterial count (as measured by flow cytometry) as a "diluent" at a range of dilutions was successful in yielding data comparable to experiments in buffer. A dilution of 10% (v/v) was again optimal, in agreement with the previous lactate experiments. This was not however surprising, as the diluent at 1000x PBS, then at 10% (v/v) was likely to have been similar to buffer in any case. Strategies for future work to assess the immunosensors in NCS include experiments blocking the tethered, unreacted sulfo-SMCC maleimide groups, to reduce non-specific binding. The inability to use the LPS assay as a commercial validation to the *E. coli* biosensors due to colour absorbance issues was another technical limitation which had to be overcome. Flow cytometry was used *in lieu* of any other suitable assay, with which all DNA containing material was stained and included, as there

was a high degree of non-specific FITC-secondary antibody staining upon initial runs. Despite this, the flow cytometry and biosensor data were significantly concordant, illustrating proof-of-principle of the sensor working in patient samples. Surprisingly, the total cell numbers measured by flow cytometry were consistently lower than those of *E. coli* alone measured by the biosensor. As with the lactate work, this was likely to be due to non-specific binding of serum proteins in the samples, increasing the impedance of the biosensors. Unfortunately there are no comparable studies in the literature that give a quantitative measurement of *E. coli* - either clinical studies with measurement after anastomotic leak, or other groups fabricating biosensors to *E. coli*. This highlights the importance of the development of the *E. coli* biosensor for clinical diagnostics. Alternate validation methods in future work are expected to include live plating techniques for quantitative microbiology in comparison to live *E. coli* measured by the biosensors for greater likeness to "fresh", point-of-care clinical samples.

Development of the TNFα immunosensor raised a number of issues. The methodology used whole antibody attached to a sensor surface *via* biotin/Avidin linkage, as anti-TNFα was only commercially available in small concentrations. This rendered half antibody cleavage unsuitable due to the low concentration yield seen after anti-*E. coli* reduction (approximately 400 fold lower concentration). The constructed TNFα biosensors initially showed very high impedance levels upon addition of spiked TNFα in buffer. Optimisation included evaluation of an alternative polymer on the electrode surface, increasing the scan rate during electro-deposition of the polymer to reduce the thickness of the surface layer, and testing a range of lower antibody concentrations. The optimised TNFα immunosensor was able to show increasing impedance upon increasing concentrations of analyte. However, data were equivalent using a myoglobin sensor control at all except the highest concentration of TNFα (100 $\mu g.ml^{-1}$), showing a high degree of non-specific binding and insensitivity of the biosensor. The levels of TNFα in patient abdominal samples measured by the commercial ELISA assay were in the order of 10^6 times lower than this concentration. Levels

shown in the literature were consistent with the assay, and therefore also much lower than the LOD of the biosensor. In clinical studies using an alternative methodology to measure TNFα in patient abdominal fluid after anastomotic leak, levels of 511 $pg.ml^{-1}$ compared to non-leak levels of 141 $pg.ml^{-1}$ were shown at post-operative day three (Fouda et al., 2011). An LOD of 1 $pg.ml^{-1}$ to 100 $pg.ml^{-1}$ was demonstrated in culture media using an antibody mixed self assembled monolayer TNFα biosensor by a biosensor group (Pui et al., 2013). Strategies for enhancing sensitivity of the TNFα biosensor in future experiments to develop a clinically useful test will consist of investigation into blocking agents on the sensor surface to reduce non-specific binding, and alternative construction strategies such as self assembled monolayers as the bioreceptor tethering layer.

For further commercial development of the *E. coli* and TNFα impedance biosensors, a number of technical issues would need to be addressed. The principle limiting factor in the ongoing development is the time taken to collect and analyse the data using EIS. The FRA system software used was out of date, with data analysis of Nyquist plot curve fitting performed manually. This required a number of hours for multiple immunosensors each at a range of analyte concentrations. To become a commercial application, the impedance reading of each sample would need to be available instantaneously. In addition to automatic curve fitting which is available with newer software, data fitting algorithms would need to be applied to achieve this, which have been shown successfully with glucose monitors. The experiments performed also utilised a single constructed immunosensor for the detection of increasing concentrations of analyte in buffer and diluent media for calibration curves, repeated for n = 5. Therefore there may have been an insulating effect caused by cumulative analyte binding, rendering the data not directly comparable to the single interrogation of patient samples. Work by Ahmed *et al*, investigated the size of this effect with bacterial immunosensors, which showed that the linear range of response was smaller with "single-shot" incubation (10^4 – 10^6 cells ml^{-1}) compared to "cumulative" incubation (10^4 – 10^7 cells ml^{-1}) (Ahmed et al., 2013). At higher concentrations of bacteria in single-shot incubation, the antibody binding

site access was hypothesised to be limited due to steric collisions. Calibration curves in diluent media should therefore be constructed using data from single immunosensors to compare most meaningfully to clinical samples. In the laboratory this would have required great expense and time beyond the scope of this study, but to proceed with any commercial application would need to be achieved. Lastly, the low yield of reduced antibody from native samples using 2-MEA in the fabrication of *E. coli* sensors (approximate 400 fold concentration reduction), whilst fortuitously being in the range of the optimum concentration for use shown by other bacterial immunosensors (Ahmed et al., 2013) should be addressed. For cost reduction, alternate reductants such as tris(2-carboxyethly)phosphine (TCEP) should be investigated, to improve antibody productivity on a commercial scale.

Ten patient drain fluid samples were used to show the biosensors gave comparable results to those of corresponding commercial assays. Five samples were from patients who suffered an anastomotic leak post-operatively, and five were from patients with an uncomplicated post-operative course. The small number reflects the number of anastomotic leaks in the cohort of drain fluid that was available to be collected. There were a total of 69 patients' samples collected over an 18 month period, with five patients who suffered an anastomotic leak, a leak rate of 7% which is consistent with national averages. Samples taken at 24 hours (post-operative day one) were used due to the availability of fluid at this time interval which was not the case on subsequent days for all patients, as well as evidence from the literature that biomarker levels are elevated this early in patients who then suffer anastomotic leak. Unfortunately, when measured by either the constructed biosensors or the commercial assays, none of the three biomarkers showed a significant difference between anastomotic leak and non-anastomotic leak groups, with large standard deviations seen in all cases. Potential reasons for this, despite evidence to the contrary in the available literature and as shown in the animal model, were considered. These were thought to be primarily the small sample size tested and variability of data seen, meaning that an individual's biomarker trend

over time may be more useful than single values with imposed arbitrary cut off points. This would need to be investigated with larger data sets, but a key advantage for this would be in using a biosensor application due to their low cost and point-of-care use. Another reason for the lack of statistical difference between groups was thought to be issues with the sample collection itself. Samples were collected from drainage bags, which were at room temperature, at 24 hour intervals. This is suboptimal, as levels of biomarkers such as lactate have been shown to vary in as little as 30 minutes in blood at room temperature due to ongoing glycolytic pathways (Seymour et al., 2011). The commercial development of the biosensor application is therefore expected to incorporate a delivery system of "fresh" fluid from the abdominal environment with immediate refrigeration to an external biosensing device. This could be in the form of a microdialysis catheter as shown by one group (Pedersen et al., 2009b), or using a biosensor flow cell device which has been successfully used to measure lactate in human sera and blood (Krawczyk et al., 1996, Yashina et al., 2010), coupled with miniaturisation of the sensor device itself. This also obviates the need for a surgical drain from which to collect samples, which are becoming less commonly used in the elective surgical setting. Measurement of the animal model samples using the biosensors would provide greater proof-of-principle that the biosensors are able to show a statistical difference between AL and non-AL, and should be performed in future work after the biosensors are fully optimised.

Current benchmarks for point-of-care diagnostics are sensors used for pregnancy tests and glucose monitors. The glucose sensor is currently the only successful electrochemical device available commercially over the counter for use in any field, and has taken a number of generations to be developed to its worldwide commercial success. Glucose monitoring by glucose biosensors currently accounts for 85% of the global market, at an estimated US$8.8 billion (Hughes, 2009). Despite the plethora of available literature on biosensors for detection of a diverse range of biomarkers at a laboratory level, none have yet come close to competing with glucose sensors in the commercial market, an "elephant in the room" for the

major biosensor companies. Key issues thought to be accountable for this, and which need to be addressed for translation of any biosensor from bench to bedside, are safe manufacture, production in large quantities under controlled conditions at minimal costs, and with adherence to regulatory standards. More specifically to the biosensors presented in this work is continued development with testing of stability and lifespan - particularly of the lactate biosensor – and testing at a range of parameters of temperature, and pH etc. The potential wider application of this work however is enormous, as the biosensors could be used to detect the immediate presence and/or progression of sepsis in not just the abdomen but in patient central venous access, urinary catheters, and for isolated ischaemic bowel complications as well as inflammatory disorders such as pancreatitis. Therefore the demand for this type of diagnostic tool strongly justifies the cost and drives development. Building on the work presented, biosensors for early detection of septic surgical complications and other clinical pathology is a promising technology that has the potential to greatly reduce morbidity and mortality from these adverse events.

Chapter 7:

References

Chapter 7. References

ABOUL-ENEIN, H. Y., STEFAN, R. I., LITESCU, S. & RADU, G. L. 2002. Biosensor for the enantioselective analysis of the thyroid hormones (+)-3,3 ',5-triiodo-L-thyronine (T-3) and (+)-3,3 ',5,5 '-tetraiodo-L-thyronine (T-4). *Journal of Immunoassay & Immunochemistry,* 23**,** 181-190.

ADHIKARI, N. K. J., FOWLER, R. A., BHAGWANJEE, S. & RUBENFELD, G. D. 2010. Critical care and the global burden of critical illness in adults. *The Lancet,* 376**,** 1339-1346.

AHMED, A., RUSHWORTH, J. V., HIRST, N. A. & MILLNER, P. A. 2014. Biosensors for Whole-Cell Bacterial Detection. *Clinical Microbiology Reviews,* 27**,** 631-646.

AHMED, A., RUSHWORTH, J. V., WRIGHT, J. D. & MILLNER, P. A. 2013. Novel impedimetric immunosensor for detection of pathogenic bacteria Streptococcus pyogenes in human saliva. *Analytical Chemistry*.

AKYOL, A. M., MCGREGOR, J. R., GALLOWAY, D. J. & GEORGE, W. D. 1992. Early postoperative contrast radiology in the assessment of colorectal anastomotic integrity. *International Journal of Colorectal Disease,* 7**,** 141-143.

ALMEIDA, A. B., FARIA, G., MOREIRA, H., PINTO-DE-SOUSA, J., CORREIA-DA-SILVA, P. & MAIA, J. C. 2012. Elevated serum C-reactive protein as a predictive factor for anastomotic leakage in colorectal surgery. *Int J Surg,* 10**,** 87-91.

ALSOP, B. 1998. Receiver operating characteristics from nonhuman animals: Some implications and directions for research with humans. *Psychonomic Bulletin & Review,* 5**,** 239-252.

ANGUS, D. C. & VAN DER POLL, T. 2013. Severe Sepsis and Septic Shock. *New England Journal of Medicine,* 369**,** 840-851.

ATES, M. 2013. A review study of (bio)sensor systems based on conducting polymers. *Materials Science & Engineering C-Materials for Biological Applications,* 33**,** 1853-1859.

BADIA, J. M., WHAWELL, S. A., SCOTT-COOMBES, D. M., ABEL, P. D., WILLIAMSON, R. C. N. & THOMPSON, J. N. 1996. Peritoneal and systemic cytokine response to laparotomy. *British Journal of Surgery,* 83**,** 347-348.

BAKER, E. A., GADDAL, S. E., AITKEN, D. G. & LEAPER, D. J. 2003. Growth factor profiles in intraperitoneal drainage fluid following colorectal surgery: Relationship to wound healing and surgery. *Wound Repair and Regeneration,* 11**,** 261-267.

BARD, A. J. & FAULKNER, L. R. 2000. *Electrochemical Methods: Fundamentals and Applications*, Wiley.

BEARD, J. D., NICHOLSON, M. L., SAYERS, R. D., LLOYD, D. & EVERSON, N. W. 1990. Intraoperative Air Testing of Colorectal Anastomoses - a Prospective, Randomized Trial. *British Journal of Surgery,* 77**,** 1095-1097.

BERGGREN, C., BJARNASON, B. & JOHANSSON, G. 2001. Capacitive biosensors. *Electroanalysis,* 13**,** 173-180.

BERGSTRAND, A., CEYLAN, I., QUASH, G., NYDEN, M. & HOLMBERG, K. 2008. Towards a biosensor immunoassay of protein-bound isopeptides in human plasma. *Colloids and Surfaces B-Biointerfaces,* 66**,** 150-153.

BERTONI, C. B., MENDIBLE, M., FLEURY, A. R., VANDERMEER, T. J., SKEIST, B. P. & CAGIR, B. 2009. Utility of Pelvic CT with Rectal Contrast to Identify Pelvic Abscess and Anastomotic Leaks. *Gastroenterology,* 136**,** A893-A893.

BILLAH, M. M., HODGES, C. S., HAYS, H. C. W. & MILLNER, P. A. 2010. Directed immobilization of reduced antibody fragments onto a novel SAM on gold for myoglobin impedance immunosensing. *Bioelectrochemistry,* 80**,** 49-54.

BINI, A., CENTI, S., TOMBELLI, S., MINUNNI, M. & MASCINI, M. 2008. Development of an optical RNA-based aptasensor for C-reactive protein. *Analytical and Bioanalytical Chemistry,* 390**,** 1077-1086.

BLACK, S., KUSHNER, I. & SAMOLS, D. 2004. C-reactive protein. *Journal of Biological Chemistry,* 279**,** 48487-48490.

BOCCOLA, M. A., BUETTNER, P. G., ROZEN, W. M., SIU, S. K., STEVENSON, A. R. L., STITZ, R. & HO, Y. H. 2011. Risk Factors and Outcomes for Anastomotic Leakage in Colorectal Surgery: A Single-Institution Analysis of 1576 Patients. *World Journal of Surgery,* 35**,** 186-195.

BONE, R. C. 1996. Toward a theory regarding the pathogenesis of the systemic inflammatory response syndrome: what we do and do not know about cytokine regulation. *Critical Care Medicine,* 24**,** 163-172.

BONE, R. C., BALK, R. A., CERRA, F. B., DELLINGER, R. P., FEIN, A. M., KNAUS, W. A., SCHEIN, R. M. H. & SIBBALD, W. J. 1992. Definitions for sepsis and organ failure and guidelines for the use of innovative therapies in sepsis. *Chest,* 101**,** 1644-1655.

BRANAGAN, G. & FINNIS, D. 2005. Prognosis after anastomotic leakage in colorectal surgery. *Diseases of the Colon & Rectum,* 48**,** 1021-1026.

BROOK, I. & FRAZIER, E. 2000. Aerobic and anaerobic microbiology in intra-abdominal infections associated with diverticulitis. *J Med Microbiol,* 49**,** 827-830.

BROOKS, H. F., OSABUTEY, C. K., MOSS, R. F., ANDREWS, P. L. R. & DAVIES, D. C. 2007. Caecal ligation and puncture in the rat mimics the pathophysiological changes in human sepsis and causes multi-organ dysfunction. *Metabolic Brain Disease,* 22**,** 353-373.

BRUCE, J., KRUKOWSKI, Z. H., AL-KHAIRY, G., RUSSELL, E. M. & PARK, K. G. M. 2001. Systematic review of the definition and measurement of anastomotic leak after gastrointestinal surgery. *British Journal of Surgery,* 88**,** 1157-1168.

BRUGIOTTI, C., CORAZZA, V., PERUZZI, A., LOZANO, C., CASADEVALL, E., QUES, F., FERRER, S., CANAVES, J., AMURRIO, R. & RODRIGUEZ, J. 2011. The efficacy of intraoperative endoscopic control of the colorectal stapled anastomosis after anterior resection of the rectum for rectal cancer. *Colorectal disease,* 13**,** 31-32.

BUSTOS, E., MANRIQUEZ, J., OROZCO, G. & GODINEZ, L. A. 2005. Preparation, characterization, and electrocatalytic activity of surface anchored, Prussian blue containing Starburst PAMAM dendrimers on gold electrodes. *Langmuir,* 21**,** 3013-3021.

CAHILL, R. A. & MORTENSEN, N. J. 2010. Intraoperative augmented reality for laparoscopic colorectal surgery by intraoperative near-infrared fluorescence imaging and optical coherence tomography. *Minerva Chir,* 65**,** 451-62.

CANCER RESEARCH UK. 2009. *Cancer Research UK* [Online]. Cancer Research UK. Available: http://www.cancerresearchuk.org/cancer-info/cancerstats/types/bowel/treatment/ [Accessed 6th August 2013].

CARRIGAN, S. D., SCOTT, G. & TABRIZIAN, M. 2005. Real-time QCM-D immunoassay through oriented antibody immobilization using cross-linked hydrogel biointerfaces. *Langmuir,* 21**,** 5966-5973.

CARUCCI, L. R., TURNER, M. A., CONKLIN, R. C., DEMARIA, E. J., KELLUM, J. M. & SUGERMAN, H. J. 2006. Roux-en-y gastric bypass surgery for morbid obesity: Evaluation of postoperative extraluminal leaks with upper gastrointestinal series. *Radiology,* 238**,** 119-127.

CAYGILL, R. L. 2012. *Developing an electrochemical assay to detect and quantify virus particles.* PhD Thesis, University of Leeds, UK.

CAYGILL, R. L., HODGES, C. S., HOLMES, J. L., HIGSON, S. P. J., BLAIR, G. E. & MILLNER, P. A. 2012. Novel impedimetric immunosensor for the detection and quantitation of Adenovirus using reduced antibody fragments immobilized onto a conducting copolymer surface. *Biosensors & Bioelectronics,* 32**,** 104-110.

CHAERON, S., TANASE, D., MARGALLO-BALBAS, E., TRIMP, P., FRENCH, P., KOMEN, N. & LANGE, J. 2007. An Optical Sensor System for Early Bacteria Detection in Drain Fluids. . *In:* JF. (ed.) *An optical sensor system for early bacteria detection in drain fluids Proceedings of SAFE.* Veldhoven, The Netherlands.

CHANDRAMOHAN, S. M., GAJBHIYE, R., AGWARWAL, A., CREEDON, E., SCHWIERS, M., WAGGONER, J. & TATLA, D. 2013. A Randomized Study Comparing Outcomes of Stapled and Hand-Sutured Anastomoses in Patients Undergoing Open Gastrointestinal Surgery. *Indian Journal of Surgery,* 75**,** 311-316.

CHANG, B. Y. & PARK, S. M. 2010. Electrochemical Impedance Spectroscopy. *Annual Review of Analytical Chemistry, Vol 3,* 3**,** 207-229.

CHEN, C. 2012. The Art of Bowel Anastomosis. *Scandinavian Journal of Surgery,* 101**,** 238-240.

CHORNOKUR, G., ARYA, S. K., PHELAN, C., TANNER, R. & BHANSALI, S. 2011. Impedance-Based Miniaturized Biosensor for Ultrasensitive and Fast Prostate-Specific Antigen Detection. *Journal of Sensors,* 2011**,** 7.

CHOWDHURY, I. & BHAT, G. K. 2009. *Tumor Necrosis Factor (TNF)-From Bench to Bed Side*, Nova Science Publishers, Inc, 400 Oser Ave, Ste 1600, Hauppauge, NY 11788-3635 USA

CHUANG, D., PADDISON, J. S., BOOTH, R. J. & HILL, A. G. 2006. Differential production of cytokines following colorectal surgery. *ANZ Journal of Surgery,* 76**,** 821-824.

CLARK, L. C. & LYONS, C. 1962. Electrode systems for continuous monitoring in cardiovascular surgery. *Annals of the New York Academy of Sciences,* 102**,** 29-&.

COLLIGHAN, N., GIANNOUDIS, P. V., KOURGERAKI, O., PERRY, S. L., GUILLOU, P. J. & BELLAMY, M. C. 2004. Interleukin 13 and inflammatory markers in human sepsis. *British Journal of Surgery,* 91**,** 762-768.

CONROY, D. J. R., MILLNER, P. A., STEWART, D. I. & POLLMANN, K. 2010. Biosensing for the Environment and Defence: Aqueous Uranyl Detection Using Bacterial Surface Layer Proteins. *Sensors,* 10**,** 4739-4755.

CONROY, P. J., HEARTY, S., LEONARD, P. & O'KENNEDY, R. J. 2009. Antibody production, design and use for biosensor-based applications. *Seminars in Cell & Developmental Biology,* 20**,** 10-26.

COOPER, M. A. 2002. Optical biosensors in drug discovery. *Nature Reviews Drug Discovery,* 1**,** 515-528.

CORCOLES, E. P., DEEBA, S., HANNA, G. B., PARASKEVA, P., BOUTELLE, M. G. & DARZI, A. 2011. Use of online rapid sampling microdialysis electrochemical biosensor for bowel anastomosis monitoring in swine model. *Analytical Methods,* 3**,** 2010-2016.

CORKE, C., GLENISTER K 2001. Monitoring Intestinal Ischaemia *Critical Care and Resuscitation* 3**,** 176-180.

COSNIER, S. 2005. Affinity biosensors based on electropolymerized films. *Electroanalysis,* 17**,** 1701-1715.

DANIELS, J. S. & POURMAND, N. 2007. Label-free impedance biosensors: Opportunities and challenges. *Electroanalysis,* 19**,** 1239-1257.

DAVIES, M. & HAGEN, P. O. 1997. Systemic inflammatory response syndrome. *British Journal of Surgery,* 84**,** 920-935.

DE RUITER, J., WEEL, J., MANUSAMA, E., KINGMA, W. & VAN DER VOORT, P. 2009. The Epidemiology of Intra-Abdominal Flora in Critically Ill Patients with Secondary and Tertiary Abdominal Sepsis. *Infection,* 37**,** 522-527.

DEARMOND, D. T., CLINE, A. M. & JOHNSON, S. B. 2010. Anastomotic Leak Detection by Electrolyte Electrical Resistance. *Journal of Investigative Surgery,* 23**,** 197-203.

DEEBA, S., CORCOLES, E., HANNA, B., PARESKEVAS, P., AZIZ, O., BOUTELLE, M. & DARZI, A. 2008. Use of Rapid Sampling Microdialysis for Intraoperative Monitoring of Bowel Ischemia. *Diseases of the Colon & Rectum,* 51**,** 1408-1413.

DEJAGER, L., PINHEIRO, I., DEJONCKHEERE, E. & LIBERT, C. 2011. Cecal ligation and puncture: the gold standard model for polymicrobial sepsis? *Trends in Microbiology,* 19**,** 198-208.

DELLINGER, R. P., LEVY, M. M., CARLET, J. M., BION, J., PARKER, M. M., JAESCHKE, R., REINHART, K., ANGUS, D. C., BRUN-BUISSON, C., BEALE, R., CALANDRA, T., DHAINAUT, J. F., GERLACH, H., HARVEY, M., MARINI, J. J., MARSHALL, J., RANIERI, M., RAMSAY, G., SEVRANSKY, J., THOMPSON, B. T., TOWNSEND, S., VENDER, J. S., ZIMMERMAN, J. L., VINCENT, J. L. & INT SURVIVING SEPSIS, C. 2008. Surviving Sepsis Campaign: International guidelines for management of severe sepsis and septic shock: 2008. *Critical Care Medicine,* 36**,** 296-327.

DEN DULK, M., NOTER, S. L., HENDRIKS, E. R., BROUWERS, M. A. M., VAN DER VILES, C. H., OOSTENBROEK, R. J., MENON, A. G., STEUP, W. H. & VAN DE VELDE, C. J. H. 2009. Improved diagnosis and treatment of anastomotic leakage after colorectal surgery. *Ejso,* 35**,** 420-426.

DINARELLO, C. A., GELFAND, J. A. & WOLFF, S. M. 1993. Anticytokine strategies in the treatment of the systemic inflammatory response syndrome. *JAMA: the journal of the American Medical Association,* 269**,** 1829-1835.

DOCHERTY, J. G., MCGREGOR, J. R., AKYOL, A. M., MURRAY, G. D. & GALLOWAY, D. J. 1995. Comparison of manually constructed and stapled anastomoses in colorectal surgery. West of Scotland and Highland Anastomosis Study Group. *Ann Surg,* 221**,** 176-84.

DORAISWAMY, A., RASMUSSEN, J., PIERCE, J., FULLER, W. & ALI, M. 2007. The utility of routine postoperative upper GI series following laparoscopic gastric bypass. *Surgical Endoscopy,* 21**,** 2159-2162.

DRAGICA, S., RUZICA, A. A., MALICEVIC, Z. & BRANKA, V. 2004. Model of sepsis (caecal ligation and puncture) in rats caused by mixed and pure bacterial cultures and changes in white blood cell counts. *Acta Veterinaria-Beograd,* 54**,** 281-287.

DUBAY, D. A. & FRANZ, M. G. 2003. Acute wound healing: the biology of acute wound failure. *Surgical Clinics of North America,* 83**,** 463-+.

EBONG, S., CALL, D., NEMZEK, J., BOLGOS, G., NEWCOMB, D. & REMICK, D. 1999. Immunopathologic alterations in murine models of sepsis of increasing severity. *Infection and Immunity,* 67**,** 6603-6610.

EININKEL, J., HOLLER, B. & HOFFMEISTER, A. 2011. Sonographic diagnosis and Endo-SPONGE assisted vacuum therapy of anastomotic leakage following posterior pelvic exenteration for ovarian cancer without using a protective stoma. *J Gynecol Oncol,* 22**,** 131-134.

ENESTVEDT, C. K., THOMPSON, S. K., CHANG, E. Y. & JOBE, B. A. 2006. Clinical review: Healing in gastrointestinal anastomoses, Part II. *Microsurgery,* 26**,** 137-143.

ENOCH, S. & LEAPER, D. J. 2005. Basic science of wound healing. *Surgery (Medicine Publishing),* 23**,** 37-42.

ESSANI, R. & BERGAMASCHI, R. 2009. Anastomotic leak in colorectal surgery: a review. *Gastroenterologia Polska,* 16**,** 123-127.

FAN, X., WHITE, I. M., SHOPOVA, S. I., ZHU, H., SUTER, J. D. & SUN, Y. 2008. Sensitive optical biosensors for unlabeled targets: A review. *Analytica Chimica Acta,* 620**,** 8-26.

FERLAY, J., SHIN, H. R., BRAY, F., FORMAN, D., MATHERS, C. & PARKIN, D. M. 2010. Estimates of worldwide burden of cancer in 2008: GLOBOCAN 2008. *Int J Cancer,* 127**,** 2893-917.

FIGUEIREDO, M. J., SOARES, D. D., MARTINS, J. M., MACHADO, R. D., SORGI, C. A., FACCIOLI, L. H., DE MELO, M. C. C., MALVAR, D. D. & SOUZA, G. E. P. 2012. Febrile response induced by cecal ligation and puncture (CLP) in rats: involvement of prostaglandin E-2 and cytokines. *Medical Microbiology and Immunology,* 201**,** 219-229.

FOUDA, E., EL NAKEEB, A., MAGDY, A., HAMMAD, E., OTHMAN, G. & FARID, M. 2011. Early Detection of Anastomotic Leakage After Elective Low Anterior Resection. *Journal of Gastrointestinal Surgery,* 15**,** 137-144.

FRACCHIOLLA, N. S., ARTUSO, S. & CORTELEZZI, A. 2013. Biosensors in clinical practice: focus on oncohematology. *Sensors (Basel),* 13**,** 6423-47.

GARCIA-GRANERO, A., FRASSON, M., FLOR-LORENTE, B., BLANCO, F., PUGA, R., CARRATALA, A. & GARCIA-GRANERO, E. 2013. Procalcitonin and C-reactive protein as early predictors of anastomotic leak in colorectal surgery: a prospective observational study. *Dis Colon Rectum,* 56**,** 475-83.

GEBBERT, A., ALVAREZICAZA, M., STOCKLEIN, W. & SCHMID, R. D. 1992. Real-time monitoring of immunochemical interactions with a tantalum capacitance flow-through cell. *Analytical Chemistry,* 64**,** 997-1003.

GERARD, M., CHAUBEY, A. & MALHOTRA, B. D. 2002. Application of conducting polymers to biosensors. *Biosensors & Bioelectronics,* 17**,** 345-359.

GIACOMELLI, C. E., BREMER, M. & NORDE, W. 1999. ATR-FTIR study of IgG adsorbed on different silica surfaces. *Journal of Colloid and Interface Science,* 220**,** 13-23.

GOLIGHER, J. C., GRAHAM, N. G. & DE DOMBAL, F. T. 1970. Anastomotic dehiscence after anterior resection of rectum and sigmoid. *Br J Surg,* 57**,** 109-18.

GREINER, M., PFEIFFER, D. & SMITH, R. D. 2000. Principles and practical application of the receiver-operating characteristic analysis for diagnostic tests. *Preventive Veterinary Medicine,* 45**,** 23-41.

GUESDON, J. L., TERNYNCK, T. & AVRAMEAS, S. 1979. Use of avidin-biotin interaction in immunoenzymatic techniques. *Journal of Histochemistry & Cytochemistry,* 27**,** 1131-1139.

GUILLOU, P. J. 1993. Biological variation in the development of sepsis after surgery or trauma. *The Lancet,* 342**,** 217-220.

HAJI-MICHAEL, P. G., LADRIERE, L., SENER, A., VINCENT, J. L. & MALAISSE, W. J. 1999. Leukocyte glycolysis and lactate output in animal sepsis and ex vivo human blood. *Metabolism-Clinical and Experimental,* 48**,** 779-785.

HALLIWELL, B. & GUTTERIDGE, J. M. C. 1990. The antioxidants of human extracellular fluids. *Archives of Biochemistry and Biophysics,* 280**,** 1-8.

HALSTED, W. S. 1887. Circular suture of the intestine: An experimental study. *Am J Med Sci,* 94**,** 436.

HAYS, H. C. W., MILLNER, P. A. & PRODROMIDIS, M. I. 2006. Development of capacitance based immunosensors on mixed self-assembled monolayers. *Sensors and Actuators B: Chemical,* 114**,** 1064-1070.

HEALY, D. A., HAYES, C. J., LEONARD, P., MCKENNA, L. & O'KENNEDY, R. 2007. Biosensor developments: application to prostate-specific antigen detection. *Trends in Biotechnology,* 25**,** 125-131.

HENDRIKS, T., BLEICHRODT, R. P., LOMME, R. M. L. M., DE MAN, B. M., VAN GOOR, H. & BUYNE, O. R. 2010. Peritoneal Cytokines Predict Mortality after Surgical Treatment of Secondary Peritonitis in the Rat. *Journal of the American College of Surgeons,* 211**,** 263-270.

HERMANSON, G. T. 2008. *Bioconjugate Techniques, 2nd Edition*, Academic Press Inc.

HERWIG, R., GLODNY, B., KÜHLE, C., SCHLÜTER, B., BRINKMANN, O., STRASSER, H., SENNINGER, N. & WINDE, G. 2002. Early Identification of Peritonitis by Peritoneal Cytokine Measurement. *Diseases of the Colon & Rectum,* 45**,** 514-521.

HIGSON, S. 2012. *Biosensors for Medical Applications*, Woodhead Publishing Limited.

HIRST, N. A., HAZELWOOD, L. D., JAYNE, D. G. & MILLNER, P. A. 2013. An amperometric lactate biosensor using H2O2 reduction via a Prussian Blue impregnated poly(ethyleneimine) surface on screen printed carbon electrodes to detect anastomotic leak and sepsis. *Sensors and Actuators B: Chemical,* 186**,** 674-680.

HIRST, N. A., TIERNAN, J. P., MILLNER, P. A. & JAYNE, D. G. 2014. Systematic review of methods to predict and detect anastomotic leakage in colorectal surgery. *Colorectal Dis,* 16**,** 95-109.

HOCK, B., SEIFERT, M. & KRAMER, K. 2002. Engineering receptors and antibodies for biosensors. *Biosensors & Bioelectronics,* 17**,** 239-249.

HOLFORD, T. R. J., DAVIS, F. & HIGSON, S. P. J. 2012. Recent trends in antibody based sensors. *Biosensors and Bioelectronics,* 34**,** 12-24.

HOLLIGER, P. & HUDSON, P. J. 2005. Engineered antibody fragments and the rise of single domains. *Nature Biotechnology,* 23**,** 1126-1136.

HOLTEN, C. H., MÜLLER, A. & REHBINDER, D. 1971. *Lactic acid: Properties and chemistry of lactic acid and derivatives*, Verlag Chemie.

HOMOLA, J., YEE, S. S. & GAUGLITZ, G. 1999. Surface plasmon resonance sensors: review. *Sensors and Actuators B-Chemical,* 54**,** 3-15.

HOOPER, L. V. & GORDON, J. I. 2001. Commensal Host-Bacterial Relationships in the Gut. *Science,* 292**,** 1115-1118.

HORIUCHI, T., MITOMA, H., HARASHIMA, S.-I., TSUKAMOTO, H. & SHIMODA, T. 2010. Transmembrane TNF-α: structure, function and interaction with anti-TNF agents. *Rheumatology,* 49**,** 1215-1228.

HUANG, Y.-C., CHIANG, C.-Y., LI, C.-H., CHANG, T.-C., CHIANG, C.-S., CHAU, L.-K., HUANG, K.-W., WU, C.-W., WANG, S.-C. & LYU, S.-R. 2013. Quantification of tumor necrosis factor-alpha and matrix metalloproteinases-3 in synovial fluid by a fiber-optic particle plasmon resonance sensor. *Analyst,* 138**,** 4599-4606.

HUGHES, M. D. 2009. The business of self-monitoring of blood glucose: a market profile. *J Diabetes Sci Technol,* 3**,** 1219-23.

HYMAN, N. H. 2009. Managing anastomotic leaks from intestinal anastomoses. *The Surgeon,* 7**,** 31-35.

IBUPOTO, Z. H., JAMAL, N., KHUN, K. & WILLANDER, M. 2012. Development of a disposable potentiometric antibody immobilized ZnO nanotubes based sensor for the detection of C-reactive protein. *Sensors and Actuators B-Chemical,* 166**,** 809-814.

IGOR, J., POLUKSHT, N., SIEGELMANN-DANIELI, N., LAVY, R., WASSERMANN, I., HALPERN, Z., GOLD-DEUTCH, R. & HALEVY, A. 2010. The role of upper gastrointestinal swallow study in patients undergoing proximal or total gastrectomy. *Isr Med Assoc J,* 12**,** 560-2.

IIJIMA, S., KATO, D., YABUKI, S., NIWA, O. & MIZUTANI, F. 2011. Enzymatically amplified electrochemical detection for lipopolysaccharide using ferrocene-attached polymyxin B and its analogue. *Biosensors & Bioelectronics,* 26**,** 2080-2084.

ISMAIL, F. & ADELOJU, S. B. 2010. Galvanostatic Entrapment of Penicillinase into Polytyramine Films and its Utilization for the Potentiometric Determination of Penicillin. *Sensors,* 10**,** 2851-2868.

IVANOV, D., CVIJANOVIC, R. & GVOZDENOVIC, L. 2011. Intraoperative Air Testing of Colorectal Anastomoses. *Srpski Arhiv Za Celokupno Lekarstvo,* 139**,** 333-338.

JAMES, E. A., SCHMELTZER, K. & LIGLER, F. S. 1996. Detection of endotoxin using an evanescent wave fiber-optic biosensor. *Applied Biochemistry and Biotechnology,* 60**,** 189-202.

JANSHOFF, A., GALLA, H. J. & STEINEM, C. 2000. Piezoelectric mass-sensing devices as biosensors - An alternative to optical biosensors? *Angewandte Chemie-International Edition,* 39**,** 4004-4032.

JOHNS HOPKINS MEDICINE. 2014. *Johns Hopkins Colon Cancer Center* [Online]. Johns Hopkins Medicine. Available: http://www.hopkinscoloncancercenter.org/CMS/CMS_Page.aspx?CurrentUDV=59&CMS_Page_ID=3ADE123E-CBF3-44ED-9122-5303AF76A32C [Accessed 25th June 2014].

JUNGER, V., JUNGER, W., MILLER, K., BAHRAMI, S., REDL, H., SCHLAG, G. & MORITZ, E. 1996. Early detection of anastomotic leaks after colorectal surgery by measuring endotoxin in the drainage fluid. *Hepato-Gastroenterology,* 43**,** 1523-1529.

KAPER, J. B., NATARO, J. P. & MOBLEY, H. L. T. 2004. Pathogenic Escherichia coli. *Nat Rev Micro,* 2**,** 123-140.

KARLICZEK, A., BENARON, D. A., BAAS, P. C., ZEEBREGTS, C. J., WIGGERS, T. & VAN DAM, G. M. 2010. Intraoperative assessment of microperfusion with visible light spectroscopy for prediction of anastomotic leakage in colorectal anastomoses. *Colorectal Disease,* 12**,** 1018-1025.

KARYAKIN, A. A., GITELMACHER, O. V. & KARYAKINA, E. E. 1995. Prussian Blue Based First-Generation Biosensor - a Sensitive Amperometric Electrode for Glucose. *Analytical Chemistry,* 67**,** 2419-2423.

KATASANI, V. G., LEETH, R. R., TISHLER, D. S., LEATH, T. D., ROY, B. P., CANON, C. L., VICKERS, S. M. & CLEMENTS, R. H. 2005. Water-soluble upper GI based on clinical findings is reliable to detect anastomotic leaks after laparoscopic gastric bypass. *Am Surg,* 71**,** 916-8; discussion 918-9.

KATE, V. 2014. *Intestinal Anastomosis* [Online]. Medscape. Available: http://emedicine.medscape.com/article/1892319-overview [Accessed 20th August 2014].

KATZ, E. & WILLNER, I. 2003. Probing biomolecular interactions at conductive and semiconductive surfaces by impedance spectroscopy: Routes to impedimetric immunosensors, DNA-Sensors, and enzyme biosensors. *Electroanalysis,* 15**,** 913-947.

KAUSAITE-MINKSTIMIENE, A., RAMANAVICIENE, A. & RAMANAVICIUS, A. 2009. Surface plasmon resonance biosensor for direct detection of antibodies against human growth hormone. *Analyst,* 134**,** 2051-2057.

KEHLET, H. 1997. Multimodal approach to control postoperative pathophysiology and rehabilitation. *Br J Anaesth,* 78**,** 606-17.

KHAN, A. A., WHEELER, J. M., CUNNINGHAM, C., GEORGE, B., KETTLEWELL, M. & MORTENSEN, N. J. 2008. The management and outcome of anastomotic leaks in colorectal surgery. *Colorectal Dis,* 10**,** 587-92.

KHOURY, W., BEN-YEHUDA, A., BEN-HAIM, M., KLAUSNER, J. M. & SZOLD, O. 2009. Abdominal computed tomography for diagnosing postoperative lower gastrointestinal tract leaks. *J Gastrointest Surg,* 13**,** 1454-8.

KINGHAM, T. P. & PACHTER, H. L. 2009. Colonic Anastomotic Leak: Risk Factors, Diagnosis, and Treatment. *Journal of the American College of Surgeons,* 208**,** 269-278.

KIYAMA, T., ONDA, M., TOKUNAGA, A., EFRON, D. & BARBUL, A. 2001. Effect of matrix metalloproteinase inhibition on colonic anastomotic healing in rats. *Journal of Gastrointestinal Surgery,* 5**,** 303-311.

KOMEN, N., DE BRUIN, R. W. F., KLEINRENSINK, G. J., JEEKEL, J. & LANGE, J. F. 2008. Anastomotic leakage, the search for a reliable biomarker. A review of the literature. *Colorectal Disease,* 10**,** 109-115.

KOMEN, N., MORSINK, M. C., BEIBOER, S., MIGGELBRINK, A., WILLEMSEN, P., VAN DER HARST, E., LANGE, J. F. & VAN LEEUWEN, W. B. 2009. Detection of colon flora in peritoneal drain fluid after colorectal surgery: Can RT-PCR play a role in diagnosing anastomotic leakage? *Journal of Microbiological Methods,* 79**,** 67-70.

KOROTCENKOV, G. 2010. *Chemical Sensors: Volume 1 General Approaches*, Momentum Press.

KOUNAVES, S. P. 1997. Voltammetric techniques. *Handbook of Instrumental Techniques for Analytical Chemistry***,** 712-713.

KRAWCZYK, T. K. V., TROJANOWICZ, M., LEWENSTAM, A. & MOSZCZYNSKA, A. 1996. Lactate solid-state biosensor with multilayer of electrodeposited polymers for flow-injection clinical analysis. *Biosensors & Bioelectronics,* 11**,** 1155-1165.

KRESGE, N., SIMONI, R. D. & HILL, R. L. 2004. The Discovery of Avidin by Esmond E. Snell. *Journal of Biological Chemistry,* 279**,** e5.

KRISHNAN, K. G., SCHACKERT, G. & STEINMEIER, R. 2005. The role of near-infrared angiography in the assessment of post-operative venous congestion in random pattern, pedicled island and free flaps. *British Journal of Plastic Surgery,* 58**,** 330-338.

KUBE, R., MROCZKOWSKI, P., GRANOWSKI, D., BENEDIX, F., SAHM, M., SCHMIDT, U., GASTINGER, I. & LIPPERT, H. 2010. Anastomotic leakage after colon cancer surgery: A predictor of significant morbidity and hospital mortality, and diminished tumour-free survival. *European Journal of Surgical Oncology (EJSO),* 36**,** 120-124.

KUDSZUS, S., ROESEL, C., SCHACHTRUPP, A. & HOER, J. J. 2010. Intraoperative laser fluorescence angiography in colorectal surgery: a noninvasive analysis to reduce the rate of anastomotic leakage. *Langenbecks Arch Surg,* 395**,** 1025-30.

LAMB, P. 2013. *123RF Royalty Free Stock Photos* [Online]. 123RF. Available: http://www.123rf.com/photo_14192057_drawing-to-show-the-detailed-structure-of-the-bowel-wall-showing-the-arteries-veins-nerves-muscle-la.html [Accessed 3rd September 2013].

LAVRIK, N. V., SEPANIAK, M. J. & DATSKOS, P. G. 2004. Cantilever transducers as a platform for chemical and biological sensors. *Review of Scientific Instruments,* 75**,** 2229-2253.

LENIGK, R., LAM, E., LAI, A., WANG, H., HAN, Y. F., CARLIER, P. & RENNEBERG, R. 2000. Enzyme biosensor for studying therapeutics of Alzheimer's disease. *Biosensors & Bioelectronics,* 15**,** 541-547.

LESLIE, D. B., DORMAN, R. B., ANDERSON, J., SERROT, F. J., KELLOGG, T. A., BUCHWALD, H., SAMPSON, B. K., SLUSAREK, B. M. & IKRAMUDDIN, S. 2012. Routine Upper Gastrointestinal Imaging Is Superior to Clinical Signs for Detecting Gastrojejunal Leak after Laparoscopic Roux-en-Y Gastric Bypass. *Journal of the American College of Surgeons,* 214**,** 208-213.

LI, J., CHEN, J. & KIRSNER, R. 2007. Pathophysiology of acute wound healing. *Clinics in Dermatology,* 25**,** 9-18.

LI, V. K., WEXNER, S. D., PULIDO, N., WANG, H., JIN, H. Y., WEISS, E. G., NOGEURAS, J. J. & SANDS, D. R. 2009. Use of routine intraoperative endoscopy in elective laparoscopic colorectal surgery: can it further avoid anastomotic failure? *Surg Endosc,* 23**,** 2459-65.

LIPSKA, M. A., BISSETT, I. P., PARRY, B. R. & MERRIE, A. E. H. 2006. Anastomotic leakage after lower gastrointestinal anastomosis: Men are at a higher risk. *ANZ Journal of Surgery,* 76**,** 579-585.

LIU, Y., KWA, T. & REVZIN, A. 2012. Simultaneous detection of cell-secreted TNF-alpha, and IFN-gamma using micropatterned aptamer-modified electrodes. *Biomaterials,* 33**,** 7347-7355.

LOCKSLEY, R. M., KILLEEN, N. & LENARDO, M. J. 2001. The TNF and TNF Receptor Superfamilies: Integrating Mammalian Biology. *Cell,* 104**,** 487-501.

LUONG, J. H. T., MALE, K. B. & GLENNON, J. D. 2008. Biosensor technology: Technology push versus market pull. *Biotechnology Advances,* 26**,** 492-500.

MACFIE, J. 2013. Surgical sepsis. *British Journal of Surgery,* 100**,** 1119-1122.

MADAN, A., STOECKLEIN, H., TERNOVITS, C., TICHANSKY, D. & PHILLIPS, J. 2007. Predictive value of upper gastrointestinal studies versus clinical signs for gastrointestinal leaks after laparoscopic gastric bypass. *Surgical Endoscopy,* 21**,** 194-196.

MAHER, K. J. & FLETCHER, M. A. 2005. Quantitative flow cytometry in the clinical laboratory. *Clinical and Applied Immunology Reviews,* 5**,** 353-372.

MALAMOU, C. A. & PRODROMIDIS, M. I. 2008. Performance of a Faradaic impedimetric immunosensor for blood group antigen A. *Microchimica Acta,* 163**,** 251-256.

MARRA, F., STEFFEN, T., KALAK, N., WARSCHKOW, R., TARANTINO, I., LANGE, J. & ZÜND, M. 2009. Anastomotic leakage as a risk factor for the long-term outcome after curative resection of colon cancer. *European Journal of Surgical Oncology (EJSO),* 35**,** 1060-1064.

MATSUI, A., WINER, J. H., LAURENCE, R. G. & FRANGIONI, J. V. 2011. Predicting the survival of experimental ischaemic small bowel using intraoperative near-infrared fluorescence angiography. *British Journal of Surgery,* 98**,** 1725-1734.

MATTHIESSEN, P. 2007. Increase of serum C-reactive protein is an early indicator of subsequent symptomatic anastomotic leakage after anterior resection. *Colorectal Dis,* 10**,** 75-80.

MATTHIESSEN, P., HALLBOOK, O., ANDERSSON, M., RUTEGARD, J. & SJODAHL, R. 2004. Risk factors for anastomotic leakage after anterior resection of the rectum. *Colorectal Dis,* 6**,** 462-9.

MATTHIESSEN, P., STRAND, I., JANSSON, K., TÖRNQUIST, C., ANDERSSON, M., RUTEGÅRD, J. & NORGREN, L. 2007. Is Early Detection of Anastomotic Leakage Possible by Intraperitoneal Microdialysis and Intraperitoneal Cytokines After Anterior Resection of the Rectum for Cancer? *Diseases of the Colon & Rectum,* 50**,** 1918-1927.

MAY, K. M. L., VOGT, A., BACHAS, L. G. & ANDERSON, K. W. 2005. Vascular endothelial growth factor as a biomarker for the early detection of cancer using a whole cell-based biosensor. *Analytical and Bioanalytical Chemistry,* 382**,** 1010-1016.

MCCAMLEY, M. K., ARTENSTEIN, A. W., OPAL, S. M. & CRAWFORD, G. P. 2007. Optical detection of sepsis markers using liquid crystal based biosensors - art. no. 64411Y. *In:* FARKAS, D. L., LEIF, R. C. & NICOLAU, D. V. (eds.) *Imaging, Manipulation, and Analysis of Biomolecules, Cells, and Tissues V.*

MERRELL, R. & LATIFI, R. 2001. *The abdomen as a source of sepsis in critically ill patient,* Munich: Zuckschwerdt.

MEYER, S. C. & GHOSH, I. 2010. *Phage Display Technology in Biosensor Development*, Springer, 233 Spring Street, New York, NY 10013, United States.

MILLAN, K. M. & MIKKELSEN, S. R. 1993. Sequence-selective biosensor for DNA-based on electroactive hybridization indicators. *Analytical Chemistry,* 65**,** 2317-2323.

MILLAN, M., GARCÍA-GRANERO, E., FLOR, B., GARCÍA-BOTELLO, S. & LLEDO, S. 2006. Early Prediction of Anastomotic Leak in Colorectal Cancer Surgery by Intramucosal pH. *Diseases of the Colon & Rectum,* 49**,** 595-601.

MILLER, K., ARRER, E. & LEITNER, C. 1996. Early detection of anastomotic leaks after low anterior resection of the rectum. *Diseases of the Colon & Rectum,* 39**,** 1081-1085.

MILLNER, P. A., HAYS, H. C. W., VAKUROV, A., PCHELINTSEV, N. A., BILLAH, M. M. & RODGERS, M. A. 2009. Nanostructured transducer surfaces for electrochemical biosensor construction—Interfacing the sensing component with the electrode. *Seminars in Cell & Developmental Biology,* 20**,** 34-40.

MINUNNI, M., TOMBELLI, S., SCIELZI, R., MANNELLI, I., MASCINI, M. & GAUDIANO, C. 2003. Detection of beta-thalassemia by a DNA piezoelectric biosensor coupled with polymerase chain reaction. *Analytica Chimica Acta,* 481**,** 55-64.

MISCORIA, S. A., BARRERA, G. D. & RIVAS, G. A. 2006. Glucose biosensors based on the immobilization of glucose oxidase and polytyramine on rodhinized glassy carbon and screen printed electrodes. *Sensors and Actuators B-Chemical,* 115**,** 205-211.

MOHAN, R., MACH, K. E., BERCOVICI, M., PAN, Y., DHULIPALA, L., WONG, P. K. & LIAO, J. C. 2011. Clinical Validation of Integrated Nucleic Acid and Protein Detection on an Electrochemical Biosensor Array for Urinary Tract Infection Diagnosis. *Plos One,* 6.

MONTROSE, A., CARGOU, S., NEPVEU, F., MANCZAK, R., GUE, A.-M. & REYBIER, K. 2013. Impedimetric immunosensor for the detection of circulating pro-inflammatory monocytes as infection markers. *Biosensors & Bioelectronics,* 49**,** 305-311.

MORRIS, E. J. A., BIRCH, R., WEST, N. P., FINAN, P. J., FORMAN, D., FAIRLEY, L. & QUIRKE, P. 2011. Low abdominoperineal excision rates are associated with high-workload surgeons and lower tumour height. Is further specialization needed? *Colorectal Disease,* 13**,** 755-761.

MOWAT, C., COLE, A., WINDSOR, A., AHMAD, T., ARNOTT, I., DRISCOLL, R., MITTON, S., ORCHARD, T., RUTTER, M., YOUNGE, L., LEES, C., HO, G., SATSANGI, J. & BLOOM, S. 2010. *Guidelines for the management of inflammatory bowel disease in adults* [Online]. British Society of Gastroenterology. Available: http://www.bsg.org.uk/images/stories/docs/clinical/guidelines/ibd/ibd_2011.pdf [Accessed 6th August 2013].

MURAMATSU, H., DICKS, J. M., TAMIYA, E. & KARUBE, I. 1987. Piezoelectric crystal biosensor modified with protein-A for determination of immunoglobulins. *Analytical Chemistry,* 59**,** 2760-2763.

MURRELL, Z. A. & STAMOS, M. J. 2006. Reoperation for anastomotic failure. *Clin Colon Rectal Surg,* 19**,** 213-6.

MYERS, C., MUTAFYAN, G., PETERSEN, R., PRYOR, A., REYNOLDS, J. & DEMARIA, E. 2009. Real-time probe measurement of tissue oxygenation during gastrointestinal stapling: mucosal ischemia occurs and is not influenced by staple height. *Surg Endosc,* 23**,** 2345-50.

NESBAKKEN, A., NYGAARD, K. & LUNDE, O. C. 2001. Outcome and late functional results after anastomotic leakage following mesorectal excision for rectal cancer. *British Journal of Surgery,* 88**,** 400-404.

NESBAKKEN, A., NYGAARD, K., LUNDE, O. C., BLUCHER, J., GJERTSEN, O. & DULLERUD, R. 2005. Anastomotic leak following mesorectal excision for rectal cancer: true incidence and diagnostic challenges. *Colorectal Dis,* 7**,** 576-81.

NEWMAN, J. D. & TURNER, A. P. F. 2005. Home blood glucose biosensors: a commercial perspective. *Biosensors and Bioelectronics,* 20**,** 2435-2453.

NGUYEN, H. B., RIVERS, E. P., KNOBLICH, B. P., JACOBSEN, G., MUZZIN, A., RESSLER, J. A. & TOMLANOVICH, M. C. 2004. Early lactate clearance is associated with improved outcome in severe sepsis and septic shock. *Critical Care Medicine,* 32**,** 1637-1642.

NICKSA, G. A., DRING, R. V., JOHNSON, K. H., SARDELLA, W. V., VIGNATI, P. V. & COHEN, J. L. 2007. Anastomotic leaks: What is the best diagnostic imaging study? *Diseases of the Colon & Rectum,* 50**,** 197-203.

O'HALLORAN, M. P., PRAVDA, M. & GUILBAULT, G. G. 2001. Prussian Blue bulk modified screen-printed electrodes for H2O2 detection and for biosensors. *Talanta,* 55**,** 605-611.

O'REGAN, T., PRAVDA, M., O'SULLIVAN, C. K. & GUILBAULT, G. G. 2003. Development of biosensor array for rapid detection of cardiac markers: Immunosensor for detection of free cardiac troponin I. *Analytical Letters,* 36**,** 1903-1920.

OFFICE FOR NATIONAL STATISTICS. 2012. *Office for National Statistics* [Online]. Office for National Statistics. Available: http://www.ons.gov.uk/ons/search/index.html?newquery=cancer+registrations [Accessed 6th August 2013].

OLIVER, J., BLAND, L., OETTINGER, C., ARDUINO, M., MCALLISTER, S., AGUERO, S. & FAVERO, M. 1993. Cytokine kinetics in an in vitro whole blood model following an endotoxin challenge. *Lymphokine Cytokine Res,* 12**,** 115-120.

PAKULA, M. P., TANASE, D., KRAAL, K., DE GRAAF, G., LANGE, J. F. & FRENCH, P. J. 2005. Optical measurements on drain fluid for the detection of anastomotic leakage. *2005 3rd IEEE/EMBS Special Topic Conference on Microtechnology in Medicine and Biology***,** 72-75.

PARSAJOO, C., KAUFFMANN, J. M. & ELKAOUTIT, M. 2012. Biosensors for drug testing and discovery. *Biosensors for Medical Applications***,** 233-262.

PASTERNAK, B., MATTHIESSEN, P., JANSSON, K., ANDERSSON, M. & ASPENBERG, P. 2010. Elevated intraperitoneal matrix metalloproteinases-8 and -9 in patients who develop anastomotic leakage after rectal cancer surgery: a pilot study. *Colorectal Dis,* 12**,** e93-8.

PCHELINTSEV, N. A. & MILLNER, P. A. 2008. A novel procedure for rapid surface functionalisation and mediator loading of screen-printed carbon electrodes. *Analytica Chimica Acta,* 612**,** 190-197.

PCHELINTSEV, N. A., VAKUROV, A. & MILLNER, P. A. 2009. Simultaneous deposition of Prussian Blue and creation of an electrostatic surface for rapid biosensor construction. *Sensors and Actuators B: Chemical,* 138**,** 461-466.

PEDERSEN, M., MORTENSEN, M., QVIST, N., PEDERSEN, S. & BEUKE, A. 2009a. Mediastinal microdialysis: early diagnosis of anastomotic leakage after resection for esophageal cancer. *Esophagus,* 6**,** 63-66.

PEDERSEN, M., QVIST, N., BISGAARD, C., KELLY, U., BERNHARD, A. & PEDERSEN, S. 2009b. Peritoneal microdialysis. Early diagnosis of anastomotic leakage after low anterior resection for rectosigmoid cancer. . *Scandanavian Journal of Surgery* 98**,** 148-154.

PEEL, A. & TAYLOR, E. 1991. Proposed definitions for the audit of postoperative infection: a discussion paper. Surgical Infection Study Group. *Ann R Coll Surg Engl,* 73**,** 385-388.

PEREZ, S. & FABREGAS, E. 2012. Amperometric bienzymatic biosensor for l-lactate analysis in wine and beer samples. *Analyst,* 137**,** 3854-3861.

PHITAYAKORN, R., DELANEY, C. P., REYNOLDS, H. L., CHAMPAGNE, B. J., HERIOT, A. G., NEARY, P., SENAGORE, A. J. & INT ANASTOMOTIC LEAK STUDY, G. 2008. Standardized algorithms for management of anastomotic leaks and related abdominal and pelvic abscesses after colorectal surgery. *World Journal of Surgery,* 32**,** 1147-1156.

PHYPERS, B. & PIERCE, J. T. 2006. Lactate physiology in health and disease. *Continuing Education in Anaesthesia, Critical Care & Pain,* 6**,** 128-132.

POHANKA, M. & SKLADAI, P. 2008. Electrochemical biosensors - principles and applications. *Journal of Applied Biomedicine,* 6**,** 57-64.

POURNARAS, A. V., KORAKI, T. & PRODROMIDIS, M. I. 2008. Development of an impedimetric immunosensor based on electropolymerized polytyramine films for the direct detection of Salmonella typhimurium in pure cultures of type strains and inoculated real samples. *Analytica Chimica Acta,* 624**,** 301-307.

POWER, N., ATRI, M., RYAN, S., HADDAD, R. & SMITH, A. 2007. CT assessment of anastomotic bowel leak. *Clinical Radiology,* 62**,** 37-42.

PUI, T. S., KONGSUPHOL, P., ARYA, S. K. & BANSAL, T. 2013. Detection of tumor necrosis factor (TNF-alpha) in cell culture medium with label free electrochemical impedance spectroscopy. *Sensors and Actuators B-Chemical,* 181**,** 494-500.

QURESHI, A., NIAZI, J. H., KALLEMPUDI, S. & GURBUZ, Y. 2010. Label-free capacitive biosensor for sensitive detection of multiple biomarkers using gold interdigitated capacitor arrays. *Biosensors & Bioelectronics,* 25**,** 2318-2323.

RAHBARI, N. N., WEITZ, J., HOHENBERGER, W., HEALD, R. J., MORAN, B., ULRICH, A., HOLM, T., WONG, W. D., TIRET, E., MORIYA, Y., LAURBERG, S., DEN DULK, M., VAN DE VELDE, C. & BÜCHLER, M. W. 2010. Definition and grading of anastomotic leakage following anterior resection of the rectum: A proposal by the International Study Group of Rectal Cancer. *Surgery,* 147**,** 339-351.

RAKOFF-NAHOUM, S., PAGLINO, J., ESLAMI-VARZANEH, F., EDBERG, S. & MEDZHITOV, R. 2004. Recognition of Commensal Microflora by Toll-Like Receptors Is Required for Intestinal Homeostasis. *Cell,* 118**,** 229-241.

RAMAN, R., RAMAN, B., RAMAN, P., ROSSITER, S., CURET, M., MINDELZUN, R. & MORTON, J. 2007. Abnormal Findings on Routine Upper GI Series following Laparoscopic Roux-en-Y Gastric Bypass. *Obesity Surgery,* 17**,** 311-316.

RANDLES, J. E. B. 1947. Kinetics of Rapid Electrode Reactions. *Discussions of the Faraday Society,* 1**,** 11-19.

RICCI, F. & PALLESCHI, G. 2005. Sensor and biosensor preparation, optimisation and applications of Prussian Blue modified electrodes. *Biosensors & Bioelectronics,* 21**,** 389-407.

RITTIRSCH, D., HUBER-LANG, M. S., FLIERL, M. A. & WARD, P. A. 2009. Immunodesign of experimental sepsis by cecal ligation and puncture. *Nature Protocols,* 4**,** 31-36.

ROBERGS, R. A., GHIASVAND, F. & PARKER, D. 2004. Biochemistry of exercise-induced metabolic acidosis. *American Journal of Physiology-Regulatory Integrative and Comparative Physiology,* 287**,** R502-R516.

ROBSON, M. C., STEED, D. L. & FRANZ, M. G. 2001. Wound healing: Biologic features and approaches to maximize healing trajectories. *Current Problems in Surgery,* 38**,** 72-140.

RODGERS, M. A., FINDLAY, J. B. C. & MILLNER, P. A. 2010. Lipocalin based biosensors for low mass hydrophobic analytes; development of a novel SAM for polyhistidine tagged proteins. *Sensors and Actuators B: Chemical,* 150**,** 12-18.

ROMERO, M. R., GARAY, F. & BARUZZI, A. M. 2008. Design and optimization of a lactate amperometric biosensor based on lactate oxidase cross-linked with polymeric matrixes. *Sensors and Actuators B: Chemical,* 131**,** 590-595.

RONKAINEN, N. J., HALSALL, H. B. & HEINEMAN, W. R. 2010. Electrochemical biosensors. *Chemical Society Reviews,* 39**,** 1747-1763.

RULLIER, E., LAURENT, C., GARRELON, J. L., MICHEL, P., SARIC, J. & PARNEIX, M. 1998. Risk factors for anastomotic leakage after resection of rectal cancer. *British Journal of Surgery,* 85**,** 355-358.

RUSHWORTH, J. V. 2013. Structure of TNF alpha. PyMOL.

RUSHWORTH, J. V., AHMED, A. & MILLNER, P. A. 2014. Midland Blotting: A Rapid, Semi-Quantitative Method for Biosensor Surface Characterization. *J Biosens Bioelectron* 4**,** 146.

RUSHWORTH, J. V., HIRST, N. A., GOODE, J. A., PIKE, D., AHMED, A. A. & MILLNER, P. A. 2013. *Impedimetric biosensors for medical applications: current progress and challenges*, ASME.

SCHIESSER, M., GUBER, J., WILDI, S., GUBER, I., WEBER, M. & MULLER, M. K. 2011. Utility of routine versus selective upper gastrointestinal series to detect anastomotic leaks after laparoscopic gastric bypass. *Obesity Surgery,* 21**,** 1238-42.

SENN, N. 1893. Enterorrhaphy; its history, technique and present status. *JAMA,* 21**,** 215-235.

SERVAIS, E. L., RIZK, N. P., OLIVEIRA, L., RUSCH, V. W., BIKSON, M. & ADUSUMILLI, P. S. 2011. Real-time intraoperative detection of tissue hypoxia in gastrointestinal surgery by wireless pulse oximetry. *Surg Endosc,* 25**,** 1383-9.

SEYMOUR, C., CARLBOM, D., COOKE, C., WATKINS, T., BULGER, E., REA, T. & BAIRD, G. 2011. Temperature and time stability of whole blood lactate: implications for feasibility of pre-hospital measurement. *BMC Research Notes,* 4**,** 169.

SHAMIYEH, A., SZABO, K., ULF WAYAND, W. & ZEHETNER, J. 2012. Intraoperative endoscopy for the assessment of circular-stapled anastomosis in laparoscopic colon surgery. *Surg Laparosc Endosc Percutan Tech,* 22**,** 65-7.

SHAO, Y., WANG, X. A., WU, X., GAO, W., HE, Q. H. & CAI, S. X. 2001. Biosensor of endotoxin and sepsis. *In:* ZHOU, Y. & XU, S. (eds.) *International Conference on Sensor Technology.*

SHINDE, S. B., FERNANDES, C. B. & PATRAVALE, V. B. 2012. Recent trends in in-vitro nanodiagnostics for detection of pathogens. *Journal of Controlled Release,* 159**,** 164-180.

SHORTHOUSE, A. J., BARTRAM, C. I., EYERS, A. A. & THOMSON, J. P. S. 1982. The water soluble contrast enema after rectal anastomosis. *British Journal of Surgery,* 69**,** 714-717.

SITUMORANG, M., GOODING, J. J., HIBBERT, D. B. & BARNETT, D. 1998. Electrodeposited polytyramine as an immobilisation matrix for enzyme biosensors. *Biosensors and Bioelectronics,* 13**,** 953-962.

SKRETAS, G. & WOOD, D. W. 2005. A bacterial biosensor of endocrine modulators. *Journal of Molecular Biology,* 349**,** 464-474.

SOLEDAD BELLUZO, M., ELIDA RIBONE, M., CAMUSSONE, C., SERGIO MARCIPAR, I. & MARINA LAGIER, C. 2011. Favorably orienting recombinant proteins to develop amperometric biosensors to diagnose Chagas' disease. *Analytical Biochemistry,* 408**,** 86-94.

SONG, S., WANG, L., LI, J., ZHAO, J. & FAN, C. 2008. Aptamer-based biosensors. *Trac-Trends in Analytical Chemistry,* 27**,** 108-117.

SONG, S., XU, H. & FAN, C. 2006. Potential diagnostic applications of biosensors: current and future directions. *International Journal of Nanomedicine,* 1**,** 433-440.

STAMOS, M. J. 2013. *Perfusion Assessment in Laparoscopic Left Anterior Resection (PILLAR II)* [Online]. Available: https://clinicaltrials.gov/ct2/show/study/NCT01560377?term=PILLAR+II&rank=1 [Accessed 12th June 2014].

STRINGER, R. C., HOEHN, D. & GRANT, S. A. 2008. Quantum dot-based biosensor for detection of human cardiac Troponin I using a liquid-core waveguide. *Ieee Sensors Journal,* 8**,** 295-300.

STUMPF, M., KLINGE, U., WILMS, A., ZABROCKI, R., ROSCH, R., JUNGE, K., KRONES, C. & SCHUMPELICK, V. 2005. Changes of the extracellular matrix as a risk factor for anastomotic leakage after large bowel surgery. *Surgery,* 137**,** 229-234.

TANG, C.-L. & SEOW-CHOEN, F. 2005. Digital rectal examination compares favourably with conventional water-soluble contrast enema in the assessment of anastomotic healing after low rectal excision: a cohort study. *International Journal of Colorectal Disease,* 20**,** 262-266.

TEEUWEN, P. H. E., DE GEUS-OEI, L. F., HENDRIKS, T., OYEN, W. J. G. & BLEICHRODT, R. P. 2010. F-18-fluorodeoxyglucose positron emission tomography of colonic anastomosis: a possibility to detect anastomotic leakage? A Pilot study. *Inflammation Research,* 59**,** S160-S161.

TENAILLON, O., SKURNIK, D., PICARD, B. & DENAMUR, E. 2010. The population genetics of commensal Escherichia coli. *Nat Rev Micro,* 8**,** 207-217.

THOMPSON, S. K., CHANG, E. Y. & JOBE, B. A. 2006. Clinical review: Healing in gastrointestinal anastomoses, Part I. *Microsurgery,* 26**,** 131-136.

THORNTON, F. J. & BARBUL, A. 1997. Healing in the gastrointestinal tract. *Surgical Clinics of North America,* 77**,** 549-&.

TOPPINO, M., CESARANI, F., COMBA, A., DENEGRI, F., MISTRANGELO, M., GANDINI, G. & MORINO, F. 2001. The role of early radiological studies after gastric bariatric surgery. *Obesity Surgery,* 11**,** 447-54.

TOTHILL, I. E. 2009. Biosensors for cancer markers diagnosis. *Seminars in Cell & Developmental Biology,* 20**,** 55-62.

TROYAN, S. L., KIANZAD, V., GIBBS-STRAUSS, S. L., GIOUX, S., MATSUI, A., OKETOKOUN, R., NGO, L., KHAMENE, A., AZAR, F. & FRANGIONI, J. V. 2009. The FLARE intraoperative near-infrared fluorescence imaging system: a first-in-human clinical trial in breast cancer sentinel lymph node mapping. *Ann Surg Oncol,* 16**,** 2943-52.

TSUJI, I., EGUCHI, H., YASUKOUCHI, K., UNOKI, M. & TANIGUCHI, I. 1990. Enzyme immunosensors based on electropolymerized polytyramine modified electrodes. *Biosensors and Bioelectronics,* 5**,** 87-101.

TURNER, A. P. F. 1996. *Biosensors: past, present and future* [Online]. Cranfield University, Institute of BioScience and Technology. Available: http://www.cranfield.ac.uk/biotech/chinap.htm. [Accessed 6th May 2013].

UGRAS, B., GIRIS, M., ERBIL, Y., GÖKPINAR, M., ÇITLAK, G., ISSEVER, H., BOZBORA, A. & ÖZTEZCAN, S. 2008. Early prediction of anastomotic leakage after colorectal surgery by measuring peritoneal cytokines: Prospective study. *International Journal of Surgery,* 6**,** 28-35.

VAKUROV, A., SIMPSON, C. E., DALY, C. L., GIBSON, T. D. & MILLNER, P. A. 2005. Acetylecholinesterase-based biosensor electrodes for organophosphate pesticide detection: II. Immobilization and stabilization of acetylecholinesterase. *Biosensors and Bioelectronics,* 20**,** 2324-2329.

VO-DINH, T. & CULLUM, B. 2000. Biosensors and biochips: advances in biological and medical diagnostics. *Fresenius' Journal of Analytical Chemistry,* 366**,** 540-551.

VOJINOVIĆ, V., AZEVEDO, A. M., MARTINS, V. C. B., CABRAL, J. M. S., GIBSON, T. D. & FONSECA, L. P. 2004. Assay of H2O2 by HRP catalysed co-oxidation of phenol-4-sulphonic acid and 4-aminoantipyrine: characterisation and optimisation. *Journal of Molecular Catalysis B: Enzymatic,* 28**,** 129-135.

WALLEY, K. R., LUKACS, N. W., STANDIFORD, T. J., STRIETER, R. M. & KUNKEL, S. L. 1996. Balance of inflammatory cytokines related to severity and mortality of murine sepsis. *Infection and Immunity,* 64**,** 4733-4738.

WANG, H., DONG, P., DI, D., WANG, C., LIU, Y., CHEN, J. & WU, X. 2013. Interdigitated microelectrodes biosensor with nanodot arrays for thyroid-stimulating hormone detection. *Micro & Nano Letters,* 8**,** 11-14.

WANG, J. 2000. From DNA biosensors to gene chips. *Nucleic Acids Research,* 28**,** 3011-3016.

WANG, J. 2001. Glucose biosensors: 40 years of advances and challenges. *Electroanalysis,* 13**,** 983-988.

WANG, J. 2006. *Analytical electrochemistry*, Wiley-VCH.

WARD, N. S., CASSERLY, B. & AYALA, A. 2008. The Compensatory Anti-inflammatory Response Syndrome (CARS) in Critically Ill Patients. *Clinics in Chest Medicine,* 29**,** 617-625.

WILCHEK, M., BAYER, E. A. & LIVNAH, O. 2006. Essentials of biorecognition: The (strept)avidin–biotin system as a model for protein–protein and protein–ligand interaction. *Immunology Letters,* 103**,** 27-32.

WILCHEK, M., BEN-HUR, H. & BAYER, E. A. 1986. p-Diazobenzoyl biocytin — A new biotinylating reagent for the labeling of tyrosines and histidines in proteins. *Biochemical and Biophysical Research Communications,* 138**,** 872-879.

WILLIAMS, C. E., MAKIN, C. A., REEVE, R. G. & ELLENBOGEN, S. B. 1991. Over-utilisation of radiography in the assessment of stapled colonic anastomoses. *European Journal of Radiology,* 12**,** 35-37.

WILSON, R. & TURNER, A. P. F. 1992. Glucose-oxidase - an ideal enzyme. *Biosensors & Bioelectronics,* 7**,** 165-185.

WOESTE, G., MULLER, C., BECHSTEIN, W. O. & WULLSTEIN, C. 2010. Increased serum levels of C-reactive protein precede anastomotic leakage in colorectal surgery. *World J Surg,* 34**,** 140-6.

XIAO, Y., LUBIN, A. A., HEEGER, A. J. & PLAXCO, K. W. 2005. Label-free electronic detection of thrombin in blood serum by using an aptamer-based sensor. *Angewandte Chemie-International Edition,* 44**,** 5456-5459.

XU, D., XU, D., YU, X., LIU, Z., HE, W. & MA, Z. 2005. Label-free electrochemical detection for aptamer-based array electrodes. *Anal Chem,* 77**,** 5107-13.

YANG, L., LI, Y. & ERF, G. F. 2004. Interdigitated Array Microelectrode-Based Electrochemical Impedance Immunosensor for Detection of Escherichia coli O157:H7. *Analytical Chemistry,* 76**,** 1107-1113.

YASHINA, E. I., BORISOVA, A. V., KARYAKINA, E. E., SHCHEGOLIKHINA, O. I., VAGIN, M. Y., SAKHAROV, D. A., TONEVITSKY, A. G. & KARYAKIN, A. A. 2010. Sol-Gel Immobilization of Lactate Oxidase from Organic Solvent: Toward the Advanced Lactate Biosensor. *Analytical Chemistry,* 82**,** 1601-1604.

YUAN, J., DUAN, R., YANG, H., LUO, X. & XI, M. 2012. Detection of serum human epididymis secretory protein 4 in patients with ovarian cancer using a label-free biosensor based on localized surface plasmon resonance. *International Journal of Nanomedicine,* 7**,** 2921-2928.

ZELADA-GUILLEN, G. A., TWEED-KENT, A., NIEMANN, M., GOERINGER, H. U., RIU, J. & XAVIER RIUS, F. 2013. Ultrasensitive and real-time detection of proteins in blood using a potentiometric carbon-nanotube aptasensor. *Biosensors & Bioelectronics,* 41**,** 366-371.

ZHAO, W., XU, J. J., SHI, C. G. & CHEN, H. Y. 2005. Multilayer membranes via layer-by-layer deposition of organic polymer protected Prussian blue nanoparticles and glucose oxidase for glucose biosensing. *Langmuir,* 21**,** 9630-9634.

ZIEGLER, C. 2004. Cantilever-based biosensors. *Analytical and Bioanalytical Chemistry,* 379**,** 946-959.

ZOUROB, M., ELWARY, S. & TURNER, A. P. F. 2008. *Principles of Bacterial Detection: Biosensors, Recognition Receptors, and Microsystems*, Springer Science+Business Media, LLC.

ZWEIG, M. H. & CAMPBELL, G. 1993. Receiver-operating characteristic (ROC) plots - a fundamental evaluation tool in clinical medicine. *Clinical Chemistry,* 39**,** 561-577.

Chapter 8:

Appendices

Chapter 8. Appendices

8.1 Patient information sheet

PATIENT INFORMATION SHEET

An invitation to take part in a research study called: Development of a biosensor for early detection of anastomotic leak after bowel resection

You have been given this information sheet to invite you to participate in a research study looking at ways to improve bowel surgery in the future. The study is being undertaken by the Leeds Teaching Hospitals Trust Hospitals – Leeds General Infirmary and St James's University Hospital. Before you decide we would like you to understand why the research is being done and what it would involve for you. We will go through the information sheet with you and answer any questions you have. We are inviting you to take part, but you do not have to and if you decide not to no-one will think badly of you and this will not affect the quality of your care.

This information sheet is designed to explain:

- The purpose of this study and what will happen to you if you take part
- Information about the conduct of the study

Please take your time to think about whether you want to take part in the study, talk to others about the study if you wish and ask us if there is anything that is not clear, or if you would like more information.

What is an anastomotic leak?

An anastomotic leak is a breakdown of the join where bowel has been stitched back together after part of it is removed in a bowel operation. It is a rare but serious complication of bowel surgery. At the moment, it can sometimes be difficult to tell when a leak occurs until a patient becomes very ill.

What is the purpose of our study?

The aim of our study is to see if it is possible to develop a new diagnostic test which would enable surgeons to detect an anastomotic leak as early as possible.

Our study involves developing a special type of test called a “biosensor” which can measure some of the cells and cellular processes from around the anastomosis/join which increase in levels when a leak begins. One of the cellular processes we will measure will be a substance called lactate which is normally produced in many cells of the body, particularly in muscle cells during exercise. Other substances we will measure are E.coli bacteria which is normally found inside the bowel, and “cytokines” which are cells which increase when body tissue starts to heal. All these substances have been shown by other studies to increase in levels locally at an anastomosis when there is an anastomotic leak.

In order to test our biosensor works, we require an abdominal fluid sample taken during bowel surgery, and fluid samples from drains from patients after surgery. We will test our biosensor in the laboratory on these fluid samples to see if it can detect levels of lactate and the other cellular substances mentioned above. There is normally a small amount of fluid in the abdomen which is suctioned out during surgery and usually discarded. Drains which we would take fluid samples from are routinely inserted into the abdomen during surgery so that any excess fluid over the next few days can drain away. They are removed a few days later on the ward.

We will also record on a computer database patient details such as name and date of birth, any other medical problems, operation details, and if an anastomotic leak develops or not. This is so we can compare the drain fluid from patients who leaked to those who did not. All the drain fluid samples and personal data will be stored securely for a period of 3 years unless stated otherwise. This is so they may be used for other research studies in the future.

Why have I been invited to take part in the study?

You have been approached to be part of this study as you are undergoing bowel surgery at Leeds Teaching Hospitals Trust. We anticipate that approximately 150 people will take part in the study.

Do I have to take part in the study?

Taking part in research is always voluntary. If you decide to take part you will be given this information sheet to keep, and will be asked to sign a consent form which will go into your medical notes, but you are still free to withdraw at any time and without giving a reason. If you decide not to take part, then you don't have to give a reason why and no-one will think badly of you for not wishing to take part. If you do not wish to participate then this will not affect your care or treatment in any way.

What will happen to me if I decide to take part in the study?

If you do choose to participate, a small amount of fluid which is usually present in the abdomen will be collected during your operation. It is usual to place a drain into the abdomen as part of your operation. This drain is connected to a small collecting bag. Small amounts of fluid will be taken out of the drainage bag once a day for as long as the drain is in place. This takes approximately 2 minutes. Emptying your drainage bag will routinely be carried out on the ward by nursing staff to empty the bag when full, and therefore is not something new for our study. It is entirely pain and discomfort free.

What are the risks and benefits of taking part in the study?

Because taking fluid from your abdomen and out of your drainage bag is not something new for our study there are no disadvantages or risks from taking part, but there is also no direct benefit to your care. The aim of the study is to try to improve bowel surgery for others in the future.

Will my taking part in the study be kept confidential?

If you decide to take part in the study, all information collected about you during the course of the study will be kept strictly confidential in the same way as all of your other medical records.

What will happen to my data and samples?

Your fluid samples will be transported to, stored and tested at the laboratory at the University of Leeds. The samples will be stored securely and used in anonymous form, ie none of your personal data will be used in the laboratory. Some of your personal data such as name, date of birth, operation details, leak or no leak, will be taken, linked to your samples and stored on a secure computer database, ensuring your confidentiality. After the study has been completed, the database containing your personal data and your anonymised fluid samples will be kept in storage for 3 years and may be used in other research studies in the future, unless you request otherwise.

What will happen if I don't carry on with the study?

If you decide to discontinue your participation in the study, this would be honoured, with no impact on your care or treatment. You can decide not to continue with the study at any point in time, but if you do we would like to keep already collected samples and data so that it may be included in the final study analysis, unless you request that it should not be.

What will happen to the results of the study?

At the end of the study, the results will form part of a degree thesis (a document submitted for a professional qualification e.g. PhD). We will also publish the results in a medical journal so that others can benefit. No individual patient information will be identified in any publications or documents.

What if there is a problem?

Whether or not you take part in the study, if you wish to complain, or have any concerns about any aspect of the way you have been approached or treated during the course of this study, the normal National Health Service complaints mechanisms would be available to you. Taking part in the study would not affect your legal rights.

Who has reviewed the study?

All research in the NHS is looked at by an independent group of people, called a Research Ethics Committee to protect your safety, rights, wellbeing and dignity. This study has been reviewed and given favourable opinion by the Leeds East Research Ethics Committee.

Who is organising and funding the research?

The research is funded by educational grants and the University of Leeds. There is no involvement of any private companies and no conflicts of interest. The surgeons involved in the study are not paid to include you in the study.

Further information

Once you have read this sheet, you will have opportunity to ask any questions to your surgeon or the research team.

If you choose to participate in the study you will be asked to sign a separate consent form which will be filed in your clinical notes.

Thank you for your time in considering being involved this study.

Contact details for researcher (Natalie Hirst): xxxxx xxxxxx

Patient information sheet for ethical approval of patient drain fluid sample collection from Leeds Teaching Hospitals Trust. National Research Ethics Service reference: 11/H1306/5, R&D approval reference: GS10/9674.

8.2 Patient consent form

Centre Number:
Study Number:
Patient Identification Number for this trial:

CONSENT FORM FOR RESEARCH STUDY

Title of Project: Development of a biosensor for early detection of anastomotic leak after bowel resection

Name of Researcher: Miss Natalie Hirst

Research Supervisor: Mr D Jayne

	Please initia to confirm
I confirm that I have read and understand the information sheet dated 11th February 2011 (version 3.0) for the above study.	_____
I have had the opportunity to consider the information, ask questions and have had these answered satisfactorily.	_____
I understand that my participation is voluntary and that I am free to withdraw at any time, without giving any reason, without my medical care or legal rights being affected.	_____
I understand that relevant sections of any of my medical notes and data collected during the study may be looked at by responsible individuals employed by the NHS, from regulatory authorities or from the NHS Trust, where it is relevant to my taking part in this research. I give permission for these individuals to have access to my records.	_____
I understand that all the fluid samples taken from me, and my personal data, will be stored for a period of 3 years and may be used for other research studies in the future	_____
I agree to take part in the above research study.	_____

_____	_____	_____
Name of Patient	Date	Signature
_____	_____	_____
Name of Person taking consent (if different from researcher)	Date	Signature
_____	_____	_____
Researcher	Date	Signature

When complete one copy for patient, one to be kept in medical notes.

Patient consent form for ethical approval of patient drain fluid sample collection from Leeds Teaching Hospitals Trust. National Research Ethics Service reference: 11/H1306/5, R&D approval reference: GS10/9674.